Imperial College London

Intra- and supra-salt strain during gravity-driven salt tectonics on passive margins

A thesis submitted to
Imperial College London

For the degree of
Doctor of Philosophy

Supervised by
Prof. Christopher A-L. Jackson

Sian Lianne Evans

Basin Research Group
Department of Earth Science and Engineering
Imperial College London

Declaration

I certify that the research presented within this thesis is my own, except where the work of others is cited appropriately. The results presented in this thesis have not previously been submitted for a degree at Imperial College London or any other institution.

Sian L. Evans

_____

Acknowledgements

First of all, a big thank you to the Basins Research Group, who I leaned on so much over the past 4 years. To my original pod squad, Alex, Tom, Steve, Francesco and Matt, whose formidable reputation clung to the BRG long after they graduated. To the MTC boys Mike, Nan and Harya who were so chilled they made it difficult to be stressed. To the not-so-new newbies Tim, David, Aurio, Gabi, and others who could always put a smile on my face. And especially to Bailey who had to put up with me at home as well as in the office. And apologies to everyone who had the misfortune to sit near us in the open-plan office.

To my supervisor, Chris, who was always in my corner, gave me a push when I needed it, and helped to navigate the murky waters of academia. And for generally being a trailblazer and a force for positive change in the world. To Becky for supporting me and the unforgettable opportunity to participate in a seismic survey in New Zealand.

To Ruth, Shinny, Jenny, Cec, Cath and our group chat who were always there to rant to, laugh with, and ultimately drag me to karaoke if I didn't escape to Waga. To all the other lovely people in the department who stopped in the corridor for a chat, baked a cake for Friday coffee mornings, or came to a GradSoc event. And to all the friends I made at conferences. You all made my PhD experience and it wouldn't have been half as fun without you.

To everyone outside the PhD bubble, especially to my family, who really have no idea what I do for a living but support me nonetheless. I promise I will have much more time to spend with you now.

And finally, to he-who-desperately-wants-to-be-named. For somehow tolerating me always putting my work first with unconditional patience, love and support. This is as much yours as mine (but mostly mine). Here's to the next chapter.

Abstract

Ductile salt units have a profound influence on the subsequent tectono-stratigraphic evolution of sedimentary basins. The development of thin-skinned, kinematic zones of updip extension and downdip contraction, driven by the interplay between gravity gliding and gravity spreading, is well established. In detail, however, there is great complexity in the range of structural styles observed on salt-influenced passive margins, and their key controls are still not fully understood. I use 3D seismic reflection data from two salt-influenced passive margin settings (the Kwanza Basin, offshore Angola and the Levantine Basin, offshore Lebanon) to interpret their post-salt tectono-stratigraphic evolutions. I assess the relationship between sub-, intra-, and supra-salt structures, with a particular emphasis on the influence of base-salt relief and intra-salt lithological heterogeneity.

A number of different tools are employed to perform this analysis, including structural restorations, strain calculations and translation measurements. Ramp syncline basins develop due to salt flow over base-salt relief and provide a record of horizontal overburden translation during gravity gliding. This record can be used to calculate rates of translation, revealing spatial and temporal variations at the basin scale in both study areas, which are linked to thick- and thin-skinned processes. On the Angolan margin, the interaction of salt flow with base-salt relief is inferred to generate local stress fields that allow synchronous extension and contraction despite closely spaced positions on the margin. On the Lebanese margin, the salt flow over large sub-salt anticlines modulates the rate of basinward translation. In both cases I show that the geometry of the base-salt surface can have an important influence on the orientation and distribution of supra-salt structures.

The seismic-based interpretations are tested using physical analogue models, designed to investigate the effect of salt thickness and heterogeneity on the degree of coupling between sub- and supra-salt structures in experiments with controlled boundary conditions. These results support and integrate the seismic case studies, showing how thinner and more heterogeneous evaporite sequences are more strongly influenced by the base-salt geometry. I conclude that the interaction between salt flow and base-salt relief is a primary control on the structural development of the salt and overburden in gravity-driven systems, and this may explain some of the observed contrast in structural styles between different salt basins.

Contents

List of Figures

1 Introduction

Salt. A simple chemical compound that gives rise to so much complexity. In this chapter I will introduce the topic to which I have devoted the past four years of my PhD research, describing the current state of knowledge in the field and the rationale behind the project. The subsequent chapters contain the main body of research and our key findings in the form of stand-alone scientific papers (some published, some in review and some in prep. at the time of submission). The final chapter will then review the body of work as a whole, explore the wider implications, and address the gaps in our knowledge that persist and may motivate future work.

1.1 The Salt Revolution

Salt tectonics is the field of research dedicated to understanding the deformation of large salt deposits observed in many sedimentary basins around the world. One of the things that first attracted me to geology was its scope, encompassing everything from the atomic structure of a crystal to the collision of planets, and similarly the world of salt tectonics embraces a huge range of scales, from microscopic flow mechanisms to plate-scale continental break-up.

1.1.1 Deposition

Salt is an evaporitic rock, meaning that it precipitates from super-saturated brines during evaporation. The most common evaporitic mineral, and the one generally associated with the term 'salt', is halite, also known as Sodium Chloride (NaCl). Halite is a colourless mineral whose regular atomic structure gives it a cubic crystal habitat (Fig. 1.1). There are, however, other minerals which also form during evaporitic processes and are also included in the general term 'salt'. During sea water evaporation the brine precipitates a predictable series of minerals as its concentration increases (Fig. 1.2) (Borchert and Muir, 1964; Carpenter et al., 1978; McCaffrey et al., 1987). Carbonate minerals, i.e. calcite or aragonite ($CaCO_3$), are usually the first to precipitate at double the concentration of seawater. When the brine reaches four or five times concentration, gypsum starts to precipitate ($CaSO_4$). Only when the brine is super-saturated at 10 to 12 times the concentration does halite begin to precipitate. And if evaporation progresses even further, bittern salts may start to precipitate when >94%

of the water has been evaporated. One kilometre of seawater evaporation results in c. 17 m of deposited salts, of which the vast majority (c. 80%) is halite (Fig. 1.2).

Thick evaporite units can only be deposited if three conditions are met (Warren, 2016): (i) arid to semi-arid climatic conditions and large volumes of brine at or near the land surface, (ii) a sedimentary depression providing accommodation, and (iii) a preservative burial environment that prevents dissolution. These conditions are commonly met in restricted basins around 30° latitude, where the outflux of water by evaporation exceeds influx (Fig. 1.3) (Hudec and Jackson, 2007).

Figure 1.1 A clear halite hand specimen showing the characteristic cubic crystal habit. Sample from salt deposits in Stassfurt, Germany. Photo credit: Rob Lavinsky, irocks.com (CC-BY-SA-3.0).

The association of salt deposits with restricted basins (i.e. basins where sea water circulation is isolated or semi-isolated from the global ocean) means that salt deposition tends to happen during certain phases of the Wilson cycle (i.e. basin opening or closing) or in certain tectonic settings (e.g. foreland basins) (Hudec and Jackson, 2007). Consequently, salt deposits are widespread around the world and present throughout the geological record (Fig. 1.4); from the ancient Precambrian salt deposits exposed in domes of the Zagros fold and thrust belt, to the young Messinian salt giant that lies beneath the Mediterranean.

To deposit the large thicknesses of evaporites observed in many of these sedimentary basins, large volumes of water must be evaporated, often many times the total volume of the basin itself. As the chemistry of the water varies through time and space during basin evolution, the precipitating evaporites may vary compositionally and form heterogeneous layered sequences of interbedded evaporite units. Our closest present day analogue for this process is the active salt deposition taking place in the Red Sea rift basin. Extensive salt precipitation also takes place in man-made salt pans, such as those along the shores of the Dead Sea, built to accelerate the natural processes for commercial distribution (Fig. 1.5).

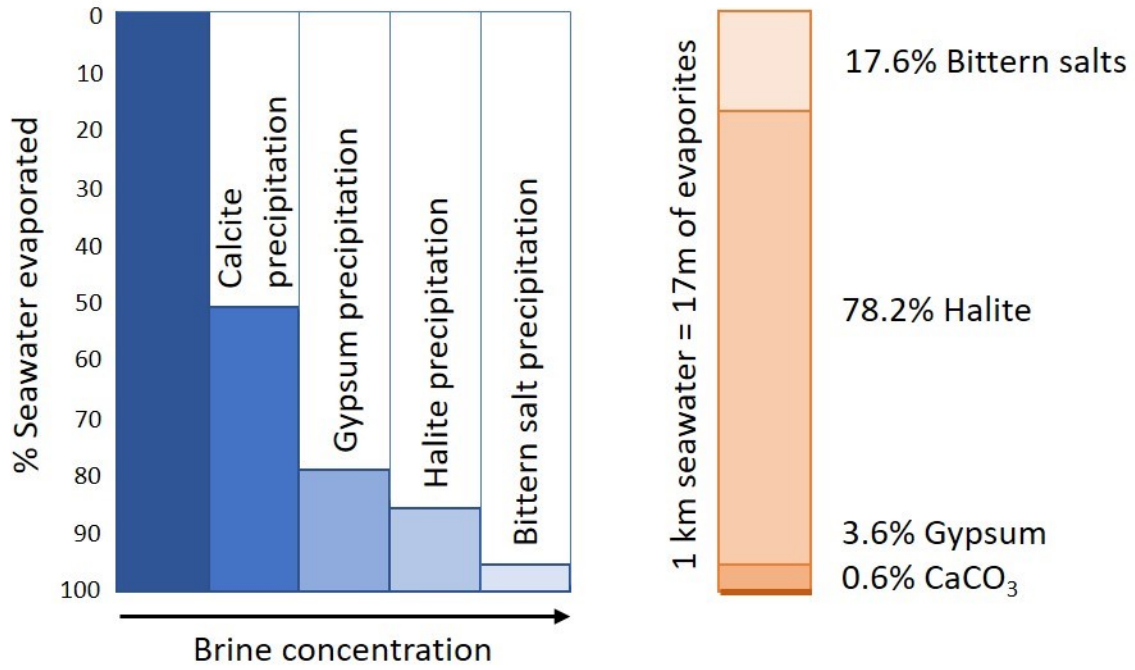

Figure 1.2 Average seawater contains about 35 ppt dissolved salts. As the seawater is evaporated, the salinity of the remaining brine increases. The concentration of the ions determines the composition of the precipitating mineral. Calcite begins to precipitate when 50% of the water is evaporated, and gypsum at 80-90%. Halite eventually precipitates at 86-94% evaporation and the brine is very dense. Bittern (k, Mg) salts only precipitate when >94% of the seawater is evaporated. Evaporation of 1km of seawater results in c. 17m of precipitated salts, of which 0.1m calcite, 0.6m gypsum, 13.3m halite and 3m of bittern salts. After Holser and Burns, 1979.

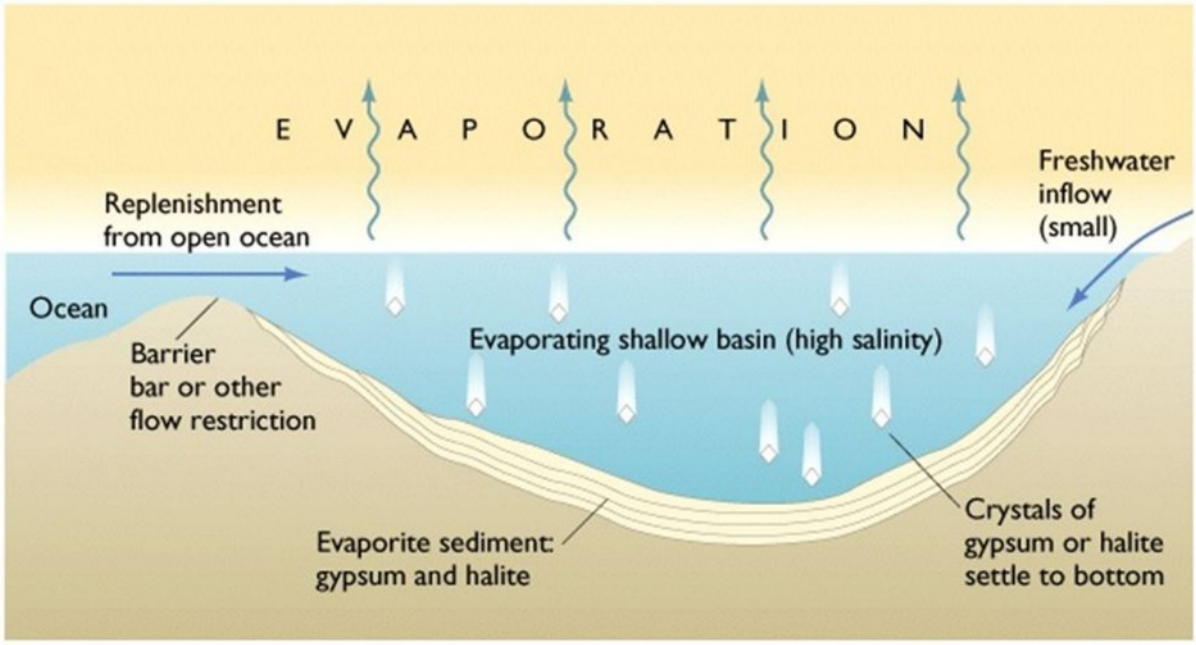

Figure 1.3 Evaporation and salt deposition in an isolated basin with restricted connection to the open ocean. After Warren, 2016.

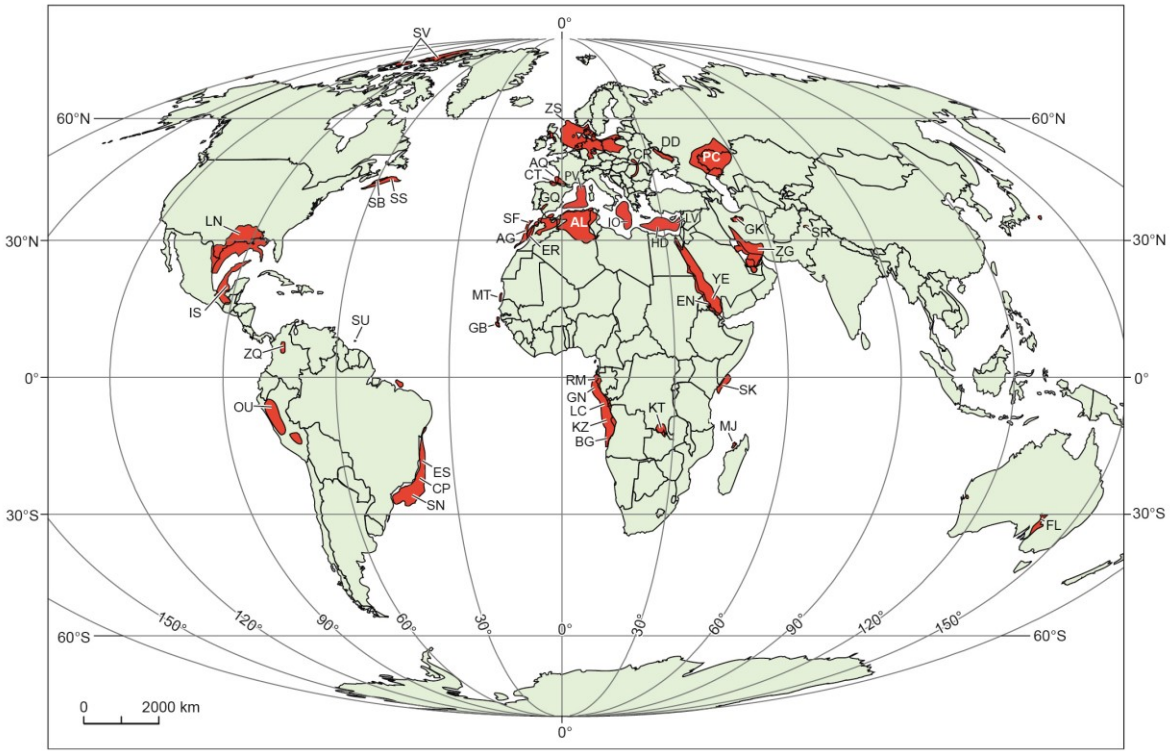

Figure 1.4 Distribution of major salt basins worldwide, highlighted in red. The age of salt and structural style varies widely among different basins. Basin abbreviations: AG = Agadir; AL = Atlas; AQ = Aquitaine; BG = Benguela–Namibe; CP = Campos; CR = Carpathian; CT = Cantabrian–West Pyrenees; DD = Dnieper–Donets; EN = Eritrean; ER = Essaouira; ES = Espírito Santo; FL = Flinders; GB = Guinea-Bissau; GK = Great Kavir–Garmsar–Qom; GN = Gabon; GQ = Guadalquivir; HD = Herodotus; IO = Ionian; IS = Isthmian; KT = Katanga; KZ = Kwanza; LC = Lower Congo; LN = Louann; LV = Levantine; MJ = Majunga; MT = Mauritania; OU = Oriente-Ucayali; PC = Precaspian; PV = Provencal; RM = Rio Muni; SB = Sable; SF = Safi; SK = Somali–Kenya; SN = Santos; SR = Salt Range; SS = Scotian Slope; SU = Suriname; SV = Sverdrup; YE = Yemeni; ZG = Zagros; ZQ = Zipaquira; ZS = Zechstein. Modified from Jackson and Hudec, 2017.

Figure 1.5 Man-made salt pans on the shores of the Dead Sea, Israel. Salt deposits are mined for commercial use.

1.1.2 Deformation

While salt had been recognised and utilised as a valuable commodity throughout much of human history, interest in salt tectonics did not start gathering momentum until the emergence of the petroleum industry (Jackson and Hudec, 2017). The 'Spindletop gusher', an oil well drilled into the top of a salt diapir in 1901 in Texas, showed just how important these salt structures could be and the huge volumes of hydrocarbons that they could hold (Owen, 1964). From that point onwards, the booming of the petroleum era brought technological advances that allowed geoscientists to explore the subsurface in ever-increasing detail. And with every advance in drilling and imaging technology, our understanding of these complex systems moved forward in leaps and bounds.

The unique property of salt that allows it to develop such a variety of structural styles is its ability to deform in a ductile manner at very low stress, and therefore behave as a fluid on geological timescales. This discovery was made remarkably early on, as the discordant contacts of onshore salt diapirs were mapped by perceptive structural geologists (Pošepný,

1871). Over the next few decades geologists scrambled to find the driving mechanism behind the apparent salt flow, and the concepts of tectonic compression and sedimentary downbuilding emerged as key drivers of salt flow in the 20th century (Barton, 1933; Stille, 1925). However, not all the ideas developed during this period stood the test of time. One of the major turning points in the history of salt tectonics was the realisation that salt tectonics is not, in fact, driven by buoyancy. The idea of buoyancy-driven deformation, likened to that of a lava lamp, was an early idea that surfaced in the 1930s and persisted into the 1980s (e.g. Fig. 1.6; Trusheim, 1960), until it was shown that salt is actually too dense to be buoyant

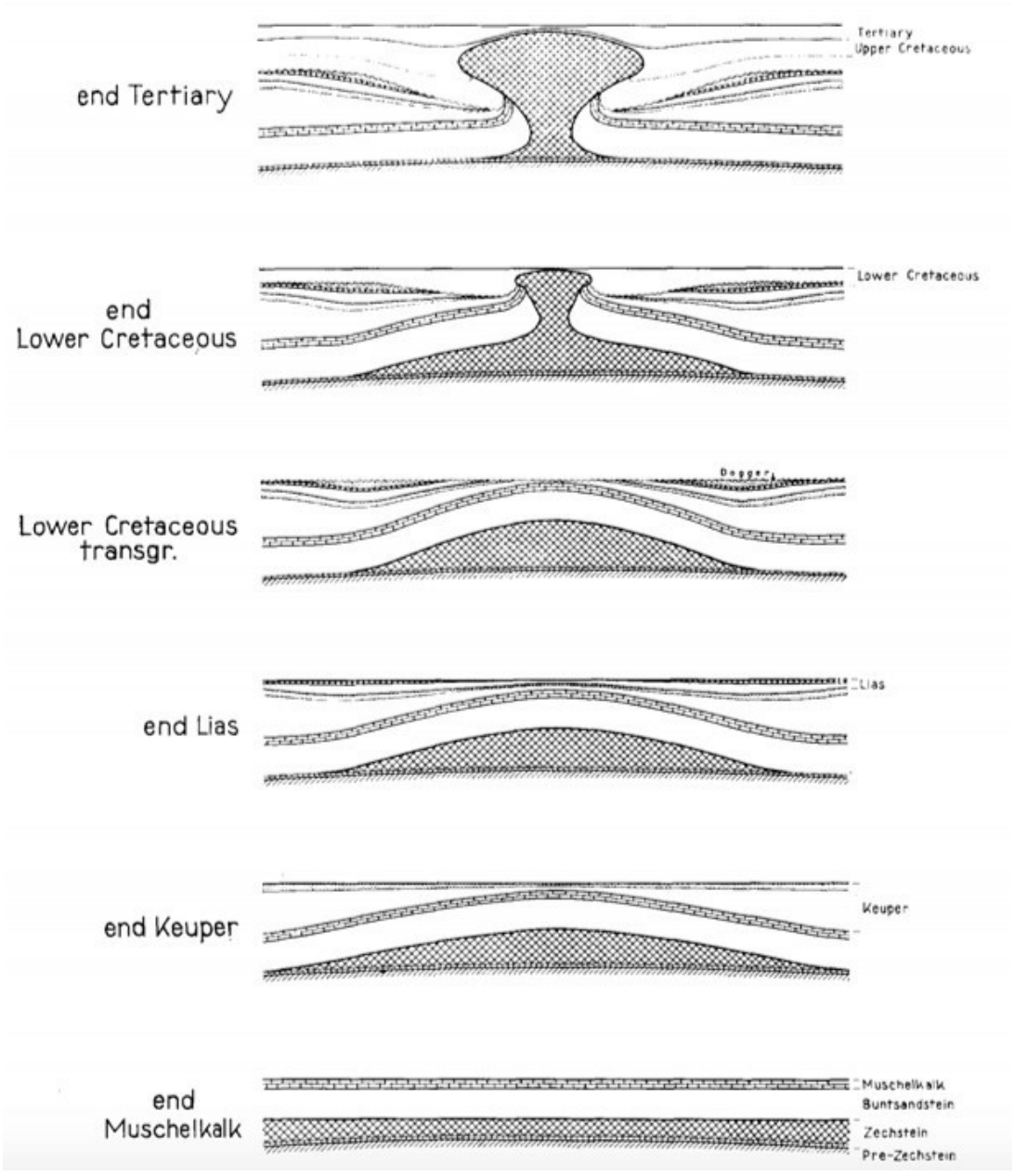

Figure 1.6 Model for diapir growth due to Rayleigh-Taylor instability. Dense sediments sinking into buoyant salt layer. From Trusheim, 1960.

during early sedimentation, and therefore that buoyancy could not be a key driving force (Baldwin and Butler, 1985; Nelson and Fairchild, 1989; Jackson, 1995). Despite being later disproven, the idea still persists in the minds of some to the present day, as I was surprised to discover when I gave a talk to a gathering of mostly retired geologists at the Hertfordshire Geological Society. At the end of the lecture an enthusiastic gentleman protested that I had 'failed to mention the fundamental driver' of salt tectonics, and I had to gently point out that this idea was a little outdated. Even some structural geology students unwittingly pick up these ideas when they take a shallow dive into some of the classic literature. I fell into this trap on a field course during my MSc in Petroleum Geoscience. Standing in the centre of an exposed diapir in the Paradox Basin, Utah, our lecturer asked the class to volunteer the driving force behind these monumental diapiric structures. I overzealously shouted 'Buoyancy!', only to sheepishly duck down behind the class as I realised my mistake.

That is not to say that buoyancy plays no role at all in salt tectonics, it certainly can influence more evolved salt tectonic systems, when actively rising diapirs uplift their overburden, but it is not a key driving force during the early stages of gravity-driven deformation (Hudec and Jackson, 2007). So if not buoyancy, what is the main driving force behind the wonderfully complex salt tectonic systems that we observe in nature? In modern salt tectonics, the evaporite unit is treated as a dense fluid, overlain by a brittle overburden (Weijermars, 1993). The salt sheet will flow in response to gravitational instability, primarily due to differential loading or differences in gravitational potential energy (Fig. 1.7).

Halite is a particularly weak rock type, under both extension and compression, and will flow in response to incredibly small applied stresses (Fig. 1.8; Weijermars et al., 1993; Jackson and Vendeville, 1994). The yield strength at which rock salt begins to creep is so low that it effectively has no strength (Fig. 1.8). Even at stress differences as low as 0.25 MPa, halite deforms by creep (Fossum and Fredrich, 2002). The rate may be so low that thousands or millions of years must pass before strain becomes evident, or it may be as fast as metres per year in extruding salt glaciers (Jackson and Hudec, 2017). Salt glaciers flow under their own weight, in the absence of additional tectonic forces, and can be observed even on human timescales. Unlithified clastic sediments may be weak at the surface, but after only 200-300 m of burial the compaction and cementation makes them stronger than salt (Fig. 1.8).

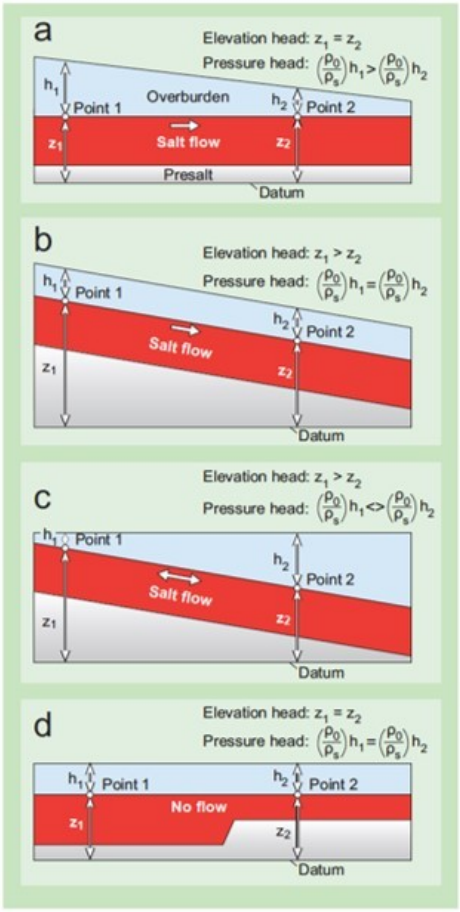

Figure 1.7 Examples of gravitationally stable and unstable configurations. (a) Salt flow driven by pressure head caused by weight of overburden. (b) Salt flow driven by an elevation head caused by margin tilt. (c) Direction of salt flow depends whether the elevation head gradient is more or less than the pressure head gradient. (d) No flow because the irregular base of salt does not create any hydraulic head gradient. From Jackson and Hudec, 2017.

The ductile behaviour of salt introduces extreme structural complexity to the basins in which it is deposited, but what are the mechanisms that allow salt to deform in this unique manner? Laboratory experiments have determined that under geological conditions, the three main microstructural processes in rock salt are: (i) microcracking and cataclastic flow, (ii) dislocation creep, and (iii) solution–precipitation creep (Fig. 1.9) (Heard, 1972; Wawersik and Zeuch, 1986; Urai et al., 1987; Carter et al., 1993; Schléder et al., 2007). The former - microcracking and cataclastic flow - are brittle, granular processes that dominate at low temperatures, low effective confining pressures, and high differential stresses, and therefore typically play only a minor role in natural salt flow (Fig. 1.9). The latter two are both types of 'creep', which describes the gradual flow of a crystalline material under a deviatoric load, leading to permanent deformation.

Dislocation creep is a form of crystal plasticity where grains are permitted to rotate and slide past one another along weakly bonded planes in the crystal lattice (Fig. 1.9). These crystallographic defects continuously heal and reform, allowing grain boundaries to migrate during ongoing deformation. The size of the subgrains is inversely proportional to the peak differential stress (Ter Heege et al., 2005). This means that where hand specimens of natural rock salt are available, the differential stress can be estimated from their average grain size. Typical values of differential stresses inside diapirs are estimated to be less than 2 MPa and rarely as much as 5 MPa (Spiers and Carter, 1998; Schléder and Urai, 2005, 2007; Schléder et al., 2007). Furthermore, the differential stresses calculated from subgrains are about twice as high in the crests of emergent diapirs as in the source layer of the same formation (Schoenherr et al. 2009).

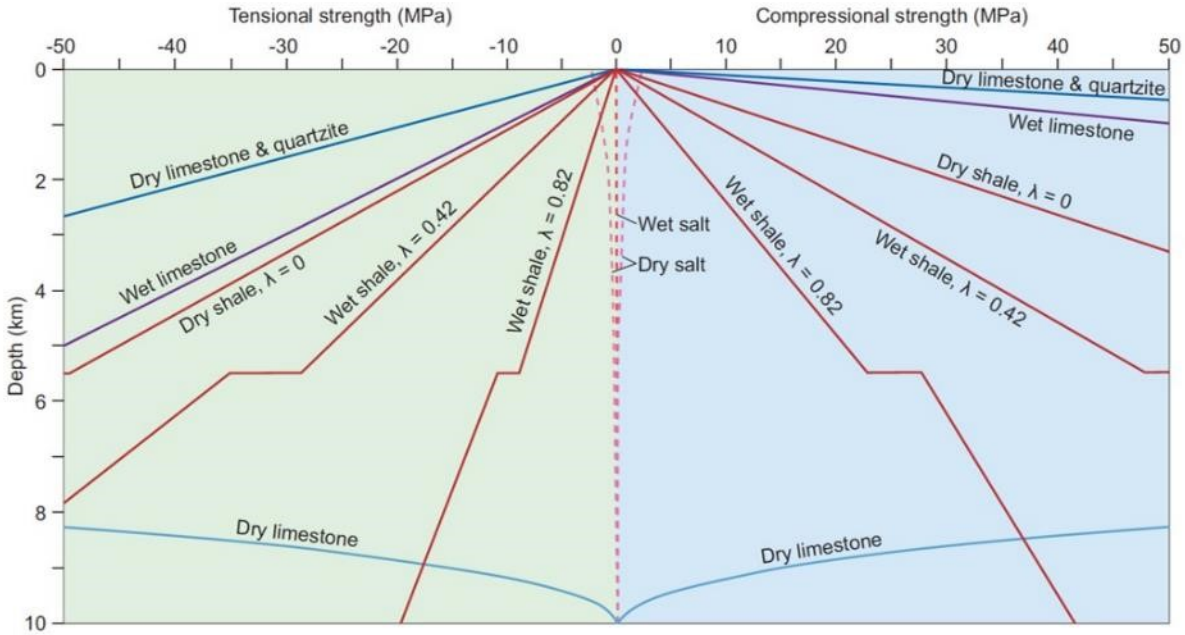

Figure 1.8 Salt is far weaker than the sedimentary rocks encasing it. Only unlithified clastics at shallow depths or lithified rocks buried to great depths can be weaker than salt. The creep strength of salt (dashed curves) is the deviatoric stress required to drive salt flow at a strain rate of 10–14/s. The strength of sedimentary rocks (solid curves) is higher in compression than in tension and increases with depth (as expressed by Byerlee's law). From Jackson and Hudec, 2017.

Solution-precipitation creep involves flow by pressure solution, where grain boundaries dissolve at points of high stress and precipitate at points of lower differential stress (Fig. 1.9). A thin fluid present along the grain boundaries facilitates the transport of ions. Unlike dislocation creep, in this case the grains change shape without internal strain. The microstructure changes little despite large ductile strains in the rock as a whole. In naturally deforming rock salt, dislocation creep and solution–precipitation creep work in parallel, with

precipitation from pressure solution filling gaps created by the sliding and rotating grains. The overall strain rate is therefore sum of the strain rates contributed by each type of creep.

Ductile salt sheets are typically encased within brittle clastic units. Deviatoric stresses in shallow crustal rocks cannot attain the magnitude required to activate flow by ductile creep because stress is first relieved by frictional slip (Goetze and Evans, 1979; Brace and Kohlstedt, 1980; Kusznir and Park, 1986; Ranalli and Murphy, 1987). Creep laws show that the brittle-ductile transition in a clastic overburden may be expected at depths between 7 and 9 km for a thermal gradient of 30 K/km and between 14 and 17 km for a thermal gradient of 15 K/km. The mechanical properties of salt are therefore unique in sedimentary basins.

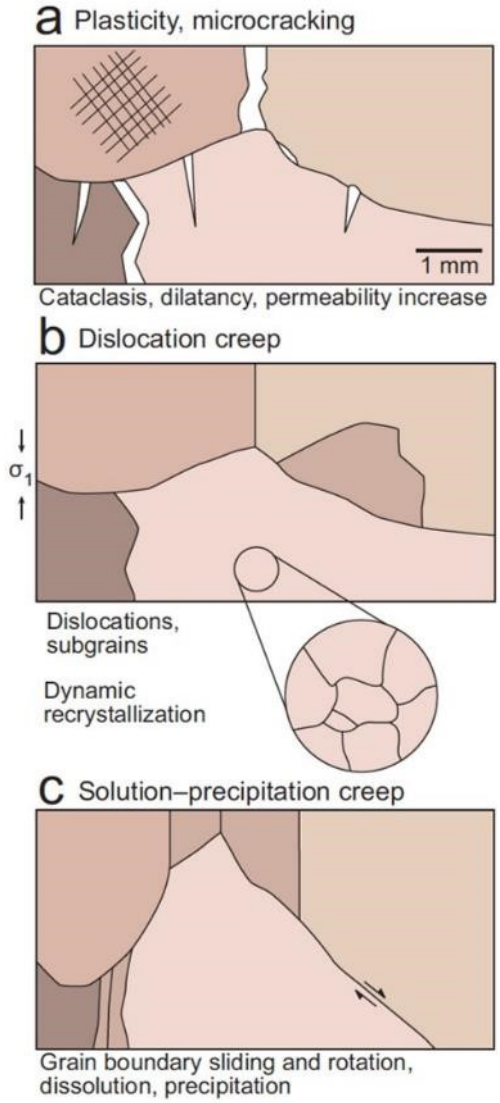

Figure 1.9 Three main types of microstructure and deformation mechanisms are known in rock salt deformed at temperatures of 20 to 200 °C: (a) microcracking, (b) dislocation creep, and (c) solution-precipitation creep. From Jackson and Hudec, 2017.

1.1.3 Diapirism

The complex interactions between salt flow, sedimentation and thick-skinned tectonics give rise to a wide range of structures observed in different salt basins around the world (Fig. 1.10; Hudec and Jackson, 2007). In an attempt to categorise the diversity of structures, the world of salt tectonics comes with a plethora of terminology: diapirs, pillows, teardrops, horns, flaps and turtles to name but a few. But with seismic data typically yielding little information within the salt body itself due to its characteristically chaotic appearance, it is the thicknesses, stratigraphic relationships and structures within the overburden that give clues as to how these structures have evolved through time.

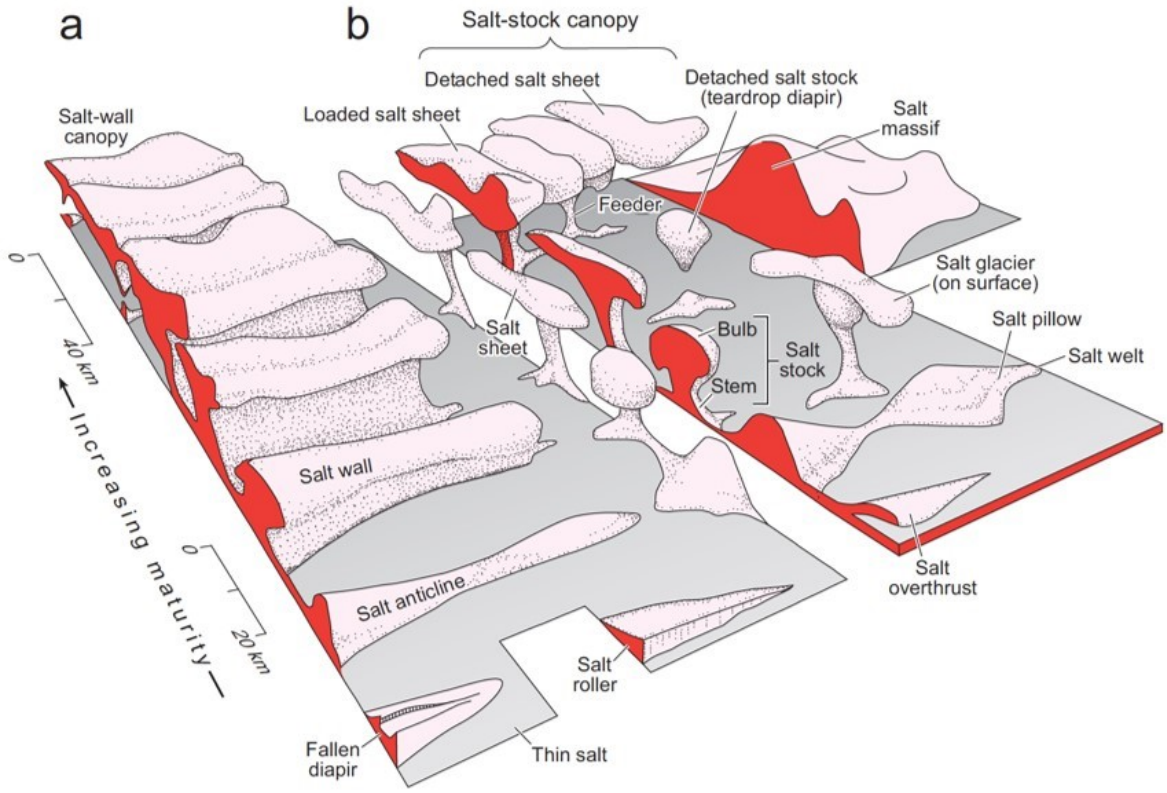

Figure 1.10 Examples of classic salt structure geometries and associated terminology. Names of salt structures are derived from cross-sectional shape and map geometry. From Jackson and Hudec, 2017.

Lateral variations in overburden thickness can record areas of relative subsidence and areas of relative uplift during halokinesis (Fig. 1.11). When salt deflation occurs (thinning by internal flow), the overburden subsides and creates more space for sediments, resulting in an isopach thick (Fig. 1.11). The salt evacuated from the subsiding areas usually supplies adjacent areas of salt inflation. The rising salt creates a local high which may be onlapped by sediments, resulting in an isopach thin (Fig. 1.11). In this way, growth strata within the different supra-

salt units record areas of relative subsidence or uplift through time. This sedimentary record is preserved long after the salt finally stops moving and is thus the most important tool for interpreting different phases of salt movement and structural development (Jackson and Hudec, 2017).

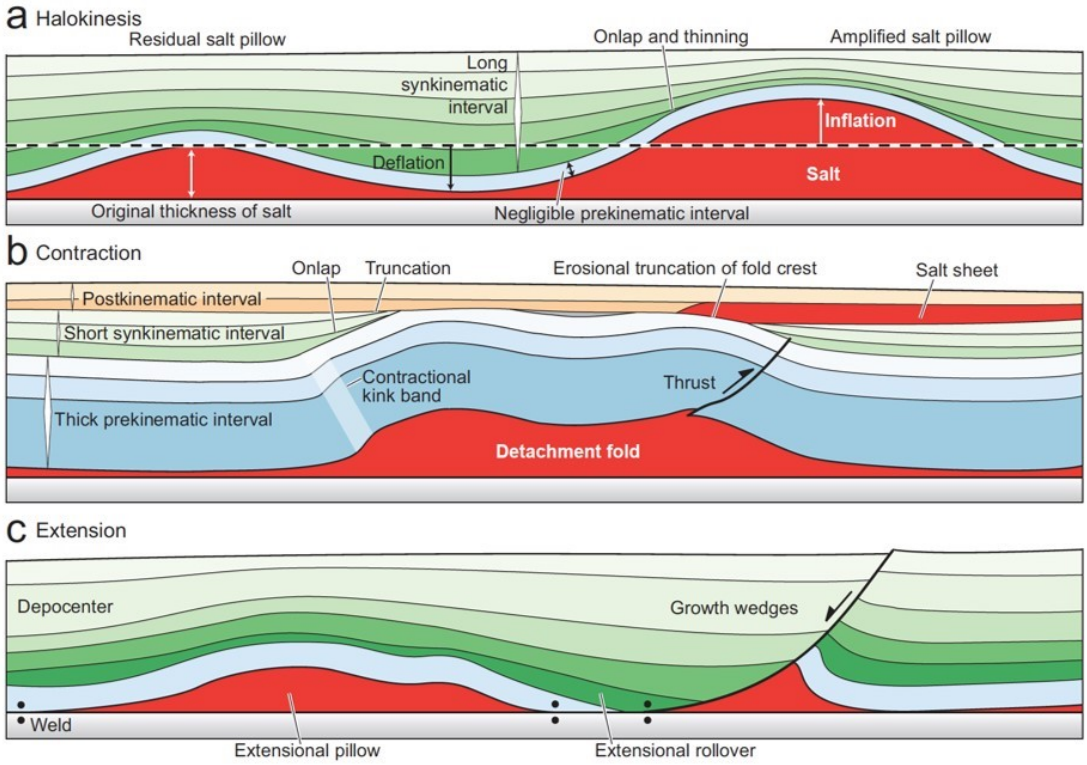

Figure 1.11 Features of salt pillows and salt anticlines formed by (a) halokinesis, (b) contraction, and (c) extension. Growth strata in the overburden show areas of relative growth versus subsidence, thereby recording the structural evolution. From Jackson and Hudec, 2017.

Analogue and numerical models have also played a pivotal role in advancing our understanding of how these complex structures develop. By the late 80's scaled physical models were widely used to understand the evolution of hydrocarbon traps in salt-influenced basins. They successfully reproduced many of the structural styles observed on seismic reflection profiles (e.g. Vendeville and Cobbold, 1988; Vendeville, 1988, 1989; Cobbold et al., 1989; Richard, 1991; Vendeville and Jackson, 1992a,b) and continue to provide further insights today (e.g. Dooley et al., 2017; Dooley and Hudec, 2017; Dooley et al., 2018; Ferrer et al., 2017a,b). Recently, computational advances have allowed for the development of complex numerical models to simulate salt tectonics systems (e.g. Daudre and Cloetingh, 1994; Albertz and Ings, 2012; Gradmann et al., 2012; Hamilton-Wright et al., 2019; Fernandez et al., 2020). Numerical models can be used to predict variables such as pore pressure which could not be reproduced by physical models. There are relative advantages and disadvantages

to both numerical and physical modelling, but both methods contribute valuable insight to our understanding of salt tectonic systems. I will consider the merits of physical modelling in more depth in Chapter 5.

1.2 Project Rationale

All these breakthroughs in our understanding of salt tectonic systems culminated in the publication of Jackson and Hudec's landmark 2017 publication; 'Salt Tectonics: Principles and Practice'. Often referred to as the 'bible of salt tectonics', this book conveniently sums up the state of play at the point of me commencing my PhD research. Having reached a broad community consensus on the triggers and drivers of salt tectonics, let's now look to where the gaps in our knowledge lie. And the more we learn, the more we realise we are only scratching the surface of the myriad of ways in which salt can influence sedimentary basin evolution. My PhD research has primarily focussed on two key themes of active interest within the salt tectonic community: base-salt relief and intrasalt heterogeneity. An in-depth introduction to each of these topics is given within the relevant chapters. Here I briefly introduce the key research questions to be investigated in this thesis.

1.2.1 Base-Salt Relief

There are two classic models for salt tectonics on passive margins: gravity gliding, where gravitational instability is induced by tilting of the margin, and gravity spreading, where gravitational instability is induced by differential loading (e.g. Schultz-Ela, 2001; Brun and Fort, 2011; Peel, 2014). These are two end-member scenarios, and in reality both gliding and spreading drive salt flow and overburden deformation, though the relative contribution from each may vary. For example, the Angolan margin is typically thought to be dominated by gravity gliding, while the Gulf of Mexico is said to be dominated by gravity spreading (Schultz-Ela, 2001). Natural salt basins can sit anywhere on this spectrum, depending on the local geological setting. Both of these models tend to envisage a perfectly smooth base of salt, gently dipping towards the centre of the basin (Fig. 1.12; Brun and Fort, 2011). In reality, such smooth surfaces are rare in nature, and while the simplified models correctly explain the presence of large-scale, kinematically-linked extensional and contractional domains, they do

not adequately predict the wide variety of structural styles observed on many passive margins.

Since salt is often deposited shortly after rifting, the base-salt surface is commonly rugose with syn-rift fault scarps (Fig. 1.13). Folds, thrusts and erosional features such as canyons can also create a rugose surface upon which evaporites are deposited. As it is deposited the salt will bury existing relief on the surface, thinning over topographic highs and thickening into topographic lows (Fig. 1.13). When gravitational instability is induced, the salt has to flow over the rugose surface toward the basin centre. Like water flowing across a bumpy surface, it follows that salt flow is also affected by the geometry of the surface that it flows across.

Some early studies recognised this and used physical models to explain some of the observed structural complexity in certain basins (e.g. Cobbold and Szatmari, 1991; Reis et al., 2008), but they were often limited by poor depth imaging of the base-salt. In recent years improved seismic imaging of sub-salt geometries has led to an increasing number of natural examples showing the profound impact that base-salt relief can have on the structural evolution of a salt tectonic system (e.g. Dooley and Hudec, 2017; Pichel et al., 2019a,b), suggesting that this may in fact be the norm rather than the exception. There are, however, still many basins where this relationship has not been explicitly studied, and the mechanisms controlling the interaction between supra-salt structure and base-salt relief are still largely unconstrained. The previous literature on this topic will be summarised in Chapter 2.

- **KEY QUESTION**: How does salt flow interact with base-salt relief and how does this affect the structural and stratigraphic development of the overburden?

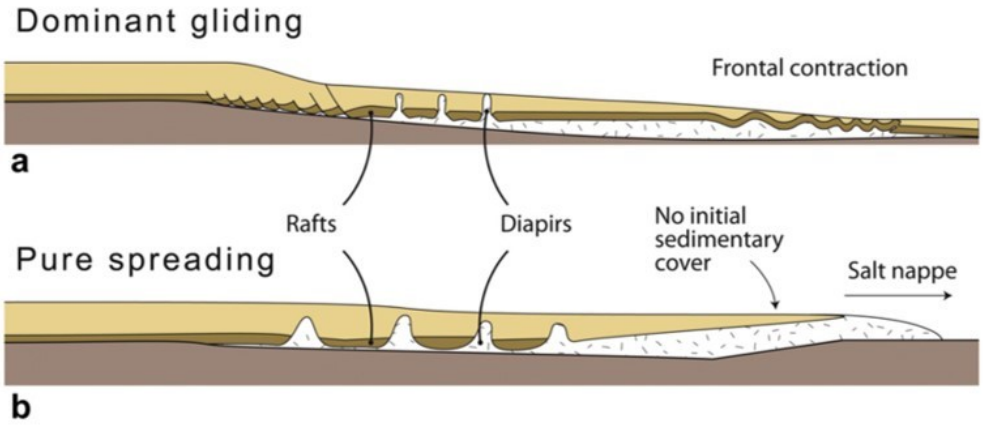

Figure 1.12 Classic end-member models of gravity-driven salt tectonics. Gravity gliding is driven by tilting of the base-salt surface (a) and gravity spreading is driven by sedimentary loading (b). In nature both gliding and spreading drive salt deformation but the relative contribution varies. In both models the base-salt surface is smooth. From Brun and Fort, 2011.

1.2.2 Intrasalt Heterogeneity

Historically salt has been treated largely as a homogeneous substance, composed of pure halite. This is primarily due to the fact that the key tool we use to study subsurface salt structures is seismic data, where salt is typically characterised by an internally chaotic and transparent seismic facies (Jones and Davison, 2014). Traditionally, focus has therefore been on the overlying stratigraphic record to reconstruct the development of salt structures, with relatively little consideration given to the internal mechanics of the salt bodies themselves.

However, we know from exposures of salt in mines (Fig. 1.14) (e.g. Balk, 1949; Hoy et al., 1962; Kupfer, 1962; Miralles et al., 2001; Schleder et al., 2008; Burliga et al., 2018) and in the field (e.g. Zak and Freund, 1980; Jackson et al., 1990; Talbot, 1998), as well as geophysical subsurface data (e.g. Van Gent et al., 2011; Strozyk et al., 2012; Raith et al., 2016), that most evaporitic sequences are actually lithologically heterogeneous. Due to temporal changes in the depositional environment, halite can be interbedded with other evaporitic minerals, and salt deposition can also be interrupted by phases of clastic deposition, or even intruded by volcanics in some basins (Fig. 1.13). Spatial changes in the depositional environment can also lead to proximal-to-distal changes in the composition of the units across the basin (Fig. 1.13). The interplay between the chemistry of the brine, organic productivity, and clastic input to the basin can result in lateral and vertical facies variations within the heterogeneous evaporite sequence.

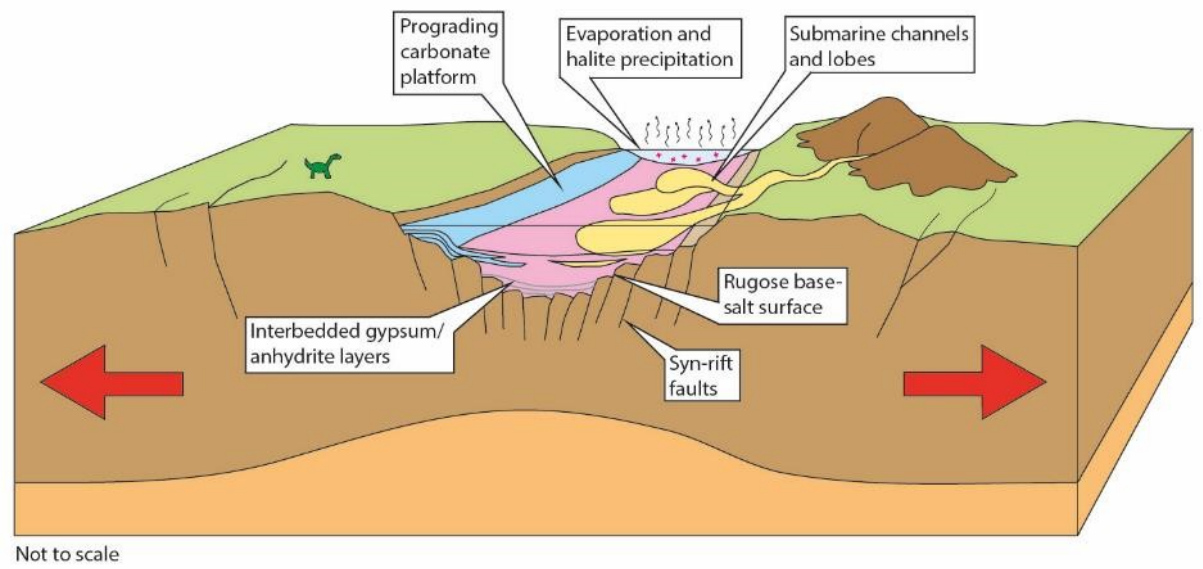

Figure 1.13 Conceptual schematic diagram showing heterogeneous salt deposition in a rift basin. Salt infills relict syn-rift bathymetry on the basin floor, and lateral facies variations occur across the basin due to changes in the depositional environment.

Different lithologies have different rheologies, and as such it follows that the rheological properties of the evaporitic sequence will affect how the salt sheet responds to applied tectonic stresses (Rowan et al., 2019). While halite-rich units may flow readily in response to small differential stresses, the stronger and more brittle units interbedded within the sequence may resist deformation. This would control the structural development of the salt and its overburden. In recent years several studies have suggested a link between the heterogeneity of the evaporite sequence and the structural and stratigraphic evolution of the overburden (e.g. Gradmann and Beaumont, 2012; Raith et al., 2016; Rowan et al., 2019). However, the way in which this heterogeneity affects the overall deformation of the salt and evolution of the basin remains poorly understood. This topic will be explored in greater depth in Chapter 3.

- **KEY QUESTION**: How does lithological heterogeneity within the evaporite sequence affect the way in which strain is partitioned within the salt sheet, and does this affect the structural and stratigraphic development of the overburden?

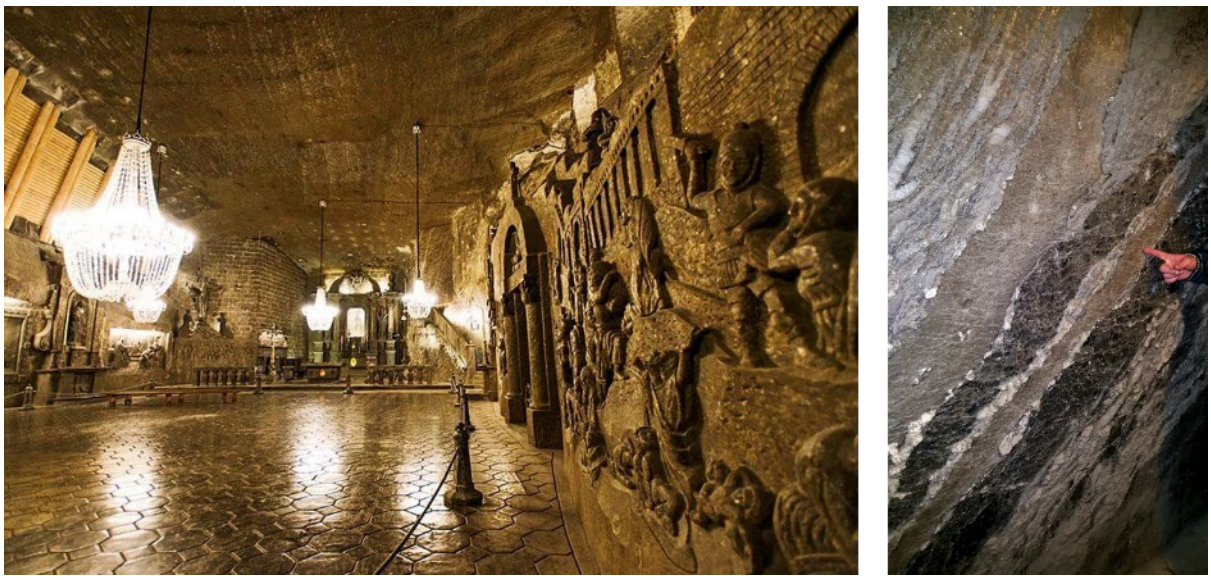

Figure 1.14 Heterogeneous salt deposits exposed in walls of the Wieliczka salt mine, near Krakow, Poland.

1.3 Seismic Datasets

The overarching aim of this research is to fill gaps in our knowledge concerning the effects of base-salt relief and intrasalt heterogeneity on the evolution of the salt and overburden. To address this I interpreted two high resolution 3D seismic datasets from different study areas that enabled me to analyse subsurface stratigraphy and structure. Here I introduce the two areas in which the datasets are located, and explain why they were selected for these studies: the Kwanza Basin offshore Angola, and the Levantine Basin in the Eastern Mediterranean. To avoid repetition, further geological context is provided within the relevant chapters.

1.3.1 Kwanza Basin, offshore Angola, West African Margin

The first dataset is located in the Kwanza Basin, offshore Angola, on the West African passive margin (Fig. 1.15). The Kwanza Basin is densely covered with 2D and 3D seismic data thanks to its history of petroleum exploration. There are several producing fields within the pre-salt strata, with the impermeable salt layer acting as the seal, including the Cameia Field which is situated within the dataset used in this study (Cazier et al., 2014).

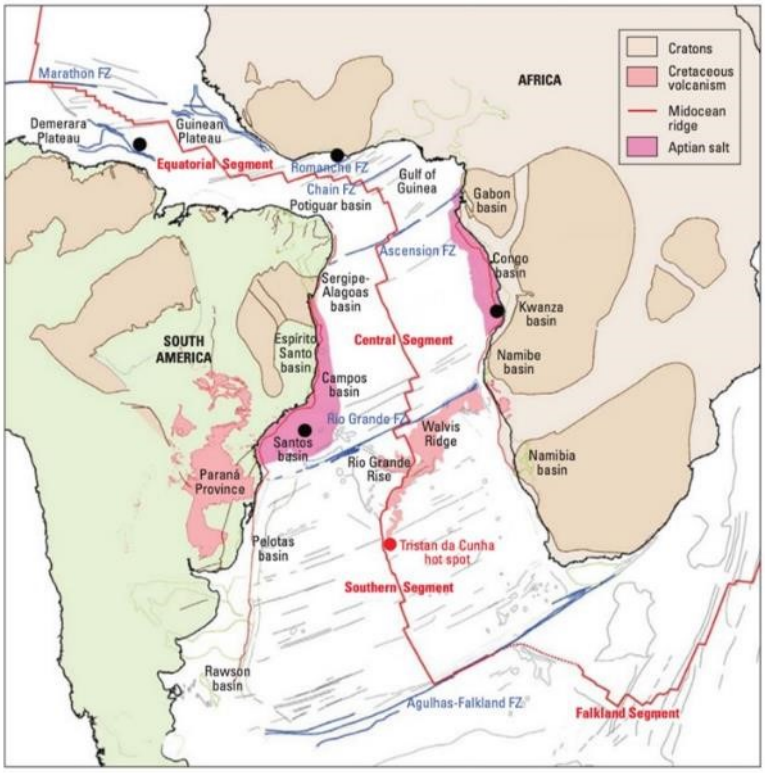

Figure 1.15 Tectonic reconstruction of the South Atlantic Ocean at 84Ma showing the regional setting of the Kwanza Basin and distribution of the Aptian salt. Black dots show locations of significant hydrocarbon discoveries: Tupi offshore Brazil, Cameia offshore Angola, Jubilee offshore Ghana, and Zaedyus offshore French Guiana. From Bryant et al., 2012.

The salt on the West African margin is Aptian (125 to 112 Ma) and was deposited shortly after the initial opening of the South Atlantic Ocean, as the continents of South America and Africa began to separate during the breakup of the Gondwana supercontinent (Bryant et al., 2012). The deposition of salt immediately follows an anomalous syn-rift sag phase which created significant accommodation in the basin (Karner and Gamboa, 2007). As the oceanic spreading system developed, the salt deposits were divided, resulting in salt of the same age located on the conjugate margin offshore Brazil in the Campos and Santos Basins (Fig. 1.15). The post-Aptian strata, both offshore Angola and offshore Brazil, are highly deformed and characterised by mature and complex diapiric salt structures, some of which are active to the present day.

The Kwanza Basin has been the focus of many salt tectonic studies over the past few decades, and is considered the type locality for structures such as rafts, turtles and ramp syncline basins (e.g. Duval et al., 1992; Lundin, 1992; Spathopoulos, 1996; Cramez and Jackson, 2000; Marton et al., 2000; Hudec and Jackson, 2002; Hudec and Jackson, 2004; Fort et al., 2004; Jackson and Hudec, 2005; Quirk et al., 2012). These studies have characterised the extensional and contractional domains, debated the relative contribution of gravity gliding vs. spreading, and estimated the rate and magnitude of basinward translation. The regional-scale salt tectonic system is therefore reasonably well understood.

The 3D depth-converted dataset used in our research covers a relatively small portion of the central margin, in an area where the base-salt is characterised by a number of large steps on the base-salt surface, presumed to be relict fault scarps inherited from the rifting phase (Hudec and Jackson, 2004). This dataset images one of those large steps and the associated supra-salt structures, therefore facilitating a 3D kinematic analysis of the salt and overburden evolution in an area where there is significant relief on the base-salt surface. The focus in this case is on understanding the detailed kinematic development of a small area and its relation to the base-salt step, in contrast to previous studies that often used only 2D data and/or focussed on characterising the broader margin-scale kinematics (e.g. Duval et al., 1992; Lundin, 1992; Spathopoulos, 1996; Cramez and Jackson, 2000; Marton et al., 2000; Hudec and Jackson, 2002; Hudec and Jackson, 2004; Fort et al., 2004; Jackson and Hudec, 2005; Quirk et al., 2012).

1.3.2 Levantine Basin, offshore Lebanon, Eastern Mediterranean

The second dataset used in this research lies in the Levantine Basin, on the Levant Margin offshore Lebanon in the Eastern Mediterranean (Fig. 1.16). Unlike the legacy of exploration offshore West Africa, the petroleum exploration potential of the Eastern Mediterranean was overlooked for many decades until dwindling resources in more prolific basins persuaded explorers to reconsider other basins. This means that until recently the area was relatively data-poor. Acquisition of new seismic datasets and application of new technologies, as well as improving geopolitical circumstances and opening of new licence rounds, has led to recent discoveries in several areas including offshore Egypt, Cyprus, Israel, Turkey and Greece (Esestime et al., 2016; Cozzi et al., 2018). It is particularly important in the current circumstances for explorers to understand the potential impact of the salt in terms of imaging, drilling and prospect derisking. This gives me an opportunity to not only study the salt tectonic deformation for academic purposes, but to also consider the implications of my work for the energy industry.

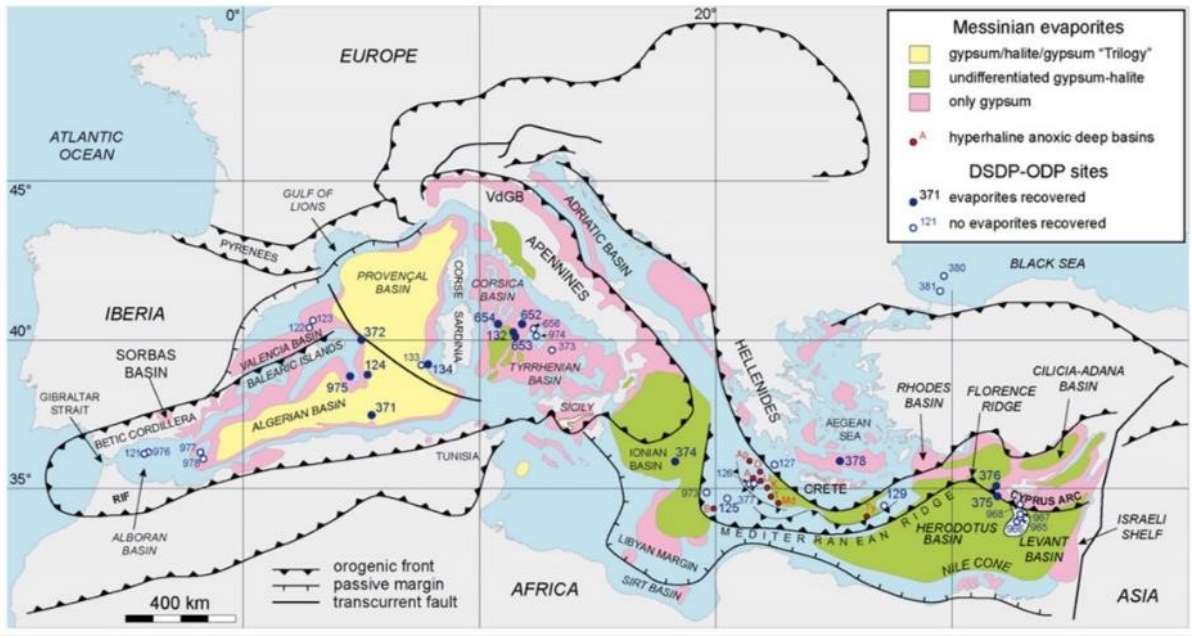

Figure 1.16 Tectonic setting of the present Mediterranean Basin showing distribution of the Messinian evaporites and connection to the Atlantic via the Gibraltar Strait. The Messinian in the western Mediterranean basins differs compositionally from basins in the eastern Mediterranean. From Roveri et al., 2014.

The Messinian salt sheet covers a large area of the Mediterranean Basin and is the youngest salt giant in the world (5.97 to 5.33 Ma) (Fig. 1.16; Roveri et al., 2014). It was deposited during the infamous Messinian Salinity Crisis (MSC), when the connection between the Mediterranean and the Atlantic Ocean via the Gibraltar Strait was cut off (or severely

restricted), resulting in sea level drawdown and extensive evaporite precipitation (Roveri et al., 2014). The magnitude of sea level drawdown during the MSC has been a topic of heated debate among researchers for many decades (e.g. Roveri et al., 2014; Camerlenghi and Aloisi, 2020), with some estimates as low as 50 m and others greater than 2 km (Ryan, 1976; Clauzon et al., 1996; Gargani and Rigollet, 2007; Bartol and Govers, 2009; Urgeles et al., 2011; Al-Balushi et al., 2016). The seismic facies of the Messinian in the western Mediterranean basins differs from that in the eastern Mediterranean, indicating lateral changes in the depositional environment and possibly poor connectivity during the MSC (Fig. 1.16) (Camerlenghi et al., 2020). The Zanclean flood marked the reopening of the Gibraltar Strait and a clastic overburden was subsequently deposited above the salt.

Thanks to its comparatively young age, the Messinian salt is much shallower and much less deformed than the Aptian salt in the Kwanza Basin. It is therefore well-imaged by seismic data, and has garnered much interest from the salt tectonic community in particular due to its internal reflectivity imaged in seismic data (e.g. Netzeband et al., 2006; Lofi et al., 2011; Gvirtzman et al., 2013; Feng et al., 2016; Camerlenghi et al., 2020). The internal reflectivity, which indicates lithological heterogeneity within the evaporite sequence, is relatively unusual due to limitations in seismic imaging associated with mature salt structures and their intense internal deformation (Jones and Davison, 2014). These internal reflections can be used as strain markers and provide rare insights into the internal flow mechanics within a deforming sheet (e.g. Cartwright et al., 2012).

Both the Kwanza Basin and the Levantine Basin datasets are located on passive margins, but the tectonic setting of the Levant Margin differs from the West African margin in several important ways. The Kwanza Basin lies on a stable passive margin far from any major plate boundaries and is characterised by limited tectonic activity, whereas the Eastern Mediterranean region is geodynamically complex and characterised by abundant seismicity (Fig. 1.16). The Levantine Basin is currently under active compression due to the northward migration of the African plate and subduction under the stable Eurasian plate, creating the Mediterranean Ridge and Cyprus Arc to the north of basin (Fig. 1.16). Furthermore, the Eratosthenes Seamount, a large continental block, bounds the basin to the west, separating it from the Herodotus Basin (Fig. 1.16). An active transpressional fault network lies onshore to the east through Lebanon and Israel, and the Nile delta progrades into the basin from the

South (Fig. 1.16). The young Messinian salt sheet is therefore influenced by a multitude of tectonic drivers.

The 3D dataset on the Levant Margin therefore provides an ideal natural laboratory to investigate early stage deformation of a heterogeneous salt sheet during gravity gliding, without having to deconvolve later tectonic overprinting. Whereas most previous studies in this area have focussed on the southern Levantine Basin, offshore Israel and the circum-Nile deformation belt, the northern Levant Margin has been relatively under-studied due to restrictions on data availability. In this research I use a recently acquired and previously confidential dataset to test existing hypotheses and identify new controls on salt flow and supra-salt structure.

1.4 Thesis Structure

The following chapters of the thesis are structured as follows:

- Chapter 2: The first study investigates the impact of salt flow over base-salt relief in the Kwanza Basin, offshore Angola, where large ramps on the base-salt surface appear to have played a key role in determining the structural development of the salt and overburden.
- Chapter 3: The second study takes us to the Levantine Basin, eastern Mediterranean, where rare intrasalt reflectors provide some insight into the internal mechanics of salt deformation.
- Chapter 4: Staying in the Levantine Basin, the third study explores the stratigraphic record of salt-detached basinward translation provided by ramp syncline basins, and implications for salt flow interaction with large base-salt anticlines.
- Chapter 5: The final study presents initial results of analogue modelling to consolidate our interpretations of the seismic data and examine the role of base-salt relief and intrasalt heterogeneity under controlled boundary conditions.
- Chapter 6: The discussion section allows me to integrate the findings of these studies and critically evaluate the importance of base-salt relief and intrasalt heterogeneity in complex salt tectonic systems.

Enjoy.

References

Al-Balushi, A.N., Neumaier, M., Fraser, A.J. and Jackson, C.A., 2016. The impact of the Messinian salinity crisis on the petroleum system of the Eastern Mediterranean: a critical assessment using 2D petroleum system modelling. Petroleum Geoscience, 22(4), pp.357-379.

Albertz, M. and Ings, S.J., 2012. Some consequences of mechanical stratification in basin-scale numerical models of passive-margin salt tectonics. Geological Society, London, Special Publications, 363(1), pp.303-330.Baldwin, B., Butler, C.O., 1985. Compaction curves. AAPG Bulletin 69, 622–626.

Balk, R. 1949. Structure of Grand Saline salt dome. AAPG Bulletin, 33, 1791–1829.

Bartol, J. and Govers, R., 2009. Flexure due to the Messinian-Pontian sea level drop in the Black Sea. Geochemistry, Geophysics, Geosystems, 10(10).

Barton, D.C., 1933. Mechanics of formation of salt domes with special reference to Gulf Coast salt domes of Texas and Louisiana. AAPG Bulletin, 17(9), pp.1025-1083.

Borchert, H. and Muir, R.O., 1964. Salt deposits: the origin, metamorphism and deformation of evaporites. Van Nostrand Ltd., London.

Brace, W.F. and Kohlstedt, D.L., 1980. Limits on lithospheric stress imposed by laboratory experiments. Journal of Geophysical Research: Solid Earth, 85(B11), pp.6248-6252.

Brun, J.P. and Fort, X., 2011. Salt tectonics at passive margins: Geology versus models. Marine and Petroleum Geology, 28(6), pp.1123-1145.

Bryant, I., Herbst, N., Dailly, P., Dribus, J.R., Fainstein, R., Harvey, N., McCoss, A., Montaron, B., Quirk, D. and Tapponnier, P., 2012. Basin to basin: Plate tectonics in exploration. Oilfield Review, 24(3), pp.38-57.

Burliga, S., P. Krzywiec, K. Dąbroś, J. Przybyło, E. Włodarczyk, M. Źróbek and M. Słotwiński. 2018. Salt tectonics in front of the Outer Carpathian thrust wedge in the Wieliczka area (S Poland) and its exposure in the underground salt mine: Geology, Geophysics & Environment, v. 44, p. 71-90.

Camerlenghi, A. and Aloisi, V., 2020. Uncovering the Mediterranean Salt Giant (MEDSALT)-Scientific Networking as Incubator of Cross-disciplinary Research in Earth Sciences. European Review, 28(1), pp.40-61.

Camerlenghi, A., Del Ben, A., Hübscher, C., Forlin, E., Geletti, R., Brancatelli, G., Micallef, A., Saule, M. and Facchin, L., 2020. Seismic markers of the Messinian salinity crisis in the deep Ionian Basin. Basin Research, 32(4), pp.716-738.

Carpenter, A.B., 1978, January. Origin and chemical evolution of brines in sedimentary basins. In SPE Annual Fall Technical Conference and Exhibition. Society of Petroleum Engineers.

Carter, N.L., Horseman, S.T., Russell, J.E. and Handin, J., 1993. Rheology of rocksalt. Journal of Structural Geology, 15(9-10), pp.1257-1271.

Cartwright, J., Jackson, M., Dooley, T. and Higgins, S., 2012. Strain partitioning in gravity-driven shortening of a thick, multilayered evaporite sequence. Geological Society, London, Special Publications, 363(1), pp.449-470.

Cazier, E.C., Bargas, C., Buambua, L., Cardoso, S., Ferreira, H., Inman, K., Lopes, A., Nicholson, T., Olson, C., Saller, A. and Shinol, J., 2014, September. Petroleum geology of Cameia field, deepwater pre-salt Kwanza basin, Angola, West Africa. In AAPG International Conference and Exhibition. Istanbul, Turkey, September (pp. 14-17).

Clauzon, G., Suc, J.P., Gautier, F., Berger, A. and Loutre, M.F., 1996. Alternate interpretation of the Messinian salinity crisis: controversy resolved?. Geology, 24(4), pp.363-366.

Cobbold, P.E.T.E.R., Rossello, E. and Vendeville, B., 1989. Some experiments on interacting sedimentation and deformation above salt horizons. Bulletin de la Société Géologique de France, (3), pp.453-460.

Cobbold, P.R. and Szatmari, P., 1991. Radial gravitational gliding on passive margins. Tectonophysics, 188(3-4), pp.249-289.

Cozzi, A., Cascone, A., Bertelli, L., Bertello, F., Brandolese, S., Minervini, M., Ronchi, P., Ruspi, R. and Harby, H., 2018. Zohr giant gas discovery: A paradigm shift in Nile Delta and East Mediterranean exploration. Search and Discovery, 20414.

Cramez, C. and Jackson, M.P.A., 2000. Superposed deformation straddling the continental-oceanic transition in deep-water Angola. Marine and Petroleum Geology, 17(10), pp.1095-1109.

Daudré, B. and Cloetingh, S.A.P.L., 1994. Numerical modelling of salt diapirism: influence of the tectonic regime. Tectonophysics, 240(1-4), pp.59-79.

Dooley, T.P., Hudec, M.R., Carruthers, D., Jackson, M.P. and Luo, G., 2017. The effects of base-salt relief on salt flow and suprasalt deformation patterns—Part 1: Flow across simple steps in the base of salt. Interpretation, 5(1), pp.SD1-SD23.

Dooley, T.P. and Hudec, M.R., 2017. The effects of base-salt relief on salt flow and suprasalt deformation patterns—Part 2: Application to the eastern Gulf of Mexico. Interpretation, 5(1), pp.SD25-SD38.

Dooley, T.P., Hudec, M.R., Pichel, L.M. and Jackson, M.P., 2018. The impact of base-salt relief on salt flow and suprasalt deformation patterns at the autochthonous, paraautochthonous and allochthonous level: insights from physical models. Geological Society, London, Special Publications, 476(1), pp.287-315.

Duval, B., Cramez, C. and Jackson, M. P. A., 1992. Raft tectonics in the Kwanza Basin, Angola. Marine and petroleum geology, 9(4), pp.389-404.

Esestime, P., Hewitt, A. and Hodgson, N., 2016. Zohr–a newborn carbonate play in the Levantine Basin, East-Mediterranean. First Break, 34(2).

Feng, Y. E., A. Yankelzon, J. Steinberg, and M. Reshef, 2016, Lithology and characteristics of the Messinian evaporite sequence of the deep Levant Basin, eastern Mediterranean: Marine Geology, 376, 118-131.

Fernandez, N., Hudec, M.R., Jackson, C.A.L., Dooley, T.P. and Duffy, O.B., 2020. The competition for salt and kinematic interactions between minibasins during density-driven subsidence: observations from numerical models. Petroleum Geoscience, 26(1), pp.3-15.

Ferrer, O., Dooley, T.P., Corti, G., Vidal-Royo, O., Hearon IV, T.E., Reber, J. and Graveleau, F., 2017a. Introduction to special section: Analog modeling as an aid to structural interpretation.

Ferrer, O., Gratacós, O., Roca, E. and Muñoz, J.A., 2017b. Modeling the interaction between presalt seamounts and gravitational failure in salt-bearing passive margins: The Messinian case in the northwestern Mediterranean Basin. Interpretation, 5(1), pp.SD99-SD117.

Fort, X., Brun, J.P. and Chauvel, F., 2004. Salt tectonics on the Angolan margin, synsedimentary deformation processes. Aapg Bulletin, 88(11), pp.1523-1544.

Fossum, A. F., and J. T. Fredrich, 2002, Salt mechanics primer for near-salt and sub-salt deepwater Gulf of Mexico field developments: Albuquerque, NM, Sandia National Laboratories, report SAND2002-2063, 67 p.

Gargani, J. and Rigollet, C., 2007. Mediterranean Sea level variations during the Messinian salinity crisis. Geophysical Research Letters, 34(10).

Goetze, C. and Evans, B., 1979. Stress and temperature in the bending lithosphere as constrained by experimental rock mechanics. Geophysical Journal International, 59(3), pp.463-478.

Gradmann, S. and Beaumont, C., 2012. Coupled fluid flow and sediment deformation in margin-scale salt-tectonic systems: 2. Layered sediment models and application to the northwestern Gulf of Mexico. Tectonics, 31(4).

Gradmann, S., Beaumont, C. and Ings, S.J., 2012. Coupled fluid flow and sediment deformation in margin-scale salt-tectonic systems: 1. Development and application of simple, single-lithology models. Tectonics, 31(4).

Gvirtzman, Z., M. Reshef, O. Buch-Leviatan and Z. Ben-Avraham, 2013, Intense salt deformation in the Levant Basin in the middle of the Messinian salinity crisis: Earth and Planetary Science Letters, 379, 108–119.

Hamilton-Wright, J., Dee, S., von Nicolai, C. and Johnson, H., 2019. Investigating controls on salt movement in extensional settings using finite-element modelling. Petroleum Geoscience, 25(3), pp.258-271.

Heard, H.C., 1972. Steady-state flow in polycrystalline halite at pressure of 2 kilobars. GMS, 16, pp.191-209.

Holser, W.T. and Burns, R.G., 1979. Marine minerals. Reviews in Mineralogy, Mineralogical Society of America, 6, pp.230-239.

Hoy, R. B., Foose,R.M. and O'Neill, B. J. 1962. Structure of Winnfield salt diapir. AAPG Bulletin, 46, 1444–1459.

Hudec, M.R. and Jackson, M.P., 2002. Structural segmentation, inversion, and salt tectonics on a passive margin: Evolution of the Inner Kwanza Basin, Angola. Geological Society of America Bulletin, 114(10), pp.1222-1244.

Hudec, M.R. and Jackson, M.P. A., 2004. Regional restoration across the Kwanza Basin, Angola: Salt tectonics triggered by repeated uplift of a metastable passive margin. AAPG bulletin, 88(7), pp.971-990.

Hudec, M.R. and Jackson, M.P. A., 2007. Terra infirma: Understanding salt tectonics. Earth-Science Reviews, 82(1-2), pp.1-28.

Jackson, M. P. A., 1995. Retrospective salt tectonics. In: Jackson, M.P.A., Roberts, D.G., Snelson, S. (Eds.), Salt Tectonics: a Global Perspective. AAPG Memoir, vol. 65, pp. 1–28.

Jackson, M. P. A., Cornelius, R. R., Craig, C. H., Gansser, A., Stocklin, J. and Talbot, C. J., 1990. Salt Diapirs of the Great Kavir. Geological Society of America, Boulder, Memoir, 177.

Jackson, M. P. A. and Hudec, M.R., 2005. Stratigraphic record of translation down ramps in a passive-margin salt detachment. Journal of Structural Geology, 27(5), pp.889-911.

Jackson, M. P. A. and Hudec, M.R., 2017. Salt tectonics: Principles and practice. Cambridge University Press.

Jackson, M. P. A. and Talbot, C.J., 1986. External shapes, strain rates, and dynamics of salt structures. Geological Society of America Bulletin, 97(3), pp.305-323.

Jackson, M. P. A. and B. C. Vendeville, 1994. Regional extension as a geologic trigger for diapirism: Geological Society of America Bulletin, 106, 57–73.

Jones, I.F. and Davison, I., 2014. Seismic imaging in and around salt bodies. Interpretation, 2(4), pp.SL1-SL20.

Karner, G.D. and Gambôa, L.A.P., 2007. Timing and origin of the South Atlantic pre-salt sag basins and their capping evaporites. Geological Society, London, Special Publications, 285(1), pp.15-35.

Kupfer, D. H. 1962. Structure of Morton salt company mine, Weeks Island salt dome. AAPG Bulletin, 46, 1460–1467.

Kusznir, N.J. and Park, R.G., 1986. Continental lithosphere strength: the critical role of lower crustal deformation. Geological Society, London, Special Publications, 24(1), pp.79-93.

Lofi, J., Déverchère, J., Gaullier, V., Gillet, H., Gorini, C., Guennoc, P., Loncke, L., Maillard, A., Sage, F. and Thinon, I., 2011. Seismic atlas of the Messinian Salinity Crisis markers in the Mediterranean and Black Seas (Vol. 179, pp. 1-72). Société Géologique de France.

Lundin, E.R., 1992. Thin-skinned extensional tectonics on a salt detachment, northern Kwanza Basin, Angola. Marine and Petroleum Geology, 9(4), pp.405-411.

Marton, L.G., Tari, G.C. and Lehmann, C.T., 2000. Evolution of the Angolan passive margin, West Africa, with emphasis on post-salt structural styles. Geophysical Monograph-American Geophysical Union, 115, pp.129-150.

McCaffrey, M.A., Lazar, B.H.D.H. and Holland, H.D., 1987. The evaporation path of seawater and the coprecipitation of Br (super-) and K (super+) with halite. Journal of Sedimentary Research, 57(5), pp.928-937.

Miralles, L., Sans, M., Gali, S. and Santanach, P. 2001. 3-D rock salt fabrics in a shear zone (Sú ria Anticline, South-Pyrenees). Journal of Structural Geology, 23, 675–691.

Nelson, T.H., Fairchild, L., 1989. Emplacement and evolution of salt sills in the northern Gulf of Mexico (abs.). Houston Geological Society Bulletin 32, 6–7.

Netzeband, G. L., C. P. Hübscher, & D. Gajewski, 2006, The Structural Evolution of the Messinian Evaporites in the Levantine Basin: Marine Geology, 230(3–4), 249–73.

Owen, E. W., 1964. An historical sketch of petroleum geology in the Gulf Coast region: Gulf Coast Association of Geological Societies Transactions, 14, 51–65.

Peel, F.J., 2014. The engines of gravity-driven movement on passive margins: Quantifying the relative contribution of spreading vs. gravity sliding mechanisms. Tectonophysics, 633, pp.126-142.

Pichel, L.M., Jackson, C.A.L., Peel, F. and Dooley, T.P., 2019a. Base-salt relief controls salt-tectonic structural style, São Paulo Plateau, Santos Basin, Brazil. Basin Research, 32(3), pp.453-484.

Pichel, L.M., Huuse, M., Redfern, J. and Finch, E., 2019b. The influence of base-salt relief, rift topography and regional events on salt tectonics offshore Morocco. Marine and Petroleum Geology, 103, pp.87-113.

Pošepný, F., 1871. Studien aus dem Salinargebiete Siebenbürgens: Kaiserlich-Königlichen Geologischen Reichsanstalt Jahrbuch, 21, 123–186.

Quirk, D.G., Schødt, N., Lassen, B., Ings, S.J., Hsu, D., Hirsch, K.K. and Von Nicolai, C., 2012. Salt tectonics on passive margins: examples from Santos, Campos and Kwanza basins. Geological Society, London, Special Publications, 363(1), pp.207-244.

Raith, A.F., Strozyk, F., Visser, J. and Urai, J.L., 2016. Evolution of rheologically heterogeneous salt structures: a case study from the NE Netherlands. Solid Earth, 7(1), p.67.

Ranalli, G. and Murphy, D.C., 1987. Rheological stratification of the lithosphere. Tectonophysics, 132(4), pp.281-295.

Reis, A.T.D., Gorini, C., Weibull, W., Perovano, R., Mepen, M. and Ferreira, É., 2008. Radial gravitacional gliding indicated by subsalt relief and salt-related structures: the example of the gulf of Lions, western Mediterranean. Revista Brasileira de Geofísica, 26(3), pp.347-365.

Richard, P., 1991. Experiments on faulting in a two-layer cover sequence overlying a reactivated basement fault with oblique-slip. Journal of Structural Geology, 13(4), pp.459-469.

Roveri, M., Flecker, R., Krijgsman, W., Lofi, J., Lugli, S., Manzi, V., Sierro, F.J., Bertini, A., Camerlenghi, A., De Lange, G. and Govers, R., 2014. The Messinian Salinity Crisis: past and future of a great challenge for marine sciences. Marine Geology, 352, pp.25-58.

Rowan, M.G., Urai, J.L., Fiduk, J.C. and Kukla, P.A., 2019. Deformation of intrasalt competent layers in different modes of salt tectonics. Solid Earth, 10(3), pp.987-1013.

Ryan, W.B., 1976. Quantitative evaluation of the depth of the western Mediterranean before, during and after the Late Miocene salinity crisis. Sedimentology, 23(6), pp.791-813.

Schléder, Z., Burliga, S. and Urai, J.L., 2007. Dynamic and static recrystallization-related microstructures in halite samples from the Kłodawa salt wall (central Poland) as revealed by gamma-irradiation. Neues Jahrbuch für Mineralogie-Abhandlungen: Journal of Mineralogy and Geochemistry, 184(1), pp.17-28.

Schléder, Z., and J. L. Urai, 2005. Microstructural evolution of deformation-modified primary halite from the Middle Triassic Röt Formation at Hengelo, The Netherlands: International Journal of Earth Sciences, 94, 941–956, doi:10.1007/s00531-005–0503-2.

Schléder, Z., and J. L. Urai, 2007, Deformation and recrystallization mechanisms in mylonitic shear zones in naturally deformed extrusive Eocene–Oligocene rocksalt from Eyvanekey plateau and Garmsar hills (central Iran): Journal of Structural Geology, 29, 241–255, doi:10.1016/j.jsg.2006.08.014.

Schléder, Z., Urai, J. L., Nollet, S. and Hilgers, C. 2008. Solution–precipitation creep and fluid flow in halite: a case study from the Zechstein (Z1) rocksalt from Neuhof salt mine (Germany). Geologisches Rundschau, 97, 1045–1056.

Schoenherr, J., L. Reuning, P. A. Kukla, R. Littke, J. L. Urai, M. Siemann, and Z. Rawahi, 2009, Halite cementation and carbonate diagenesis of intra-salt reservoirs from the late Neoproterozoic to Early Cambrian Ara Group (South Oman Salt Basin): Sedimentology, 56, 567–589, doi:10.1111/j.1365–3091.2008.00986.

Schultz-Ela, D.D., 2001. Excursus on gravity gliding and gravity spreading. Journal of structural geology, 23(5), pp.725-731.

Spathopoulos, F., 1996. An insight on salt tectonics in the Angola Basin, South Atlantic. Geological Society, London, Special Publications, 100(1), pp.153-174.

Spiers, C. J., and N. L. Carter, 1998. Microphysics of rocksalt flow in nature, in M. Aubertin and H. R. Hardy, eds., The mechanical behavior of salt: Proceedings of the 4th conference: Clausthal-Zellerfeld, Trans Tech Publications, Series on Rock and Soil Mechanics, 22, 115–128.

Stille, H., 1925. The upthrust of the salt masses of Germany. AAPG Bulletin, 9(3), pp.417-441.

Strozyk, F., Van Gent, H., Urai, J.L. and Kukla, P.A., 2012. 3D seismic study of complex intra-salt deformation: An example from the Upper Permian Zechstein 3 stringer, western Dutch offshore. Geological Society, London, Special Publications, 363(1), pp.489-501.

Talbot, C. J., 1998. Extrusions of Hormuz salt in Iran. In: Blundell,D.J.& Scott, A. C. (eds) Lyell, the Past is the Key to the Present. Geological Society, London, Special Publications, 143, 315–334.

Ter Heege, J.D., De Bresser, J.H.P. and Spiers, C.J., 2005. Dynamic recrystallization of wet synthetic polycrystalline halite: dependence of grain size distribution on flow stress, temperature and strain. Tectonophysics, 396(1-2), pp.35-57.

Trusheim, F., 1960. Mechanism of salt migration in northern Germany. AAPG Bulletin, 44(9), pp.1519-1540.

Urai, J.L., Spiers, C.J., Peach, C.J., Franssen, R.C.M.W. and Liezenberg, J.L., 1987. Deformation mechanisms operating in naturally deformed halite rocks as deduced from microstructural investigations. Geologie en Mijnbouw, 66(2), pp.165-176.

Urgeles, R., Camerlenghi, A., Garcia-Castellanos, D., De Mol, B., Garcés, M., Vergés, J., Haslam, I. and Hardman, M., 2011. New constraints on the Messinian sealevel drawdown from 3D seismic data of the Ebro Margin, western Mediterranean. Basin Research, 23(2), pp.123-145.

Van Gent, H., Urai, J.L. and De Keijzer, M., 2011. The internal geometry of salt structures–a first look using 3D seismic data from the Zechstein of the Netherlands. Journal of Structural Geology, 33(3), pp.292-311.

Vendeville, B., 1988. Modèles expérimentaux de fracturation de la couverture contrôlée par des failles normales dans le socle. Comptes rendus de l'Académie des sciences. Série 2, Mécanique, Physique, Chimie, Sciences de l'univers, Sciences de la Terre, 307(8), pp.1013-1018.

Vendeville, B.C., 1989. Scaled experiments on the interaction between salt flow and overburden faulting during syndepositional extension. In SEPM Gulf Coast Section, 10th Annual Research Conference, Houston, Program and Extended Abstracts (pp. 131-136).

Vendeville, B. and Cobbold, P.R., 1988. How normal faulting and sedimentation interact to produce listric fault profiles and stratigraphic wedges. Journal of structural Geology, 10(7), pp.649-659.

Vendeville, B.C. and Jackson, M.P., 1992a. The rise of diapirs during thin-skinned extension. Marine and Petroleum Geology, 9(4), pp.331-354.

Vendeville, B.C. and Jackson, M.P.A., 1992b. The fall of diapirs during thin-skinned extension. Marine and Petroleum Geology, 9(4), pp.354-371.

Warren, J. K., 2016. Evaporites: A Geological Compendium, 2nd edition. Springer, Berlin, Germany.

Wawersik, W.R. and Zeuch, D.H., 1986. Modeling and mechanistic interpretation of creep of rock salt below 200 C. Tectonophysics, 121(2-4), pp.125-152.

Weijermars, R., M. P. A. Jackson, and B. C. Vendeville, 1993, Rheological and tectonic modeling of salt provinces: Tectonophysics, 217, 143–174.

Zak, I. and Freund, R., 1980. Strain measurements in eastern marginal shear zone of Mount Sedom salt diapir, Israel. AAPG Bulletin, 64(4), pp.568-581.

2 Base-Salt Relief Controls Salt-Related Deformation in the Outer Kwanza Basin, Offshore Angola

This work presented in this chapter has been published in **Basin Research**:

Evans, S.L. and Jackson, C.A.L., 2020. Base-salt relief controls salt-related deformation in the Outer Kwanza Basin, offshore Angola. Basin Research, 32(4), pp.668-687. https://doi.org/10.1111/bre.12390

The accepted manuscript is also available as a pre-print on **EarthArxiv**:

https://eartharxiv.org/repository/view/778/

Acknowledgements

The data used in this study is confidential and was generously provided under license by CGG. Restrictions apply to the availability of these data, which were used under license for this study. I would like to thank my supervisor and co-author for valuable discussions that guided my interpretation of the data, and reviewers who provided helpful feedback to improve the manuscript (Tim Dooley and an anonymous reviewer).

Abstract

Salt-influenced passive margins are widespread and commonly hydrocarbon-rich. However, they can be structurally complex, with their kinematic development being poorly understood. Classic models of salt tectonics divide such margins into updip extensional, mid-slope translational, and downdip contractional kinematic domains. Furthermore, the faults, folds, and salt walls associated with each kinematic domain are typically assumed to form perpendicular to the maximum principal stress, which in gravitationally driven systems means broadly perpendicular to base salt dip. We use high-resolution 3D seismic reflection data from the Outer Kwanza Basin, offshore Angola to show that these models cannot explain the diversity of salt structures developing on passive margins, especially those defined by considerable relief on the base-of-salt surface.

Overburden seismic-stratigraphic patterns record the basinward translation and rotation, allowing us to reconstruct the origin and evolution of the salt structures. We show structures in the transitional domain of the Outer Kwanza Basin display three dominant trends, each characterised by different structural styles: i) salt walls perpendicular to the overall base salt dip, ii) salt walls parallel to the base salt dip, and iii) salt walls oblique to the base salt dip.

We show that each set of walls has a unique history, with synchronous phases of extension and compression occurring in adjacent structures despite their close spatial relationship. Our analysis suggests that, in the Outer Kwanza Basin, the structural evolution of the salt and overburden is predominantly controlled by translation over relief on the base-salt surface formed above fault scarps associated with a preceding phase of rifting.

Changes in the downdip volumetric flux and velocity of the salt over topographic features can cause local extension or contraction of the salt and its overburden, associated with local acceleration or deceleration of the salt, respectively. This interaction with base-salt relief creates locally variable stress fields that deform the salt and its overburden, overprinting the broader, margin-scale salt tectonics typically associated with gravity gliding and spreading.

2.1 Introduction

2.1.1 Passive margin salt tectonics

There are two end-member models of gravity-driven salt tectonics on passive margins; 'gravity gliding', which occurs due to seaward tilting of the margin during continental uplift and basin subsidence, and 'gravity spreading', which occurs due to differential loading of the margin, principally by subsalt sediments eroded and shed from the rising continent (Jackson et al., 1994; Schultz-Ela, 2001; Fort et al. 2004; Hudec and Jackson, 2004; Brun and Fort, 2011; Peel, 2014). Salt-influenced passive margins dominated by gravity gliding (e.g. offshore Israel, eastern Mediterranean) are typically divided into broad, kinematically-linked zones of updip extension, mid-slope translation and downdip contraction (Fig. 2.1)). Each zone is associated with a distinct suite of structures within the salt and its overburden. The updip extensional zone is commonly associated with salt-detached normal faults, salt rollers, rafts, graben and turtles, whereas the downdip contractional zone is associated with salt-cored anticlines and thrusts (Brun and Fort, 2011). In both zones, the long-axes of these structures are subparallel to the strike of the margin, reflecting their formation perpendicular to the maximum principal stress, which is aligned in the direction of the base-salt dip.

Similar structures and trends characterize margins dominated by gravity-spreading (e.g. Nile Delta, eastern Mediterranean), which are also divided into kinematic zones of lateral extension within the proximal part of the load and contraction near the distal pinchout of the load. However, in these cases the orientation of the extensional and contractional structures will be determined by the geometry of the load. For example, in the case of a delta prograding out into a basin containing salt, the fold-and-thrust belt will be arcuate, thus mimicking the arcuate geometry of the delta front (Fig. 2.1). Both the gravity gliding and spreading models typically envisage a smoothly seaward-dipping base-salt, despite the fact that many salt basins formed above substantial, pre- or syn-depositional structural relief (e.g. Rowan, 2012; Dooley et al., 2017; Dooley et al. 2018).

2.1.2 Influence of Base-Salt Relief on Gravity-Driven Deformation

Over geological timescales, the rheological behaviour of salt can be approximated as highly viscous fluid (Weijermars et al., 1993). Fluids such as these are responsive to the geometry of the surface they flow across, and since salt can be deposited shortly after rifting, the base-salt surface is commonly rugose at varying scales (e.g. Hudec et al. 2013). Physical and numerical analogue models, as well as observations from seismically imaged passive margins, show that gravity gliding and the otherwise free seaward flow of salt may be complicated by residual topography on the base-salt surface. Underlying fault scarps or folds can both create an uneven base-salt surface with which the salt interacts as it flows basinward.

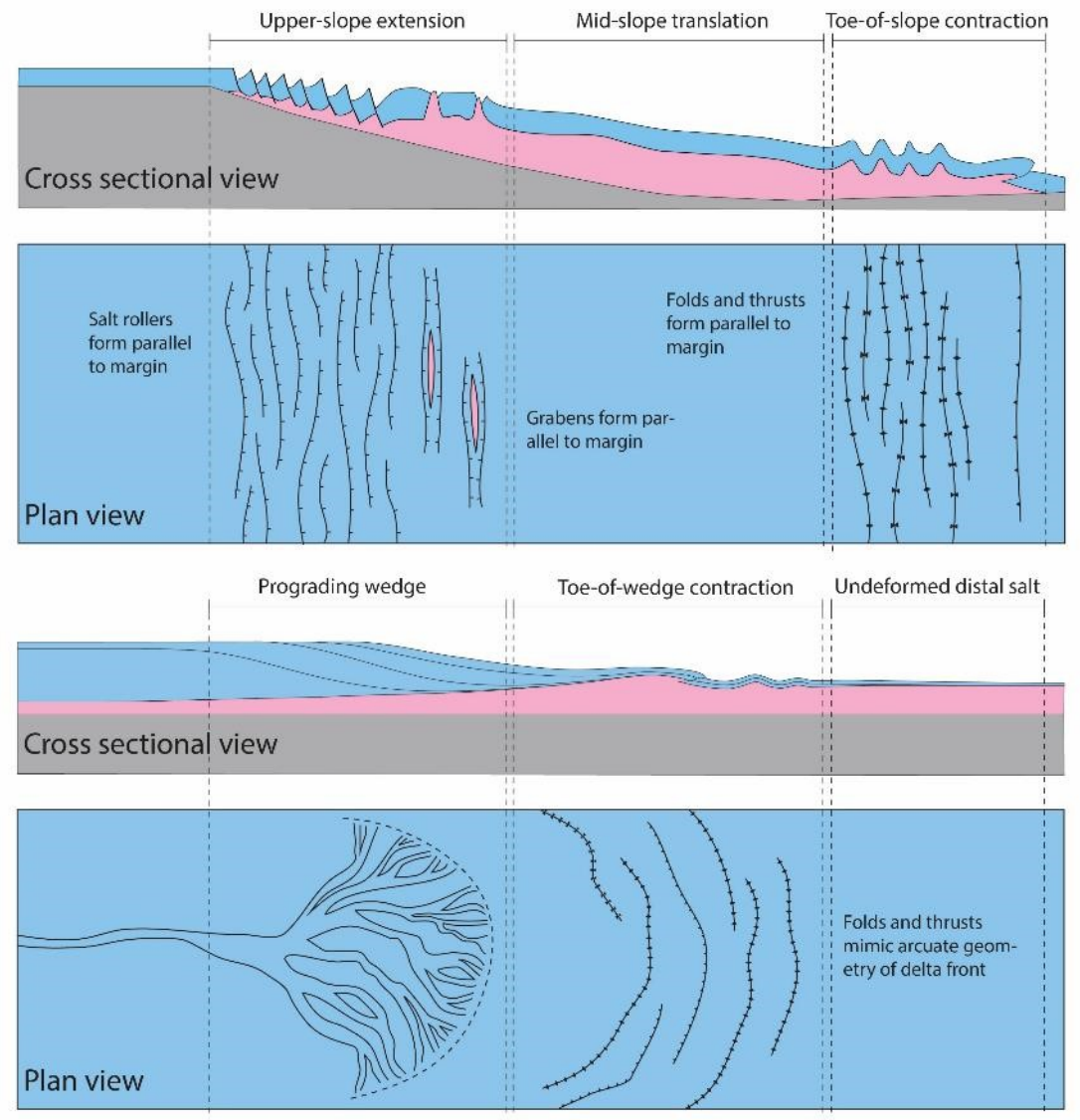

Figure 2.1 Cross sectional and plan view schematic diagrams of end member models of salt tectonic systems: a) gravity gliding, and b) gravity spreading, showing the types of structures and orientations associated with each kinematic domain.

For example, Gaullier et al. (1993) use physical analogue models to simulate salt flow over base-salt steps related to relict syn-rift fault scarps. Base-salt steps oblique to the overall gliding direction generate oblique faults in the overburden, demonstrating a strong correlation between structural trends below the salt décollement and those in the overburden. Cobbold and Szatmari (1991) and Tadeu dos Reis et al. (2008) also use physical models, in the latter case supported by natural examples from the western Mediterranean Gulf of Lion, to show how local changes in the base-salt dip direction can locally redirect salt flow. More specifically, they show that convex and concave base-salt surfaces can generate bi-directional or radial gliding patterns. Concave geometries lead to convergent salt flow that can generate compressional structures, whereas convex geometries lead to divergent salt flow that can generate extensional structures.

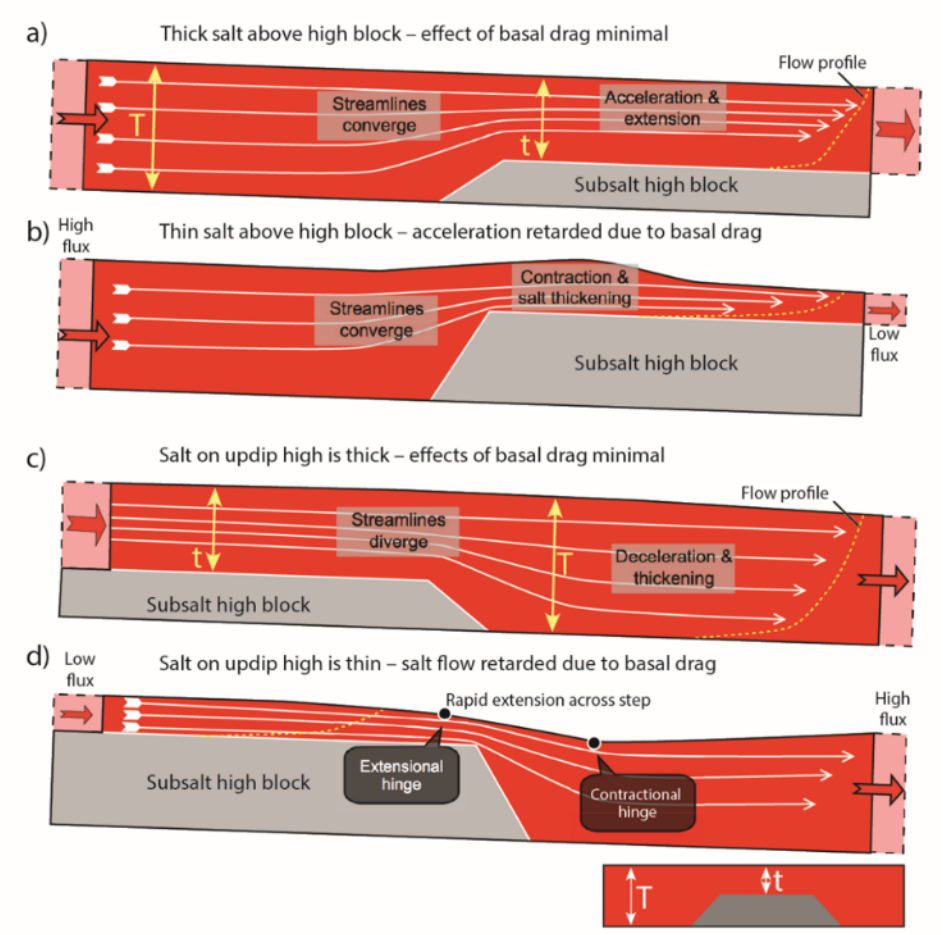

Figure 2.2 Synoptic diagram showing the complex interaction of base-salt relief with salt flow, as determined from physical models. Base-salt relief causes local acceleration and deceleration which in turn causes local extensional and contractional stress fields. The effect on salt flow is different for thick salt cases, a) and c), compared to thin salt cases, b) and d) respectively. Note that these stress fields may also vary through time. From Dooley et al. (2017).

More recently, Dooley et al. (2017) (see also Dooley et al., 2018) further investigate salt flow over downflow- and upflow-facing steps in the base-salt, showing that the change in salt flux over a step can be associated with local acceleration and deceleration (Fig. 2.2). The ratio of initial salt thickness to the height of step is important as this controls the change in flux across the step, and the contribution of basal drag is greater for thin salt (Fig. 2.2b and 2.2d) vs. thick salt (Fig. 2.2a and 2.2c). In the case of a downflow-facing step, these spatial changes in salt flux can generate an extensional hinge at the top of the step, and a contractional hinge at the base (Fig. 2.2d). Further complexity arises when we consider that local stress fields may vary through time as a function of the net seaward salt flow. For example, Dooley et al. (2017) show that as salt contracts at the top of an upflow-facing ramp (Fig. 2.2b), it thickens and gradually allows the salt velocity to increase, which results in overburden extension. However, the reactive or passive diapir that forms in this position may then be squeezed as it translates seaward and later passes through the contractional hinge of another step. Salt structures and their overburden may thus go through multiple phases of extension and contraction, with these local changes in stress fields overprinting the margin-scale kinematic zones associated with classic models of gravity gliding and spreading (Dooley et al. 2018) (Fig. 2.1). These studies show the significant impact base-salt relief can have on the structural evolution of salt-influenced passive margins. More specifically, they show that extension and contraction can occur anywhere on a passive margin, and that structures may develop oblique to the regional dip, more closely mimicking the trend of features on the base-salt surface which influence their growth. There are, however, relatively few natural examples showing how base salt relief can control salt flow and supra-salt deformation patterns.

High-quality 3D seismic reflection data from the Kwanza Basin, offshore Angola, provides us with an opportunity to assess the salt-tectonic development of an area defined by significant base-salt relief. We first characterize the large-scale structure and kinematics of the study area, before focusing in on the development of individual structures during basinward translation of the salt and its overburden. By analysing and interpreting structural and stratigraphic relationships in the overburden, we are able to reconstruct the origin and growth of salt structures. In doing so, we highlight the important role of base-salt relief in controlling the patterns and products of salt flow during passive margin development, and the overall structural evolution of the basin. These data support the observations from

physical models discussed above that the widely accepted and applied gravity gliding/spreading models envisaging broad, margin-scale kinematic zones (Fig. 2.1) do not fully capture the variety of structural styles and orientations of salt structures present on many salt-influenced passive margins. Although based on observations from the Kwanza Basin, the implications of the study are likely applicable to other salt-influenced basins and passive margins defined by significant base-salt relief.

2.2 Geological Setting

The Kwanza Basin forms part of the salt-influenced passive margin characterising much of offshore Angola (Evans, 1978). The basin is >300 km wide, stretching from onshore exposures in the Precambrian Congo Craton westwards to the abyssal plain (Hudec and Jackson, 2004). The southern margin of the basin is marked by a line of seamounts and volcanic rocks that separate the Kwanza Basin from the Benguela Basin. The northern margin of the basin is poorly defined, with the Kwanza Basin passing gradually into the Lower Congo Basin.

Rifting of the Kwanza Basin initiated in the Early Cretaceous, associated with the opening of the South Atlantic Ocean during breakup of the supercontinent Gondwana (Brice et al., 1982; Lentini et al., 2010). The distribution of extension and associated subsidence patterns were controlled by pre-existing basement structures, giving rise to an anomalous syn-rift sag phase that created deep basins along the margins which were filled with thick syn-rift deposits (Karner and Gamboa, 2007; Lentini et al., 2010). A thick layer (locally up to 4 km; Hudec and Jackson, 2004) of Aptian salt was deposited shortly after rifting, draping the residual syn-rift relief. The sag sequence in Angola is relatively thinner compared to the adjacent Lower Congo and Gabon basins (Lentini et al., 2010), allowing greater preservation of syn-rift relief. A thick layer (locally up to 4 km; Hudec and Jackson, 2004) of Aptian salt was deposited shortly after rifting, draping the residual syn-rift relief. The salt was deposited in two sub-basins separated by a margin-parallel chain of platforms, known as the Atlantic hinge zone, where salt is thin or absent (Fig. 2.3b) (Brink, 1974; Hudec and Jackson, 2004). The sub-basins are termed the Inner (eastern and landward) and Outer (western and seaward) Kwanza Basins. Analogous salt basins are present across the Atlantic on the conjugate South American margin (Figure 1.15) (Evans, 1978; Quirk et al., 2012).

Since the deposition of the Aptian salt, salt tectonics have dominated the tectono-stratigraphic evolution of the Kwanza Basin (Marton et al., 2000). Hudec and Jackson (2004) interpreted key structures on a regional 2D seismic line, and defined the updip extensional and downdip contractional domains (Fig. 2.3a, location shown in Fig. 2.4). They restored the section shown in Figure 2.3, and used this restoration to describe three principal phases of salt-related deformation in the Kwanza Basin. First, an early Albian phase of gravity gliding initiated shortly after salt deposition, as the margin tilted during post-rift thermal subsidence. The rate of gravity gliding slowed in the late Albian due to thinning of the salt beneath the updip extensional domain. Second, a phase of rejuvenated salt tectonics occurred in the Campanian, linked to crustal uplift in the distal basin. During this phase the Angola salt nappe was expelled seaward above the distal ramp and onto newly emplaced oceanic crust. Finally, in the Miocene, the rate of downslope translation increased once more as the basin slope (and base-salt) steepened in response to uplift of the West African continental margin (Bond, 1978). This uplift has been attributed to mantle plume-related dynamic topography (Walford and White, 2005).

Due to these phases of salt-related deformation, the Kwanza Basin is now characterised by a diverse range of salt-related structures associated with complex supra-salt deformation patterns (Duval et al., 1992; Lundin, 1992; Spathopoulos, 1996; Peel et al., 1998; Marton et

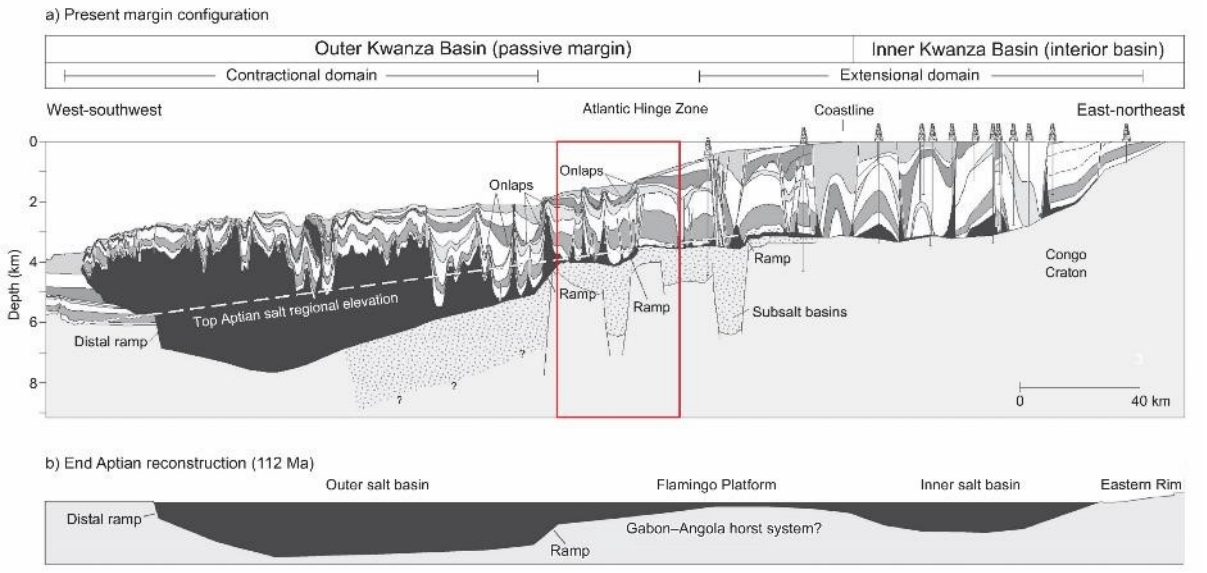

Figure 2.3 a) Regional line showing present day configuration of the Angolan margin from shelf to distal salt nappe. Note the presence of several ramps on the base-salt surface. Location of line shown in Figure 4. Red box highlights approximate position of dataset used in this study. b) End Aptian reconstruction showing initial division of Inner and Outer salt basins. Modified from Hudec and Jackson (2004).

al., 2000; Jackson et al., 2001; Hudec and Jackson, 2002; Fort et al., 2004; Hudec and Jackson, 2004; Quirk et al., 2012). The Albian 'Pinda' carbonate group directly overlies the salt, followed by clastic deposition of a mud-dominated Upper Cretaceous and Tertiary sequence.

In terms of the regional structural framework established by Hudec and Jackson (2004), the study area falls within the intermediate domain between pure updip extension and pure downdip contraction (i.e. the relatively undeformed zone of pure translation is lacking cf. Fig. 2.1a) (Fig. 2.3). Hudec and Jackson (2004) refer to this area as the 'monocline' and 'diapir' domains. The monocline domain is characterised by subhorizontal or landward-dipping packages of sediments that terminate against prominent onlap surfaces. The diapir domain is characterised by a diverse variety of salt structures including salt-cored anticlines, salt rollers, stocks, walls and allochthonous sheets.

2.3 Data and Methods

We use a 3D seismic cube, acquired by CGG, covering a broadly rectangular area of 2915 km^2 offshore Angola (Fig. 2.4). The Pre-Stack Depth Migrated (PSDM) BroadSeis^{TM} data are excellent quality and image down to the base-salt, which lies up to 5.5 km below the seabed. Due to confidentiality restrictions we present annotated geosections with sub-salt strata removed. The data are zero phase and normal polarity, with a downward increase in acoustic impedance (e.g. top salt) defined by a positive/negative reflection (i.e. blue/red on displayed seismic profiles). The vertical and horizontal resolution are approximated by a quarter of the dominant wavelength of the data, yielding c. 3.5 m (λ=14 m) at the seabed and c. 30 m (λ=120 m) at a depth of 5 km (Brown, 2011).

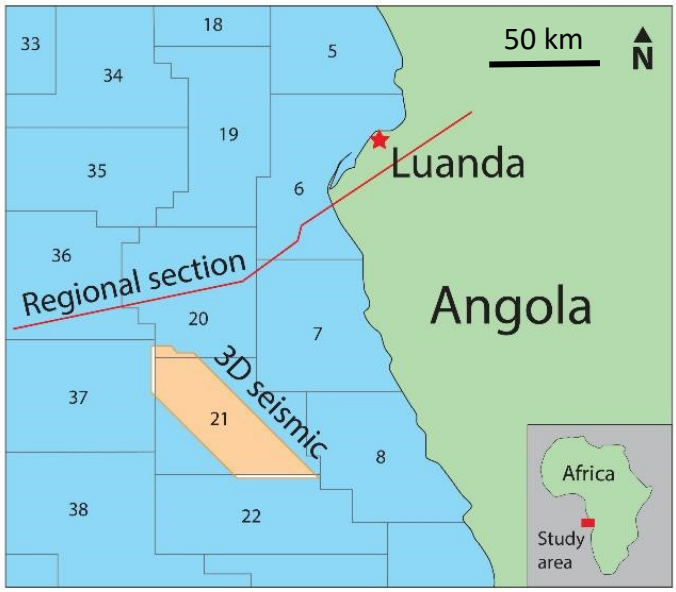

Figure 2.4 Regional map showing location of 3D dataset used in this study (orange) and regional line (see Figure 2.3). Dataset covers Licensing Block 21 of the offshore Angolan margin.

We mapped several key horizons across the dataset; these were selected based on their regional significance (i.e. truncation marking an unconformity, or change in seismic character inferred to mark a significant lithological boundary). The mapped surfaces show the present basin geometry. These surfaces are used to calculate isopachs that show the distribution and evolution of sedimentary depocentres through time, and which we primarily relate to salt-driven deformation and related changes in accommodation. A lack of available well data means that lithologies and absolute ages are unconstrained. However, in order to approximate horizontal translation rates, Top Albian, Top Eocene and Top Miocene ages are tentatively assigned based on a correlation with surfaces and units published by Hudec and Jackson (2004). Note, however, that we focus primarily on the *relative* timing of events based on seismic-stratigraphic analysis, rather than the *absolute* timing with regards to the regional tectono-stratigraphic framework.

2.4 Basin Structure

2.4.1 Base-Salt

The base-salt surface (Fig. 2.5a) dips dominantly to the SW with an average dip of 7°, although we observe significant local changes in both dip and dip direction. The most striking feature is the NW-trending, SW-dipping ramp across the eastern, updip edge of the study area (Fig. 2.5a; see also Fig. 2.6). The ramp, presumed to be a degraded relict fault scarp, formed during the earlier rifting phase (Fig. 2.3a; see also Hudec and Jackson, 2004) and has c. 1.3 km of relief and an average dip of 12°. In detail, despite being broadly perpendicular to the base-salt dip direction, the ramp trend changes along strike. Furthermore, some segments of the ramp, in plan-view, have a convex-, whereas others have a concave-, towards-the-basin geometry. We also note several sub-circular, isolated base-salt highs (Fig. 2.5a).

2.4.2 Salt Thickness

The salt isopach map (Fig. 2.5b) shows the distribution of salt structures across the study area. These structures display a wide range of orientations and geometries, with no clear systematic pattern to their spatial distribution. The salt structures, in addition to displaying different trends across the study area, vary in structural style (e.g Fig. 2.6). For example, some are associated with normal faults and salt rollers, whereas others are spatially related to thrust faults and buckle folds. We provide a detailed description of these salt structures, and their relationship to the base-salt geometry and overburden structures in Section 2.6.

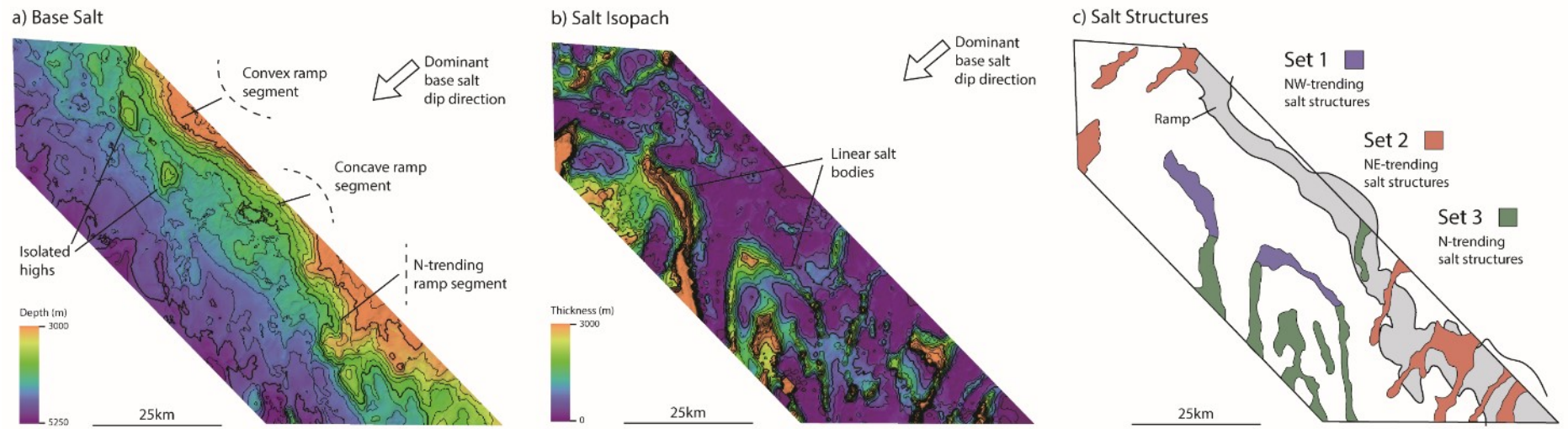

Figure 2.5 a) Depth map of base-salt surface showing dominant dip to the SW. Ramp runs across updip edge of the dataset, broadly sub-parallel to margin but with variable geometry along strike. b) Salt isopach map. Areas of increased thickness correspond to location of salt structures. Areas of minimal thickness show where salt is close to welding. c) Schematic distribution of salt structures across the study area, dividing the structures into three broad sets characterised by their orientation and structural style. Shaded area shows location of base-salt ramp. Seismic data supplied by CGG.

2.4.3 Overburden

We map four main supra-salt seismic-stratigraphic units (Fig. 2.8a-d; corresponding to units highlighted in Fig. 2.6). The thickness map for Unit 1, which broadly equates to the Albian interval, is the most uniform, showing a gradual increase in thickness to the south-east (from c. 400 to c. 1200 m) (Fig. 2.8a). The unit is absent where it has been subsequently pierced by the underlying salt (e.g. Fig. 2.6), but unlike the overlying units, there are only minor and local, salt-related thickness changes, on the order of c. 200-300m). Minor local thickness changes are attributed to filling of early relief on the top-salt surface. This relief could be due to minor syn-depositional deformation of the salt, or simply due to fact that the salt was not deposited perfectly smooth. These minor local thickness changes do not reflect a significant phase of salt tectonic activity or structural development, and are thus discounted from the kinematic model.

By comparison, the thickness patterns for Units 2-4 (Fig. 2.8b-d) are considerably more complex. Of particular note are the prominent, NNE-to-NNW-trending depocentres visible in all three isopachs, where the unit thickness increases from c. 500 m to >1500 m over a relatively short (<5 km) length scale. These depocentres contain stacked packages of landward-thickening and dipping strata that onlap or downlap their immediately underlying units (Fig. 2.6). These are the same packages of landward-dipping strata identified by Hudec and Jackson (2004) in their monocline domain (see Section 2.2). We describe and interpret the origin of these complex overburden thickness patterns below (Section 2.5).

2.5 Basin-scale Kinematics

We interpret that the landward-thickening and -dipping packages described in Section 2.4.3 (Fig. 2.6) form a series of stacked ‘ramp-syncline basins’ (RSBs) that developed in response to the progressive downdip translation of the salt and its overburden across the major base-salt ramp located along the updip edge of the study area (Fig. 2.5a) (Peel et al., 1998; Marton et al., 1998; Jackson et al., 2001; Jackson and Hudec, 2005; Dooley et al., 2017; Pichel et al., 2018; Dooley et al., 2018; Pichel et al., 2019). A RSB is defined as a “translating growth syncline that gradually moves seaward on a dipping detachment as if on a conveyor belt” by Hudec and Jackson (2017). Translation over the seaward-dipping ramp continually creates accommodation on the downdip side of the ramp, causing syn-kinematic strata to thicken landward into the ramp (Fig. 2.7). As displacement continues, strata are rotated downward such that primary onlap relationships now appear as downlap relationships.

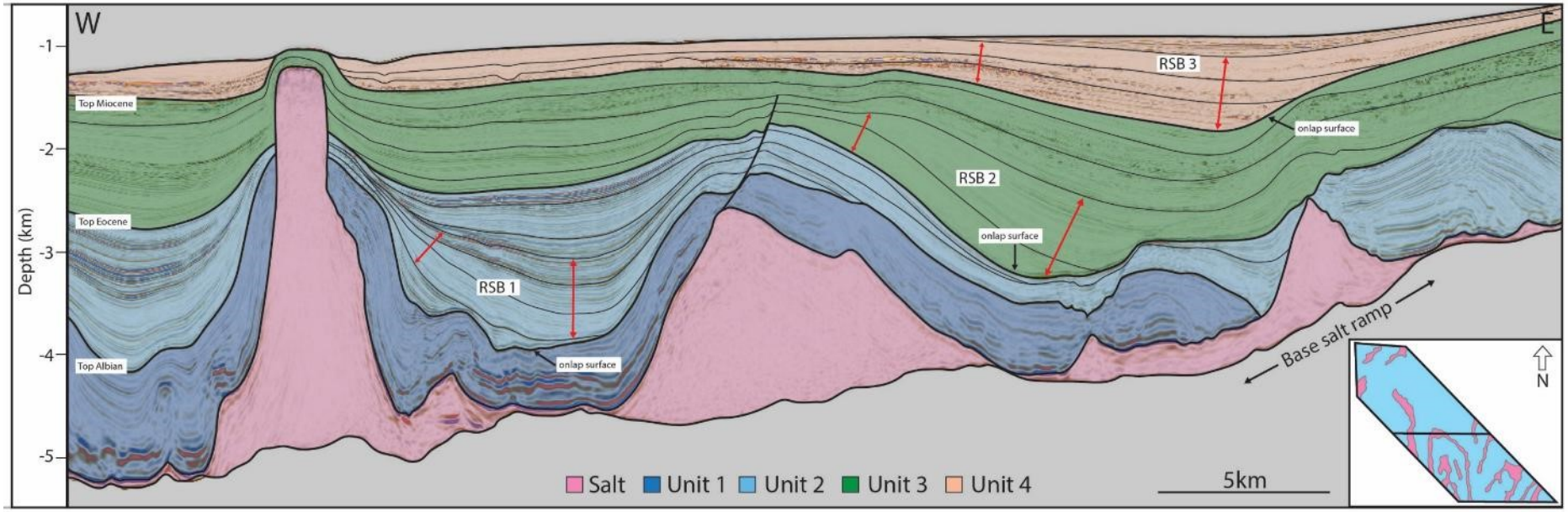

Figure 2.6 Representative seismic geosection showing series of salt structures (see inset map for location). Key interpreted units in the overburden (1-4) and approximate ages of key surfaces (Top Albian, Top Eocene, Top Miocene). Stacked ramp syncline basins (RSB1, RSB2, RSB3) and location of updip base-salt ramp. Seismic data supplied by CGG.

The RSBs are therefore recognised by their characteristic pseudo-downlap surface and monoclinal geometry of the growth strata (Jackson and Hudec, 2005). Similar examples have previously been described on the Angolan margin using 2D seismic data (Peel et al., 1998; Marton et al., 1998; Jackson et al., 2001; Jackson and Hudec, 2005), and using 3D data from the conjugate margin in the Santos Basin, offshore Brazil (Pichel et al. 2018). RSBs have also been produced in physical analogue models (Dooley et al., 2017; Dooley et al., 2018) and numerical models (Pichel et al., 2018) (Fig. 2.7).

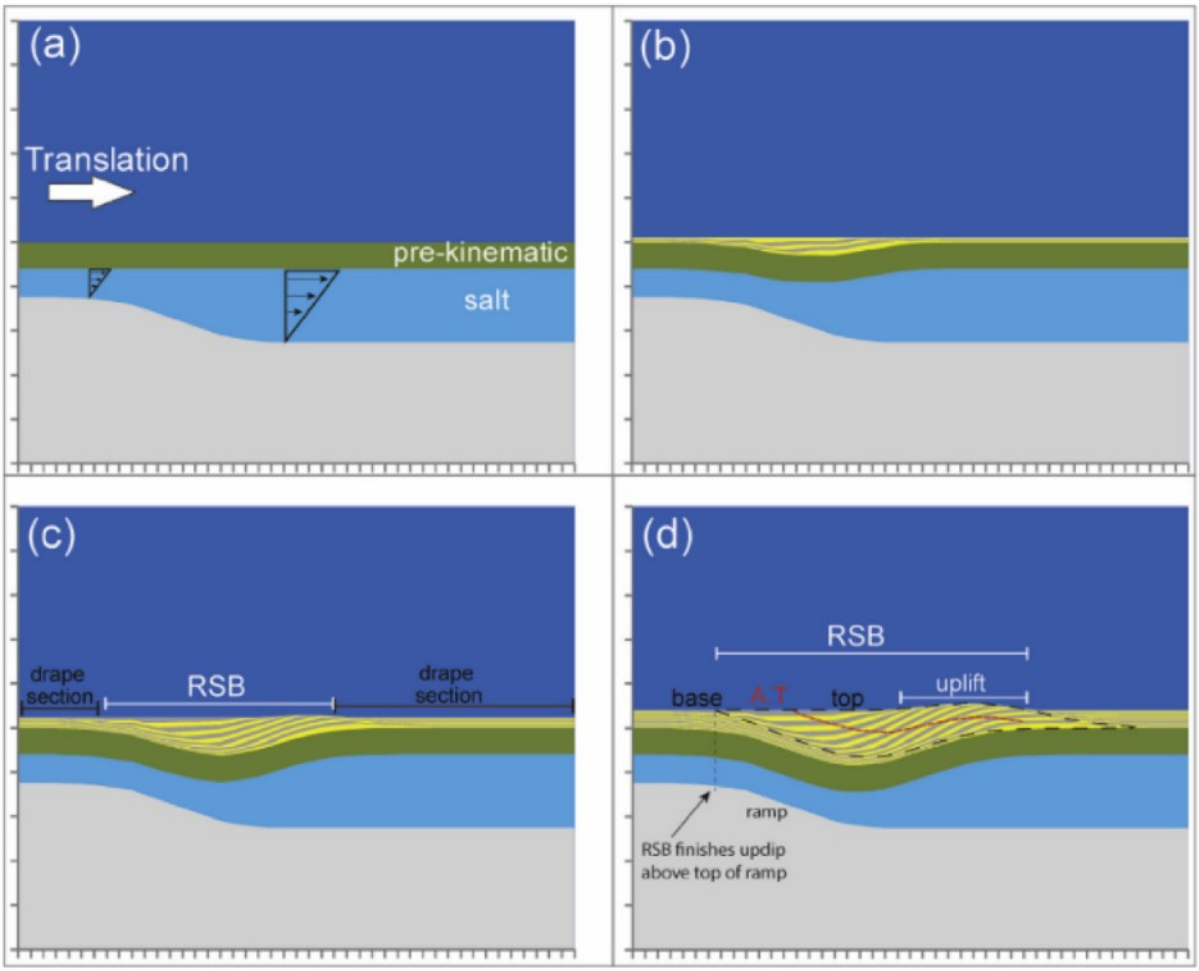

Figure 2.7 Numerical model showing incremental development of ramp syncline basin during basinward translation. a) Isopachous pre-kinematic strata prior to translation. b) Imbalance of salt flux creates accommodation space above ramp which fills which growth strata thickening into ramp. c) Early growth strata are rotated and moved downdip as translation continues. d) Fully developed ramp syncline basin showing monoclinal geometry of growth strata, basal onlap surface and distal uplift. From Pichel et al. (2018).

We interpret that the RSBs imaged in the dataset are genetically related to the base-salt ramp located immediately updip (Fig. 2.5a). Given that each RSB forms at the same position above the major base-salt ramp and is subsequently translated seaward as salt flow progresses, we can reconstruct the overburden translation through time by mapping-out the sedimentary depocentres and their onlaps, and laterally restoring them to their initial positions adjacent to the ramp. The lowermost, and thus earliest, onlap onto the base of each RSB is laterally restored to its original position above the updip

hinge of the ramp (Fig. 2.6), and the associated depocentres are fitted as closely as possible to their (inferred) original positions directly overlying the ramp (Fig. 2.8e-g), as shown by physical and numerical models (Dooley et al., 2017; Dooley et al., 2018; Pichel et al., 2018). This process is relatively straightforward for the large, elongate RSB depocentres, hence their original positions are quite well-constrained. However, it is more difficult to restore the original positions of the smaller, more rounded, yet clearly RSB-related depocentres located in the NW of the study area (Fig. 2.8e-g). We therefore focus the discussion here on the N-trending, linear RSBs for which we can make a confident restoration. The approximate original positions of the smaller depocentres use the vectors and displacement magnitudes given by the larger RSBs to guide their restorations.

	Time (Ma)	**Displacement (km)**	**Rotation (deg)**	**Translation rate (mm/yr)**	**Rotation rate (deg/Myr)**
	100.5	0	0		
RSB 1	33.9	11.9	20	0.18	0.30
RSB 2	5.3	17.8	27	0.21	0.24
RSB 3	0	23.2	32	1.0	0.90

Table 2.1 Translation and rotation recorded by ramp syncline basins. Ages are derived from those assigned to the corresponding boundary in the GSA Geologic Time Scale.

The earliest onlap contained within the RSB defines the net distance of translation (Pichel et al., 2018). Our analysis shows that the oldest RSB, RSB 1, records c. 23.2 km of seaward translation, and c. 32° of clockwise rotation from its original position to its present day position (Fig. 2.8e). Note that this is a minimum estimate of the total horizontal translation, as it does not include any translation that may have occurred during the Albian, prior to the development of the RSB. Our estimate does, however, broadly agree with the estimate of Hudec and Jackson (2004), who calculated at least 20 km of lateral translation based on their structural restoration. We infer the earliest onlap surface is approximately end Albian in age (see Section 2.3), which equates to c. 23.2 km of lateral translation in c. 100.5 Ma (i.e. from the end of the Albian to the present). This yields an average translation rate of c. 0.23 mm/yr (± 0.02 mm/yr), and an average rotation rate of 0.3°/Myr (± 0.03 °/Myr). Previous translation estimates using RSBs used 2D seismic sections and were therefore unable to determine any syn-translation rotation; we think this is the first time this phenomenon has been quantified from a salt basin. Plan-view rotation of salt structures associated with salt flow over base-salt relief has been suggested from analysis of seismic reflection data in the Santos Basin, offshore Brazil (Pichel et al., 2019), and documented in physical models (Dooley and Hudec, 2017).

RSB 2 overlies RSB 1 (Fig. 2.6), and is now located c. 11.3 km seaward from, and has rotated clockwise c. 12° from, its causal ramp (Fig. 2.8f), whereas the youngest, RSB 3, is located c. 5.4 km seaward of the ramp and has undergone c. 5° of clockwise rotation (Fig. 2.8g). If we apply the approximate ages

to these units (see Section 2.3), we can estimate the incremental change in rates of translation and rotation through time (Table 2.1).

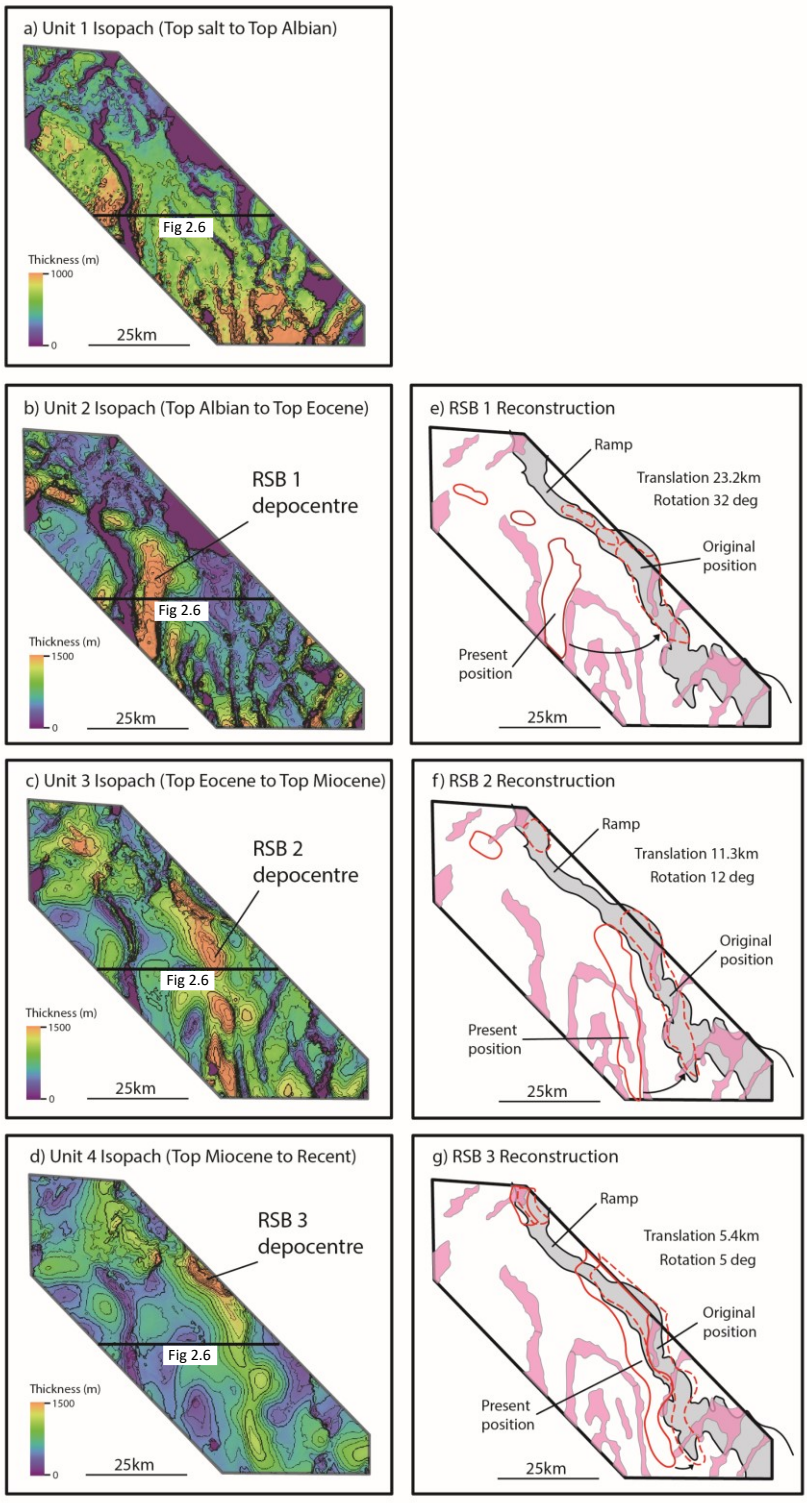

Figure 2.8 a-d) Isopach maps for key units (see Figure 2.6). Thick, linear depocentres correspond to ramp syncline basins. Location of Figure 6 section is shown for reference. e-g) Reconstructed positions of ramp syncline basins above the causal base-salt ramp, allowing translation and rotation to be quantified through time. Seismic data supplied by CGG.

This analysis suggests that translation and rotation rates were approximately constant from the end of the Albian up to the Miocene, at which point they both increased (see Fig. 2.9), an observation is consistent with a previous study by Hudec and Jackson (2004). Translation rates are usually highest during the initial stages of salt tectonics, and decrease through time due to salt thinning and overburden thickening (Jackson and Hudec, 2005). However, in the case of the Kwanza Basin, basement uplift during the Miocene steepened the bathymetric gradient and greatly accelerated downslope translation during the latter stages of margin development (Hudec and Jackson, 2004). This is attributed to continental uplift related to the West African mantle plume, which may have initiated as early as the Oligocene, evidenced by a change in course of the Congo river and increase in course clastic sedimentation to the Lower Congo and Kwanza basins (Lavier et al., 2001). Due to the relatively poor age constraints within strata filling the RSBs, we cannot resolve shorter periods of acceleration or deceleration that may have occurred. Rather, our values are broad averages of the rates of translation and rotation for each time step.

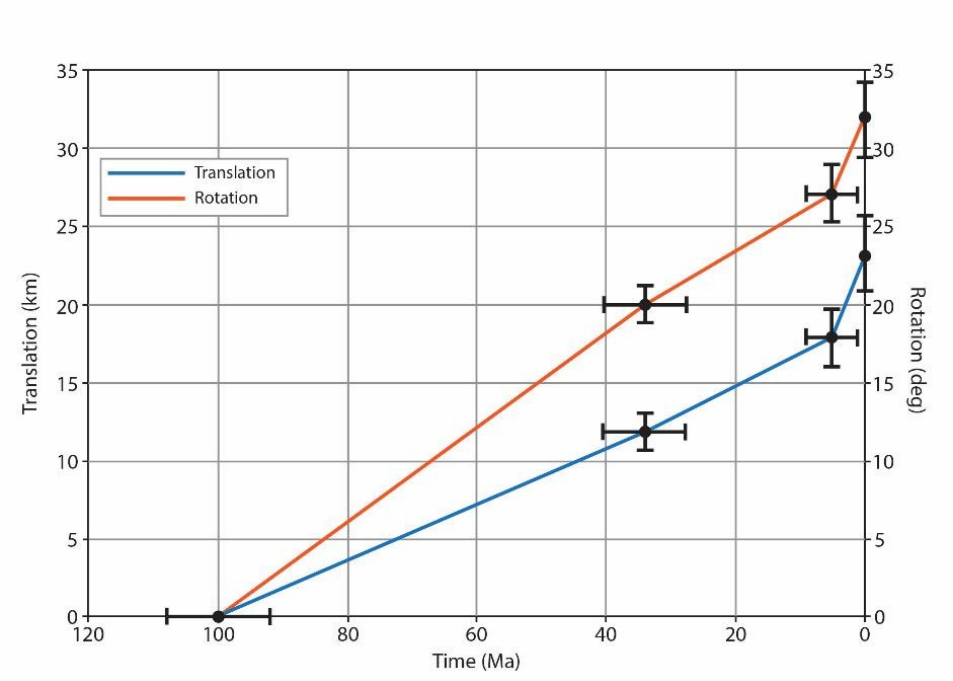

Figure 2.9 Graph showing translation and rotation through time since end Albian, as derived from ramp syncline basins (see Table 1). 10% error bars shown for each data point.

The RSBs show that the dominant direction of translation is westward, oblique to the dominant, broadly south-westerly base-salt dip direction (Fig. 2.5a). Clockwise rotation of the RSBs may be explained by variations in the depositional thickness of underlying salt. Due to reduced basal drag, areas of thick salt (in the south) would flow faster seaward than areas of

thin salt (in the north), thereby causing a net-clockwise rotation of the translating overburden (Jackson and Hudec, 2017). Von Nicolai (2011) used backstripping and isostatic balancing to determine the initial distribution of salt deposited during the Aptian, showing early local thickness changes that suggest the original salt isopach thickened to the south in this area (see her Fig. 4.11).

Having used the RSBs to interpret and quantify the net overburden translation and rotation associated with salt flow in the region of interest, we now proceed with a seismic-stratigraphic analysis of the individual salt structures. Given that we now know how these structures have moved through time from their original positions on the margin, we can interpret their evolution in the context of this basinward translation and their interaction with base-salt relief.

While we are confident applying these translation and rotation estimates to the evolution of local salt structures, we would caution against applying these more widely. A series of thick-skinned transfer faults, which run perpendicular to the margin and segment the Kwanza Basin, are said to allow different amounts of translation on either side of the faults (Duval et al., 1992; Spathopoulos, 1996). This could mean that the rates of translation and rotation calculated here may only apply locally and may differ along the margin.

2.6 Local Salt Structure Evolution

The salt structures can be grouped into three broad sets defined by their orientations (Fig. 2.5c): (i) Set 1 - Parallel to margin (NW-SE); (ii) Set 2 - Perpendicular to margin (NE-SW); and (iii) Set 3 - Oblique to margin (N-S). Each of these sets is also associated with distinctly different structural styles (e.g. salt rollers and turtle structures vs. thrusts and buckle folds). In a classic gravity gliding-dominated view of salt-influenced passive margins, we might expect elongate salt-related structures (i.e. faults, folds and walls) to be oriented subparallel to the margin (Bally, 1981). As we demonstrate below, the trend and styles of salt structures in this part of the Kwanza Basin deviate from this view, suggesting other processes, such as salt flow over base-salt relief, controlled the structural development of the salt and its overburden. In the following section we describe and interpret the characteristic structural styles of each of

the sets, and explore how the base-salt relief may have influenced their structural development during seaward translation.

2.6.1 Set 1: Margin-Parallel Structures

Geometry and Seismic Stratigraphy

There are two NW-trending, margin-parallel salt walls, oriented perpendicular to the general base-salt dip direction and oblique to the dominant (westerly) gliding direction (Fig. 2.5c). The major base-salt ramp is located c. 15 km updip of, and is subparallel to, these two walls. Both salt walls have a broadly triangular shape in cross section, defined by a wide base and narrow crest, and share similar structural characteristics, but the more northerly structure is significantly larger (Fig. 2.10a). Furthermore, the structural characteristics of the larger wall (Fig. 2.10a) vary along strike. Near the centre, the wall has rounded crests, and is flanked by more steeply dipping strata that only onlap the wall in their upper part (Fig. 2.11a). In contrast, at its end, the wall has lower relief and an irregular crestal geometry defined by 'horn-like' projections of salt (Fig. 2.11b). In this location, two large, inward-dipping, salt-detached normal faults bound a supra-wall graben.

Unit 1 is broadly tabular, terminating against the salt wall on both flanks (Fig. 2.10a). However, strata at the base of Unit 1 are folded, with growth strata preserved within synclines (Fig. 2.10b). The folds and related growth strata are draped by more tabular, largely deformed strata. Unit 2, however, thins onto both flanks of the salt wall, and forms part of the fill of RSB 1 on the updip side of the structure (Fig. 2.10a). Unit 3 marks a significant change in structural style as it thickens across a series of inward-dipping, graben-defining normal faults developed above the salt wall (Fig. 2.10a). Updip, Unit 3 thickens into a salt-detached normal fault located above the major base-salt ramp. Unit 4 is also faulted over the crest of the salt wall, but overall thickens updip into RSB 3.

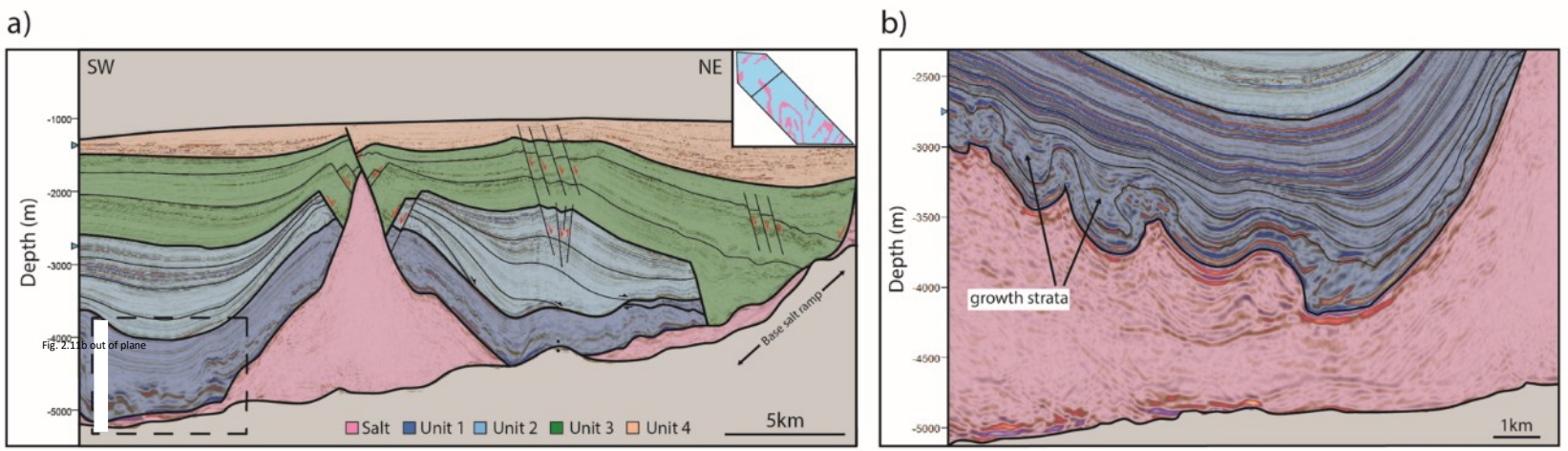

Figure 2.10 a) Seismic geosection through Set 1 salt wall (see inset map for location). Note the triangular geometry, inward-dipping crestal normal faults and updip base-salt ramp. b) Enlarged section showing buckle folds and growth strata on the flank of the salt wall at base of Unit 1 (out of plane of box shown in a). Seismic data supplied by CGG.

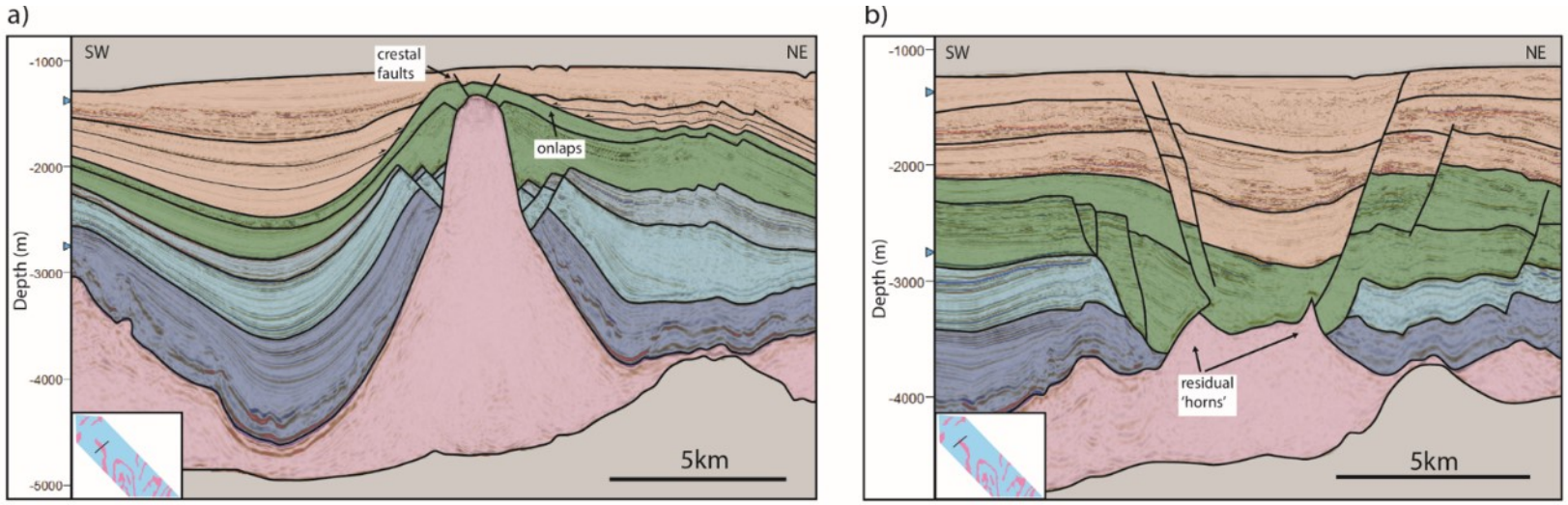

Figure 2.11 a) Seismic geosection through central Set 1 salt wall showing characteristics indicative of active rise. b) Seismic geosection through end of Set 1 salt wall showing characteristics indicative of diapir collapse. Locations shown in inset maps. Seismic data supplied by CGG.

Based on the geometry and seismic-stratigraphy of the overburden, the structural evolution of the Set 1 salt walls, and their relation to the updip RSB, is summarised here and illustrated schematically in Figure 2.12.

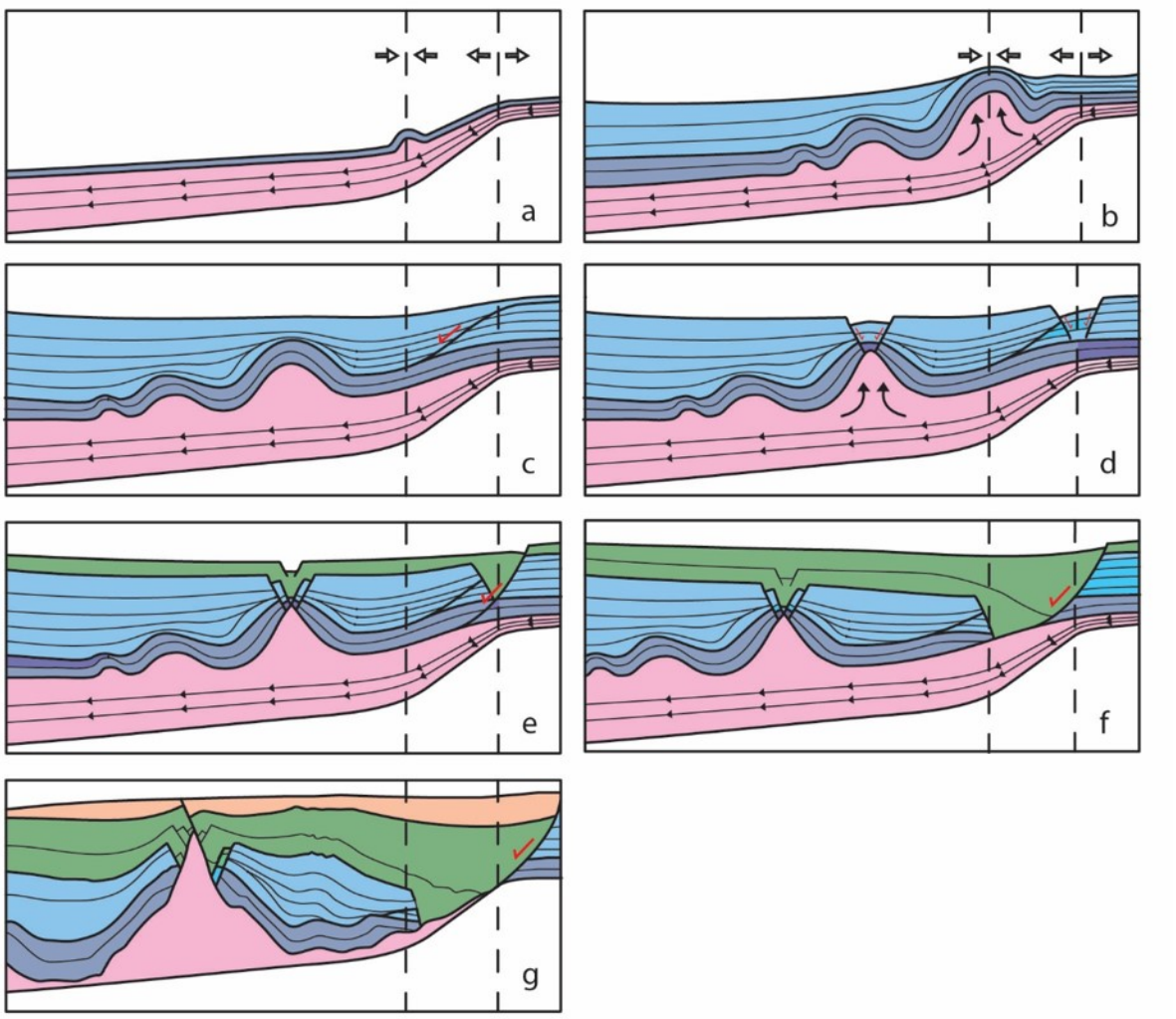

Figure 2.12 Schematic evolution of the Set 1 salt structures. Location of each schematic time step shown in Figure 2.17. a) Initial contraction as salt decelerates at base of ramp. b) Overburden thickening and sediment loading drives growth of salt-cored anticline as translation continue. c) Overburden strengthens and normal fault develops above ramp. d) Local extension as grabens open at points of overburden weakness – top of the ramp and crest of the salt-cored anticline. e) Syn-kinematic sediments thicken over crest as reactive rise drives further growth of salt wall. Normal fault above ramp grows and detaches into salt. f) Normal fault facilitates continued downdip translation of the salt and overburden. e) Present day geometry.

The presence of growth strata shows that the buckle folds formed during deposition of Unit 1, implying salt-related deformation initiated when the overburden was very thin (only c. 0.1 km thick, based on the thickness of the tabular strata underlying the growth strata; Fig. 2.10b). Our earlier analysis of the RSBs showed that a significant amount (at least c. 23 km) of basinward translation has occurred in the area. We therefore propose that this very early

contractional deformation may reflect overburden shortening at the base of the ramp as salt flowed seaward (Fig. 2.2d) (e.g. Dooley et al., 2017; 2018). As a result, the thin overburden buckled to form low-amplitude, small-wavelength folds at the base of the ramp (Fig. 2.12a; Fig. 2.17a). The buckle folds were subsequently translated further downdip to their present position. These kinematics and related structural style are analogous to the translated fold-belt of prekinematic strata generated in a physical model by Dooley et al. (2017) (see their Fig. 25).

Thinning of Unit 2 onto the large salt wall indicates that it had a topographic expression on the seafloor during deposition. The associated buckle folds suggest a possible contractional origin for the diapiric structure, which may have initially formed as a salt-cored anticline (Fig. 2.12b; Fig. 2.17b). An alternative interpretation is that the structure formed at the extensional hinge at the top of the ramp (Fig. 2.2d), but we favor the contractional origin because buckle folds of similar age occur on the updip flank of the structure. Once the initial anticline had formed, subsidence of strata immediately flanking the walls occurred as salt was drawn into the core of the growing structure. Sediment loading would have then amplified this effect and driven continued growth of the structure as it translated basinward.

Following continued sediment deposition, the overburden reached a critical thickness where it became too strong to buckle at the base of the ramp. The buckle folds and salt-cored anticlines were thus passively translated downdip as gliding continued, and a RSB formed above the ramp due to an imbalance in salt flux (Fig. 2.12c). The RSB is essentially the expression of the hinge pair/monocline as the roof thickens and strengthens.

A phase of extension, possibly related to salt acceleration as the margin steepened and base-salt dip increased, then caused two graben to develop. One graben developed over the crest of the salt-cored anticline where the overburden was thin and therefore mechanically weak, whereas the other formed over the extensional hinge of the ramp where the stress is greatest (Fig. 2.12d). Overburden extension initiated reactive diapiric rise and allowed the salt to penetrate to the seafloor (Vendeville and Jackson, 1992a) (Fig. 2.17c).

As the diapir rose reactively and drew in more salt, the seaward-dipping, graben-bounding fault above the ramp became dominant, growing and detaching into the salt (Fig. 2.12e).

Normal displacement on the fault facilitated the downslope transport of material in this location (Fig. 2.12f), laterally equivalent to RSB 2 developing along strike to the SE. Eventually, diapir growth slowed and it became buried, as the source layer thinned and almost welded (Fig. 2.12g). The 'turtle' structure in Unit 2 developed due to subsidence of the minibasin flanks as it reached base-salt. Growth strata indicate that this 'inversion' of the minibasin (from syncline to anticline) occurred during the deposition of Unit 4, as the salt is withdrawn into the adjacent diapir on the downdip side, and the hangingwall subsides due to normal fault displacement on the updip side.

Following reactive rise, the salt wall was tall enough, and the overburden thin enough, to permit active rise by buoyancy in the centre of the salt wall. The diapir assumed a more rounded geometry characteristic of active rise in this location (Jackson and Hudec, 2017) (Fig. 2.11a; Fig. 2.17d). In order to feed the actively rising central diapir, salt flowed along-strike from its ends, causing the ends of the salt wall to collapse/fall (Vendeville and Jackson, 1992b) (Fig. 2.11b). The diapir welded on its north-eastern margin, and only a thin connection to the adjacent salt pillow on the south-western edge remains (Fig. 2.10a), thus salt flowed more easily within the salt wall itself. Onlapping strata in the youngest package indicate active rise may be ongoing, although the lack of topographic expression on the present seafloor suggests that either the sediment accumulation rate keeps pace with the rate of diapir rise, or that the active rise has very recently ceased (Fig. 2.17e).

2.6.2 Set 2: Margin-Perpendicular Structures

Geometry and Seismic Stratigraphy

The NE-trending salt walls are oriented perpendicular to the margin and parallel to the general base-salt dip (Fig. 2.5c). These walls have strikingly different structural characteristics to Set 1 (Fig. 2.13). For example, in contrast to walls defining Set 1, which are broad and normal faulted across the crest, walls in Set 2 are short and narrow, each being associated with a thrust fault that detaches in the crest of the structure (Fig. 2.13a). The predominantly SE-dipping thrust faults are confined to Units 1 and 2, terminating at the contact between Units 2 and 3.

Unit 1 comprises a series of discrete rafts, within which strata thicken to the south-east (Fig. 2.13a). Unit 2 overlies Unit 1 conformably and fills depocentres between detached blocks of Unit 1. Locally, Unit 2 strata define antiformal 'turtle' structures filled with growth strata (Fig. 2.13b). Unit 3 drapes the salt walls and intervening depocentres unconformably, and overlying units are undeformed. Strata at the base of Unit 4 appear to downlap Unit 3; this relationship arises because Fig. 2.13a represents an oblique, NW-trending section through a broadly N-trending RSB. Of particular note in Unit 3 is the broad anticline directly above a topographic high on the base-salt surface; we return to the significance of this structure below.

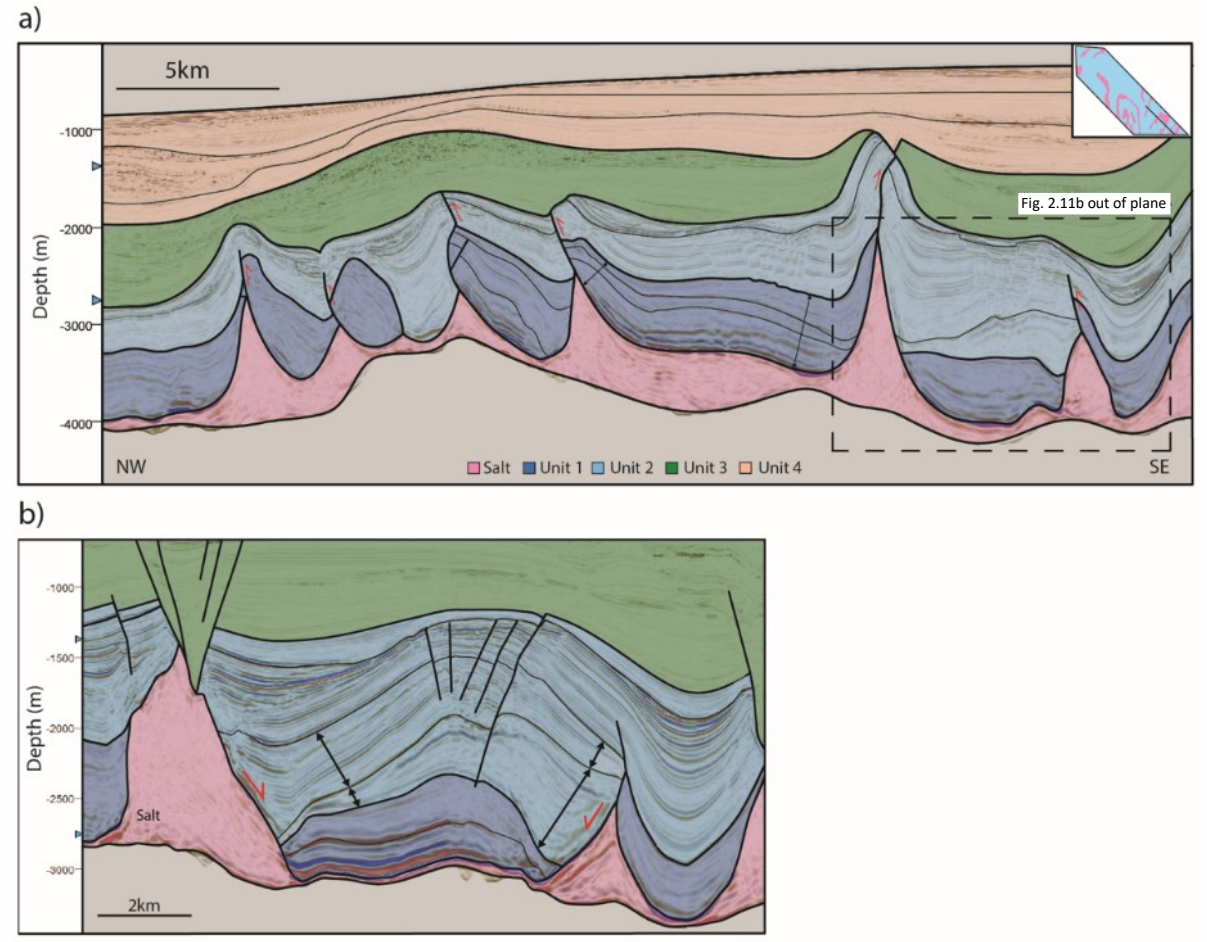

Figure 2.13 a) Seismic geosection through Set 2 salt structures (see inset map for location; note that as this section is taken perpendicular to the Set 2 salt walls, the net flow direction of salt is out of the page, towards the viewer). Note the rafts of Unit 1 and the thrust faults associated with each salt wall. b) Enlarged section showing turtle anticline structure (out of plane of box shown in a). Seismic data supplied by CGG.

Structural Evolution

The schematic structural evolution of the Set 2 salt walls is shown in Figure 2.14. We propose that these salt walls initiated in response to a phase of early extension, which was accommodated by formation of predominantly W-dipping normal faults and associated salt rollers (that later evolved into walls; Fig. 2.14a; Fig. 2.17a). Continued extension eventually dissected Unit 1 into a series of detached rafts, with Unit 2 filling the accommodation between the rafts as the salt thinned (Fig. 2.14b; Fig. 2.17b). An extensional turtle structure formed out-of-plane to the NE (Fig. 2.13b), similar to asymmetric turtle structures previously been identified in the Kwanza Basin (Duval et al., 1992).

Using the translation and rotation increments given by the RSBs (Section 2.5), we can restore the original position of the structures. This shows that the Set 2 structures initially formed outside of the area imaged in our seismic data (Fig. 2.17a). It is therefore difficult to suggest a mechanism for the extension that triggered salt roller formation. However, based on the magnitude of rotation recoded in the RSBs, we can infer that Set 2 structures originally trended broadly N (Fig. 2.17a), before being rotated into their present NE trend (Fig. 2.17e). Furthermore, the dominant (restored; see Fig. 2.17a) westward dip direction of the normal faults bounding the rollers and rafts suggests formation in response to bulk westward sliding. We therefore tentatively infer that the base-salt dips locally to the west (rather than south-westwards) where the Set 2 structures originated. This would be in line with the regional gliding direction indicated by the RSBs, and consistent with observations of roller and raft development elsewhere (e.g. Duval et al., 1992).

The contact between Units 2 and 3 defines the onset of contraction; this exploited the pre-existing planes of weakness created by the salt rollers, which were relatively weaker than the flanking rafts (Fig. 2.14c; Fig. 2.17c). Note that the thrust faults dip to the SE and cross-cut the oppositely dipping, salt-detached, raft-bounding normal faults, likely because the latter were too steep to be reactivated in a reverse sense. The thrust faults uplifted strata above the salt rollers, which were then locally eroded prior to deposition of Unit 3.

The bulk (i.e. regional) shortening direction responsible for squeezing and inversion the Set 2 structures is difficult to determine given contraction exploited pre-existing, weak salt rollers;

i.e. the maximum principal stress may have been oblique, rather than perpendicular, to the orientation of the salt walls (Duffy et al., 2018). At the onset of shortening the structures would have been approaching a concave-into-the-basin ramp segment (Fig. 2.17c). Local contraction at this time may therefore relate to the onset of convergent radial gliding associated with translation over this concave-into-the-basin ramp (Cobbold and Szatmari, 1991; Tadeu dos Reis et al, 2008).

From the deposition of Unit 3 onward, there is little evidence of salt-related deformation, with Unit 3 draping and burying the established salt walls (Fig. 2.14d; Fig. 2.17d). The broad fold defined at the top of Unit 3, and associated thinning of Unit 4 above the base-salt high, formed as the overburden was folded during overall basinward translation across base-salt relief (Fig. 2.14f).

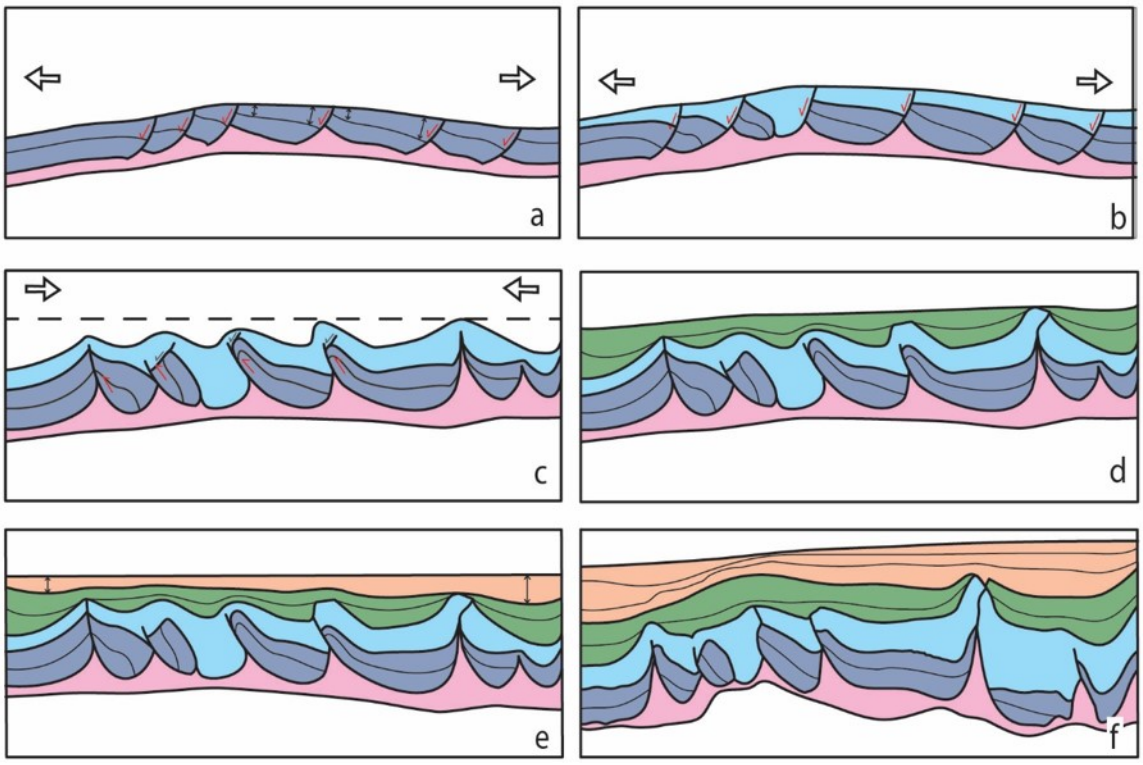

Figure 2.14 Schematic evolution of the Set 2 salt structures. Locations of each schematic time step shown in Figure 17. a) Early development of extensional salt rollers and associated growth strata. Normal faults detach in salt and dip to the west. b) Continued extension leads to rafting (turtle anticline develops out of plane). c) Onset of contraction exploiting weak salt rollers and causing rafts to thrust over each other. Local erosion of uplifted strata. d) Sediments onlap residual highs and salt walls become buried. e) Inactivity of salt structures and continued burial. Growth strata shows asymmetric subsidence as downdip translation progresses. f) Present day geometry.

2.6.3 Set 3: Oblique Salt Structures

Geometry and Seismic Stratigraphy

The N-trending salt structures are (presently) oriented oblique to the general base-salt dip direction, perpendicular to the dominant (westerly) gliding direction (see Section 2.5), and parallel to the RSBs. Unlike those in sets 1 and 2, most of the structures in Set 3 are high-amplitude salt-cored anticlines that do not pierce the overlying stratigraphy (i.e. they are not diapirs; Hudec and Jackson, 2011) (Fig. 2.15). There is one exception that has pierced the overburden and penetrates close to the present day sea floor (furthest west in Fig. 2.15). Unit 1 is largely isopachous across the salt-cored anticlines, whereas Unit 2 thins over the crests and thickens dramatically into flanking synclines (Fig. 2.15). Unit 3 onlaps the salt-cored topographic highs, whereas Unit 4 does not markedly changed in thickness across the underlying salt structures.

Structural Evolution

The stratigraphic occurrence of growth strata indicates that Set 3 salt structures had a rapid and short-lived phase of growth during deposition of Unit 2. This is in contrast to Sets 1 and 2, which formed early during deposition of Unit 1. Set 3 salt structures also differ from Sets 1 and 2 in that they do not show diagnostic characteristics associated with either compression or extension. For example, salt-cored anticlines in Set 3 may have formed as – 1) halokinetic folds, in response to sedimentary loading in the absence of lateral tectonic forces, or 2) contractional folds, in response to lateral compressive forces. Halokinetic folds typically form gradually and are associated with low-relief salt pillows or anticlines, whereas the short-wavelength and tight geometry of these folds, in addition to their relatively rapid growth, is perhaps most consistent with a compressive origin (Jackson and Hudec, 2017).

The schematic structural evolution of the Set 3 salt structures is shown in Fig. 2.16. The N-trending salt-cored anticlines are parallel to the N-trending axes of the RSBs and the N-trending segment of the base-salt ramp responsible for their development (Fig. 2.5a). It therefore follows that the compression that generated the folds and salt pillows was also associated with a deceleration during translation across the base-salt ramp. Decelerating flow at the base of the N-trending ramp could have generated the compressive stress in the same

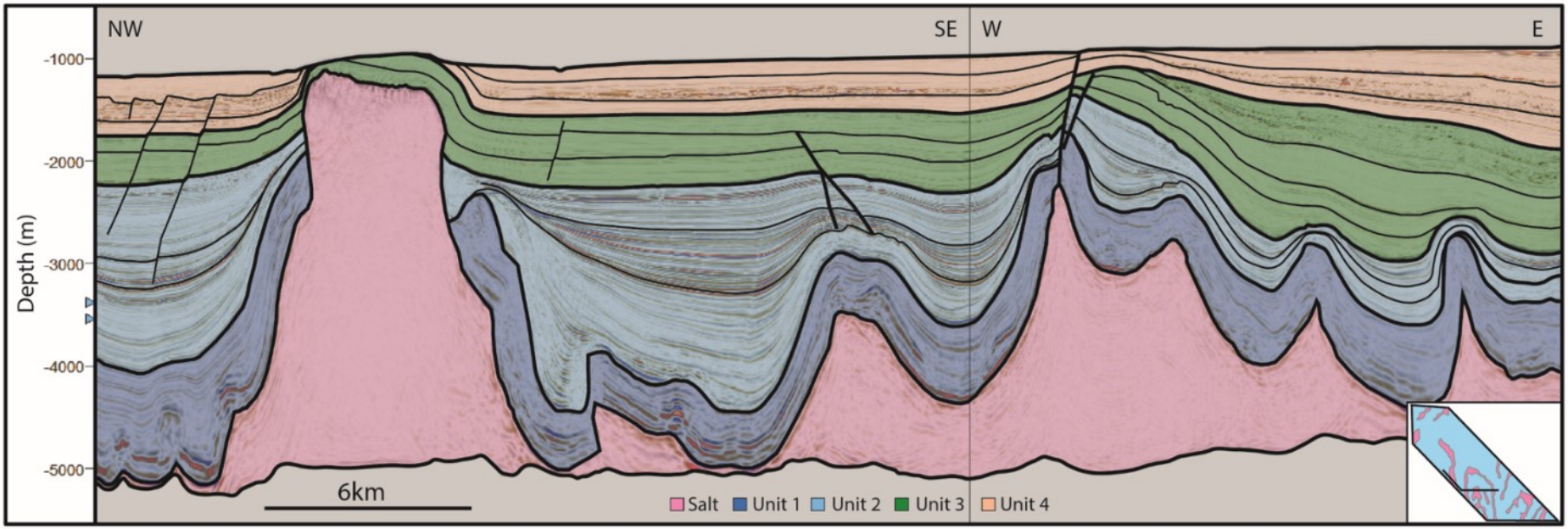

Figure 2.15 Seismic geosection through Set 3 salt structures (see inset map for location; note that line bends in order to cross a larger Set 3 salt wall, the only one to pierce the overburden). Note the isopachous nature of Unit 1 and prominent growth strata of Unit 2. Seismic data supplied by CGG.

way described for the early buckle folds in Section 2.6.1, but since the amplitude and wavelength of the folds is proportional to the overburden thickness, the folds generated in this case were larger (see Price and Cosgrove, 1990). Downdip welding during this time may also have served to enhance the deceleration and salt accumulation, though the timing of welding is difficult to constrain from the available data. Subsequent downbuilding and sediment loading then drove rapid growth of the anticlines, and in one case the differential loading was sufficient to actively pierce the roof (furthest west in Fig. 2.15).

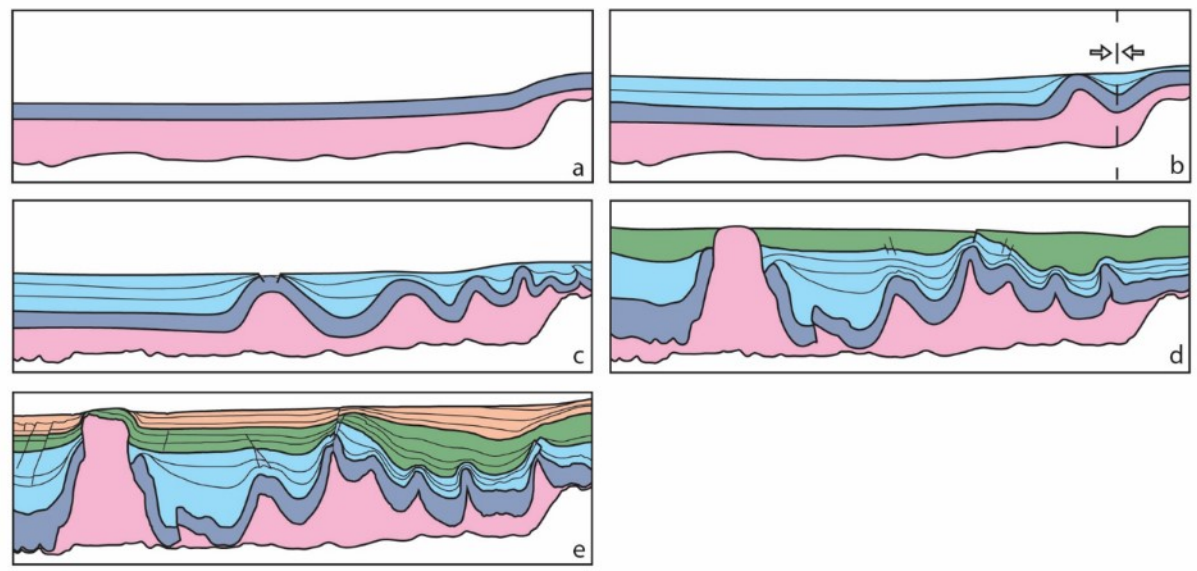

Figure 2.16 Schematic evolution of the Set 3 salt structures. Locations of each schematic time step shown in Figure 17. a) Pre-kinematic, isopachous deposition of Unit 1. b) Rapid growth of salt-cored anticlines. c) Salt-cored anticlines translated away from base-salt ramp and amplified by sediment loading. New ones develop in their place. d) Growth of anticlines slows and most become buried. The buoyancy associated with the oldest and largest anticline is enough to generate active rise and pierce the overburden. e) Present day geometry.

2.7 Synthesis

As described in Section 2.5, the geometry, position and orientation of the three main RSBs indicate c. 23.2 km of seaward translation, and up to 32° of rotation; this indicates that related salt structures are now situated a significant distance from where they originated. Fig. 2.17 shows the active salt-related deformation at each time step, as discussed below.

2.7.1 Albian

The broadly isopachous nature of the Albian indicates: (i) the seabed was broadly flat during its deposition, and thus that the salt had infilled relict, rift-related topography, and broadly thickened seaward; and (ii) regional gravity gliding commenced post-Albian (i.e. the RSBs are strictly post-Albian). However, Albian growth strata indicate that local thin-skinned deformation did occur in at least two areas at this time: (i) at the base of the ramp, in an area of salt and overburden contraction; and (ii) updip, outside of the area of data coverage, where we suggest that early extension drove formation of the somewhat enigmatic, slope-parallel, Set 2 salt rollers (Fig. 2.17a).

2.7.2 Upper Cretaceous to Eocene

Regional gliding had fully initiated by the end of the Albian, by which time the overburden had thickened and strengthened. This resulted in the development of the first RSB as the salt and overburden were translated over the base-salt ramp (Fig. 2.17b). As the thick salt continued to flow seaward, away from the ramp, accommodation was created adjacent to the ramp, producing landward-thickening and dipping growth packages that onlapped underlying Albian strata. The onset of regional gliding can be attributed to regional tilting of the base-salt driven by thermal subsidence to the SW within the deep basin (Brice et al., 1982; Hudec and Jackson, 2004). The angle necessary to create basin-scale gravitational instability and to thus induce regional gliding can be as little as 1-2° (Peel, 2014).

We suggest the salt-cored anticlines formed at this time at the base of the ramp as the mismatch in salt flux causes deceleration and contraction of the thickening overburden (Dooley et al., 2017). Syn-kinematic sediments accumulated within synclinal depocentres, driving further growth of the anticlines. Updip of the growing salt-cored anticlines, extension

continues to dominate the development of the Set 2 structures, creating rafts and turtle structures. Albian rafting has previously been documented elsewhere in the Kwanza Basin (Burollet, 1975; Duval et al., 1992; Lundin, 1992; Mauduit et al., 1997). In these studies the orientation of the early formed rafts was inferred to be parallel to the margin, although they were imaged on 2D seismic lines (i.e. the true relationship between base-salt dip, margin trend, and raft trend was unknown).

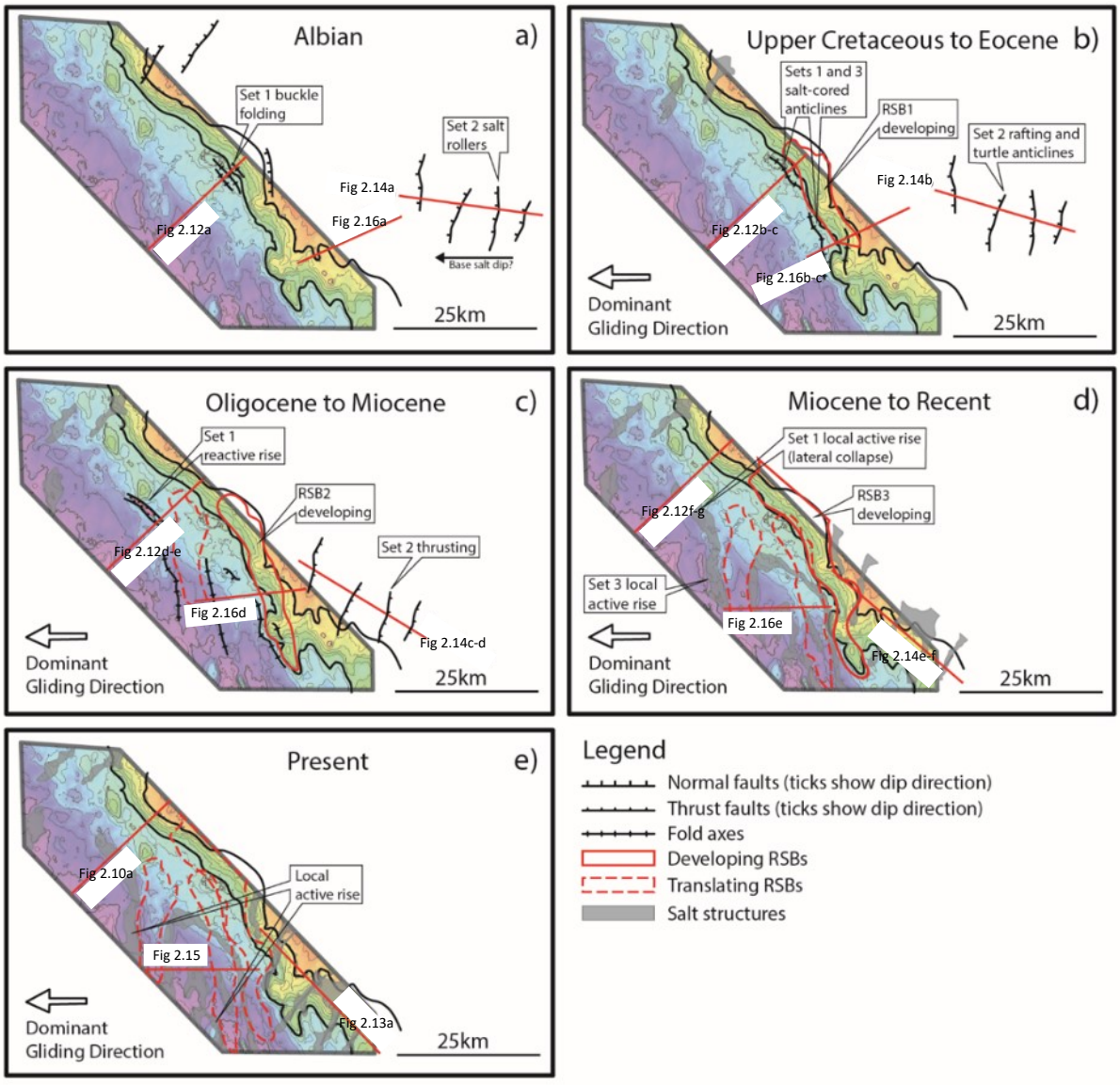

Figure 2.17 Reconstructed salt structure evolution through time using reconstructed positions of ramp syncline basins (see Figure 2.8). Shows active structures and development of RSBs at each time step, overlaid on map of base-salt relief. See Figures 2.12, 2.14 and 2.16 for schematic structural evolutions.

2.7.3 Oligocene to Miocene

The Set 1 salt structures are translated away from the base of the ramp and enter an extensional stress field, which transforms the salt-cored anticline into a reactive diapir (Fig. 2.17c). This extension may relate to local acceleration resulting from translation over a steeper part of the base-salt surface, which served to locally increase the rate of seaward salt flow. We argue that local rather than regional stresses drove this change in deformation style, given that the adjacent Set 2 structures enter a phase of contraction at this time.

Whilst structures within Sets 1 and 2 continued to grow during this period due to squeezing and reactive rise, those within Set 3 became inactive and were eventually buried.

2.7.4 Miocene to Recent

The RSBs record an increase in translation rate at this time (from c. 0.2 to 1 mm/yr), despite thinning of the salt (Fig. 2.9). This is attributed to margin uplift during the Miocene, which thereby increased gravitational instability (Lunde et al., 1992; Lundin, 1992; Hudec and Jackson, 2004). Thinning and onlapping of strata across major salt structures indicate that some were tall enough (relative to their overburden thickness) to actively rise and arch their overburden (Fig. 2.17d). Other structures were passively translated and buried as the salt source layer was too thin to feed them. Welds develop and translation rates consequently slowed.

2.7.5 Present

The salt thickness map shows that, at present, most of the study area adjacent to the well-developed salt walls is very close to welding (Fig. 2.5b). This means that there is increased basal drag on the salt, and that seaward translation of salt and overburden is correspondingly slow. The youngest strata still thicken into the youngest RSB, but rather than onlapping its seaward-dipping flank, they thin up onto the ramp, indicating basinward translation persists at a slow rate. This is further supported by the fact that the seabed shows no expression of the RSB, indicating that aggradation keeps up with the rate of displacement. Two salt structures continue to actively rise and thus deform the seabed, but the majority of salt structures are inactive and are being buried (Fig. 2.17e).

2.8 Discussion

Classic models of salt-influenced passive margins cannot explain the diversity of structural styles and orientations of the salt structures observed in the Outer Kwanza Basin, offshore Angola. Each salt structure set is associated with a unique structural evolution, with many showing evidence for multiple phases of reactivation and inversion. Another key observation is that phases of extension and contraction were synchronous in closely spaced salt structures (Fig. 2.18). This means we cannot appeal to basement-involved shortening as in the Inner Kwanza Basin (Hudec and Jackson, 2002). We suggest this complexity reflects the interaction of seaward salt flow with considerable base-salt topography. A key consequence of this process is that the mid-slope zone of translation, which in classic models is shown to be largely undeformed (Fig. 2.1a; see Jackson et al., 1994; Schultz-Ela, 2001; Fort et al. 2004; Hudec and Jackson, 2004; Brun and Fort, 2011; Peel, 2014), may in fact be an area of very complex deformation.

Salt deformation on the Angolan margin initiated early in response to gravity gliding but the interaction of salt flow with base-salt topography controlled the subsequent structural evolution, and produced a much more complicated set of salt structures than would typically be associated with salt-influenced passive margins (i.e. margin-parallel structures defining extensional, translational and compressional domains). Ramp syncline basins record more than 20 km of basinward salt flow, driven by gravity gliding as the base-salt dip is increased by thermal subsidence in the first instance and later by Tertiary uplift of the west African Margin.

Physical models by Dooley et al. (2017) and Dooley et al. (2018) show that the basinward flow of salt and overburden across base-salt relief can generate local extension and contraction anywhere along a margin. Because of this, pre-existing, diapiric and non-diapiric structures can be inverted multiple times as they migrate through these various stress fields. These local stress fields explain how structures from the Kwanza Basin comprise extensional diapirs which are subsequently squeezed during contraction, and folds which evolved into reactive diapirs due to late extension. These structures are very similar to those developed in the multi-ramp models by Dooley et al. (2018), with even greater complexities seen in models with isolated ramps (see their model 5; Fig. 2.16. These local stress fields also explain how structures

experience very different tectonic evolutions, depending on their starting position on the margin and path taken during downdip translation. Consequently, salt structures in the Kwanza Basin have complex evolutionary histories comprising phases of both extension and compression, and different salt structures are associated with different evolutionary histories as they respond to local stresses caused by the underlying topography over which they are translated.

In the Kwanza Basin, steep, seaward-dipping ramps, which change orientation along strike, had the greatest impact on salt-related deformation. Changes in the flux of salt over these ramps generate local stresses that deform the salt and its overburden. Convex- and concave-into-the-basin segments of the ramps may have also initiated locally divergent and convergent gliding (Cobbold and Szatmari, 1991; Tadeu dos Reis et al., 2008). The effect of these local stresses on overburden deformation depends on the thickness of the latter, and the presence and orientation of any pre-existing weaknesses (e.g. precursor diapirs).

Unlike the strike-elongate, broadly linear base-salt ramps, the more isolated, sub-circular base-salt highs are not obviously associated with any salt structures or specific style of overburden deformation. The reason for this is not yet clear, although this observation may suggest there is a critical ratio between salt thickness and relief height; i.e. a threshold value must be reached before stresses induced at the base of the salt are transferred into the overburden. Or put another way, low-relief features only produce stress perturbations sufficient to deform the overburden when the salt is very thin. An alternative interpretation for the apparent lack of structures above isolated base-salt highs is that any structures that did form have since been translated out of the study area or overprinted by later deformation. Other controls on the structural evolution of the salt and overburden which require further study include: sedimentation rate and distribution, the composition and rheology of both the salt (i.e. in case where the salt is mechanically layered; e.g. Van Gent et al., 2010; Fiduk and Rowan, 2012; Jackson et al., 2014, 2015) and overburden, and the role of active basement-involved tectonics.

This study concludes that, in this area downdip translation over base-salt topography played a key role in the structural evolution of the salt walls. The diversity of salt wall orientations and structural styles in the Kwanza Basin demonstrates the significant impact which salt flow

over base-salt topography can have on the structural evolution of the basin. We suggest that the effects of base-salt relief in the Kwanza Basin are important because the ratio of base-salt relief to depositional salt thickness is high. Only when this ratio is low (e.g. for a smooth base-salt surface) may simple models of gravity gliding and spreading accurately capture the origin and evolution of salt structures on a margin.

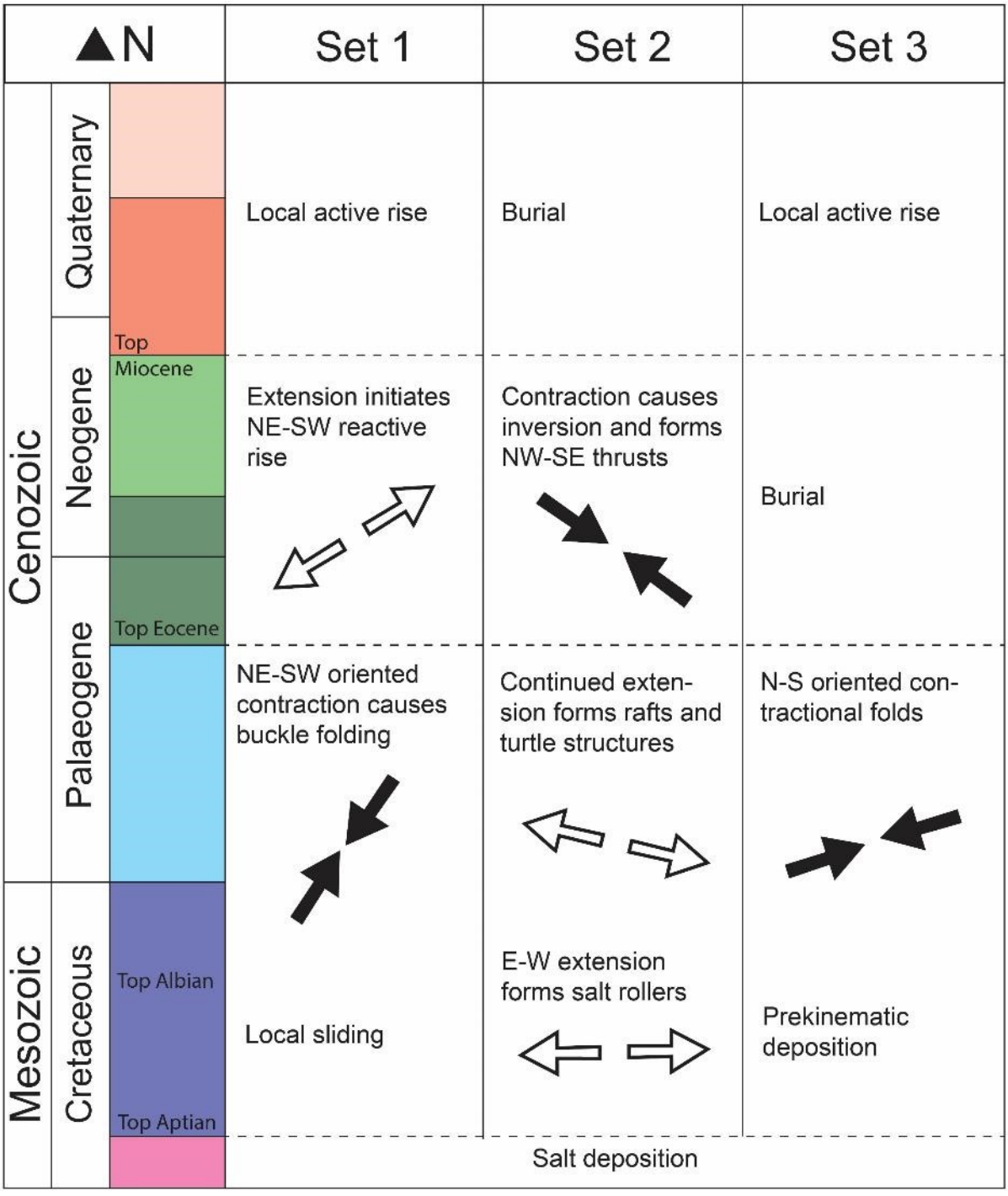

Figure 2.18 Summary chart

2.9 Conclusions

We used 3D seismic data to reconstruct the tectono-stratigraphic evolution of the Outer Kwanza Basin, with the aim being to investigate how the interaction of salt flow with base-salt relief influenced the origin and growth of salt structures on the margin. The key conclusions of our study are:

- Ramp-syncline basins record a minimum of 23 km of translation and 32 degrees of rotation in the mid-slope domain of the Outer Kwanza Basin
- Clockwise direction of rotation suggests increasing velocities, and therefore increasing salt thickness, to the south
- Salt tectonics in the Kwanza Basin is characterised by advanced diapiric salt structures. The salt structures can be divided broadly into three sets characterised by their orientations and structural styles.
- The stratigraphic relationships in the overburden indicate that the evolutionary history of each set is unique and cannot be explained in terms of conventional models of gravity gliding and gravity spreading on salt-influenced passive margins.

The effects of salt flow over base-salt relief played a crucial role in the development of the salt structures. The local variations in salt flux cause local compression or extension, thereby fundamentally controlling the spatial distribution, orientation and structural style of the salt structures.

References

Bally, A.W., 1981. Thoughts on the tectonics of folded belts. Geological Society, London, Special Publications, 9(1), pp.13-32.

Bond, G., 1978. Evidence for late Tertiary uplift of Africa relative to North America, South America, Australia and Europe. The Journal of Geology, 86(1), pp.47-65.

Brice, S.E., Cochran, M.D., Pardo, G. and Edwards, A.D., 1982. Tectonics and Sedimentation of the South Atlantic Rift Sequence: Cabinda, Angola: Rifted Margins: Field Investigations of Margin Structure and Stratigraphy.

Brink, A.H., 1974. Petroleum geology of Gabon basin. AAPG Bulletin, 58(2), pp.216-235.

Brown, A.R., 2011. Interpretation of three-dimensional seismic data. Society of Exploration Geophysicists and American Association of Petroleum Geologists.

Brun, J.P. and Fort, X., 2011. Salt tectonics at passive margins: Geology versus models. Marine and Petroleum Geology, 28(6), pp.1123-1145.

Burollet, P.F., 1975. Tectonique en radeaux en Angola. Bulletin de la Société géologique de France, 7(4), pp.503-504.

Cobbold, P.R. and Szatmari, P., 1991. Radial gravitational gliding on passive margins. Tectonophysics, 188(3-4), pp.249-289.

Dooley, T.P. and Hudec, M.R., 2017. The effects of base-salt relief on salt flow and suprasalt deformation patterns—Part 2: Application to the eastern Gulf of Mexico. Interpretation, 5(1), pp.SD25-SD38.

Dooley, T.P., Hudec, M.R., Carruthers, D., Jackson, M.P. and Luo, G., 2017. The effects of base-salt relief on salt flow and suprasalt deformation patterns—Part 1: Flow across simple steps in the base of salt. Interpretation, 5(1), pp.SD1-SD23.

Dooley, T.P., Hudec, M.R., Pichel, L.M. and Jackson, M.P., 2018. The impact of base-salt relief on salt flow and suprasalt deformation patterns at the autochthonous, paraautochthonous and allochthonous level: insights from physical models. Geological Society, London, Special Publications, 476, pp.SP476-13.

Duffy, O.B., Dooley, T.P., Hudec, M.R., Jackson, M.P., Fernandez, N., Jackson, C.A. and Soto, J.I., 2018. Structural evolution of salt-influenced fold-and-thrust belts: a synthesis and new insights from basins containing isolated salt diapirs. *Journal of Structural Geology*, *114*, pp.206-221.

Duval, B., Cramez, C. and Jackson, M.P.A., 1992. Raft tectonics in the Kwanza basin, Angola. Marine and Petroleum Geology, 9(4), pp.389-404.

Evans, R., 1978. Origin and significance of evaporites in basins around Atlantic margin. AAPG Bulletin, 62(2), pp.223-234.

Fort, X., Brun, J.P. and Chauvel, F., 2004. Contraction induced by block rotation above salt (Angolan margin). Marine and Petroleum Geology, 21(10), pp.1281-1294.

Gaullier, V., Brun, J.P., Gue, G. and Lecanu, H., 1993. Raft tectonics: the effects of residual topography below a salt decollement. Tectonophysics, 228(3-4), pp.363-381.

Hudec, M.R. and Jackson, M.P., 2002. Structural segmentation, inversion, and salt tectonics on a passive margin: Evolution of the Inner Kwanza Basin, Angola. Geological Society of America Bulletin, 114(10), pp.1222-1244.

Hudec, M.R. and Jackson, M.P., 2004. Regional restoration across the Kwanza Basin, Angola: Salt tectonics triggered by repeated uplift of a metastable passive margin. AAPG bulletin, 88(7), pp.971-990.

Hudec, M.R., Norton, I.O., Jackson, M.P. and Peel, F.J., 2013. Jurassic evolution of the Gulf of Mexico salt basin. AAPG bulletin, 97(10), pp.1683-1710.

Jackson, M.P. and Hudec, M.R., 2005. Stratigraphic record of translation down ramps in a passive-margin salt detachment. Journal of Structural Geology, 27(5), pp.889-911.

Jackson, M.P. and Hudec, M.R., 2017. Salt tectonics: Principles and practice. Cambridge University Press.

Jackson, M.P., Hudec, M.R., Fraenkl, R., Sikkema, W., Binga, L. and Da Silva, J., 2001. Minibasins translating down a basement ramp in the deepwater monocline province of the Kwanza Basin, Angola [abs.]. In American Association of Petroleum Geologists Annual Meeting Official Program (Vol. 10, p. A99).

Jackson, M.P., Vendeville, B.C. and Schultz-Ela, D.D., 1994. Structural dynamics of salt systems. Annual Review of Earth and Planetary Sciences, 22(1), pp.93-117.

Karner, G.D. and Gambôa, L.A.P., 2007. Timing and origin of the South Atlantic pre-salt sag basins and their capping evaporites. Geological Society, London, Special Publications, 285(1), pp.15-35.

Lavier, L.L., Steckler, M.S. and Brigaud, F., 2001. Climatic and tectonic control on the Cenozoic evolution of the West African margin. Marine Geology, 178(1-4), pp.63-80.

Lentini, M.R., Fraser, S.I., Sumner, H.S. and Davies, R.J., 2010. Geodynamics of the central South Atlantic conjugate margins: implications for hydrocarbon potential. Petroleum Geoscience, 16(3), pp.217-229.

Lunde, G., Aubert, K., Lauritzen, O. and Lorange, E., 1992. Tertiary uplift of the Kwanza Basin in Angola. Géologie Africaine: Coll. Géol. Libreville, Recueil des Communications. Elf Aquitaine, Boussens, France, pp.99-117.

Lundin, E.R., 1992. Thin-skinned extensional tectonics on a salt detachment, northern Kwanza Basin, Angola. Marine and Petroleum Geology, 9(4), pp.405-411.

Marton, L.G., Tari, G.C. and Lehmann, C.T., 2000. Evolution of the Angolan passive margin, West Africa, with emphasis on post-salt structural styles. Geophysical Monograph-American Geophysical Union, 115, pp.129-150.

Mauduit, T., Guerin, G., Brun, J.P. and Lecanu, H., 1997. Raft tectonics: the effects of basal slope angle and sedimentation rate on progressive extension. Journal of Structural Geology, 19(9), pp.1219-1230.

Peel, F.J., 2014. The engines of gravity-driven movement on passive margins: Quantifying the relative contribution of spreading vs. gravity sliding mechanisms. Tectonophysics, 633, pp.126-142.

Peel, F., Jackson, M. and Ormerod, D., 1998. Influence of major steps in the base of salt on the structural style of overlying thin-skinned structures in deep water Angola. In American Association of Petroleum Geologists International Conference and Exhibition, Rio de Janeiro, Brazil, November, Extended Abstracts Volume (pp. 366-367).

Pichel, L.M., Peel, F., Jackson, C.A. and Huuse, M., 2018. Geometry and kinematics of salt-detached ramp syncline basins. Journal of Structural Geology, 115, pp.208-230.

Pichel, L.M., Jackson, C.A.L., Peel, F. and Dooley, T.P., 2019. Base-Salt Relief Controls on Salt-Tectonic Structural Style, São Paulo Plateau, Santos Basin, Brazil. Basin Research.

Price, N.J. and Cosgrove, J.W., 1990. Analysis of geological structures. Cambridge University Press.

Quirk, D.G., Schødt, N., Lassen, B., Ings, S.J., Hsu, D., Hirsch, K.K. and Von Nicolai, C., 2012. Salt tectonics on passive margins: examples from Santos, Campos and Kwanza basins. Geological Society, London, Special Publications, 363(1), pp.207-244.

Rowan, M.G., Peel, F.J., Vendeville, B.C. and Gaullier, V., 2012. Salt tectonics at passive margins: Geology versus models–Discussion. Marine and Petroleum Geology, 37(1), pp.184-194.

Schultz-Ela, D.D., 2001. Excursus on gravity gliding and gravity spreading. Journal of Structural Geology, 23(5), pp.725-731.

Spathopoulos, F., 1996. An insight on salt tectonics in the Angola Basin, South Atlantic. Geological Society, London, Special Publications, 100(1), pp.153-174.

Tadeu dos Reis, A., Gorini, C., Weibull, W., Perovano, R., Mepen, M. and Ferreira, É., 2008. Radial gravitational gliding indicated by subsalt relief and salt-related structures: the example of the Gulf of Lions, western Mediterranean. Revista Brasileira de Geofísica, 26(3), pp.347-365.

Vendeville, B.C. and Jackson, M.P., 1992a. The rise of diapirs during thin-skinned extension. Marine and Petroleum Geology, 9(4), pp.331-354.

Vendeville, B.C. and Jackson, M.P.A., 1992b. The fall of diapirs during thin-skinned extension. Marine and Petroleum Geology, 9(4), pp.354-371.

von Nicolai, C., 2011. The Interplay of Salt Movements and Regional Tectonics at the Passive Continental Margin of the South Atlantic, Kwanza Basin. Unpublished PhD thesis. Universität Potsdam. [https://goo.gl/8LwQBY]

Walford, H.L. and White, N.J., 2005. Constraining uplift and denudation of west African continental margin by inversion of stacking velocity data. Journal of Geophysical Research: Solid Earth, 110(B4).

Weijermars, R., Jackson, M.T. and Vendeville, B., 1993. Rheological and tectonic modeling of salt provinces. Tectonophysics, 217(1-2), pp.143-174.

3 Intrasalt Structure and Strain Partitioning in Layered Evaporites: Implications for Drilling Through Messinian Salt in the Eastern Mediterranean

This manuscript is currently under review with **Petroleum Geoscience**.

A pre-print is available on **EarthArxiv**:

https://eartharxiv.org/repository/view/146/

Acknowledgements

The data used in this study is confidential and was generously provided under license by the Lebanese Petroleum Administration. I would like to gratefully acknowledge Ramadan Ghalayini for help acquiring the data, and Wissam Chbat for sanctioning the material for publication. I would also like to thank my supervisor and co-author, Chris Jackson, for valuable discussions that guided my interpretation of the data, and help with editing the manuscript.

Abstract

We use 3D seismic reflection data from the Levant margin, offshore Lebanon to investigate the structural evolution of the Messinian evaporite sequence, and how intrasalt strain varies within a thick salt sheet during early-stage salt tectonics. Intra-Messinian reflectivity reveals lithological heterogeneity within the otherwise halite-dominated sequence. This leads to rheological heterogeneity, with the different mechanical properties of the various units controlling strain accommodation within the deforming salt sheet. We assess the distribution and orientation of structures, and show how intrasalt strain varies both laterally and vertically along the margin. We argue that units appearing weakly strained in seismic data, may in fact accommodate considerable sub-seismic or cryptic strain. We also argue that the intrasalt stress state varies through time and space in response to the gravitational forces driving deformation. We conclude that efficient drilling through thick, heterogeneous salt requires a holistic understanding of the mechanical and kinematic development of the salt and its overburden. This will also enable us to build better velocity models that account for intrasalt lithological and structural complexity in order to accurately image sub-salt geological structures.

3.1 Introduction

Thick salt deposits have a dramatic effect on the subsequent structural evolution of a basin due to their unique ability to behave as a fluid on geological timescales, and thus to flow in response to gravitational driving forces (e.g. Jackson et al., 1994; Jackson, 1995; Hudec and Jackson, 2007; Jackson and Hudec, 2017). The interaction between sedimentation and salt deformation can lead to extreme structural complexity in salt-influenced basins, which presents unique challenges when exploring for and producing hydrocarbons from the subsurface (e.g. Quirk et al., 2012).

Advances in seismic imaging have revolutionised our understanding of the way in which overburden rocks are deformed by flowing salt. However, due to its characteristic chaotic and transparent appearance in seismic reflection data, the internal composition and kinematics of salt bodies have been overlooked. Salt is frequently thought of as a homogeneous body composed of pure halite, but exposures of salt in mines (e.g. Balk, 1949; Hoy et al., 1962; Kupfer, 1962; Miralles et al., 2001; Schleder et al., 2008; Burliga et al., 2018) and in the field (e.g. Zak and Freund, 1980; Jackson et al., 1990; Talbot, 1998), as well as geophysical subsurface data (Van Gent et al., 2011; Strozyk et al., 2012; Jackson et al., 2015; Raith et al., 2016), show that most evaporitic sequences are in fact lithologically heterogeneous (Fig. 3.1) (see also Rowan et al., 2019). Despite this, the impact of this lithological heterogeneity on the resulting intrasalt deformation and structural evolution is poorly understood.

The young Messinian (latest Miocene) salt giant in the Mediterranean provides a perfect natural laboratory to study active, early-stage salt tectonics of a thick, lithologically heterogeneous salt sheet. The Messinian Salinity Crisis (MSC) is a remarkable geological event that occurred between 5.96 and 5.33 Ma (e.g. Gautier et al., 1994; Ryan, 2009; Roveri et al., 2014). During this time, the Mediterranean Sea was isolated from the Atlantic due to the closure of the Gibraltar Straits, causing rapid evaporitic drawdown and extensive salt precipitation. This resulted in the widespread deposition of a thick (up to 2 km), layered evaporite unit across much of the Mediterranean basin. When the Straits reopened in the Pliocene, the Mediterranean was flooded by marine Atlantic waters, and a clastic overburden (up to 1.5 km thick) was deposited above the salt. Tectonically-driven tilting of the basin margins, as well as differential loading of the salt by prograding clastic wedges, triggered

gravity-driven deformation of the Messinian salt, resulting in the development of kinematically-linked zones of updip extension and downdip contraction (Fig. 3.2) (Cartwright and Jackson, 2008; Gvirtzman et al., 2013; Allen et al., 2016). Salt-related deformation in the Levantine Basin is thought to be dominantly driven by gravity gliding in the north (due to tilting of the margin), and by gravity spreading in the south (due to loading of the salt where the Nile delta is prograding into the basin) (Allen et al., 2016). This gravity-driven deformation of the salt remains active to the present day.

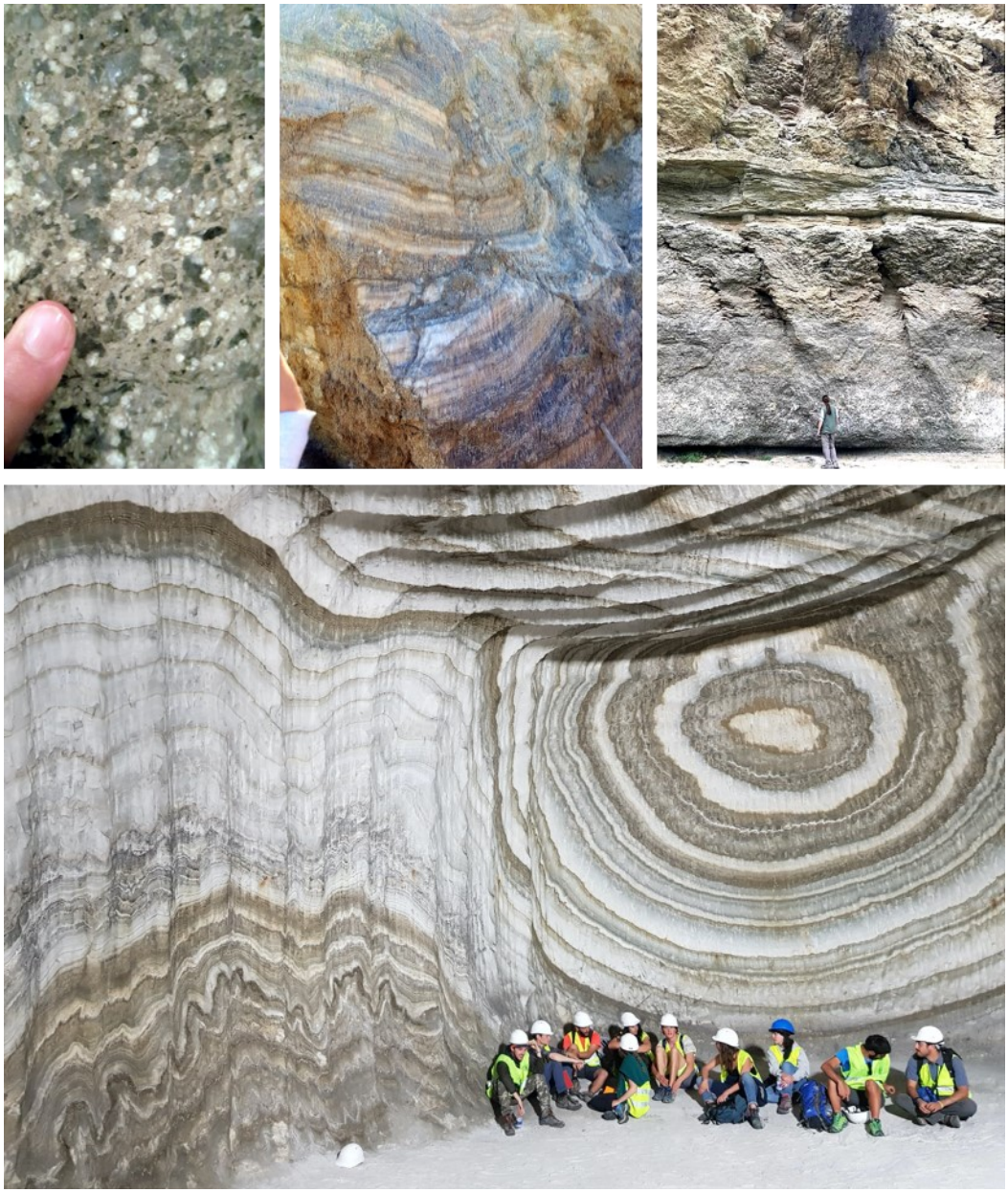

Figure 3.1 Compositional intrasalt heterogeneities on a range of scales: a) Coarse, angular crystals of halite and anhydrite in a clay-rich matrix from the Serravallian evaporite sequence exposed in the Wieliczka Salt Mine, situated close to Krakow in Poland; b) Interbedded layers of halite, gypsum and anhydrite from the Late Miocene-Pliocene evaporite sequence of the Mount Sodom diapir, Israel; c) Microbial gypsum trees and layered gypsum deposits in Sorbas, southern Spain; d) Deformed layers of Messinian age halite, gypsum, anhydrite ad clay layers exposed in the Realmonte salt mine, Sicily.

In recent years the eastern Mediterranean region has attracted renewed interest from petroleum explorers. Following the Zohr discovery offshore Egypt in 2015, the proven pre-salt plays have become the focus of intense exploration efforts (Esestime et al., 2016). Accurate seismic imaging of the subsalt geology is necessary to successfully target prospects in the pre-salt. Velocity models must therefore consider the complex lithological heterogeneity and internal structure of the Messinian salt. Furthermore, determining the stress state within the deforming salt sheet is important for safe and efficient drilling through the thick, actively flowing salt. For example, Weijermars and Jackson (2014) show that wells drilling through thick salt are at greater risk of lost time and are overall costlier, primarily due to issues related to wellbore stability. Many of these issues could be mitigated by planning well paths that account for the present and likely future stress state within the salt. However, due to typically poor seismic imaging within thick salt, and a lack of outcrop and well data, there have been relatively few studies to constrain the relationship between the intrasalt stratigraphy, structure and the evolution of stress and strain within the deforming salt sheet.

Furthermore, the few previous studies investigating Messinian intrasalt deformation have yielded contradictory results. Cartwright et al. (2012) calculate strain on intrasalt layers using seismic data from offshore Israel (Fig. 3.2) and interpret an asymmetric Poiseuille flow profile, suggesting a dominantly pressure-induced flow (Fig. 3.3a). In contrast, Cartwright et al. (2018) and Kirkham et al., (2019) more recently identified deformed gas pipes within the salt in the deep Levantine Basin (Fig. 3.2), which if taken as direct kinematic indicators suggest a Couette flow profile, indicative of drag-induced flow (Fig. 3.3b). In this study, we use a 3D seismic reflection dataset located offshore Lebanon in the northern Levantine Basin (Fig. 3.2) to investigate how intrasalt structure and strain develop within thick salt during the early phase of evaporite deformation. We compare our results to those arising from previous studies and thus attempt to resolve existing contradictions regarding intrasalt flow. Insights gathered from the Mediterranean can also be used to develop our understanding of intrasalt structure and kinematics in other salt-influenced basins around the world.

3.2 Data and Methods

Because the Messinian evaporite sequence is young, shallow, and only weakly deformed, it is well-imaged by seismic reflection data. The large (c. 10,000 km^2) 3D seismic reflection dataset used in this study is located offshore Lebanon (Fig. 3.2). It has near-zero phase with reverse polarity, i.e. an increase in acoustic impedance (hard kick) corresponds to a negative amplitude, coloured red (a trough), while a decrease in acoustic impedance (soft kick) corresponds to a positive amplitude, coloured black/blue (a peak). The seismic data are presented in two-way-time (TWT) and dimensions quoted in ms TWT are estimated in equivalent depth using velocities given by Reiche et al. (2014) and Feng et al. (2016) for the intrasalt units and overburden. The vertical resolution (λ/4) of the Messinian interval is estimated to be 16.8 m using an average velocity of 4200 m/s, but this varies with precise composition. In this study we investigate the nature and distribution of intrasalt and supra-salt deformation by mapping intrasalt reflections and seismic facies within the Messinian salt, analysing stratigraphic relationships within the salt and overburden, generating structure maps, and measuring intrasalt strain.

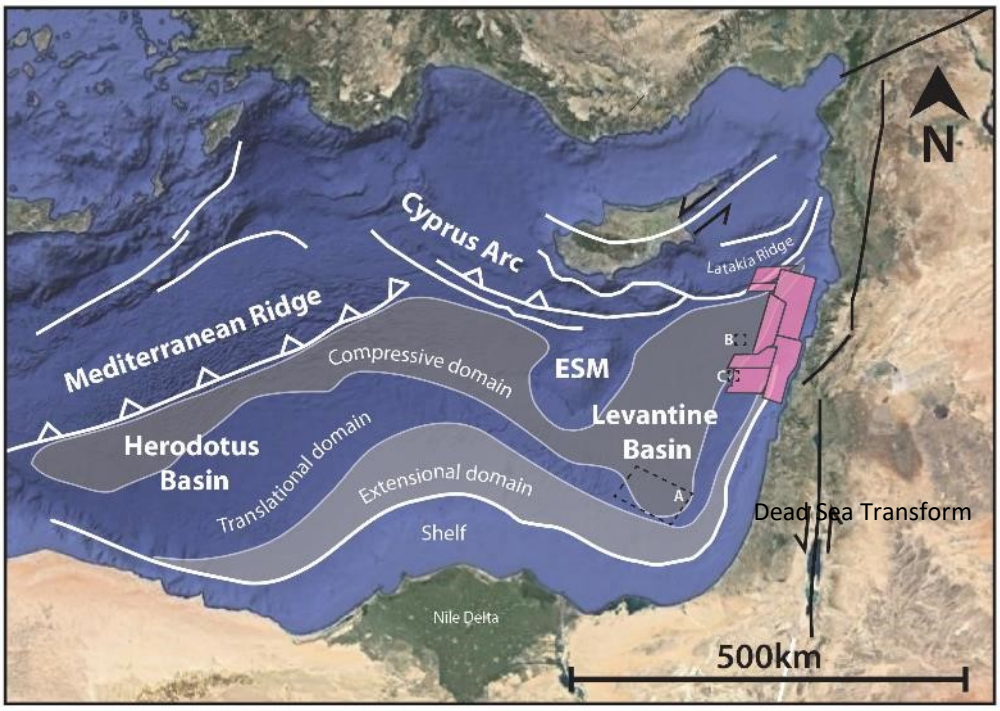

Figure 3.2 Location of 3D seismic data used in this study (pink polygons), and regional context showing distribution of key tectonic elements in the eastern Mediterranean (modified from Allen et al. 2016). ESM = Eratosthenes Seamount. Boxes A, B and C indicate the locations of previous studies by Cartwright et al., (2012), Cartwright et al., (2018) and Kirkham et al., (2019) respectively.

Reflections within the Messinian evaporite sequence allow us to measure strain at different levels within the deforming salt sheet. We follow Cartwright et al. (2012) and calculate the strain along mapped intrasalt reflections on a series of seismic cross-sections through the contractional domain (dominated by reverse shear zones and related folds; this allows us to examine how strain varies horizontally and vertically across the study area. 2D sections are taken perpendicular to the dominant structural trend (NNE-SSW), which is thus parallel to the direction of bulk salt flow (WNW). Strain is calculated using simple line-length analysis on individual reflections (i.e. change in line length divided by original line length; Fig. 3.4). Line-length analysis measures the total undeformed length of the same horizon, and thus only includes deformation due to seismically-resolved faulting and folding.

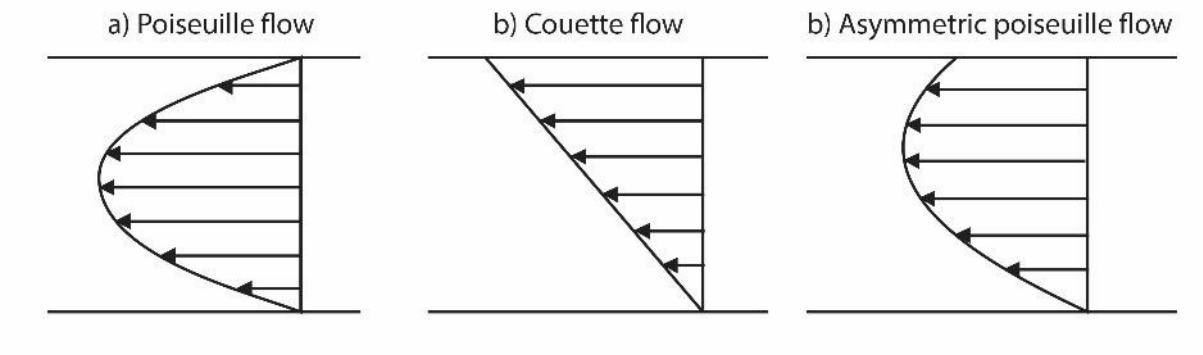

Figure 3.3 Idealised flow profiles through a viscous salt sheet: (A) Poiseuille flow (pressure-induced), (B) Couette flow (drag-induced), and (C) asymmetric Poiseuille flow (combination of pressure- and drag-induced).

A similar approach to calculating strain has been previously applied in many different tectonic settings, both with and without salt, using seismic data and/or analogue models (e.g. Cartwright et al., 2012; Burberry, 2015; Coleman et al., 2017; Butler and Paton, 2010; Steventon et al., 2019). This method assumes plane strain deformation and preservation of bed lengths and areas, and thus provides a minimum estimate of shortening. It does *not* include tectonic layer-parallel compaction, which would thicken the layers prior to thrusting and folding. Where reflections are truncated by the overburden, we extrapolate them to where they would intersect with the projected shear zone plane (e.g. Fig. 3.9). This introduces greater uncertainty in the uppermost layers, but the resulting trends are consistent with those observed even where the evaporite sequence is fully preserved. We therefore design this study to analyse and interpret relative, rather than absolute, values in strain magnitude.

Since the measurements of bed-length are dominantly sub-horizontal, lateral velocity variations would not impact these significantly and so the vertical axis of the seismic data is given in two-way-time (TWT). We conclude our study by comparing our results to previous seismic-based studies of intrasalt strain distribution, and integrating observations from exposures of compositionally analogous deformed evaporites.

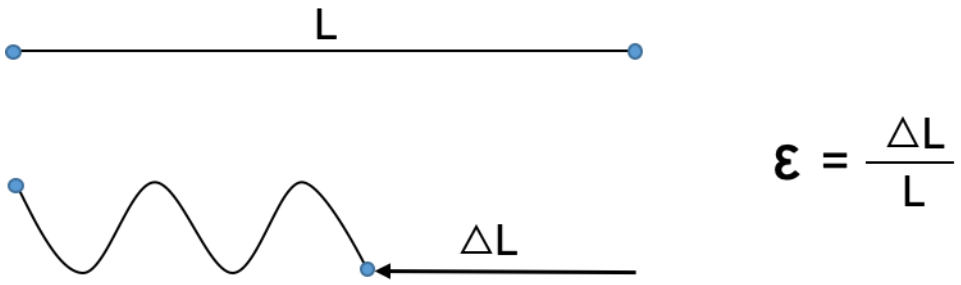

Figure 3.4 Calculation of strain using preservation of bed lengths during contraction (change in length as a proportion of original bed length).

3.3 Geological Setting

The East Mediterranean Basin comprises two sub-basins; the Levantine Basin to the east and the Herodotus Basin to the west, separated by the Eratosthenes Seamount (Fig. 3.2). The basins contain up to 20 km of clastic material overlying thin, oceanic crust (Aal et al., 2000). The seismic data used in this study is situated offshore Lebanon, on the eastern passive margin of the Levantine Basin (Fig. 3.2).

The eastern Mediterranean is a tectonically complex region. Ongoing convergence between the northward-migrating African plate and the stable Eurasian plate gives rise to active subduction zones along the northern and western basin margins (Ben-Avraham, 1978). The deformation front of the Cyprus Arc, dominated by the Latakia Ridge, forms the northern boundary, in a location where remnant Tethyan oceanic crust is being subducted (Hall et al., 2005). The eastern extension of the Hellenic Arc, forming an accretionary wedge known as the Mediterranean Ridge, bounds the basin to the west.

The Levant passive margin provides the eastern limit to the basin (Hawie et al., 2013). N-S oriented strike-slip faulting occurs onshore in association with the Dead Sea Transform Zone,

and the northwards motion of the Arabian plate relative to the African plate. The north African passive margin forms the southern boundary, where the Nile river system is draining the African continental interior and supplying large quantities of clastic material to the basin. The Nile Delta is therefore rapidly prograding northward out into the basin.

The present structure of the basin thus records the complex interplay of thick-skinned tectonic processes related to the geodynamic boundary conditions, and thin-skinned tectonics due to the gravitationally-driven flow of the Messinian evaporites.

3.4 Margin Characterisation

In this section we focus on characterising the structure and stratigraphy of the salt and overburden imaged in the present dataset. In the proceeding section we then integrate these observations to present an interpretation of the salt tectonics.

3.4.1 Sub-Salt Structure

The base-salt surface dips predominantly to the NW but the precise dip direction rotates laterally along the margin, from a more WNW dip in the northern part of the study area to a more NNW dip at the southern edge of the study area (Fig. 3.5 and Fig. 3.6). This margin geometry is the structurally shallow expression of the Saida-Tyr Platform, also known as the Levant Ramp; a SW-trending, inversion-related high that extends from the Levant margin into the deep basin, and which was formed during Late Cretaceous continental collision (Nader et al., 2018; Hodgson, 2012).

Where the shelf edge protrudes into the basin in the south, the upper shelf plateau is incised by several Messinian (or post-Messinian) canyons (Fig. 3.6). Similar features have been described on the southern Levant margin, offshore Israel, where they are inferred to provide evidence for sea level drawdown during the Messinian Salinity Crisis (e.g. Bertoni and Cartwright, 2007). The Latakia Ridge crosses the northwestern corner of the dataset and is expressed as a large, arcuate, broadly NE-trending anticline on both the base-salt and top-salt surfaces (Fig. 3.6 and Fig. 3.7).

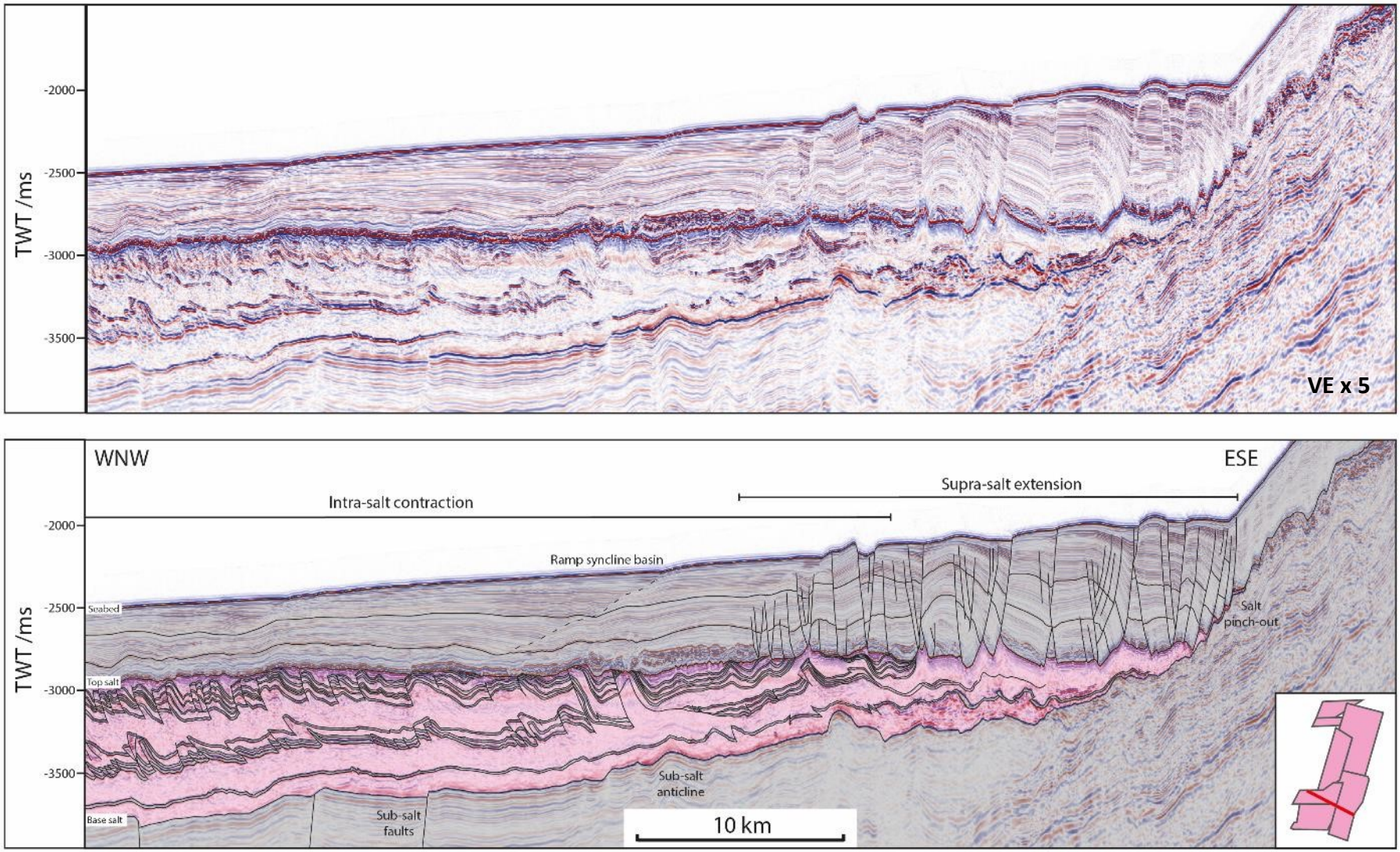

Figure 3.5 Seismic section (upper) and interpretation (lower) showing updip supra-salt extension where salt pinches out, and deformed intrasalt reflections truncating against top-salt. Location shown on inset map and Figures 6 and 7.

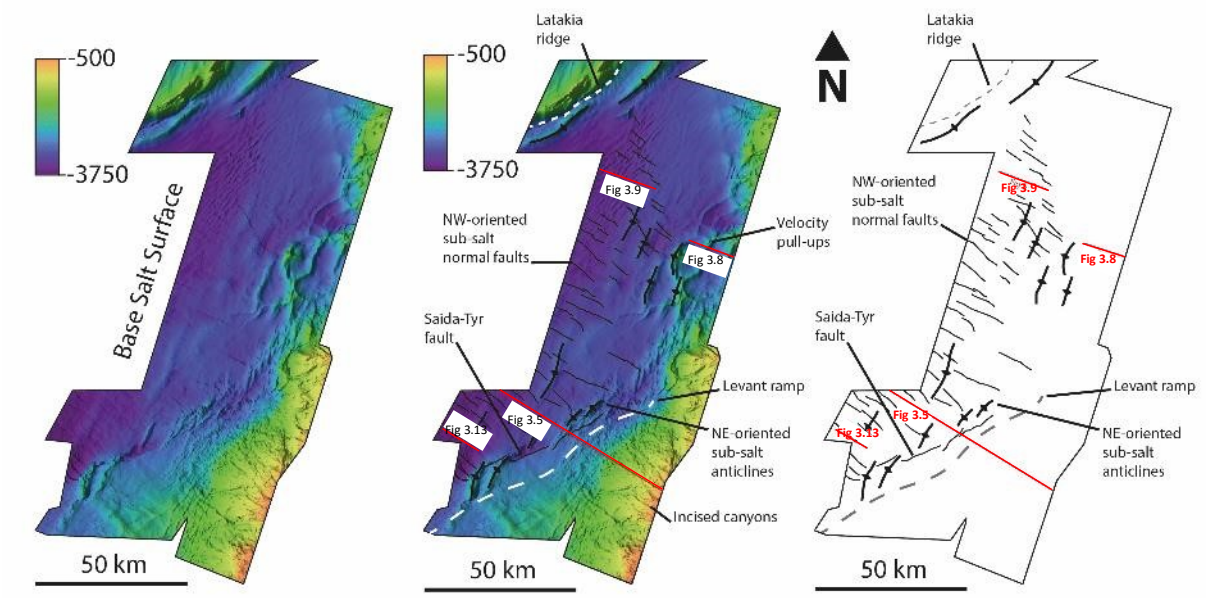

Figure 3.6 Annotated structure map showing relief on the base-salt surface, in particular the distribution of sub-salt anticlines and normal faults.

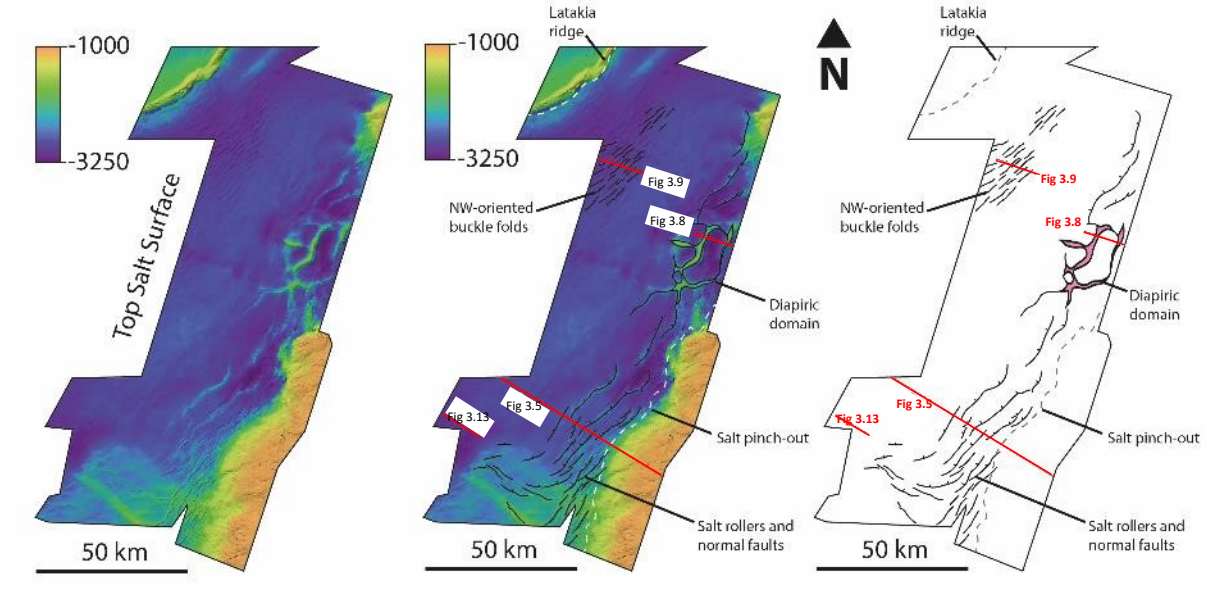

Figure 3.7 Annotated structure map showing relief on the top-salt surface, in particular the distribution of supra-salt normal faults, reactive diapirs and buckle folds.

A series of NW-SE-striking, relatively short (up to 6 km) and small-displacement (c. 30-60 ms TWT or c. 45-60 m) normal faults offset the base-salt in the deeper basin (Fig. 3.6). In cross-section these appear to be layer-bound, sub-salt restricted normal faults that terminate at the base-salt. These faults have been interpreted as syn-sedimentary, active during the late Miocene, and are attributed to an anisotropic extensional stress field (Ghalayini et al. 2017; Reiche et al, 2014).

Other features of particular interest on the base-salt surface include the prominent NE-trending anticlines that have relief of up to 650 ms (c. 1 km) (Fig. 3.6). The folds are 8-28 km long and 2-3 km wide. These features are definitively not salt-related velocity pull-ups (i.e. geophysical artefacts) given that the salt is thinner (as opposed to thicker) over their crests. These anticlines initially formed during the Late Miocene due to NW-SE regional tectonic compression, prior to the Messinian Salinity Crisis, though it is possible they may have been amplified during later shortening (Ghalayini et al. 2014).

3.4.2 Supra-Salt Structure

Normal faults and reactive diapirs dominate the updip edge of the margin, delineating an extensional regime, although the type and orientation of extensional structures vary along the margin (Fig. 3.5 and Fig. 3.7). In the northern part of the study area, supra-salt extension is accommodated by a polygonal network of mature reactive diapirs and salt rollers (Fig. 3.7). The reactive diapirs have a characteristic triangular shape in cross-section and are associated with inward-dipping normal faults across their crests (Fig. 3.8). This style of diapirism contrasts markedly with the southern part of the study area, where extension is accommodated by salt-detached normal faults, sometimes associated with small salt rollers, that are parallel or sub-parallel to the NE-oriented margin. Mature, high-relief reactive diapirs are absent in the south of the present dataset (Fig. 3.7).

Further south along the margin, offshore Israel, high-relief reactive diapirs are also absent in the extensional domain; only salt rollers occur. The reactive, high-relief diapirs therefore appear to be a relatively localised feature along the Levantine margin. However, similar diapiric structures have been documented around the circum-Nile deformation belt (CNDB) (e.g. Allen et al., 2016), and in the equivalent Messinian basins of the western Mediterranean

(e.g. Gulf of Lions; dos Reis et al., 2005). The polygonal distribution of these structures seems to suggest that the local differential stress (σ2 - σ3) in this area is small, and as such the structures show no preferred alignment.

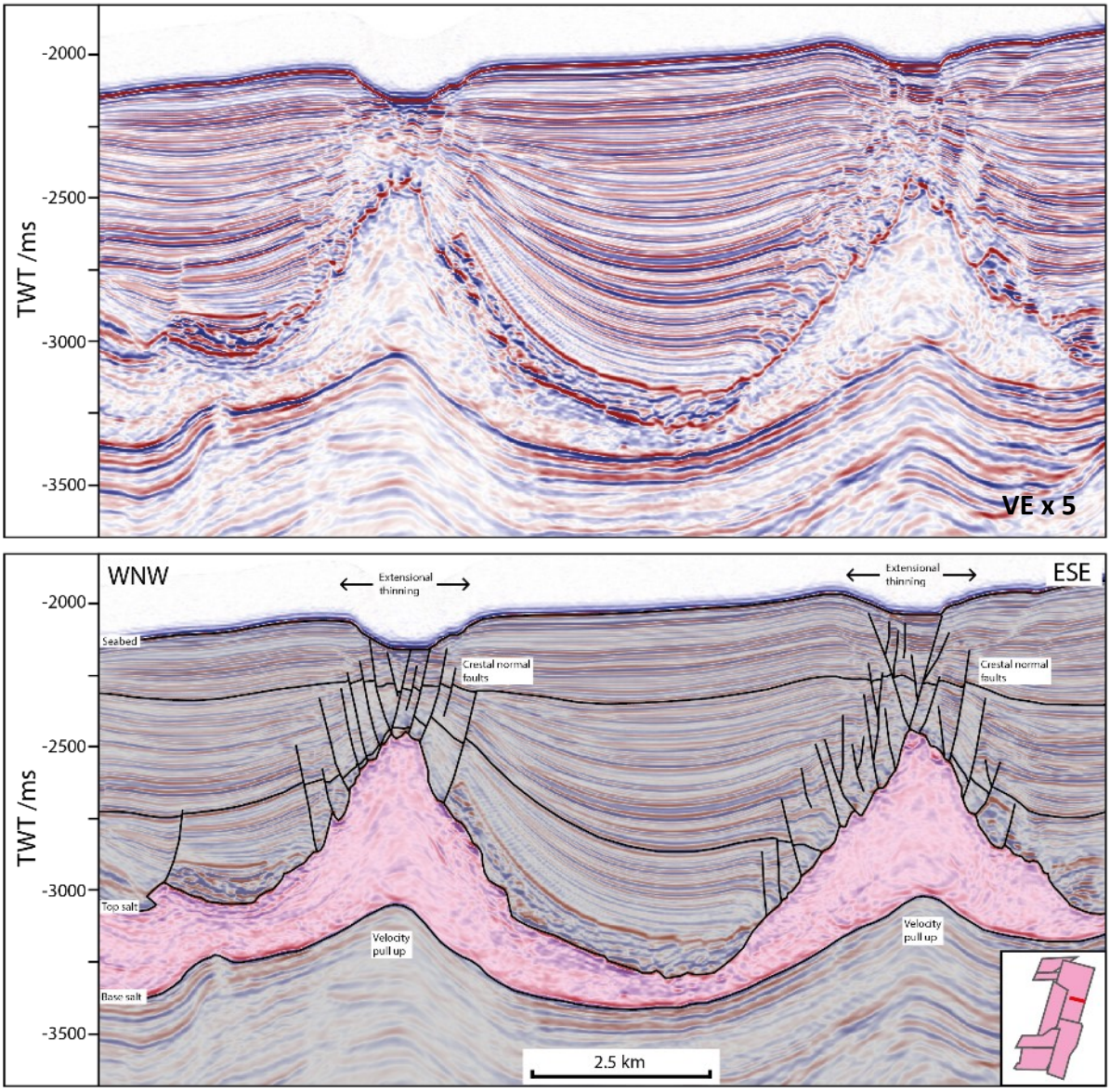

Figure 3.8 Seismic section (upper) and interpretation (lower) showing mature reactive diapirs with crestal normal faults corresponding to velocity pull-ups. Location shown on inset map and Figures 6 and 7.

The NNE-SSW-striking faults and rollers in the North rotate towards the south to strike broadly WNW-ESE (Fig. 3.7), closely following the local orientation of the shelf edge and salt pinch-out (Fig. 3.10a). In the far south a few faults even assume a perpendicular NW-SE orientation (Fig. 3.7). The major extensional faults are predominantly basinward-dipping and detach into the salt, with small throws on associated antithetic faults (Fig. 3.5). Many salt-

detached faults are listric and have an arcuate geometry in plan-view (Fig. 3.5 and Fig. 3.7). Where landward-dipping counter-regional faults do form they lead to the development of supra-salt anticlines (e.g. Fig. 3.5). Growth strata in the hangingwalls of the faults indicate that fault activity initiated in the Pliocene, after the deposition of a thin pre-kinematic layer (Allen et al., 2016; Elfassi et al., 2019).

A series of closely-spaced, supra-salt buckle folds are located down-dip of the extensional structures in the northern part of the study area (Fig. 3.7). The fold axes are NE-oriented (sub-parallel to the salt rollers in the extensional domain) and they have a peak-to-peak wavelength of c. 1.2 km. The overburden in the southern part of the dataset, however, remains largely undeformed and shows little evidence of supra-salt contraction.

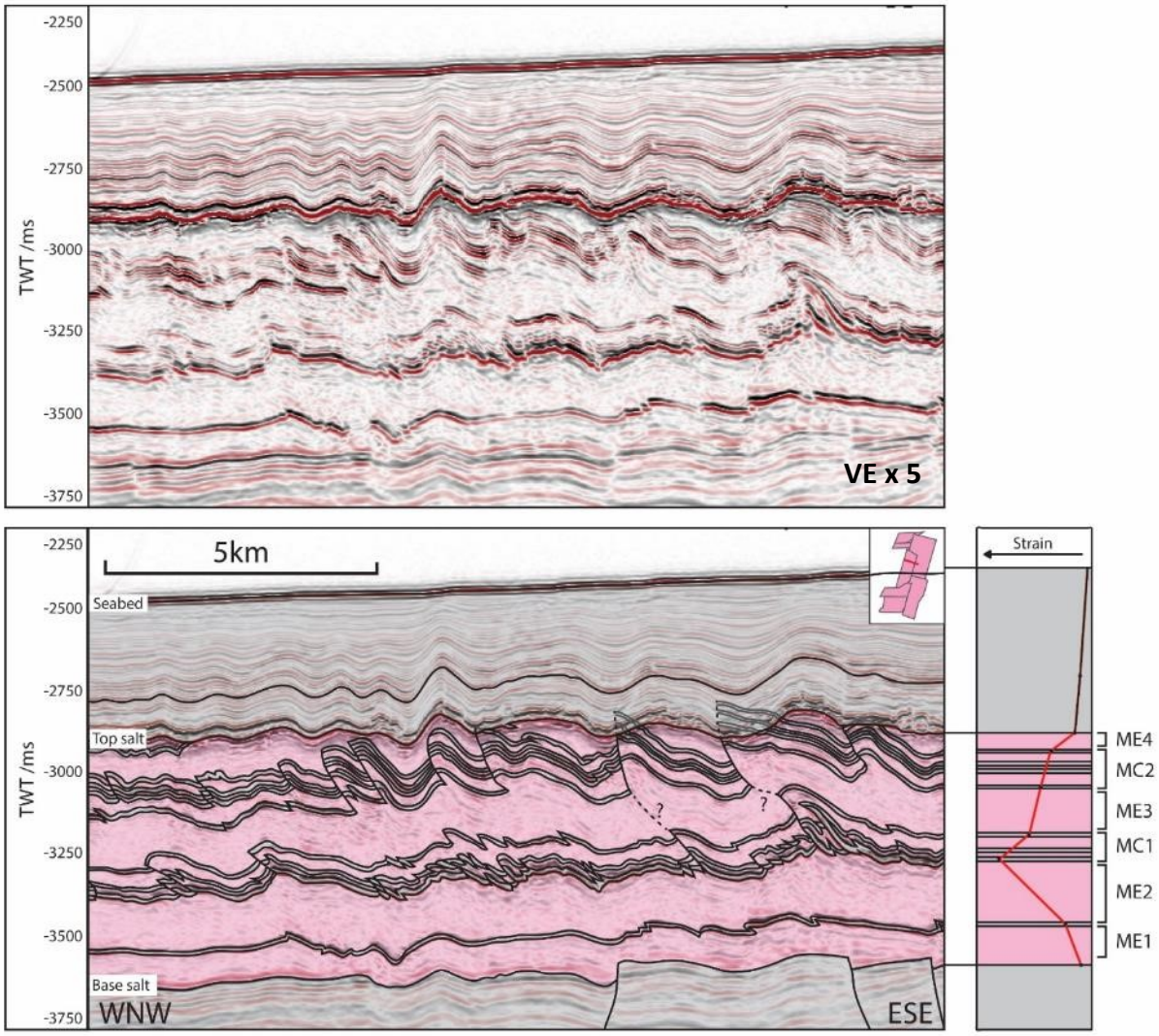

Figure 3.9 Seismic section (upper) and interpretation (lower) showing intrasalt stratigraphy and structure within the contractional domain. Vertical seismic strain profile calculated on brittlely deforming intrasalt reflectors (extrapolating upper reflectors to account for truncation at the top-salt) shows maximum strain in centre of the deforming salt sheet.

3.4.3 Intrasalt Stratigraphy

The Messinian evaporite sequence in the Levantine Basin comprises characteristically chaotic, low-amplitude, halite-dominated units interbedded with bright, semi-continuous reflections (Fig. 3.5). These reflective packages are widely documented across the eastern Mediterranean, and indicate lithological heterogeneity within the evaporite sequence (Netzeband et al., 2006; Lofi et al., 2011; Gvirtzman et al., 2013; Feng et al., 2016; Camerlenghi et al., 2019). Herein, we use the Messinian stratigraphic nomenclature defined by Feng et al. (2017), where the six intrasalt units are termed (from oldest/deepest to youngest/shallowest): ME1, ME2, MC1, ME3, MC2 and ME4 (Fig. 3.9). ME is used to refer to the chaotic (halite-dominated) units whereas MC refers to the reflective units. These correspond to Units 1 to 6 in Gvirtzman et al. (2013), and ME-I to ME-VI in Netzeband et al. (2006).

The reflective units have been variably interpreted as interbeds of evaporites (gypsum and anhydrite) and clastics (e.g. Netzeband et al., 2006; Cartwright and Jackson, 2008; Feng et al., 2016). The hazard and high drilling cost associated with the recovering of cores within the MSC has resulted in a lack of hard data to constrain the intrasalt stratigraphy. Netzeband et al. (2006) interpret the evaporitic units to reflect depositional cycles caused by temporal changes in brine salinity driven by variations in sea level. They suggest that this led to interbedding of the thick, ductile halite with more rigid evaporites and/or clastic sediments. Depositional cycles may be controlled by changes in sea level, in sea water chemistry, basin physiography or, most likely, some combination of the above. At a higher level this is controlled by the interplay between tectonics and climatic conditions.

Feng et al. (2017) and Gvirtzman et al. (2017) use petrophysical data from boreholes to interpret a succession of thin, clay-rich, clastic interbeds. Feng et al. (2017) also use an amplitude extraction on the intrasalt horizons to interpret a possible network of basin floor fans, supporting a clastic mode of deposition. Industrial activity targeting new hydrocarbon prospects has provided new data, and Meilijson et al. (2019) recently published the first publicly available report using borehole cuttings to analyse the lithologies of the units at two localities in the Levantine Basin, offshore Israel. They confirm that the reflective units comprise a high proportion of clay material, with layers of argillaceous diatomites found within MC1 and at top-ME1, and mixed clastic-evaporitic interbeds with anhydrites dominating MC2.

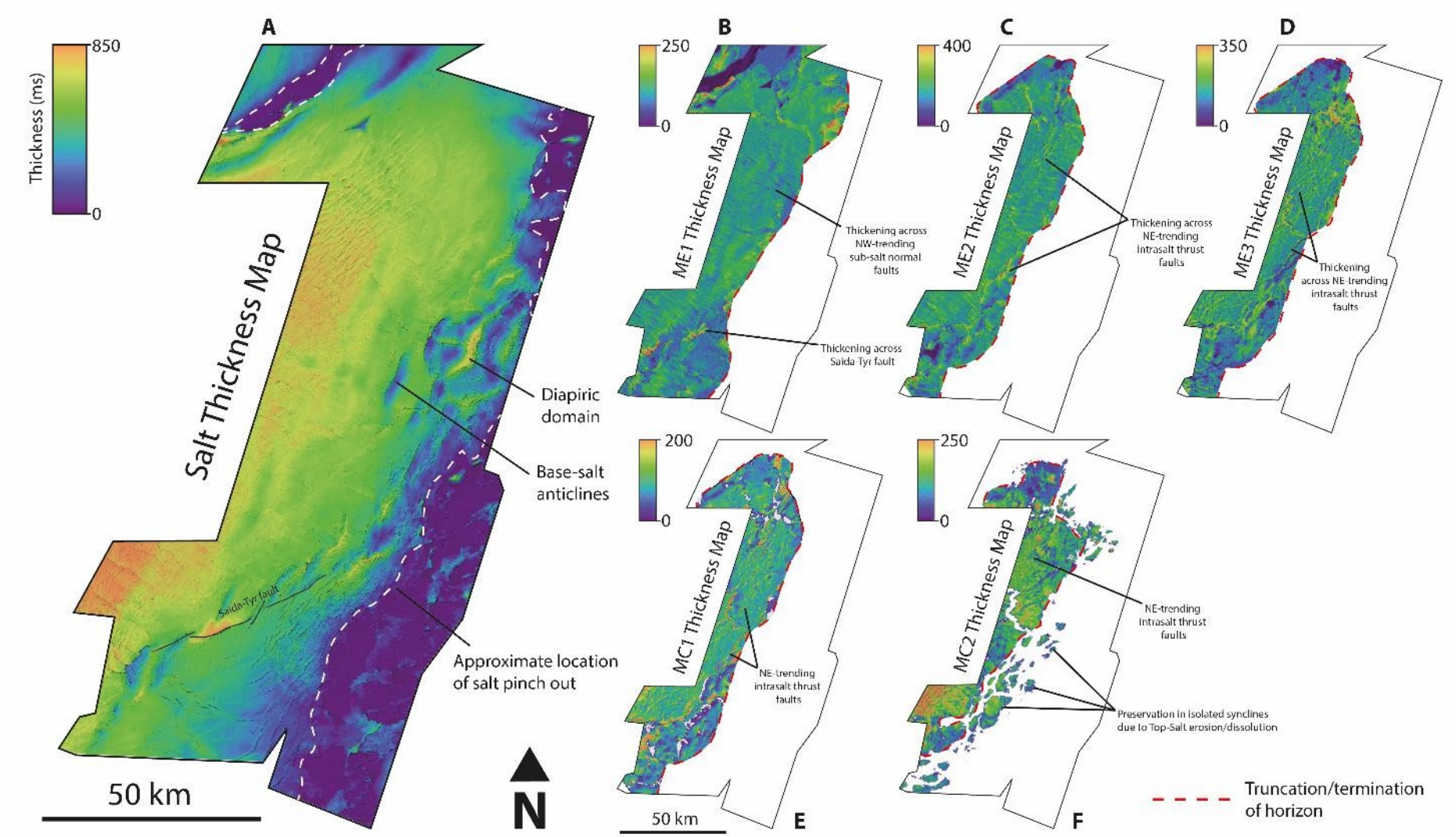

Figure 3.10 (A) Total salt thickness map showing basinward thickening and pinch-out updip. (B-F) Annotated thickness maps of individual intrasalt units within the contractional domain.

We are therefore confident that the reflective units imaged in the present dataset comprise clastic (mostly clay-rich) interbeds, but the detailed evaporitic heterogeneity and lateral facies continuity remain largely unconstrained. Local factors, such as proximity to clastic supply and topography of the basin, are likely to result in significant differences between the Messinian stratigraphic succession in different parts of the Mediterranean. Exposures of Messinian deposits in marginal basins of the Mediterranean (e.g. in the Realmonte Salt Mine, Sicily) and analogous evaporite sequences in other basins (e.g. in the Wieliczka Salt Mine, Poland), show that intrasalt heterogeneity occurs on a range of scales, from mm-scale crystalline impurities up to the decametre bedding scale (Fig. 3.1).

The total thickness of the Messinian evaporitic sequence increases seaward toward the centre of the basin and pinches out updip on the Levant margin (Fig. 3.10a). Thickness maps of the halite-dominated units ME1, ME2 and ME3 show relatively little variation across the contractional domain (Fig. 3.10b-d). The oldest unit ME1 does, however, thicken across the sub-salt normal faults (Fig. 3.9; Fig. 3.10b). The fact that there appears to be little intrasalt thickness variation across the dataset indicates that contractional (vertical) thickening of the layers has been broadly uniform across the study area.

MC1 consists of three semi-continuous, high-amplitude, sub-parallel reflections that can be traced across most of the basin (Fig. 3.9 and Fig. 3.10e). The thickness map for MC1 shows a broadly uniform average thickness of 85 ms TWT (c. 170 m) across the contractional domain of dataset (Fig. 3.10d), with local thickness variations attributed to reverse faulting (e.g. Fig. 3.9). This unit has a very similar expression and thickness in the southern Levantine Basin, offshore Israel (Gvirtzman et al., 2013; Feng et al., 2016) and in the deep basin, offshore Lebanon (Kirkham et al., 2020).

In contrast, MC2 comprises between 4-6 discrete intrasalt reflections and does show some basinward thickening into the contractional domain, largely due to the angular truncation of intrasalt reflections against the top-salt in updip areas (Fig. 3.9 and Fig. 3.10f). Where the full stratigraphy of the unit is preserved it reaches thicknesses of 180 ms TWT (c. 360 m). In comparison, MC2 is overall thicker to the south, offshore Israel, averaging 450 m (Feng et al., 2016). This may reflect lateral depositional variability, likely related to the large input of clastic material from the proximal Nile Delta in the southern Levantine Basin.

Both units MC1 and MC2, as well as the top-ME1 reflector, show some lateral variation in the amplitude and continuity of the reflections (Fig. 3.5). In some places they are very dim and the salt becomes seismically transparent, which may once again reflect lateral depositional variability in the thickness and composition of the units. The halite-dominated Messinian salt interval is immediately overlain by a unit of fluvial clastic origin known as the 'Nahr Menashe', which is characterised by high amplitudes relative to the overlying overburden (Kartveit et al., 2019).

3.4.4 Intrasalt Structure and Strain

Intrasalt reflections are folded and faulted across the basin, even where they directly underlie extensional structures in the overburden (Fig. 3.5). Structure maps of the intrasalt reflectors show that the fold axes and thrust planes strike dominantly NNE-SSW (Fig. 3.11). The thrust faults are 2-5 km long and have an arcuate trace in plan view (Fig. 3.11). They are relatively closely spaced (mostly 1-2 km apart), forming segmented, en echelon arrays separated by unbreached or breached relay ramps. The thrust planes dip exclusively to the SE with hangingwall folds verging to the NW across the study area (Fig. 3.5 and Fig. 3.9).

The strike of the faults and fold axes is consistent for all mapped horizons within the salt. While most intrasalt faults have small throws (<70 ms or c. 300 m) and are confined to their discrete reflective units, some larger faults with larger throws (up to 160 ms or c. 670 m) connect MC1 and MC2 and cross-cut the intervening halite-dominated ME3 (Fig. 3.9). The intrasalt faults are fully confined to the salt, terminating at the top-salt, and do not extend up into the overburden. Finally, we observe that some structures in the overburden appear to be concordant with intrasalt structures (i.e. overburden folds directly overlying intrasalt thrusts of the same length and orientation), but in other places intrasalt structures have no expression in the overlying overburden (Fig. 3.9).

The distribution of the seismically imaged intrasalt strain is highly heterogeneous, varying both vertically and laterally across the study area. First, strain on individual reflections can vary by significant amounts (up to 200%) laterally over relatively short length-scales (i.e. between profiles only 8 km apart). Overall strain increases southward, but with significant local variability within the area of interest (Fig. 3.12). For example, abrupt local increases in

strain occur where intrasalt thrust duplexes are developed, accommodating a large amount of shortening over a relatively short distance, with strain reducing significantly away from the structure (Fig. 3.13).

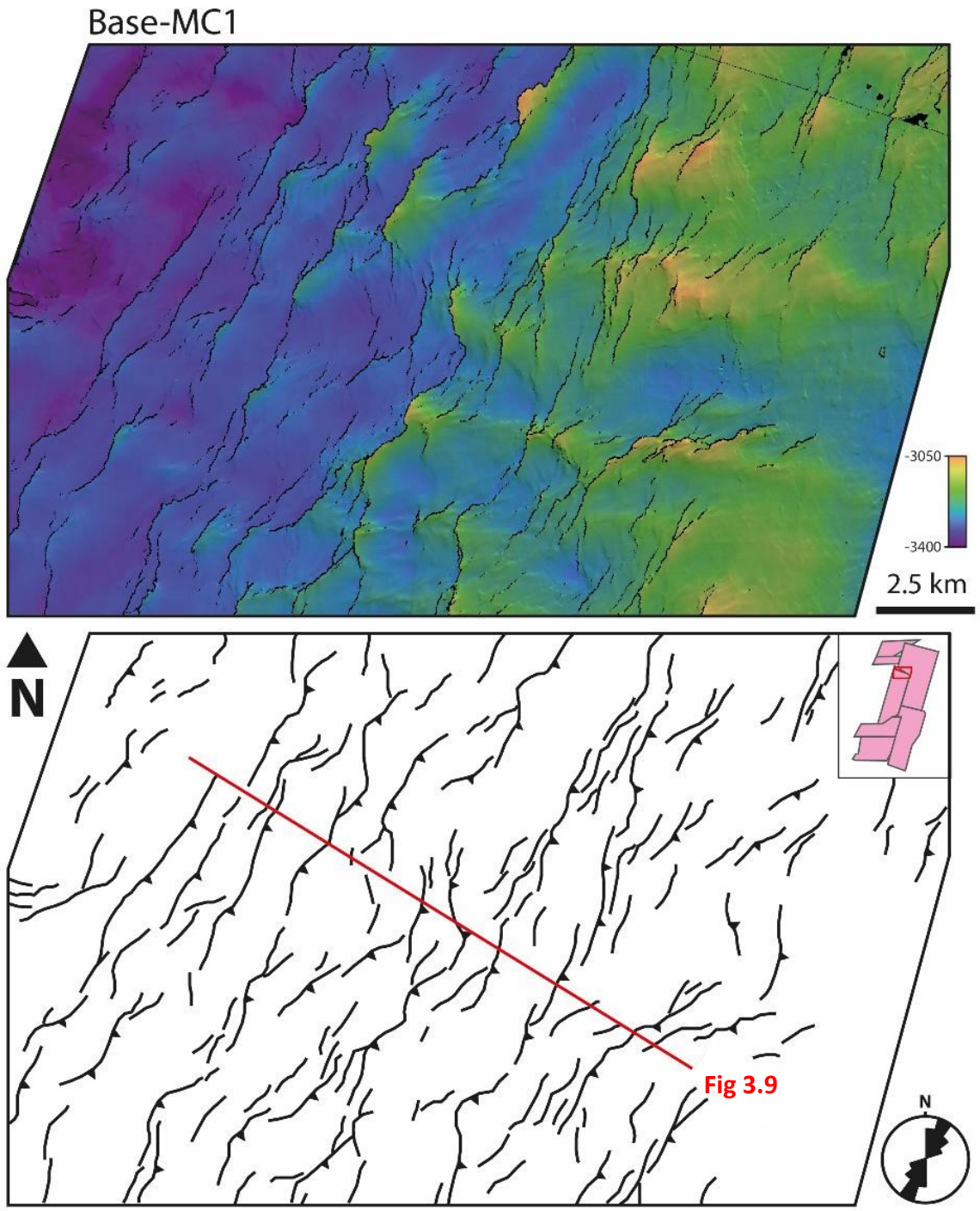

Figure 3.11 Detailed structure map of Base-MC1 (Top-ME2) reflection showing dominant NNE structural trend of intrasalt faults and folds. Rose diagram and location shown in inset.

The cause of such extreme strain localisation is unclear. One possible explanation is that it relates to relief on the base-salt surface which causes salt flow lines to converge and thus promotes local contraction (Dooley et al., 2017). The magnitude of relief on the base-salt surface appears relatively small in the presented two-way-time data, but since the reflective packages are acoustically slower than the salt (Reiche et al., 2014; Feng et al., 2016), a depth-converted section may show the true relief to be significantly greater. This highlights the importance of lithologically-controlled variations in intrasalt velocity when building velocity models and undertaking depth conversion. A uniform velocity model applied to the entire salt sheet would not account for the lateral velocity variations due to intrasalt structural complexity and would therefore inaccurately distort the base-salt structure map. Conversely, other base-salt anticlines mapped in this study are not associated with such extreme strain localisation or development of intrasalt duplex structures. An alternative interpretation is that strain localisation may reflect depositionally-controlled lateral facies changes and associated lateral variations in the bulk strength of the deforming salt sheet. If the salt was locally weaker due to, for example, an increased proportion of halite and/or thinner clastic units, this would make it more prone to accommodate any applied stress, serving to localise strain.

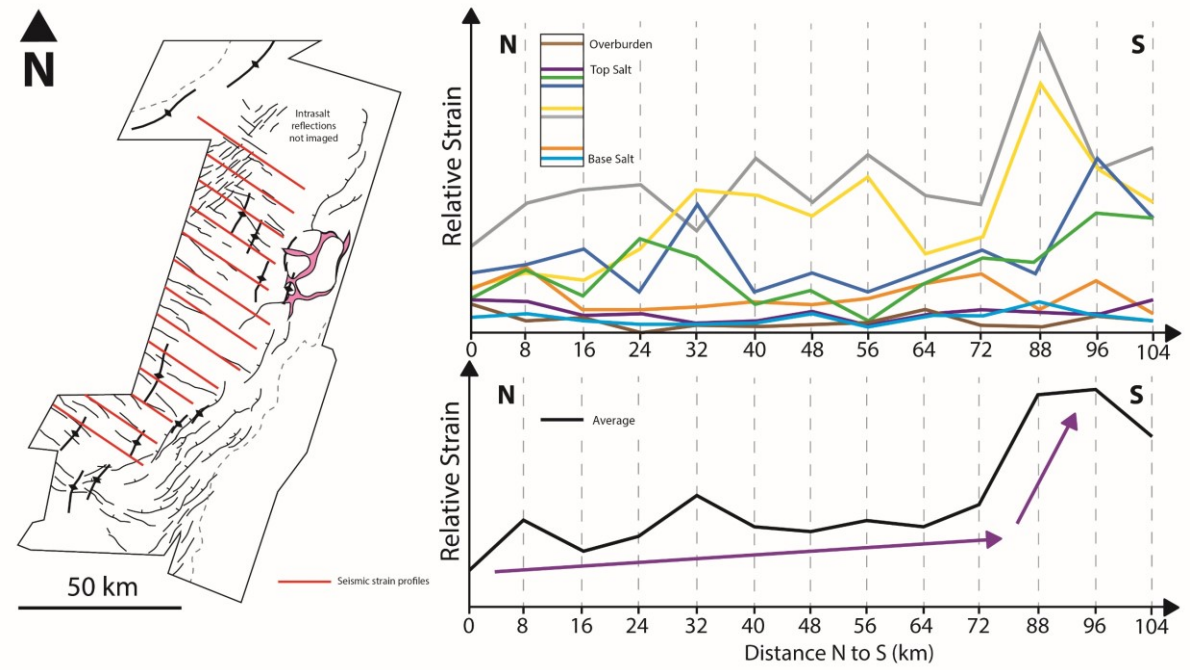

Figure 3.12 (A) Location of 2D seismic sections used in strain measurements. (B) Lateral seismic strain variations plotted along margin (North to South) calculated for individual intrasalt reflections (upper) and average across all reflections (lower). Red arrows indicate overall trend of strain increasing toward the South.

The intrasalt strain also appears to vary vertically, as well as laterally, within the deforming salt sheet (Fig. 3.9). The averaged vertical strain profile shows that the top-ME1 reflection near the base of the sheet exhibits the least strain, likely due to increased boundary drag and shear stress at the contact with the fixed base-salt surface. Maximum strains occur in the centre of the salt sheet at the base of MC1, with strain decreasing gradually toward the top of the salt sheet in MC2, and a sharp decrease at the erosional contact with the overlying clastic overburden (Fig. 3.9). In fluid mechanics, this resembles an asymmetric Poiseuille flow distribution (Fig. 3.3c). However, since strain is only measurable in the brittle units, cryptic strain within the ductile units may be even higher, as has been shown in some physical models (e.g. Fig. 3.14; Weijermars and Jackson, 2014). Strain remains very low in the overburden relative to the intrasalt units.

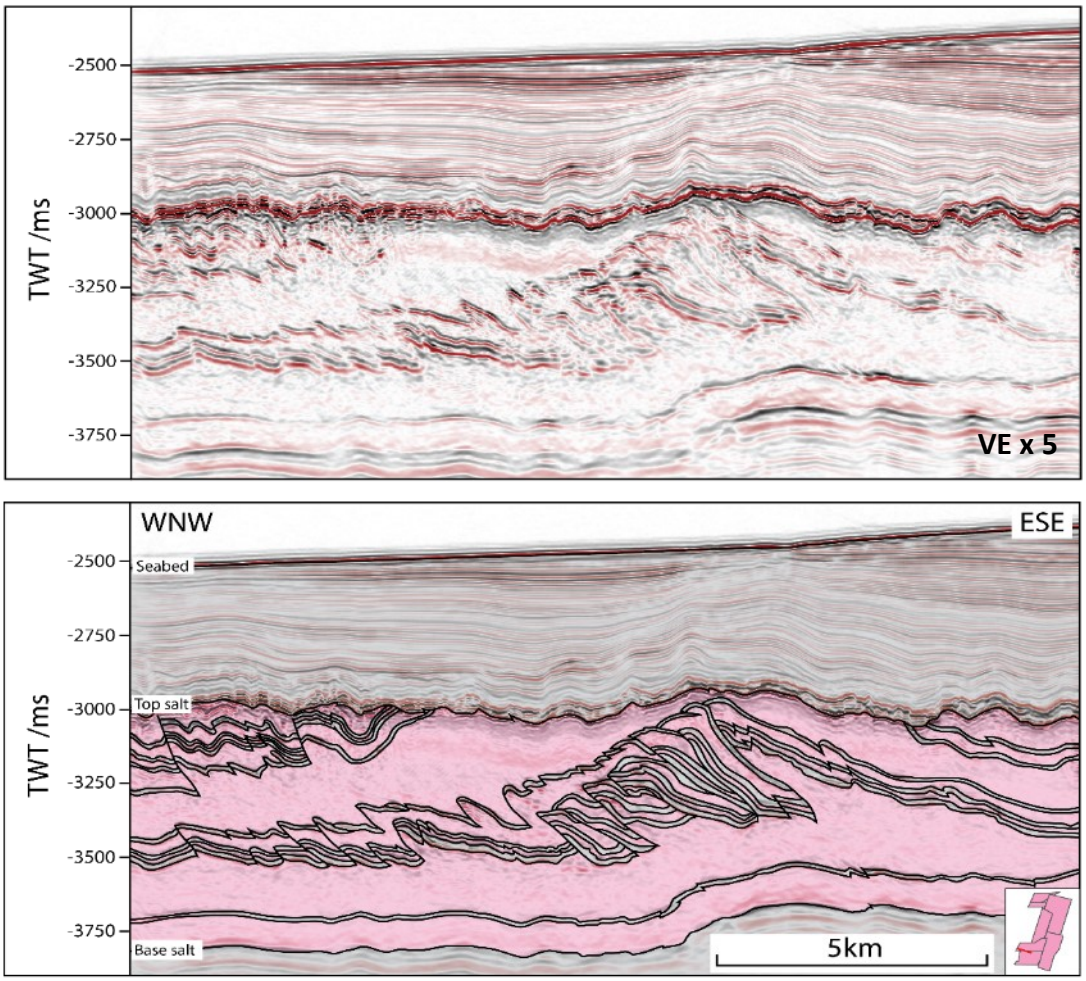

Figure 3.13 Seismic section (upper) and interpretation (lower) showing kilometre-scale thrust duplex accommodating very high strain over relatively short distance. MC2 reflections truncated at the top-salt. Note very low strain on Top-ME1 reflection. Location shown in inset and Figures 3.6 and 3.7.

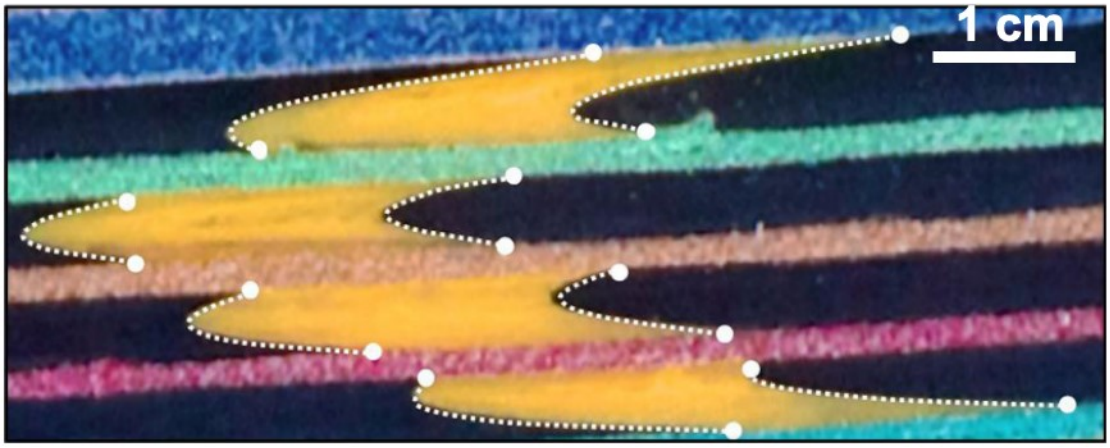

Figure 3.14 Physical model using silicone as salt analogue demonstrating overall Poiseuille flow, with passive strain markers (yellow) showing higher strains in ductile silicone layers than intervening brittle sand layers (Weijermars and Jackson, 2014).

3.5 Salt Tectonics

In this section we review the observations described in detail above and pull these together to form an integrated salt tectonic framework for the Lebanese Levant margin. We interpret the implications of our observations in terms of gravity gliding, the interaction of salt flow with base-salt relief, the rheology of the evaporite sequence, and the multiphase evolution of salt deformation.

3.5.1 Gravity Gliding

The Levant passive margin can be divided into kinematically-linked salt tectonic domains of updip extension and downdip contraction, with the listric geometry of the detached supra-salt faults typical of thin-skinned tectonics on salt-influenced margins (Fig. 3.5) (Jackson and Hudec, 2017). Their orientation parallel to the margin and closely following the base-salt dip is indicative of a system dominated by gravity gliding (Jackson et al., 1994; Jackson and Hudec, 2017) (Fig. 3.6 and Fig. 3.7). The dominant NE-SW structural trend of the supra-salt faults and buckle folds, as well as the basinward vergence and trend of the intrasalt faults and folds, indicates a dominant NW direction of transport. This differs significantly from the NE direction of transport indicated by the structural trend offshore Israel, c. 150 km to the south of the present study area (Cartwright et al., 2012). This is attributed to the proximity of the Nile

Delta and the associated increased gravity spreading component in the southern Levantine Basin, the influence of which decrease northwards along the Levant margin (Allen et al, 2016).

The supra-salt buckle folds are present only in the northern part of the study area, whereas in the southern part of the study area there is very little overburden contraction despite significant extension updip. This can be attributed to the proximity of the folds to the Latakia Ridge, which acts as a buttress to basinward salt flow and thus confines the formation of contractional structures to a relatively narrow belt. The overburden in the southern part of the study area may therefore appear weakly deformed because the contraction is more diffuse and taken up over a greater area, or because the translational zone is much wider, with the buckle folds located further downdip of the available dataset.

3.5.2 Influence of Base-Salt Relief

The flow of salt over relief on the base-salt surface has affected the structural evolution of the salt and overburden in two notable ways. First, the NE-trending base-salt anticlines have caused the development of several ramp syncline basins in the overburden, recognised by their landward-dipping growth strata and onlap surfaces adjacent to the sub-salt anticlines (Fig. 3.5) (Jackson and Hudec, 2005; Pichel et al., 2018). Ramp-syncline basins record simple basinward (horizontal) translation and are not associated with any contractional (e.g. folds or thrusts) or extensional (e.g. normal faults) structures in the overburden, therefore there is no apparent effect of changes in salt flux across the base-salt anticlines (cf. Dooley et al., 2017; Pichel et al., 2018).

Second, the expression of the underlying NW-SE-striking sub-salt faults (Fig. 3.6) can be seen in the thickness map of ME1 (Fig. 3.10b) and in the structure map of the top-ME1 reflector. Thickening across the base-salt faults likely reflects the syn-depositional infilling of residual topography on the base-salt surface, suggesting the faults were active up to, or during, the deposition of ME1 in the early stage of the Messinian Salinity Crisis. This supports the interpretation made by Reiche et al. (2014) that these faults may have contributed to the development of small fault-propagation folds that deformed the top-ME1 reflection. Reiche et al. (2014) also interpret shallower intrasalt structures in units MC1 and MC2 on 2D seismic lines, and suggest that these early fault-propagation folds may have accommodated and

focused later tectonic shortening. However, the younger evaporitic units mapped within our 3D survey do not appear to show any expression of these subsalt faults, nor any related thickness changes, and the orientation of the intrasalt contractional structures is different to that of the sub-salt faults. We therefore conclude that fault activity had ceased during the deposition of ME2, and that the residual base-salt relief does not appear to have had any significant effect on salt flow due to the orientation of the faults parallel to the direction of salt flow, as well as their small throw (c. 70 m) relative to the large evaporite thickness (up to 2 km).

3.5.3 Salt Rheology

Lithological heterogeneity gives rise to rheological heterogeneity, since the different lithologies have different mechanical properties (e.g. Albertz and Ings, 2012; Raith et al., 2016; Rowan et al., 2019). This controls the way in which the intrasalt units respond to applied stresses and accommodate strain. The reflective units MC1 and MC2 demonstrate dominantly brittle behaviour during deformation, accommodating most of the contraction with slip on reverse faults (Fig. 3.9 and Fig. 3.11). This contrasts with the intervening halite-dominated units, which deform in a bulk ductile manner, accommodating strain principally by viscous flow and thickening. No brittle deformation of these units is visible in the seismic data.

Our observations are consistent with those of Netzeband et al. (2006) and Gvirtzman et al. (2013), in that MC1 and MC2 appear to be largely independently faulted and folded, with the ductile halite-dominated layers acting as intra-Messinian detachment levels within the deforming sequence. Netzeband et al. (2006) assert that the lack of coupling between the units is evidence for syn-depositional deformation. However, mechanical decoupling of the brittle layers via the intervening ductile layers could also account for this disharmonic deformation (Cartwright et al., 2012; Allen et al., 2016). Furthermore, we observe that some of the larger reverse faults appear to cross-cut the halite-dominated ME3 unit to vertically link faults in MC1 and MC2. We therefore suggest that small, thrust-related vertical displacements may be absorbed by ductile deformation of the ME3 halite unit, allowing the development of discrete, layer-bound structures within MC1 and MC2, whereas larger vertical displacements that impose larger vertical stresses (e.g. due to hangingwall uplift) are able to propagate through the halite to link otherwise discrete structures in MC1 and MC2.

3.5.4 Multiphase Flow

The gently folded Pliocene overburden is demonstrably much less deformed than the underlying intrasalt units (Fig. 3.9). This phenomenon has been variably interpreted as a result of multiphase salt flow (Netzeband et al., 2006; Gvirtzman et al., 2013; Feng et al., 2017; Kartveit et al. 2018), or mechanical decoupling of the salt and overburden, accommodated by shear drag at the contact (i.e. top-salt) (Cartwright et al., 2012).

The contact between the salt and overburden (i.e. top-salt) is also an erosional unconformity (Fig. 3.9). The observed thickness variations across MC2 are largely attributed to erosion of the unit in the updip domain, as indicated by the truncated intrasalt reflections against the top-salt surface (Fig. 3.5 and Fig. 3.10f). This means that seaward salt flow, and erosion of the crests of developing structures, initiated prior to the deposition of the present-day overburden. This is consistent with interpretations by Gvirtzman et al. (2017) offshore Israel, and more recently by Kirkham et al. (2020) offshore Lebanon, who postulate dissolution of structural highs due to impingement of the halocline in a stratified water column. This truncation is conclusive evidence that there have been at least two discrete phases of salt flow on the Levant margin, first pre- and then post-overburden deposition (cf. Netzeband et al., 2006; Gvirtzman et al., 2013; Gvirtzman et al., 2017; Feng et al. 2017; Kartveit et al. 2018). Gvirtzman et al. (2013) also use thickness changes within salt layers and intrasalt onlaps as evidence of syn-depositional flow but no such evidence is documented in the present dataset. We note that even post-depositional deformation can lead to thickness changes within the mobile, halite-dominated salt layers, and that geophysical artefacts may resemble apparent onlaps (Albertz and Ings, 2012; Allen et al., 2016).

The multiphase flow model also explains the observed differences between the type and distribution of structures in the intrasalt units compared to the overburden. If both were deformed together we would expect more concordance between overburden and intrasalt structures (i.e. intrasalt faults with large throws associated with uplift in the overlying supra-salt strata).

Shallow growth strata in the overburden and relief on the seabed indicate that active salt tectonics continue to influence the structural evolution of the Levant margin to the present

day. Whereas some salt-related structures appear to show recent growth, as indicated by their expression in the overlying overburden and recent growth strata, others have become inactive and show no evidence of activity post-overburden burial (e.g. Fig. 3.9).

3.6 Discussion

The Poiseuille strain profile derived from seismic data in this study is consistent with strain measurements offshore Israel (Cartwright et al., 2012), although the net direction of tectonic transport and salt flow is different (i.e. NW as opposed to NE). However, recent studies by Cartwright et al. (2018) and Kirkham et al. (2019), which utilise a series of deformed fluid escape pipes and related pockmarks within the post-salt overburden, suggest that the salt layer deformed predominantly by Couette (Fig. 3.3b) rather than Poiseuille flow (Fig. 3.3a). The passively deformed fluid escape pipes are interpreted as direct kinematic indicators and show the greatest amount of strain at the top of the salt, decreasing exponentially toward its base. Here we discuss two ways in which these seemingly contrasting flow patterns (Poiseuille vs. Couette) may be reconciled.

3.6.1 Subseismic Strain

First, we discuss the way in which strain is accommodated by the different brittle units, decoupled by the intervening halite-dominated, ductile layers. Seismic data show differences between units MC1 and MC2 in terms of the number and spacing of intrasalt reflections; however, seismic data alone does not allow us to determine the detailed lithological heterogeneity. We know that lithological heterogeneity is common in evaporitic sequences (Fig. 3.1) and that this heterogeneity occurs at a range of scales; seismic data images only the very upper end of this scale (i.e. >10 m). The available well data also suggest lithological differences between MC1 and MC2, and that they comprise slightly different thicknesses of clastic interbeds (Meilijson et al., 2019).

Constraining the intrasalt lithological heterogeneity of the Messinian salt is important, given it controls how the unit deforms and what we can image seismically. Deformed, heterogeneous evaporites exposed in the Wieliczka Salt Mine show that strain is accommodated differently between different units (Fig. 3.15; Burliga et al., 2018). A m-scale

thrusted and recumbently folded structure exposed in the wall of the mine contains within it several smaller broken units which are too small to be imaged by seismic reflection data. This means we would be unable to identify, map, and measure the associated strain with seismic data. Although the Serravallian evaporites exposed in the mine are older and more deformed than the Messinian, it is plausible that the different units within the Messinian sequence, with different rheological behaviours, would also accommodate strain differently.

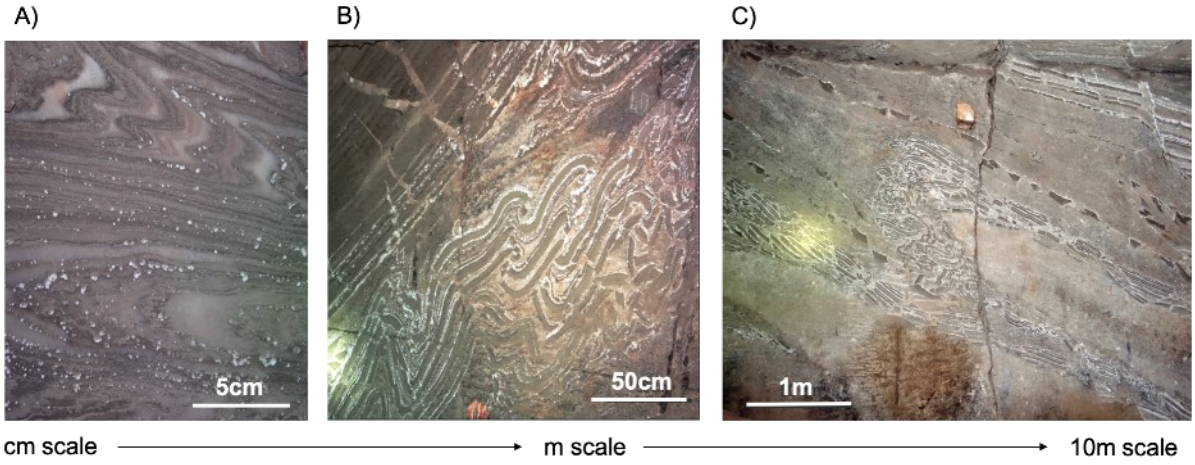

Figure 3.15 Structures exposed in the Wieliczka Salt Mine in Poland show different ways in which strain is accommodated by different units depending on their physical properties (e.g. viscosity), thickness and position in the sequence. Mine exposes Serravalian age deposits comprising interbedded evaporites and clastic material. Modified from Burliga et al. (2018).

If the upper reflective unit MC2 accommodates more sub-seismic deformation (i.e., short-wavelength folds and/or low-displacement faults), the unit may falsely appear to be more weakly strained in seismic reflection data than it actually is (Fig. 3.16). It is also noted that even though the reflective layers appear to deform in a dominantly brittle manner, some strain may also be accommodated by cryptic compaction and/or bed thickening. Again, a seismic-based strain analysis would not detect this and we may therefore be missing a significant and as yet unquantified percentage of the actual strain (Fig. 3.16). This could account for the discrepancy between the lower strain calculated for MC2 in the seismic data, versus the higher strain indicated by the deformed pipes.

This leads us to speculate as to the composition of MC2, such that it accommodates more strain by the formation of sub-seismic structures, and therefore appears at the seismic-scale to be more weakly deformed than MC1. Even small differences in the lithological stratigraphy

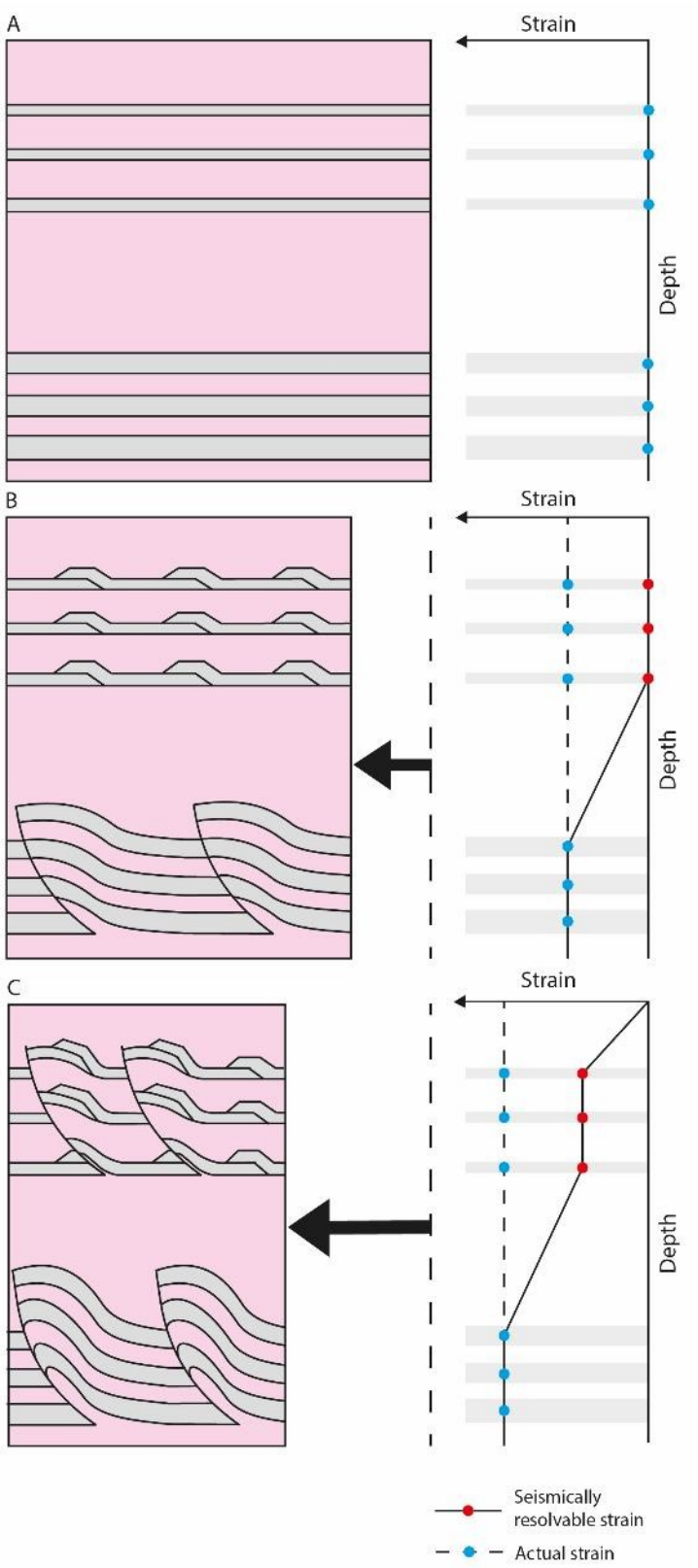

Figure 3.16 Schematic cartoon showing evolution of strain within a heterogeneous salt sheet. (A) Undeformed brittle intrasalt units within halite-rich ductile sequence. (B) The upper unit with a lower brittle:ductile ratio accommodates shortening via small, sub-seismic structures while the lower unit with a higher brittle:ductile ratio develops seismically-resolvable thrust faults. (C) The upper unit accommodates strain on two new, seismically-resolvable thrust faults while the lower unit accommodates strain with slip on pre-existing structures. The result is that the upper unit appears less strained on seismic data than the lower unit, despite both having accommodated the same magnitude of shortening.

of the units may have a significant effect on how they respond to applied stress. The thickness and spacing of the interbeds, as well as their competency contrast with the intervening halite-rich layers, play an important role here, exerting a first-order control on how contractional strain is accommodated within a multilayer sequence (Ramberg, 1962; Johnson and Flether, 1994; Schmid and Podladchikov, 2006; Schmalholz and Mancktelow, 2016; Fossen, 2016). Firstly, thicker, stronger beds develop folds with a greater dominant wavelength than thinner, weaker beds (Fossen, 2016). The individual brittle intra-salt layers are too thin to separately resolve their top and base with seismic data (i.e. the 'soft kick' of the top of the layer is immediately followed by the 'hard kick' of the base of the layer, with the resulting superposition generating a single wavelet; Brown, 2011). There may therefore be unresolved differences in bed thicknesses between MC1 and MC2. Since fold amplitude is proportional to bed thickness and strength, if MC2 were composed of thinner or weaker beds it is possible that more of the strain would be accommodated by short-wavelength, small-amplitude, sub-seismic structures than MC1, within which thicker or stronger beds promote the development of large-amplitude, seismically resolvable structures (Fig. 16). Discordant folding of beds with different thicknesses is evident in onshore exposures of Messinian evaporites in marginal basins, such as those in Sicily (Butler et al., 2015).

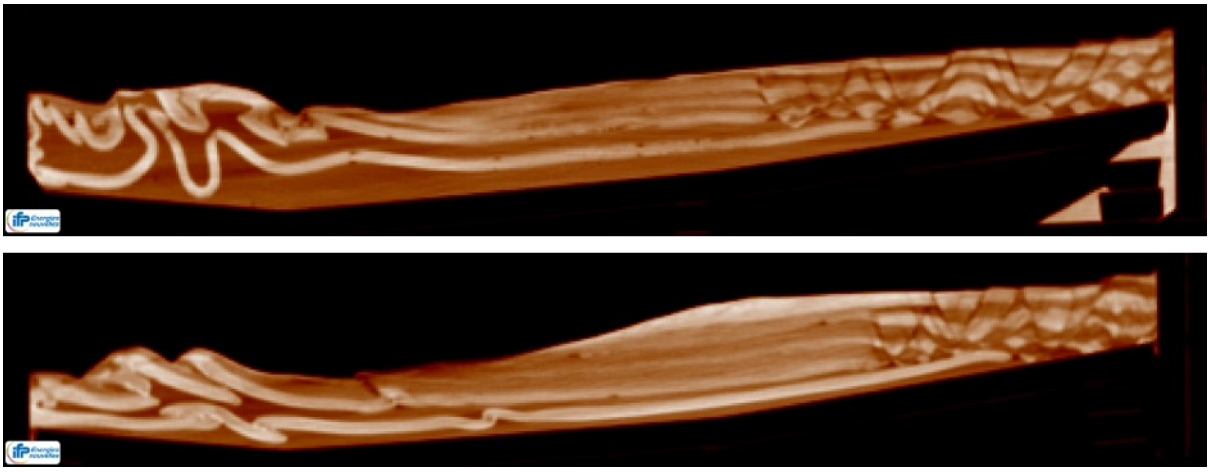

Figure 3.17 Cross sectional CT scans of physical analogue models of salt tectonics on a passive margin. The interbedded sand layer deforms in a ductile manner when encased in thick silicone (upper) and in a brittle manner when encased in thin silicone (lower). Models run at IFP Energies Nouvelles, Paris.

The way in which the reflective units accommodate strain is not only determined by the lithology and thickness of individual beds within the sequence, but also by the properties of the sequence as a whole. For example, physical models show that the rheology of an individual sand layer is sensitive to the thickness of silicone within which it is encased (Fig.

3.17). In a closed, gravity-driven system, sand layers encased in thick silicone accommodated horizontal shortening by large-amplitude ductile folding, whereas sand layers encased in thin silicone accommodated strain on discrete brittle thrusts (Fig. 3.17). Therefore, perhaps it is the overall ratio of brittle-ductile materials in the sequence that exerts a primary control on the resulting deformation.

Physical models using silicone as a salt analogue have previously shown that higher brittle-ductile strength ratios result in greater localisation of strain whereas more ductile sequences result in more distributed strain. Davy et al. (1995) define the brittle-ductile parameter (Γ), which controls the large-scale localization of deformation, and associated fault patterns (both density and fault length distribution). Schueller and Davy (2008) use physical models to show that strain localization occurs when Γ = >0.5. For smaller Γ, the large-scale deformation, although heterogeneous, never localizes. Γ = 0.5 can be considered as a rheological transition between ductile-like macroscale rheology and brittle-like one. In order for seismic-scale thrusts to develop, strain must localise on individual structures such that they accumulate a critical amount of displacement that can be seismically resolved. We could therefore speculate that MC2 has a smaller Γ than MC1, which means that it is more prone to accommodating strain on distributed, sub-seismic scale structures, as opposed to the larger, discrete thrusts developed in the middle unit (Fig. 3.16).

3.6.2 Spatial and Temporal Variability in Salt Flow

An alternative way to explain the apparent discrepancy between flow profiles is that the salt layer was subject to both Poiseuille and Couette flow, but that the relative contribution of each (and related deformation) varied through time. On geological timescales, salt deformation can be approximated as a viscoplastic fluid that flows in response to applied stresses, from areas of high pressure to low pressure to reach an equilibrium state. Viscoplastic materials are defined by the presence of a yield strength, under which strain increases linearly with stress and beyond which the material deforms at constant stress. Materials that yield to applied stresses by continuous deformation are known as ductile materials, as opposed to brittle materials which are characterized by the fact that rupture occurs without any noticeable prior change in shape. If we treat the behaviour of the salt unit as viscoplastic and the brittle intrasalt layers act as passive strain gauges, the salt will exhibit

a Poiseuille flow profile when responding to a pressure gradient such as a differential load, and a Couette profile when the flow is drag-induced by a translating overburden.

In nature, seismic data image finite structural style but this may not be representative of the present day stress state within the deforming sequence. Physical analogue models and numerical finite element models have generated both Poiseuille (e.g. Cartwright et al., 2012; Gradmann and Beaumont, 2012) and Couette flow (e.g. Brun and Mauduit, 2009; Schultz-Ela and Walsh, 2002), demonstrating that salt flow is highly sensitive to the applied boundary conditions, i.e. the relative contribution of gravity gliding vs. gravity spreading. It is therefore probable that the dominant flow regime varies through time and space depending on the stresses applied locally to the salt sheet. When differential loading dominates, salt will deform via Poiseuille flow, and when overburden drag dominates, the salt will deform via Couette flow. These are end-members of a spectrum, and in cases where the salt sheet experiences both differential loading and overburden drag, the resulting flow profile will take a hybrid form (i.e. asymmetric Poiseuille profile; Fig. 3.3c).

Based on the mechanical and kinematic arguments detailed above, two phases of deformation are required to explain the present structure of the salt and its overburden (Fig. 3.18). The first phase is said to have occurred syn-depositionally or shortly thereafter, during the Messinian, culminating in erosion of structural highs, followed by a second, later phase in the Plio-Pleistocene, during which time thin-skinned tectonics were reactivated, deforming both the salt and overburden (Netzeband et al., 2006; Gvirtzman et al., 2013; Gvirtzman et al., 2017; Feng et al. 2017; Kartveit et al. 2018). During the early phase of deformation, when there was little gravitational instability due to base-salt tilt, salt flow could have been driven predominantly by a pressure gradient caused by differential loading (i.e., Poiseuille flow) (Fig. 3.18b). These clastic wedges could then have been eroded in the same basinwide margin uplift event that created the truncation of intrasalt reflections against the top-salt (Fig. 3.18c) (Gvirtzman et al., 2017; Kirkham et al., 2020). Later, as basin subsidence resumed and a clastic overburden was deposited above the salt, additional loading, combined with wholesale tilting of the margin, could have caused a change to drag-induced (i.e., Couette) flow (Fig. 3.18e). This is consistent with the model proposed by Cartwright et al. (2018) showing that the first fluid escape pipe formed when some overburden (c. 250 m) had already been deposited. This means that the strain recorded by the deformation of the intrasalt layers is the total flow (i.e., Poiseuille + Couette) experienced by the salt (Fig. 3.19), whereas the strain recorded by the pipes reflects only the later Couette phase of flow.

It is possible that this second phase of salt-related deformation, triggered by uplift of the margin, is related to the regional plate tectonics. Transpressional activity on the Dead Sea transform fault adjacent to the Lebanese Margin (Fig. 2), accomodating the northwards migration of Arabia and opening of the Red Sea, could have also been associated with the apparent uplift and associated gravitational stability.

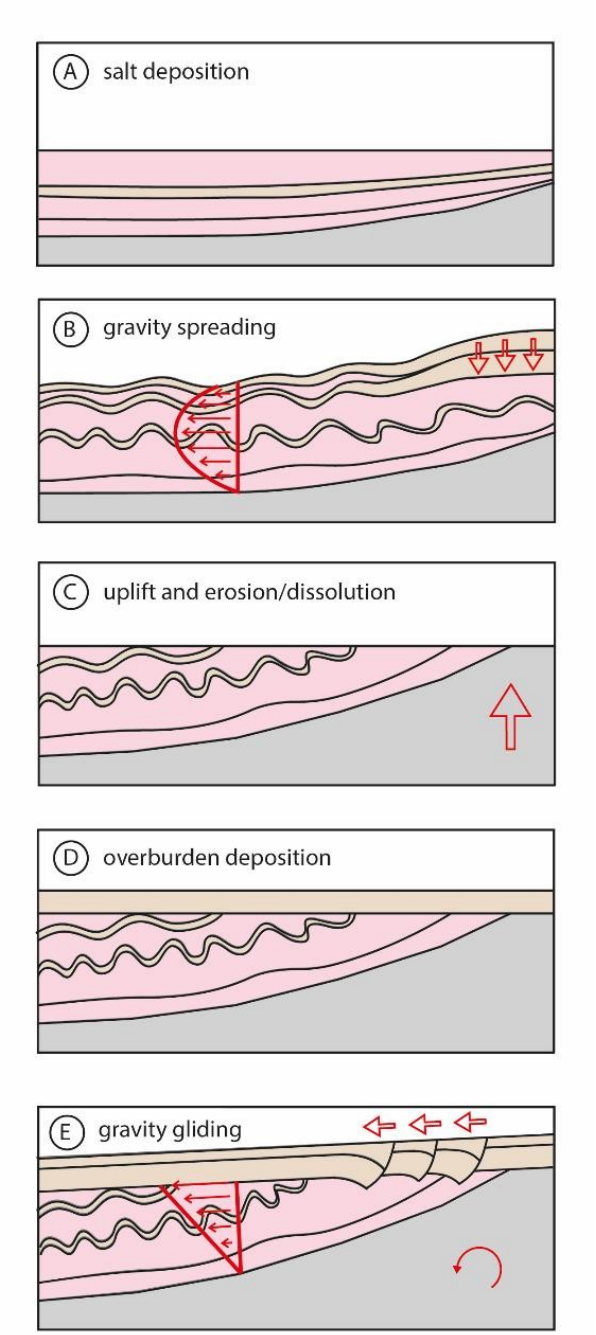

Figure 3.18 Schematic structural evolution of the salt deformation on the Levant margin. (A) Deposition of salt layers, thinning updip toward the shelf. (B) Thick sediments on shelf are deposited contemporaneously with upper brittle intrasalt units, resulting in gravity spreading due to pressure difference and basinward Poiseuille flow. The middle intrasalt units accommodate more shortening than upper and lower units where drag against top- and base-salt hinders basinward flow. (C) Uplift of the Levant margin causes erosion and dissolution of the sediments and salt layers updip. (D) Basin subsidence resumes and an overburden is deposited on top of the deformed salt sheet. (E) Greater subsidence in the deep basin causes margin tilt and gravity gliding is initiated, resulting in a drag-induced basinward Couette flow.

3.6.3 Implications

We have shown that planning well paths to account for the present stress state within thick salt bodies must consider the structural evolution of the salt and overburden, since strain profiles derived from seismic data may be misleading. Complex rheological sequences mean that stress and strain are not proportional, and that strain may not be accommodated uniformly within the deforming salt body. Furthermore, temporal and spatial variability in the dominant flow regime could mean that the cumulative strain distribution may not be representative of the present intrasalt stress state. It is therefore important to develop an integrated understanding of the regional and local forces acting upon the salt sheet, and driving deformation in the system, in order to predict the present stress state. On the Lebanese Levant margin the salt in now undergoing a drag-induced Couette flow, and as such a deviated drilling trajectory would be required to minimise shear stress on the borehole (Fig. 3.20; Weijermars and Jackson, 2014). While such a deviation may minimise stress on the borehole related to horizontal salt flow, other risks may be amplified. Well planning must also consider, for example, the risk of borehole collapse, stuck pipes, and problems with electric logging.

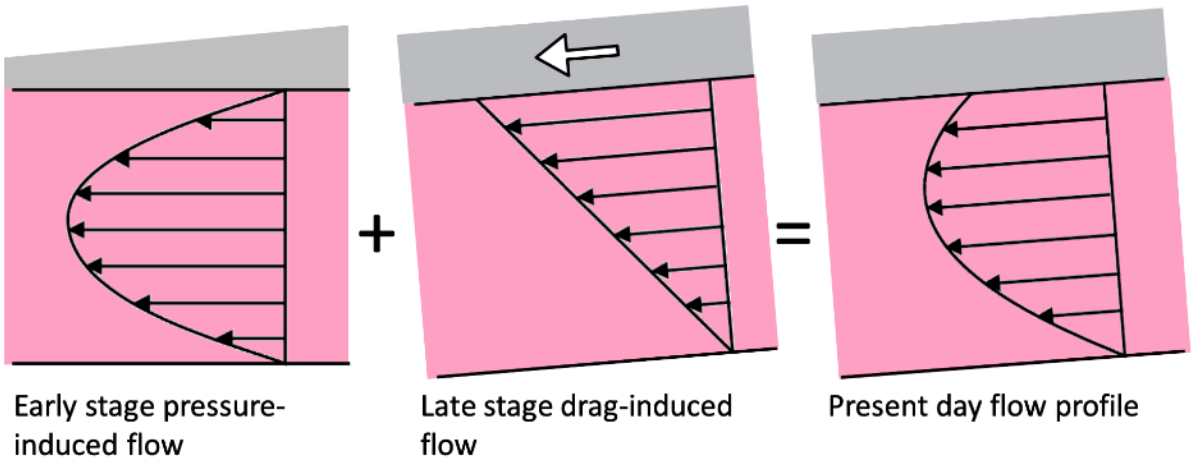

Figure 3.19 Summing the strain resulting from an early pressure-induced Poiseuille flow followed by a later drag-induced Couette flow results in an asymmetric Poiseuille flow profile.

The heterogeneous distribution of strain within the deforming salt body also means that we must account for intrasalt heterogeneity when building velocity models to accurately seismically image and depth convert sub-salt structures. The presence of interbeds with relatively slow seismic velocities will disrupt travel times, and as such the travel times will be sensitive to the geometry and distribution of intrasalt structures, particularly where large

stacked duplex structures occur (e.g. Fig. 3.13). We therefore conclude that intrasalt structure and strain partitioning is an important consideration for successful petroleum exploration and production, with implications for accurate velocity modelling and efficient drilling through thick salt.

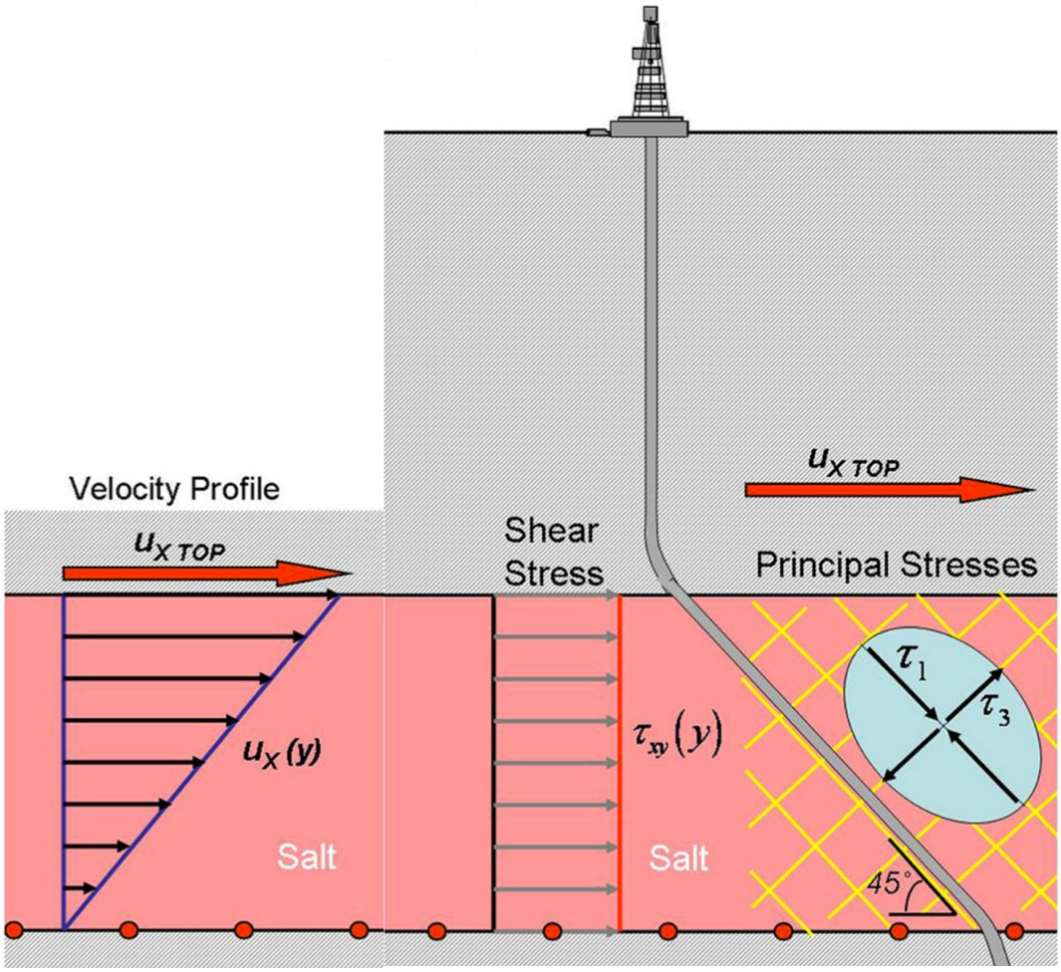

Figure 3.20 Optimal drilling trajectory through a salt sheet deforming via Couette flow in order to minimise shear stresses acting on the well bore. Peak shear stress of salt layers having Couette flow can be mitigated by drilling at 45° to the direction of flow in the salt layer. Modified from Weijermars and Jackson, (2014).

3.7 Conclusions

- Gravitationally-driven salt tectonics have dominated the Levant passive margin since the Messinian, with a dominant NW direction of transport
- Salt flow is locally restricted around the Latakia Ridge leading to more intense supra-salt deformation
- Reflective units within Messinian salt deform in a brittle manner and allow us to measure the relative seismic-scale intrasalt strain distribution
- The lateral seismic strain distribution is irregular, with locally high strains that reflect locally developed thrust duplexes
- Vertical strain profiles derived from seismic reflection data may not represent true flow profiles due to limitations in seismic resolution and differences in the way in which strain is accommodated between units with different rheologies
- The dominant flow regime (Poiseuille vs. Couette) may vary through time and space, predominantly due to changes in the relative contribution of differential loading (i.e. gravity spreading) and margin tilting (i.e. gravity gliding)
- Deviated well paths may be implemented to minimise borehole stress where the present dominant salt flow regime is well-constrained

References

Aal, A.A., El Barkooky, A., Gerrits, M., Meyer, H., Schwander, M. and Zaki, H., 2000. Tectonic evolution of the Eastern Mediterranean Basin and its significance for hydrocarbon prospectivity in the ultradeepwater of the Nile Delta. The Leading Edge, 19(10), pp.1086-1102.

Albertz, M. and Ings, S.J., 2012. Some consequences of mechanical stratification in basin-scale numerical models of passive-margin salt tectonics. Geological Society, London, Special Publications, 363(1), pp.303-330.

Allen, H., C.A.-L. Jackson and A.J. Fraser, 2016, Gravity-driven deformation of a youthful saline giant: the interplay between gliding and spreading in the Messinian basins of the Eastern Mediterranean: Petroleum Geoscience, v. 22, p. 340-356.

Balk, R. 1949. Structure of Grand Saline salt dome. AAPG Bulletin, 33, 1791–1829.

Ben-Avraham, Z., 1978. The structure and tectonic setting of the Levant continental margin, eastern Mediterranean. Tectonophysics, 46(3-4), pp.313-331.

Bertoni, C. and Cartwright, J.A., 2006. Controls on the basinwide architecture of late Miocene (Messinian) evaporites on the Levant margin (Eastern Mediterranean). Sedimentary Geology, 188, pp.93-114.

Bertoni, C. and Cartwright, J.A., 2007. Major erosion at the end of the Messinian Salinity Crisis: evidence from the Levant Basin, Eastern Mediterranean. Basin Research, 19(1), pp.1-18.

Brown, A.R., 2011. Interpretation of three-dimensional seismic data. Society of Exploration Geophysicists and American Association of Petroleum Geologists.

Brun, J.P. and Mauduit, T.P.O., 2009. Salt rollers: Structure and kinematics from analogue modelling. Marine and Petroleum Geology, 26(2), pp.249-258.

Burberry, C.M., 2015. Spatial and temporal variation in penetrative strain during compression: Insights from analog models. Lithosphere, 7(6), pp.611-624.

Burliga, S., P. Krzywiec, K. Dąbroś, J. Przybyło, E. Włodarczyk, M. Źróbek and M. Słotwiński. 2018. Salt tectonics in front of the Outer Carpathian thrust wedge in the Wieliczka area (S Poland) and its exposure in the underground salt mine: Geology, Geophysics & Environment, v. 44, p. 71-90.

Butler, R.W., Maniscalco, R., Sturiale, G. and Grasso, M., 2015. Stratigraphic variations control deformation patterns in evaporite basins: Messinian examples, onshore and offshore Sicily (Italy). Journal of the Geological Society, 172(1), pp.113-124.

Butler, R.W.H. and Paton, D.A., 2010. Evaluating lateral compaction in deepwater fold and thrust belts: How much are we missing from “nature’s sandbox”. GSA Today, 20(3), pp.4-10.

Camerlenghi, A., Del Ben, A., Hübscher, C., Forlin, E., Geletti, R., Brancatelli, G., Micallef, A., Saule, M. and Facchin, L., 2019. Seismic markers of the Messinian salinity crisis in the deep Ionian Basin. Basin Research.

Cartwright, J.A. and M.P.A. Jackson, 2008, Initiation of gravitational collapse of an evaporite basin margin: The Messinian saline giant, Levant Basin, eastern Mediterranean. Geological Society of America Bulletin, 120(3-4), pp.399-413.

Cartwright, J.A., M.P.A. Jackson, T.P. Dooley and S. Higgins, 2012, Strain partitioning in gravity-driven shortening of a thick, multilayered evaporite sequence, in G.I. Alsop, S.G. Archer, A.J. Hartley, N.T. Grant and R. Hodgkinson, eds., Salt Tectonics, Sediments and Prospectivity: GSL Special Publication 363, p. 449-470.

Cartwright, J., C. Kirkham, C. Bertoni, N. Hodgson and K. Rodriguez, 2018, Direct calibration of salt sheet kinematics during gravity-driven deformation: Geology, v. 46, p. 623-626.

Coleman, A.J., Jackson, C.A-L. and Duffy, O.B., 2017. Balancing sub-and supra-salt strain in salt-influenced rifts: Implications for extension estimates. Journal of Structural Geology, 102, pp.208-225.

Dooley, T.P., Hudec, M.R., Carruthers, D., Jackson, M.P.A. and Luo, G., 2017. The effects of base-salt relief on salt flow and suprasalt deformation patterns—Part 1: Flow across simple steps in the base of salt. Interpretation, 5(1), pp.SD1-SD23.

dos Reis, A.T., Gorini, C. and Mauffret, A., 2005. Implications of salt–sediment interactions on the architecture of the Gulf of Lions deep-water sedimentary systems—western Mediterranean Sea. Marine and Petroleum Geology, 22(6-7), pp.713-746.

Elfassi, Y., Gvirtzman, Z., Katz, O. and Aharonov, E., 2019. Chronology of post-Messinian faulting along the Levant continental margin and its implications for salt tectonics. Marine and Petroleum Geology, 109, pp.574-588.

Esestime, P., A. Hewitt, and N. Hodgson, 2016, Zohr–A newborn carbonate play in the Levantine Basin, East-Mediterranean: First Break, 34(2), 87-93.

Feng, Y.E., Steinberg, J. and Reshef, M., 2017. Intra-salt deformation: Implications for the evolution of the Messinian evaporites in the Levant Basin, eastern Mediterranean. Marine and Petroleum Geology, 88, pp.251-267.

Feng, Y. E., A. Yankelzon, J. Steinberg, and M. Reshef, 2016, Lithology and characteristics of the Messinian evaporite sequence of the deep Levant Basin, eastern Mediterranean: Marine Geology, 376, 118-131.

Fiduk, J.C. and Rowan, M.G., 2012. Analysis of folding and deformation within layered evaporites in Blocks BM-S-8 &-9, Santos Basin, Brazil. Geological Society, London, Special Publications, 363(1), pp.471-487.

Fossen, H., 2016. Structural geology. Cambridge University Press.

Gautier, F., G. Clauzon, J.P. Suc, J. Cravatte and D. Violanti, 1994, Age and duration of the Messinian salinity crisis: R. Acad. Sci., Paris (IIA) 318, p. 1103–1109.

Ghalayini, R., Daniel, J.M., Homberg, C., Nader, F.H. and Comstock, J.E., 2014. Impact of Cenozoic strike-slip tectonics on the evolution of the northern Levant Basin (offshore Lebanon). Tectonics, 33(11), pp.2121-2142.

Ghalayini, R., Homberg, C., Daniel, J.M. and Nader, F.H., 2017. Growth of layer-bound normal faults under a regional anisotropic stress field. Geological Society, London, Special Publications, 439(1), pp.57-78.

Gradmann, S. and Beaumont, C., 2012. Coupled fluid flow and sediment deformation in margin-scale salt-tectonic systems: 2. Layered sediment models and application to the northwestern Gulf of Mexico. Tectonics, 31(4).

Gvirtzman, Z., M. Reshef, O. Buch-Leviatan and Z. Ben-Avraham, 2013, Intense salt deformation in the Levant Basin in the middle of the Messinian salinity crisis: Earth and Planetary Science Letters, 379, 108–119.

Gvirtzman, Z., Manzi, V., Calvo, R., Gavrieli, I., Gennari, R., Lugli, S., Reghizzi, M. and Roveri, M., 2017. Intra-Messinian truncation surface in the Levant Basin explained by subaqueous dissolution. Geology, 45(10), pp.915-918.

Hall, J., Calon, T.J., Aksu, A.E. and Meade, S.R., 2005. Structural evolution of the Latakia Ridge and Cyprus Basin at the front of the Cyprus Arc, eastern Mediterranean Sea. Marine Geology, 221(1-4), pp.261-297.

Hawie, N., Gorini, C., Deschamps, R., Nader, F.H., Montadert, L., Granjeon, D. and Baudin, F., 2013. Tectono-stratigraphic evolution of the northern Levant Basin (offshore Lebanon). Marine and Petroleum Geology, 48, 392-410.

Hodgson, N., 2012. The Miocene hydrocarbon play in southern Lebanon. First Break, 30(12).

Hoy, R. B., Foose,R.M.& O'Neill, B. J. 1962. Structure of Winnfield salt diapir. AAPG Bulletin, 46, 1444–1459.

Hudec, M.R. and Jackson, M.P., 2007. Terra infirma: Understanding salt tectonics. Earth-Science Reviews, 82(1-2), pp.1-28.

Jackson,M.P.A., Cornelius, R. R., Craig, C. H., Gansser, A., Stocklin,J.& Talbot, C. J. 1990. Salt Diapirs of the Great Kavir. Geological Society of America, Boulder, Memoir, 177.

Jackson, M. P. A. 1995. Retrospective salt tectonics. In: Jackson, M.P.A., Roberts,D. G.& Snelson,S. (eds) Salt Tectonics, A Global Perspective. American Association of Petroleum Geologists, Tulsa, Memoir, 65, 1–28.

Jackson, M.P. and Hudec, M.R., 2017. Salt tectonics: Principles and practice. Cambridge University Press.

Jackson, M.P.A., B.C. Vendeville and D.D. Schultz-Ela, 1994, Structural dynamics of salt systems: Annual Review of Earth and Planetary Sciences, 22(1), pp.93-117.

Jackson, C.A.L., Jackson, M.P., Hudec, M.R. and Rodriguez, C.R., 2015. Enigmatic structures within salt walls of the Santos Basin—Part 1: Geometry and kinematics from 3D seismic reflection and well data. Journal of Structural Geology, 75, pp.135-162.

Jackson, M.P. and Hudec, M.R., 2005. Stratigraphic record of translation down ramps in a passive-margin salt detachment. Journal of Structural Geology, 27(5), pp.889-911.

Kartveit, K.H., Omosanya, K.O., Johansen, S.E., Eruteya, O.E., Reshef, M. and Waldmann, N.D., 2018. Multiphase structural evolution and geodynamic implications of Messinian salt-related structures, levant basin, offshore Israel. Tectonics, 37(5), pp.1210-1230.

Kartveit, K.H., Ulsund, H.B. and Johansen, S.E., 2019. Evidence of sea level drawdown at the end of the Messinian salinity crisis and seismic investigation of the Nahr Menashe unit in the northern Levant Basin, offshore Lebanon. Basin Research, 31(5), pp.827-840.

Kirkham, C., Cartwright, J., Bertoni, C., Rodriguez, K. and Hodgson, N., 2019. 3D kinematics of a thick salt layer during gravity-driven deformation. Marine and Petroleum Geology, 110, pp.434-449.

Kirkham, C., Bertoni, C., Cartwright, J., Lensky, N.G., Sirota, I., Rodriguez, K. and Hodgson, N., 2020. The demise of a 'salt giant'driven by uplift and thermal dissolution. Earth and Planetary Science Letters, 531, p.115933.

Kupfer, D. H. 1962. Structure of Morton salt company mine, Weeks Island salt dome. AAPG Bulletin, 46, 1460–1467.

Lofi, J., Déverchère, J., Gaullier, V., Gillet, H., Gorini, C., Guennoc, P., Loncke, L., Maillard, A., Sage, F. and Thinon, I., 2011. Seismic atlas of the Messinian Salinity Crisis markers in the Mediterranean and Black Seas (Vol. 179, pp. 1-72). Société Géologique de France.

Meilijson, A., Hilgen, F., Sepúlveda, J., Steinberg, J., Fairbank, V., Flecker, R., Waldmann, N.D., Spaulding, S.A., Bialik, O.M., Boudinot, F.G. and Illner, P., 2019. Chronology with a pinch of salt: Integrated stratigraphy of Messinian evaporites in the deep Eastern Mediterranean reveals long-lasting halite deposition during Atlantic connectivity. Earth-Science Reviews.

Miralles, L., Sans, M., Gali,S.& Santanach, P. 2001. 3-D rock salt fabrics in a shear zone (Su´ria Anticline, South-Pyrenees). Journal of Structural Geology, 23, 675–691.

Nader, F.H., Inati, L., Ghalayini, R., Hawie, N. and Daher, S.B., 2018. Key geological characteristics of the Saida-Tyr Platform along the eastern margin of the Levant Basin, offshore Lebanon: implications for hydrocarbon exploration. Oil & Gas Science and Technology–Revue d'IFP Energies nouvelles, 73, p.50.

Netzeband, G. L., C. P. Hübscher, & D. Gajewski, 2006, The Structural Evolution of the Messinian Evaporites in the Levantine Basin: Marine Geology, 230(3–4), 249–73.

Pichel, L.M., Peel, F., Jackson, C.A. and Huuse, M., 2018. Geometry and kinematics of salt-detached ramp syncline basins. Journal of Structural Geology, 115, pp.208-230.

Quirk, D.G., Schødt, N., Lassen, B., Ings, S.J., Hsu, D., Hirsch, K.K. and Von Nicolai, C., 2012. Salt tectonics on passive margins: examples from Santos, Campos and Kwanza basins. Geological Society, London, Special Publications, 363(1), pp.207-244.

Raith, A.F., Strozyk, F., Visser, J. and Urai, J.L., 2016. Evolution of rheologically heterogeneous salt structures: a case study from the NE Netherlands. Solid Earth, 7(1), p.67.

Reiche, S., Hübscher, C. and Beitz, M., 2014. Fault-controlled evaporite deformation in the Levant Basin, Eastern Mediterranean. Marine Geology, 354, pp.53-68.

Roveri, M., R. Flecker, W. Krijgsman, J. Lofi, S. Lugli, V. Manzi, F.J. Sierro, A. Bertini, A. Camerlenghi, G. De Lange, R. Govers, F.J. Hilgen, C. Hübscher, P.T. Meijer, & M. Stoica, 2014, The Messinian salinity crisis: Past and future of a great challenge for marine sciences: Marine Geology, 352, 25–58.

Rowan, M.G., Urai, J.L., Fiduk, J.C. and Kukla, P.A., 2019. Deformation of intrasalt competent layers in different modes of salt tectonics. Solid Earth, 10(3), pp.987-1013.

Ryan, W.B.F., 2009, Decoding the Mediterranean salinity crisis: Sedimentology 56, 95–136.

Schleder, Z., Urai, J. L., Nollet,S.& Hilgers,C. 2008. Solution–precipitation creep and fluid flow in halite: a case study from the Zechstein (Z1) rocksalt from Neuhof salt mine (Germany). Geologisches Rundschau, 97, 1045–1056.

Schueller, S., and P. Davy, 2008, Gravity influenced brittle-ductile deformation and growth faulting in the lithosphere during collision: Results from laboratory experiments, J. Geophys. Res., 113, B12404.

Schultz-Ela, D.D. and Walsh, P., 2002. Modeling of grabens extending above evaporites in Canyonlands National Park, Utah. Journal of Structural Geology, 24(2), pp.247-275.

Steventon, M.J., Jackson, C.A.L., Hodgson, D.M. and Johnson, H.D., 2019. Strain analysis of a seismically imaged mass-transport complex, offshore Uruguay. Basin Research, 31(3), pp.600-620.

Strozyk, F., Van Gent, H., Urai, J.L. and Kukla, P.A., 2012. 3D seismic study of complex intra-salt deformation: An example from the Upper Permian Zechstein 3 stringer, western Dutch offshore. Geological Society, London, Special Publications, 363(1), pp.489-501.

Talbot, C. J. 1998. Extrusions of Hormuz salt in Iran. In: Blundell,D.J.& Scott, A. C. (eds) Lyell, the Past is the Key to the Present. Geological Society, London, Special Publications, 143, 315–334.

Van Gent, H., Urai, J.L. and De Keijzer, M., 2011. The internal geometry of salt structures–a first look using 3D seismic data from the Zechstein of the Netherlands. Journal of Structural Geology, 33(3), pp.292-311.

Weijermars, R. and M.P.A. Jackson, 2014, Predicting the depth of viscous stress peaks in moving salt sheets: Conceptual framework and implications for drilling: AAPG Bull., v. 98, p. 911–945.

Zak, I. and Freund, R., 1980. Strain measurements in eastern marginal shear zone of Mount Sedom salt diapir, Israel. AAPG Bulletin, 64(4), pp.568-581.

4 Taking the Pulse of Salt-Detached Gravity Gliding in the Eastern Mediterranean

This manuscript is currently under review with **Tectonics**.

A pre-print is available on **EarthArxiv**:

https://eartharxiv.org/repository/view/45/

Acknowledgements

The data used in this study is confidential and was generously provided under license by the Lebanese Petroleum Administration. I would like to gratefully acknowledge Ramadan Ghalayini for help acquiring the data, and Wissam Chbat for sanctioning the material for publication. I would also like to thank my supervisor and co-authors, Chris Jackson and Davide Oppo, for valuable discussions that guided my interpretation of the data, and help with editing the manuscript.

This study was part of a collaboration that produced two companion papers: this work presented here and led by me, and a second led by my co-author Davide Oppo. Whilst my study focuses on the salt tectonics implications, the latter focuses on the fluid escape implications. The companion paper is currently under review in **Basin Research** and available as a pre-print on **EarthArxiv**:

https://eartharxiv.org/repository/view/46/

Abstract

Despite having a profound impact on the structural evolution of salt-influenced basins, spatial and temporal variations in rates of salt flow, and their key controls, remain largely unconstrained. We investigate early-stage salt-detached gliding using a 3D seismic dataset from the Levant Margin in the Eastern Mediterranean, where gravitational instability due to margin uplift has caused north-westward translation of the Messinian salt sheet and its Plio-Pleistocene clastic overburden. Large, NE-trending, base-salt anticlines have allowed the basinward translation to be recorded by the development of supra-salt ramp syncline basins (RSBs) and fluid escape pipes, the latter forming due to the leakage of gas and fluid from the anticline crests. The trails of fluid escape pipes provide direct kinematic vectors of transport direction, while the stratigraphic record of the RSBs not only constrains the relative ages of the pipes, but allows us to quantify the magnitude of basinward translation. Correlating intra-RSB horizons across the margin provides relative age constraints, which we use to analyse lateral variations in translation rates along the margin, and how these vary through time. We show that translation rates are broadly uniform on the length scale of individual anticlines and related RSBs (c. 10 km), but that there is significant margin-scale (c. 100 km) lateral variability in both the direction and magnitude of translation. We attribute temporal variations in rates of translation to cyclical 'pulses' of salt flow due to volumetric flux imbalances across the anticlines, while the distribution of elastic strain in the overburden modulates the overall basin-scale trend. These results demonstrate the importance of local stresses in controlling the local direction and rate of salt flow at any point in time.

4.1 Introduction

Salt-influenced basins and passive margins are structurally complex, globally distributed, and hydrocarbon-rich. The variety of structural styles in different salt basins around the world is testament to the myriad of ways in which salt-related deformation can affect the tectono-stratigraphic evolution of sedimentary basins. Over the past few decades seismic reflection data have transformed our understanding of subsurface salt tectonics, allowing us to investigate the regional structural evolution of salt basins (Jackson et al., 1994; Hudec and Jackson, 2007; Jackson and Hudec, 2017). However, the various controls on the evolution of these stress-sensitive systems are still debated. Gravity gliding and spreading are simplified end-member models used to describe gravitationally-driven salt tectonics along passive margins (e.g. Brun and Fort, 2011; Peel, 2014; Schultz-Ela, 2001), but the effects of other variables that introduce further complexity into the system, such as base-salt relief (e.g. Dooley et al., 2017; Pichel et al., 2019; Evans and Jackson, 2019) and intrasalt heterogeneity (e.g Albertz and Ings, 2012; Raith et al., 2016; Rowan et al., 2019), have remained poorly understood.

Due to the internally chaotic and low-amplitude appearance of salt bodies in seismic reflection data (Jones and Davison, 2014), the deformation history of seismically-imaged salt structures is commonly reconstructed using stratigraphic relationships and structures in the overburden (e.g. Quirk et al., 2012). While this approach is invaluable in reconstructing vertical salt movements (e.g. diapir growth), it often neglects that overburden structures may have also been laterally translated tens of km downdip. Estimations of lateral translation on salt-detached margins have relied heavily on summing extensional fault heaves (in the updip domain) and/or line-length balancing techniques (see Coleman et al., 2017). Typically, the 'undeformed' translational domain has yielded little information of use in this regard (Schultz-Ela, 2001).

Ramp syncline basins (RSBs) are one of the few stratigraphic features that record, and thus allow us to quantify, basinward translation of salt overburden (Jackson and Hudec, 2005). Although they were first recognised in the Gulf of Lyon, offshore France more than two decades ago (e.g. Benedicto et al., 1999), they are still often overlooked and under-utilised in many basins (Pichel et al., 2018). Salt-detached RSBs form as a result of salt and overburden

translation across a sub-salt topographic high (Marton et al., 2000; Jackson and Hudec et al., 2005; Pichel et al., 2018; Evans and Jackson, 2019). This creates a local sediment depocentre adjacent to the high, above its downdip flank. Syn-kinematic strata thicken into this accommodation space, and onlap towards the updip high. As translation continues, the onlapping growth strata are progressively transported away from the high in the direction of salt flow. This creates an 'onlap surface' in the stratigraphic record, with the horizontal distance from the first onlap to the sub-salt high giving the total magnitude of translation (Jackson and Hudec, 2005). Recent studies have begun to exploit the uses of RSBs as records of translation on salt-influenced passive margins, demonstrating how stacked RSBs of different ages may be used to reconstruct the history of salt-detached gravity gliding offshore Brazil (Pichel et al., 2018) and offshore Angola (Evans and Jackson, 2019).

Transient strain markers such as fluid escape pipes may also be used to reconstruct translation on salt-influenced passive margins (Cartwright et al., 2018; Kirkham et al., 2019). The first study identified a trail of diachronous pipes in the deep Levantine Basin, offshore Lebanon, and determine that each pipe originated from the crest of a sub-salt anticline (termed the Oceanus structure; Fig. 4.1) before being transported basinward due to gravity gliding (Cartwright et al., 2018). A subsequent study then interpreted four distinct pipe trails originating from a single anticline nearby (termed the Saida-Tyr structure; Fig. 4.1) (Kirkham et al., 2019). By treating the pipes as direct kinematic markers the authors estimate the velocity of the overburden and viscosity of the deforming salt sheet. However, both studies are forced to make assumptions about the ages of the pipes, and they are limited to relatively small areas (each <35 km^2) due to the distribution of pipes, thus giving only local constraints on the kinematics of a much larger salt layer.

In this study we apply a new approach to investigating gravity-driven salt translation at the margin-scale (covering an area of c. 5000 km^2) by integrating the geological records given by RSBs and trails of fluid escape pipes. The young Messinian (latest Miocene) evaporite sequence of the Mediterranean Basin provides a perfect natural laboratory to study active, early-stage, gravity-driven salt tectonics of a thick salt sheet. We analyse eight RSBs and twelve associated fluid escape pipe trails in the updip domain of the northern Levantine Basin, offshore Lebanon. Because the Messinian salt giant is shallowly buried and only weakly deformed, it is well-imaged in seismic reflection data. Furthermore, unlike older basins (e.g.

offshore Brazil and Angola), the RSBs are well-preserved and not yet overprinted by later tectonic deformation. They therefore provide an ideal opportunity to investigate early RSB development, quantify translation along the margin and assess implications for salt flow kinematics.

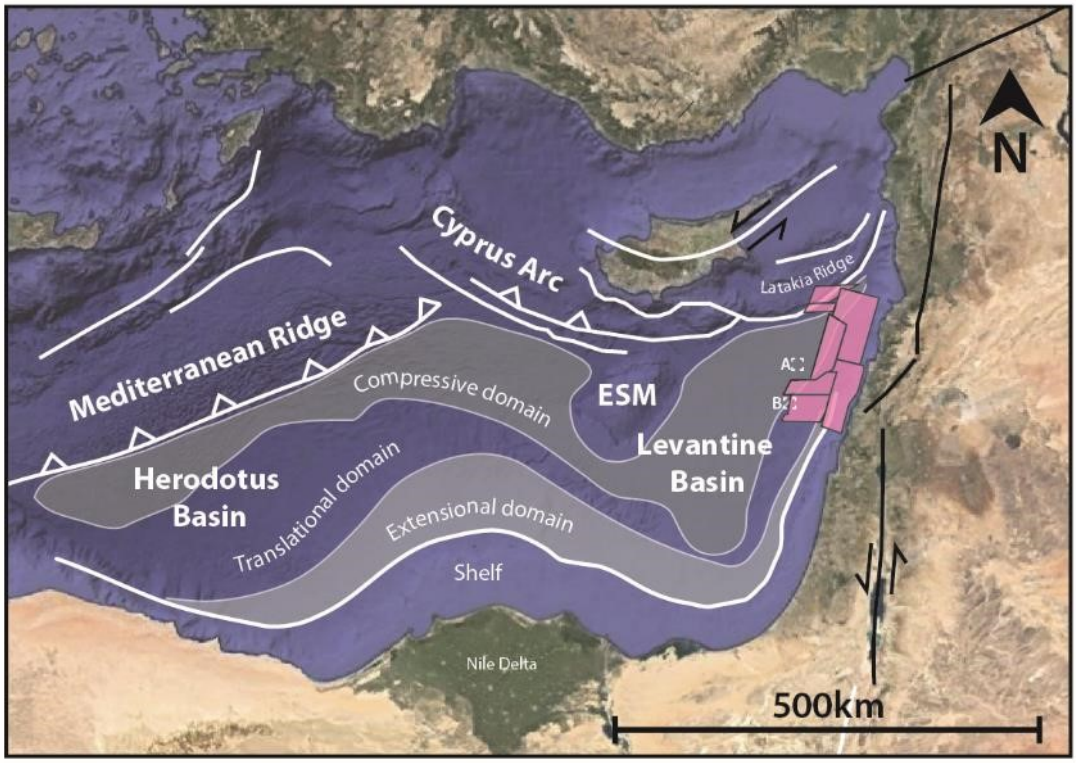

Figure 4.1 Location of dataset (pink polygon) and distribution of key tectonic elements in the Eastern Mediterranean. Boxes A and B denote location of previous studies of the Oceanus Structure (Cartwright et al., 2018) and the Saida-Tyr Structure (Kirkham et al., 2019), respectively.

4.2 Data and Methods

We use a large (c. 10,000 km^2) 3D seismic reflection dataset located offshore Lebanon in the northern Levantine Basin (Fig. 4.1) to investigate the stratigraphic record of RSBs in an area of early-stage gravity gliding. The dataset comprises a merge of seven time-migrated 3D seismic surveys acquired by PGS that have been processed to near-zero phase with reverse SEG polarity, i.e. an increase in acoustic impedance has a negative amplitude. Bin dimensions were 25 x 25 m during data processing. The dominant frequencies of seismic data are 50 Hz in the overburden, 25 Hz in the Messinian evaporites, and 17 Hz in the sub-salt units. The seismic resolution, calculated as a quarter of the wavelength (λ/4; Brown, 2011), varies according to lithology and depth below seabed, but is estimated to be c. 10 m in the clastic supra-salt overburden, c. 42 m in the Messinian salt interval and c. 44 m in the sub-salt, using

average P-wave velocities of 2000 m/s, 4200 m/s, and 3000 m/s respectively (Gardosh and Druckman, 2006; Reiche et al., 2014; Feng et al., 2016). Where thicknesses and depths are measured and quoted in ms two-way-time (TWT), we use the average interval velocities to estimate the equivalent thickness in m.

In order to analyse the development of RSBs we map reflections in the supra-salt stratigraphy, analyse their seismic-stratigraphic relationships, and generate structure and thickness (isopach) maps. Key horizons include base-salt, top-salt and seabed. The distribution of the salt and orientation of supra-salt faults and folds give context to the salt tectonic regime and basin evolution. We identify eight well-developed RSBs that have clearly defined onlap surfaces, and select 9 onlapping intra-RSB horizons (O2-O10; Fig. 4.2) that can be confidently correlated across the margin (spanning c. 100 km from NE to SW). Correlating seismic horizons between different RSBs allows us to compare the magnitude of translation along the margin during different time intervals, identifying lateral changes along strike. For the most part we discuss relative, rather than absolute, translation rates due the absence of accurate age constraints in the supra-salt strata. One key horizon is tentatively assigned an absolute age of 1.8 Ma based on a calibration with Kirkham et al. (2019) and Cartwright et al. (2018), who mapped this horizon northwards from wells in the southern Levantine Basin into their study areas. Should future data (i.e. from drilling) yield further meaningful age constraints within the supra-salt strata, this may be used to calculate absolute translation rates. Finally, we sum the heaves of salt-detached growth faults in the updip extensional domain to compare to the translation estimates given by the RSBs. Fault heave measurements are taken on seismic sections perpendicular to the dominant structural trend (i.e. parallel to the direction of extension).

We also generate variance and RMS amplitude attribute maps derived from the top-salt surface to identify and map fluid escape pipes (Barnes, 2016). Features related to subsurface fluid migration have been interpreted following the criteria described in literature (e.g. Cartwright and Santamarina, 2015). Variance maps highlight fluid escape features due their internally chaotic nature in comparison to the continuous reflections characterising the surrounding stratigraphy, whereas RMS amplitude maps show the anomalously low-amplitude regions where the otherwise high-amplitude, top-salt reflection has been disrupted by fluid escape.

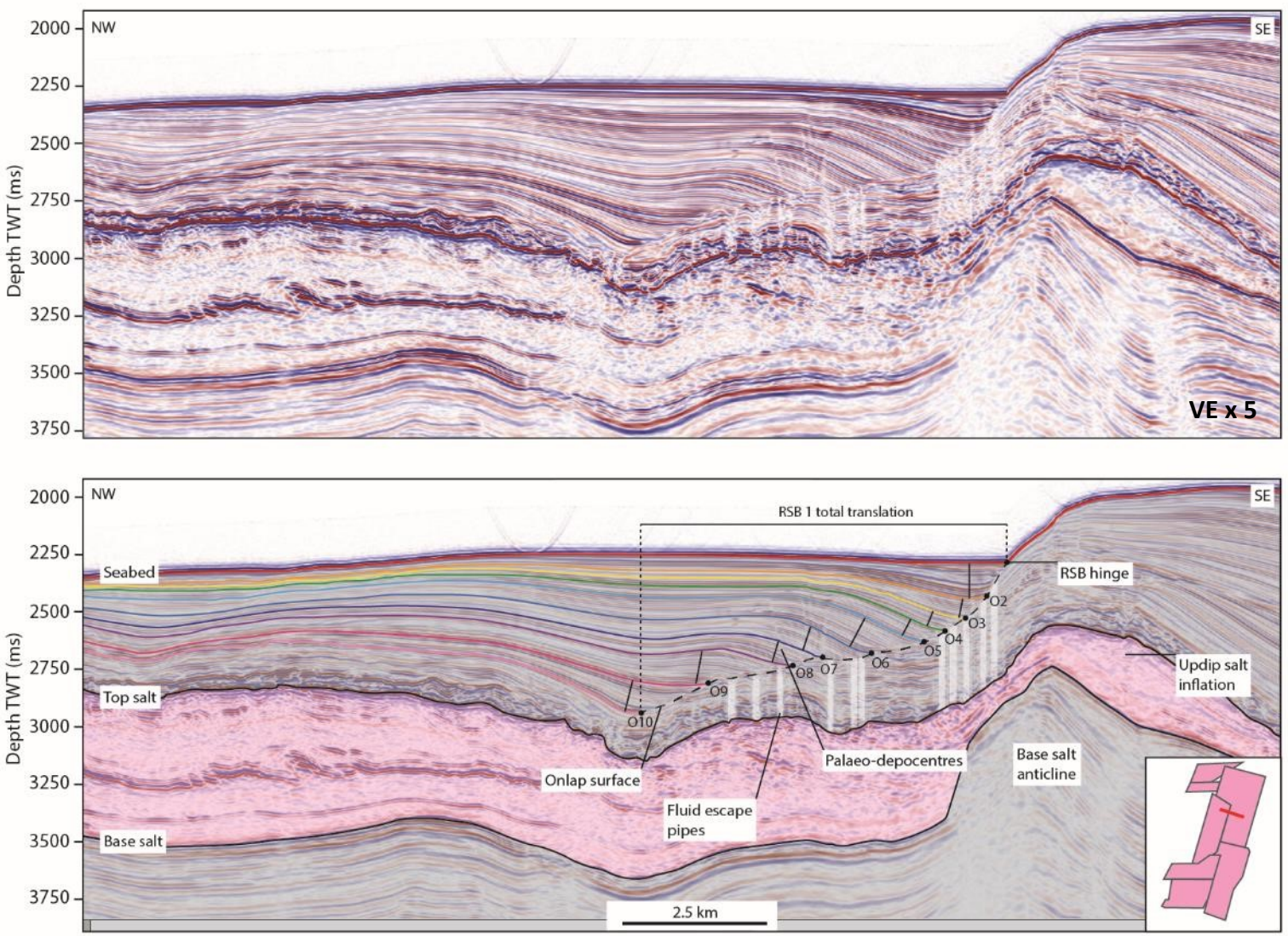

Figure 4.2 Seismic cross section showing base-salt anticline and associated ramp syncline basin downdip (RSB 1). Coloured lines show mapped intra-RSB horizons. Vertical white lines show fluid escape pipes. RSB depocentres form adjacent to the crest of the anticline and is subsequently translated downdip, preserving a stratigraphic record of downdip translation.

4.3 Geological Setting

The seismic dataset used in this study is situated offshore Lebanon in the Levantine Basin. The Eastern Mediterranean comprises the Levantine and Herodotus Basins, separated by the Eratosthenes Seamount (Fig. 4.1). The Levantine Basin formed during Permo-Triassic and Jurassic multiphase rifting events (Nader et al., 2018) and contains up to 20 km of clastic material overlying thinned continental crust (Aal et al., 2000; Inati et al., 2016). The African plate collided with the Eurasian plate in the Late Cretaceous, initiating active subduction along the northern boundary of the basin. The complex collision geodynamics of the region led to additional phases of folding, thrusting, and sinistral strike-slip fault movements during the Late Miocene-Pliocene (Hall et al., 2005). Compression led to folding and thrusting along the basin eastern margin, leading to the generation of NE-trending anticlines that deformed the Oligo-Miocene sedimentary units prior to, or at the onset of, the Messinian Salinity Crisis (MSC) (Ghalayini et al., 2014; Hawie et al., 2013). The lack of visible deformation of the post-Messinian overburden, possibly because of the accommodation of anticline amplification within the salt, makes it difficult to confidently demonstrate post-Messinian growth of the sub-salt anticlines (Ghalayini et al., 2014).

A thick (up to 2 km), layered evaporitic sequence was deposited across the eastern Mediterranean during the Messinian Salinity Crisis (MSC) between 5.96 and 5.33 Ma (e.g. Gautier et al., 1994; Ryan, 2009; Roveri et al., 2014). During this time, the Mediterranean Sea was isolated from the Atlantic Ocean due to the closure of the Strait of Gibraltar, causing evaporitic drawdown and extensive salt precipitation. When the Strait of Gibraltar reopened in the Pliocene, marine Atlantic waters flooded the Mediterranean and a clastic overburden (up to 1.5 km thick) was deposited above the salt. Tectonically-driven tilting of the basin margins, as well as differential loading of the salt by prograding clastic wedges, triggered gravity-driven deformation of the Messinian salt (Gvirtzman et al., 2013; Allen et al., 2016). This resulted in the development of kinematically-linked zones of updip extension and downdip contraction (Fig. 4.1) (e.g. Jackson et al., 1994). The salt deformation is thought to be dominantly driven by gravity gliding in the northern Levantine Basin (due to tilting of the margin), whereas gravity spreading dominates in the south due to sediment load by the Nile deep-sea fan (Allen et al., 2016).

The present-day Eastern Mediterranean region remains tectonically active. The deformation front of the Cyprus Arc, dominated by the Latakia Ridge, forms the northern boundary of the Levantine Basin, where ongoing plate convergence maintains active subduction zones (Fig. 4.1) (Ben-

Avraham, 1978; Hall et al., 2005). The western extension of the subduction zone forms an accretionary wedge, known as the Mediterranean Ridge, which bounds the Herodotus Basin to the north and west (Fig. 4.1). The Levant passive margin provides the eastern limit to the basin, offshore Lebanon and Israel (Hawie et al., 2013). N-S oriented strike-slip tectonics occur onshore adjacent to the margin along the Dead Sea Transform Zone, as the Arabian plate slides northwards past the African plate (Fig. 4.1). The north African passive margin forms the southern boundary to the basin, where the Nile river system is draining the African continental interior and supplying large quantities of clastic material to the rapidly prograding Nile Delta (Fig. 4.1).

4.4 Results

4.4.1 Base-Salt Relief

Salt flow is known to be sensitive to the geometry of the surface that it flows across (e.g. Dooley et al., 2017; Pichel et al., 2019; Evans and Jackson, 2019). Offshore Lebanon the base-salt surface dips generally to the NW, but with significant rugosity on this part of the Levant Margin (Fig. 4.3). The depth to base-salt shallows to the south of the dataset across the Saida Fault, a Mesozoic normal fault which bounds an elevated Mesozoic structural element known as the Saida-Tyr Platform (Fig. 4.3) (Ghalayini et al., 2018). The Latakia Ridge crosses the northwestern corner of the dataset and is expressed as a large, arcuate, broadly NE-trending anticline on both the base-salt and top-salt surfaces (Fig. 4.3 and Fig. 4.4b).

There are several, NE-trending anticlines distributed across the margin which vary from 100 ms up to 820 ms in height (c. 200 m up to 1.6 km respectively) (Fig. 4.3). In map view they are between 8 and 28 km long, and are typically 2-3 km wide (Fig. 4.3). Although the seismic data are presented in TWT, we know these anticlines are real geological structures and not seismic data artefacts (i.e. velocity pull-up features) as the salt is thinner (as opposed to thicker) above the anticlines crest. Above one of the largest anticlines the salt thins to as little as 30 ms (c. 70 m), from an adjacent thickness of 500 ms (c. 1.3 km) (Fig. 4.2). These anticlines are thought to have developed during the Late Miocene due to the NW-SE oriented regional tectonic compression associated with continental convergence. Some are symmetric anticlinal structures while other show an asymmetric geometry with steep forelimbs and gentle backlimbs, interpreted as fault-propagation folds overlying deeper thrust faults (e.g. Fig. 4.2) (Ghalayini et al., 2014; Ghalayini et al., 2018). Several of the folds were formed during transpressional reactivation of the Saida Fault

(Fig. 4.3). They therefore predate deposition of the Messinian salt (Hawie et al., 2013), although it is possible that there may have been some later amplification of these structures in response to ongoing compression (Ghalayini et al. 2014).

We also note the base-salt is offset by evenly-spaced, NW-SE striking, short (up to 6 km), low-displacement (30-60 ms TWT; c. 50-90 m) normal faults that are particularly common in the deeper basin (Fig. 4.3). In cross section these appear to be layer-bound, sub-salt normal faults terminating at the base-salt, and that do not extend upwards into the overlying salt. These have been interpreted as Late Miocene syn-sedimentary faults that formed in response to an anisotropic stress field (Ghalayini et al. 2017; Reiche et al, 2014).

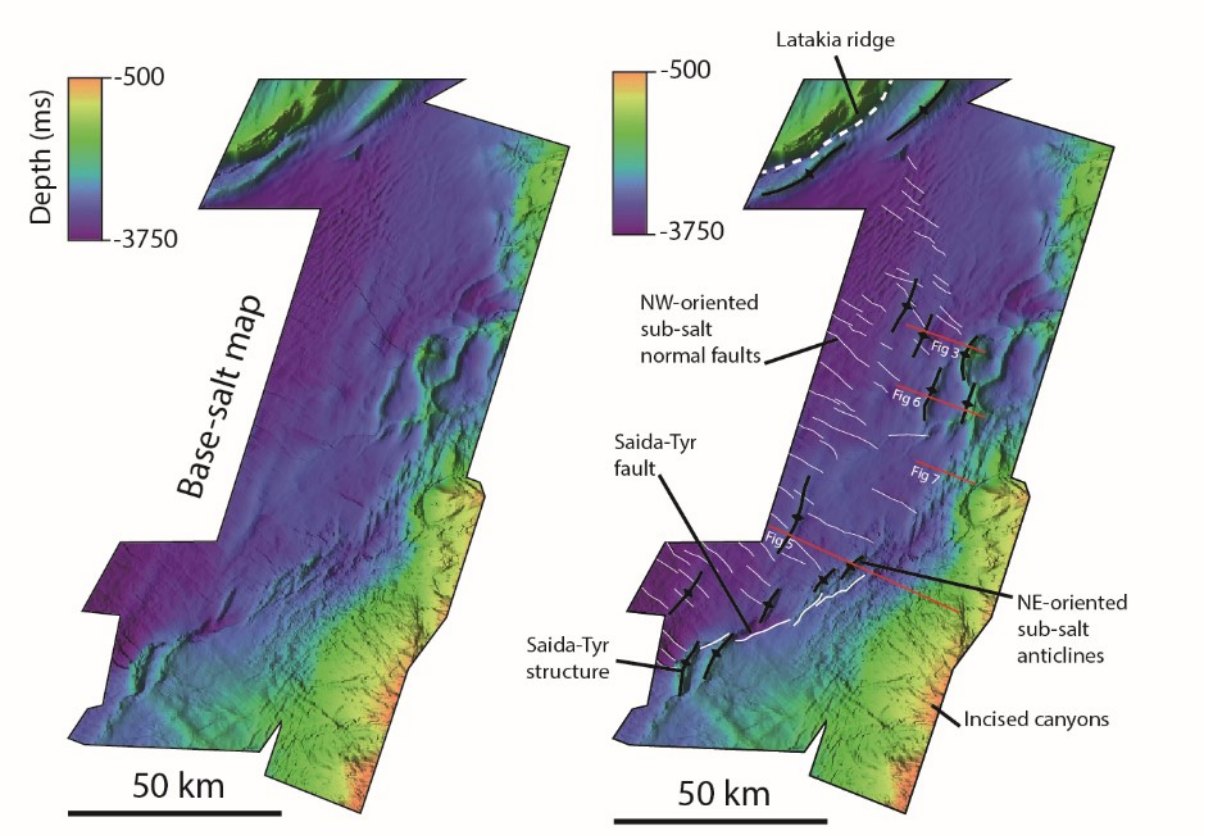

Figure 4.3 TWT depth map of the base-salt surface showing the distribution of NE-trending anticlines (black) and NW-trending normal faults (white). Red lines show locations of seismic sections used in other figures.

4.4.2 Salt Distribution and Supra-Salt Structure

The Messinian salt layer overall thickens westward into the deep Levantine Basin and thins updip, pinching out onto the Levant Margin (Fig. 4.4a). The evaporite sequence is lithologically heterogeneous, leading to internal seismic reflectivity within the deforming salt sheet (e.g. Fig. 4.5) (Gvirtzman et al., 2013; Feng et al., 2016; Meilijson et al., 2019; Evans and Jackson, 2020).

The intrasalt reflections are folded and faulted, and are truncated landward against the top-salt due to an earlier, syn-depositional phase of deformation, erosion, and dissolution (Gvirtzman et al., 2013; Gvirtzman et al., 2017; Feng et al., 2017; Kartveit et al., 2018; Kirkham et al., 2020; Evans and Jackson, 2020).

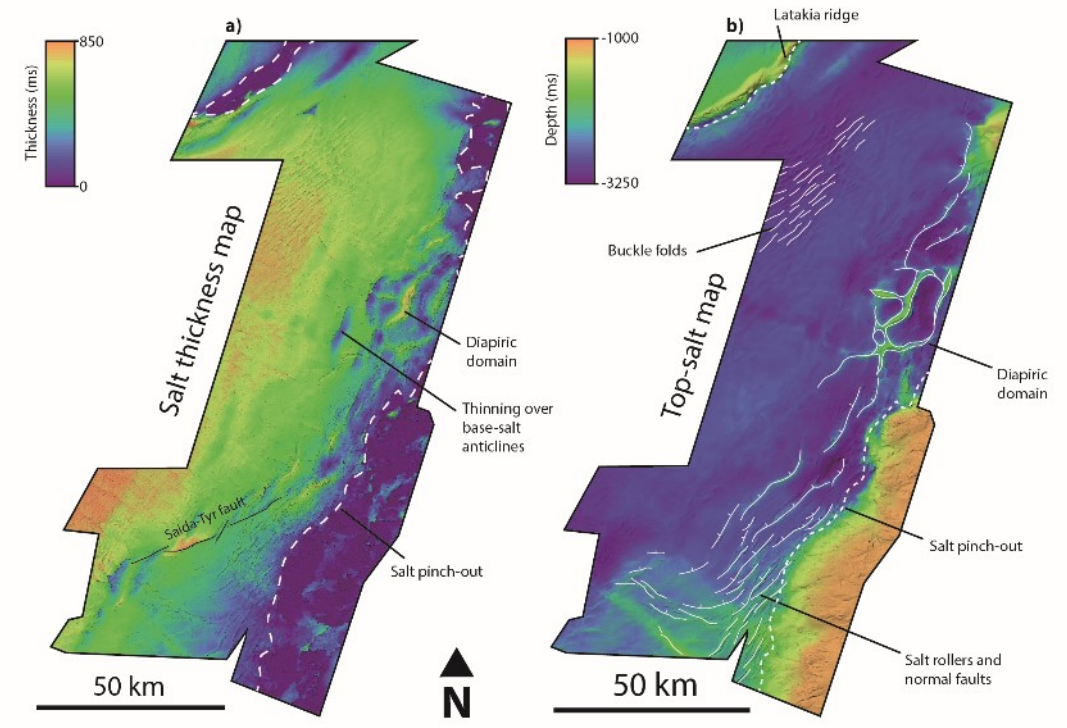

Figure 4.4 (a) Salt thickness map showing thinning over base-salt anticlines and pinch-out updip onto the Levant margin. (b) Top-salt depth map showing extensional structures along the margin and buckle folds around the Latakia Ridge.

The supra-salt structure of the basin can be divided into kinematically-linked domains of updip extension and downdip contraction, separated by a relatively undeformed translational domain (Fig. 4.1). The present dataset mostly covers the extensional and upper translational domains, with minimal contraction in the overburden, except where the Latakia Ridge locally restricts salt flow in the north, resulting in the formation of NE-trending buckle folds (Fig. 4.4b; Evans and Jackson, 2020). The extensional domain is dominated by salt-detached normal faults and associated salt rollers striking sub-parallel to the margin, perpendicular to the base-salt dip (Fig. 4.4b and Fig. 4.5). The trend of these structures is entirely consistent with a dominant NW direction of translation driven by gravity gliding (Evans and Jackson, 2020). The dominant strike of the supra-salt faults rotates toward the south, from NNE to ENE, closely following the geometry of the base-salt surface and orientation of the salt pinch-out (Fig. 4.4b). A small region towards the north of the dataset is dominated by a polygonal network of mature reactive diapirs (Fig. 4.4b).

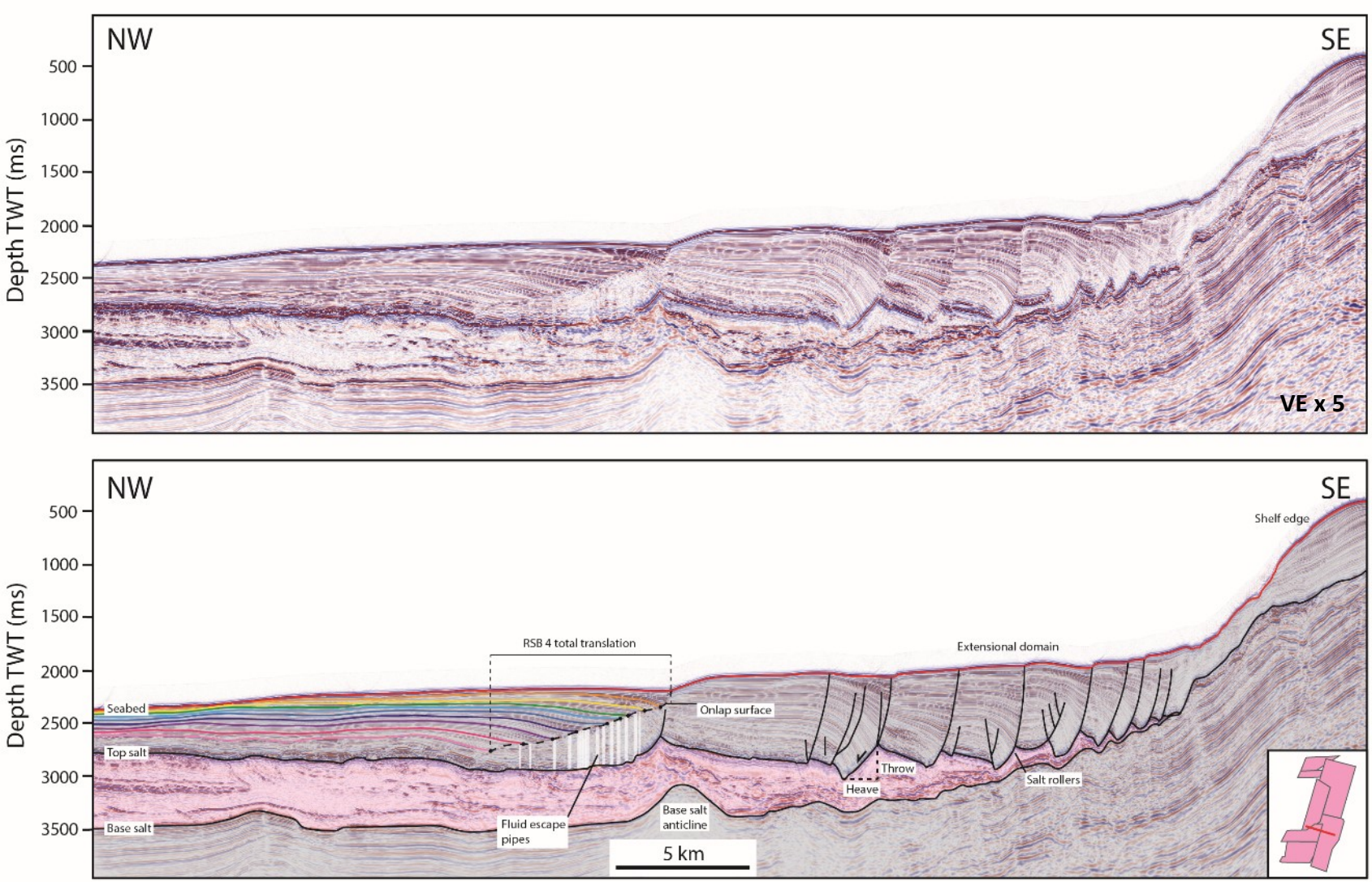

Figure 4.5 Seismic cross section showing thin-skinned extensional faults facilitating basinward translation of the overburden across the base-salt anticline. Coloured lines show mapped intra-RSB horizons. Vertical white lines show fluid escape pipes.

4.4.3 Ramp Syncline Basins

The NE-trending sub-salt anticlines are associated with supra-salt RSBs positioned above and adjacent to their basinward flanks, recording the progressive basinward translation of the salt and overburden over the anticlines. They can be easily recognised in cross section by their characteristic landward-dipping, asymmetric growth strata (Fig. 4.2). The growth strata packages thicken toward, and terminate against, the basal RSB 'onlap surface'. The onlap surface is diachronous, cutting up through the stratigraphy and younging toward the anticline. It typically has a listric geometry in cross section, being steepest at the youngest stratigraphic level and flattening with depth and distance from the anticline (Fig. 4.2). The listric geometry causes the onlapping intra-RSB horizons to rotate downward as they are translated away from the anticline, thus forming pseudo-downlaps (Fig. 4.2). The thickness of sediment beneath the RSB (i.e. between the onlap surface and the top-salt) also increases toward the anticline, reflecting the amount of sediment accumulated updip prior to basinward translation into the RSB depocentre. These observations are all consistent with RSB geometries generated by numerical models of overburden translation over base-salt steps (see Pichel et al., 2018).

Two of the RSBs are situated adjacent to one another, above two parallel base-salt anticlines with an across-strike spacing of only c. 10 km (Fig. 4.6). The dual development of the two RSBs means that strata in the basinward RSB onlaps strata in the landward RSB, such that the two basins may become vertically juxtaposed with continued translation (forming stacked RSBs; see Pichel et al., 2018).

Small base-salt anticlines (c. 100 ms) are associated with poorly-developed RSBs whose onlap surface is difficult to trace, and that show only very subtle landward expansion of growth strata. This is attributed to the small amplitude of the anticline relative to the total salt thickness, which means that the associated depocentre is relatively small (Pichel et al., 2018). We also observe partially-formed RSBs within the extensional domain, disrupted by normal faults (Fig. 4.7). These appear to represent a kinematic system whereby basinward translation of undeformed overburden is intermittently interrupted by slip on normal faults, causing RSB development to 'switch on and off' (Fig. 4.7). This observation shows that RSB development is not limited to the translational domain, as suggested by previous studies, but can occur

anywhere on the margin where salt translates over base-salt relief. However, RSBs developing in extensional settings are more likely to be disrupted by normal faulting and associated salt rollers. Such structures likely preferentially nucleate over the crest of the anticlines where there is a salt flux imbalance (Dooley et al., 2017), thus disrupting the continuous basinward translation that is required to maintain the RSB depocentre.

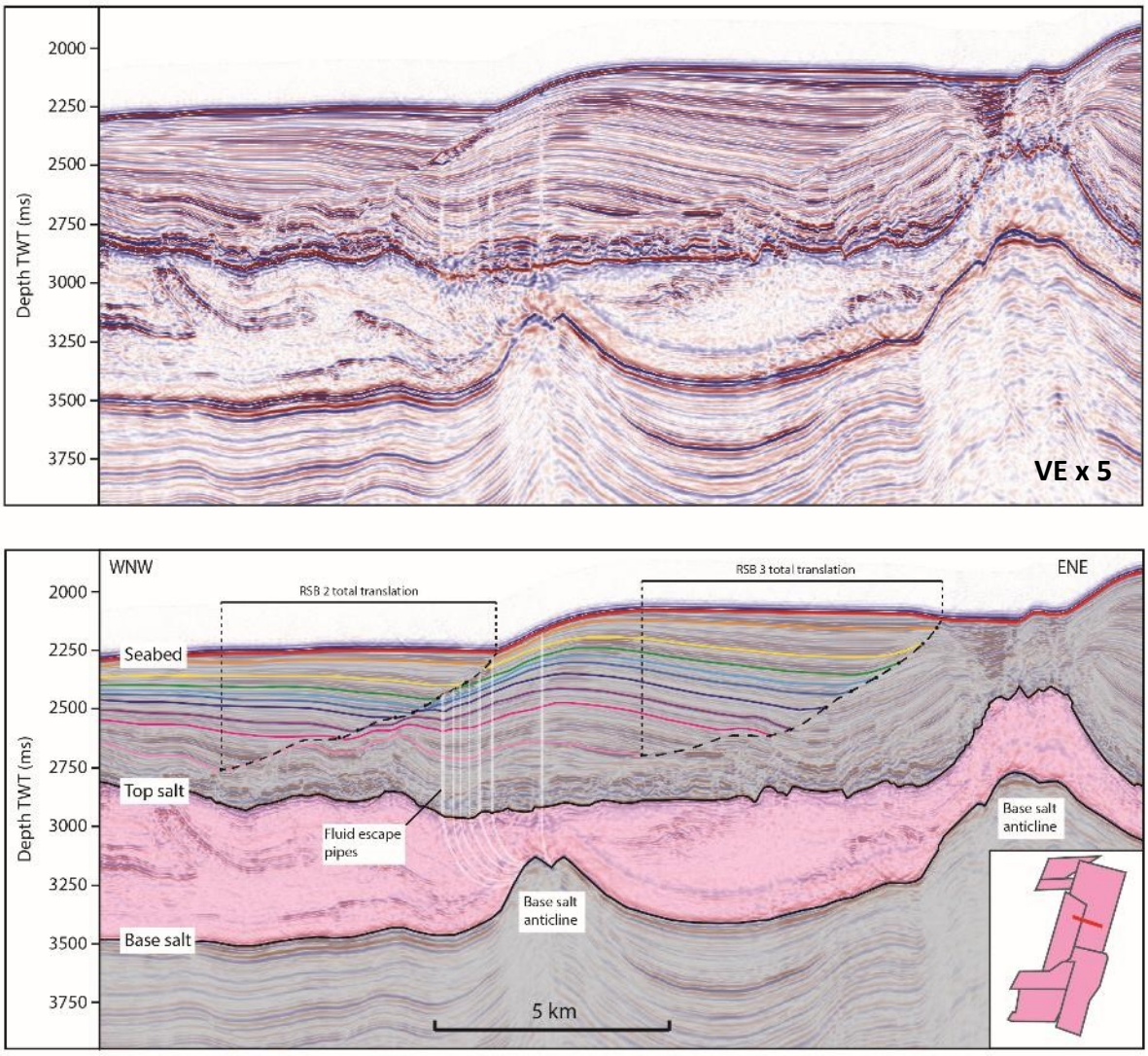

Figure 4.6 Dual ramp syncline basins adjacent to parallel base-salt anticlines (basinward RSB 2 and landward RSB 3). Coloured lines show mapped intra-RSB horizons. Vertical white lines show fluid escape pipes.

In this study we identify and map in 3D the internal stratigraphy of eight well-developed RSBs (Fig. 4.8e), whose onlap surface is clearly defined and which thus provide a reliable record of continuous basinward translation. Onlaps can be observed adjacent to the anticline at the present-day sea floor, where the RSB 'hinge' is typically represented by a bathymetric low, indicating ongoing RSB development and basinward translation (e.g. Fig. 4.2). The onlap surface does not, however, reach down to the top-salt, instead terminating against a thin (average 170 ms or c. 170 m), largely isopachous (but overall basinward-thinning) supra-salt unit. This is interpreted as a pre-kinematic layer (deposited prior to initiation of RSB development). The oldest intra-RSB strata therefore directly onlap onto the pre-kinematic unit (e.g. Fig. 4.2).

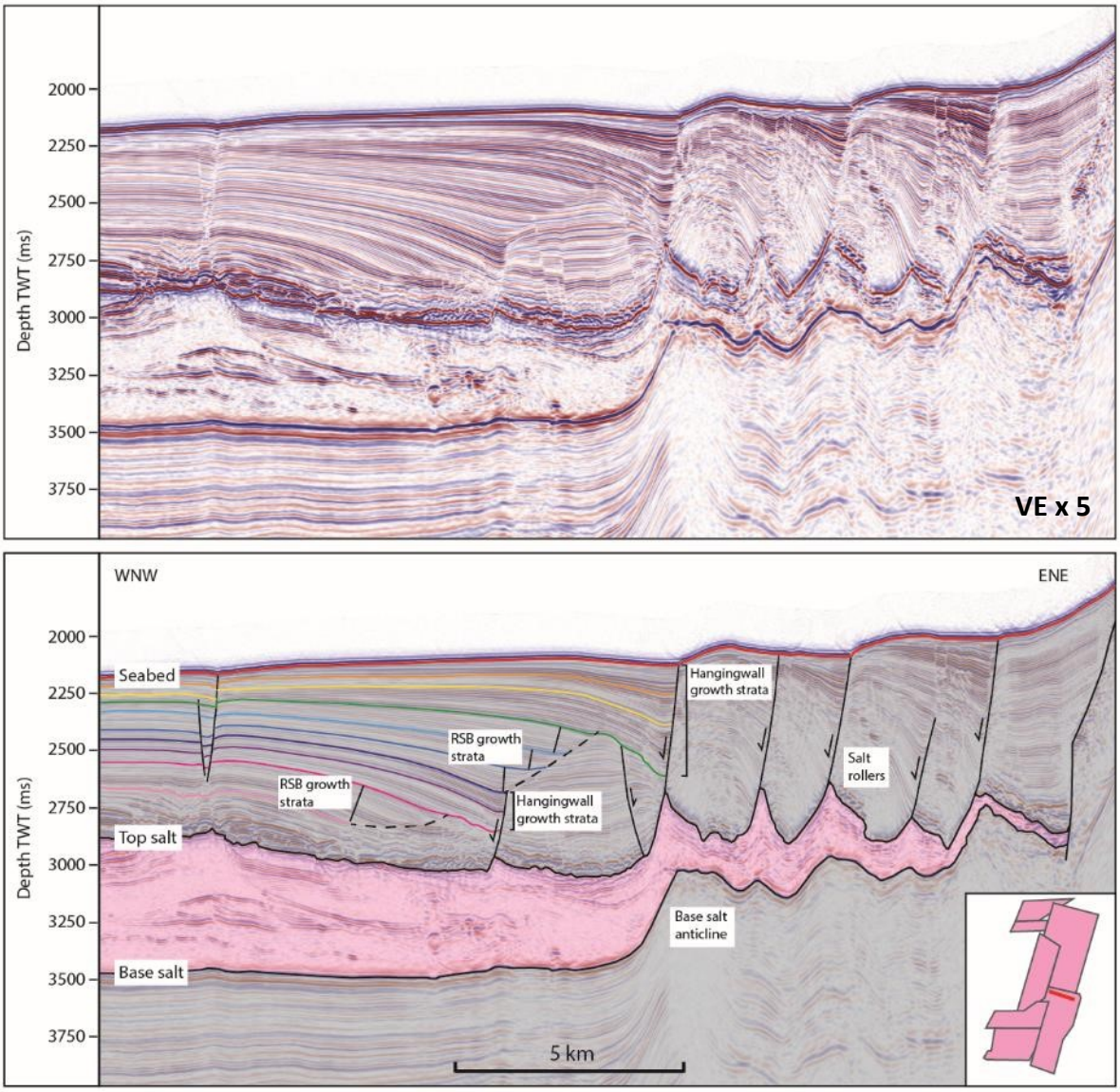

Figure 4.7 Disrupted RSB development due to intermittent normal faulting. Packages of RSB growth strata and hangingwall growth strata indicate phases of continuous translation and phases of faulting. Coloured lines show mapped intra-RSB horizons.

We map selected intra-RSB horizons that can be traced confidently across the margin (O2-O10; Fig. 4.2). Intra-RSB units show elongate depocentres with maximum thickness in the centre of the RSB, and a corresponding onlap sub-parallel to the origin anticline (Fig. 4.8a). Similarly, onlap surfaces show the greatest depression in the centre of the RSB, adjacent to the maximum height of the anticline (Fig. 4.8b). Intra-RSB units show the migration of depocentres away from the anticline with increasing age (Fig. 4.8c) (see also Pichel et al., 2018 and Pichel et al., 2019). The intra-RSB depocentres may be used to determine the direction of salt flow by tracing the position of the thickest part of the depocentre through time (Fig. 4.8c). In older, more deeply buried basins, the precision of this technique may be limited by later faulting, diapirism, and other tectonic processes that subsequently deform the intra-RSB isopachs. However, the original geometries of the young RSBs on the Levant Margin are exceptionally well-preserved. The present-day RSB hinges and the intra-RSB onlaps have a linear or curvilinear expression in map-view, trending parallel or sub-parallel to the anticline from which they originate (Fig. 4.8d). The length of the onlaps (and of the corresponding RSB depocentre) is determined by the length of the adjacent anticline (Fig. 4.8e).

4.4.4 Fluid Escape Pipes

Several of the RSBs are cross-cut by vertical features that have an internally chaotic or transparent seismic expression (Fig. 4.2, Fig. 4.5 and Fig. 4.6). They extend vertically between the top-salt and the diachronous RSB onlap surface, commonly being capped by a pockmark. In map view they form linear trails and are interpreted as series of fluid escape pipes (Fig. 4.9) (Cartwright et al., 2018; Kirkham et al., 2019; Oppo et al., 2020). As well as the vertical pipes preserved within the overburden, we can also identify the arcuate traces of the deformed pipes preserved within the salt sheet itself, connecting the base of the pipe at the top-salt to its origin in the sub-salt anticline (Fig. 4.6). The pipes invariably root to the crest or the downdip flank of the anticlines, indicating a sub-salt origin for the escaped fluids, with the anticlines acting as traps and the salt as an imperfect seal (Al-Balushi et al., 2016; Cartwright et al., 2018; Oppo et al., 2020).

We identify twelve pipe trails in the dataset, all of which originate from sub-salt anticlines that also generate RSBs (Fig. 4.8e). The pipe trails record the progressive basinward translation of the overburden due to their transient nature (Cartwright et al., 2018): each pipe

forms vertically above the crest of the anticline, releasing pressure accumulated in the sub-salt trap in a single event, before being passively translated basinward into the RSB depocentre where they become buried (Fig. 4.10). As it is translated into the RSB depocentre, the pockmark is onlapped by the RSB growth strata (Fig. 4.10). Critically, this means that the age of each pipe is approximately equivalent to the age of the horizon that meets the pockmark at the onlap surface (Fig. 4.10). All pipes are thought to be inactive fluid pathways once they are translated away from the crest of the anticline. The sub-salt trap then recharges until it once again exceeds the critical pressure required for the fluids to hydro-fracture the overlying salt and generate a new fluid escape pipe (Fig. 4.10) (Cartwright et al., 2018; Oppo et al., 2020). The immense pressure required to hydro-fracture the salt, which is traditionally thought of as an excellent seal, could also cause a blow out of clastic material from the crest of the anticline. This is evidenced by the dip observed at the crest of the structure in Fig. 4.6.

Pipe trails can therefore be used to determine the direction of translation by tracking a single point through time (Fig. 4.9). Some trails form a well-defined linear trend, whereas others show significantly more scatter, indicating that the precise emission point may vary slightly through time (Fig. 4.8d). They can be treated as direct kinematic vectors of transport direction at different localities along the margin, with the intra-RSB horizons constraining the relative ages of the pipes between different, widely spaced RSBs (Fig. 4.8d). All pipe trails identified in the present study trend broadly NW, indicating a NW direction of translation, which is consistent with the orientation of supra-salt faults updip. They do, however, show some variation in the precise direction of translation along margin, rotating from a more NNW bearing in the northern part of the dataset (295°) to a more WNW bearing in the south (335°). This rotation in transport direction is consistent with the observed change in the strike of faults in the updip extensional domain (Evans and Jackson, 2020).

The deformed pipes provide a unique means to examine the internal flow dynamics of a deforming salt sheet, whereas in the past much of our understanding has had to rely on numerical and physical analogue models, with few ways of constraining the natural systems themselves (e.g. Davison et al., 1996; Albertz and Ings, 2012). We observe arcuate pipe geometries that flatten with depth and are largely consistent with those of the previous studies (Cartwright et al., 2018; Kirkham et al., 2019), where the authors use the inclined nature of the deformed pipes to infer a dominant Couette (i.e. drag-induced) flow profile within the salt sheet.

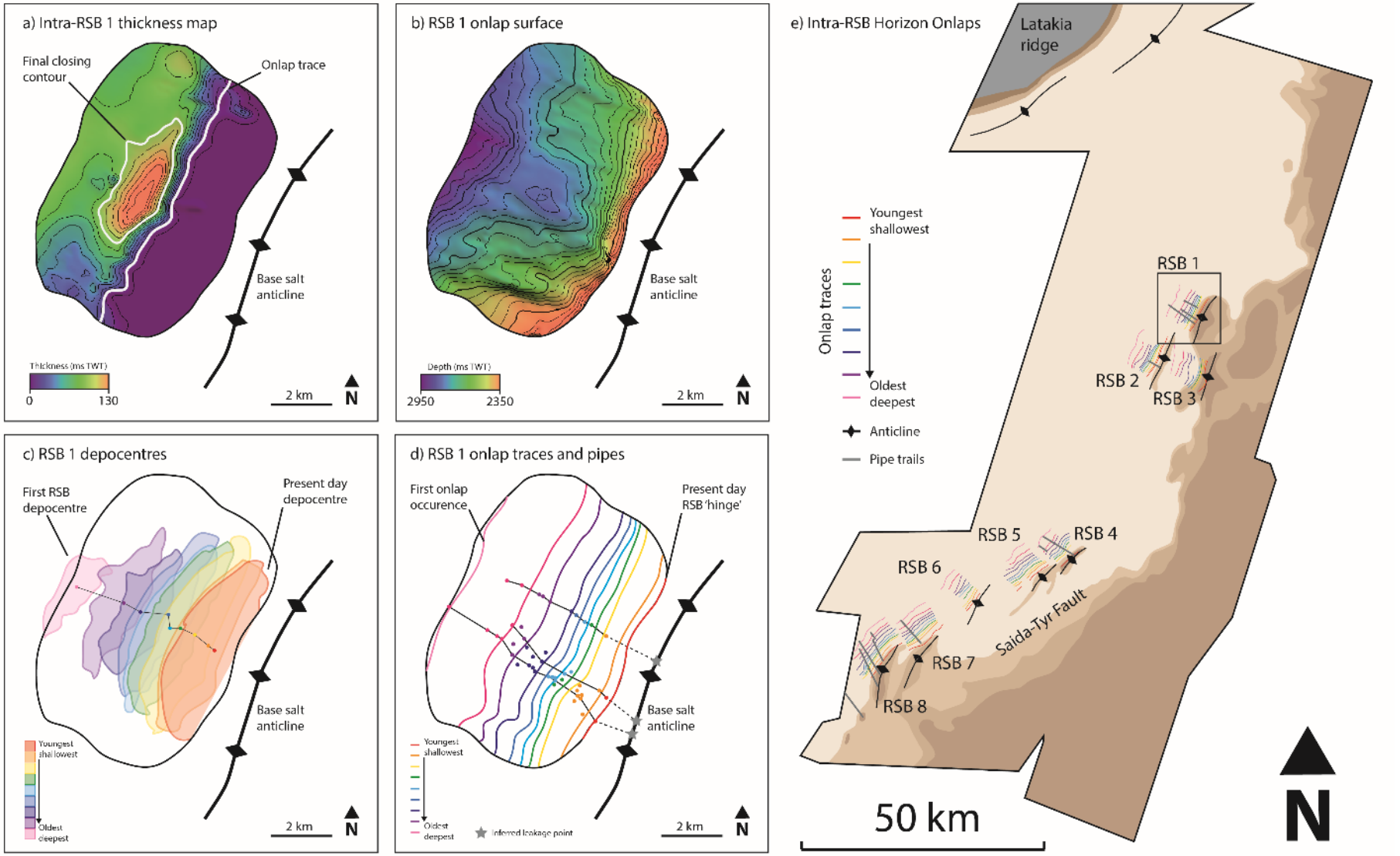

Figure 4.8 (a) Example thickness map of intra-RSB unit showing final closing contour and onlap trace. (b) Geometry of the onlap surface. (c) Stacked RSB depocentre outlines showing their migration away from the anticline with increasing age. Tracing the thickest succession of each unit gives the direction of translation. (d) Mapped onlap traces for RSB 1 and fluid escape pipe trails coloured by age of corresponding intra-RSB unit. (e) Distribution of base-salt anticlines and mapped onlap traces for RSBs presented in this study. Grey lines show associated pipe trails. Square indicates location of (a-d).

4.4.5 Kinematic Analysis

Integrating the information given by the RSBs and fluid escape pipes, we can analyse lateral variations in the magnitude and direction of translation recorded at different localities along the northern Levantine Basin margin. The intra-RSB onlaps give the magnitude of translation and some indication of the direction, but since their orientation is most sensitive to the orientation of the anticline from which they originate, they may be oblique to the actual direction of translation shown by the pipes (e.g. RSB 8 in Fig. 4.8e). The translation direction is therefore more precisely constrained by either the orientation of the pipe trails or the migration of the RSB depocentres (Fig. 4.8c-d).

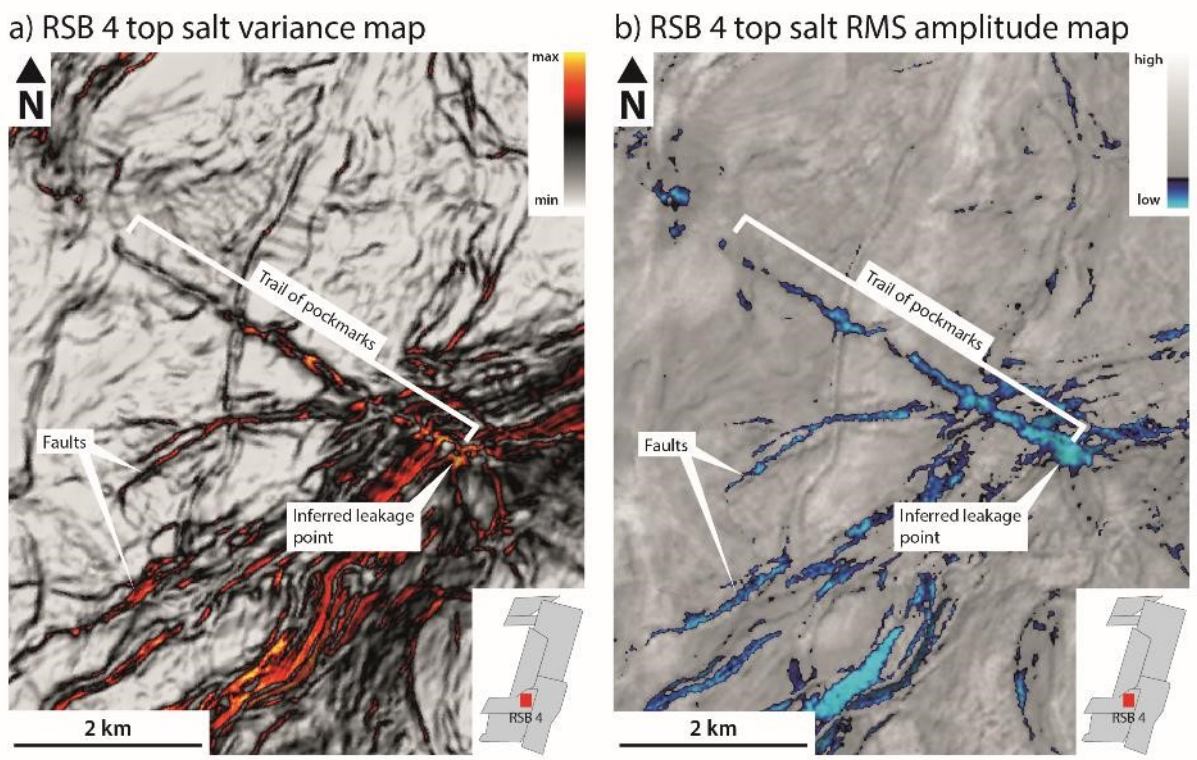

Figure 4.9 Variance (a) and RMS amplitude (b) maps of the top-salt surface showing the RSB 4 pipe trail. Location shown in inset map. Seismic section along trail shown in Fig 4.5.

The first onlap onto the pre-kinematic layer at the base of the RSB records the initiation of RSB development, and therefore the onset of salt-detached gravity gliding of the overburden (O10 in Fig. 4.2). Note that this constitutes the second main phase of salt deformation, with an earlier phase of syn-depositional deformation occurring prior to overburden deposition (Gvirtzman et al., 2013; Gvirtzman et al., 2017; Feng et al., 2017; Kartveit et al., 2018; Kirkham et al., 2020; Evans and Jackson, 2020). The age of this first onlap appears to be the same (or

within two reflections) for all of the RSBs mapped in this study, meaning that the onset of gravity gliding was broadly synchronous across the margin. This horizon also appears to correspond to the 1.8 Ma age horizon indicated by Kirkham et al. (2019) (based on a correlation with well data from the southern Levantine Basin, offshore Israel).

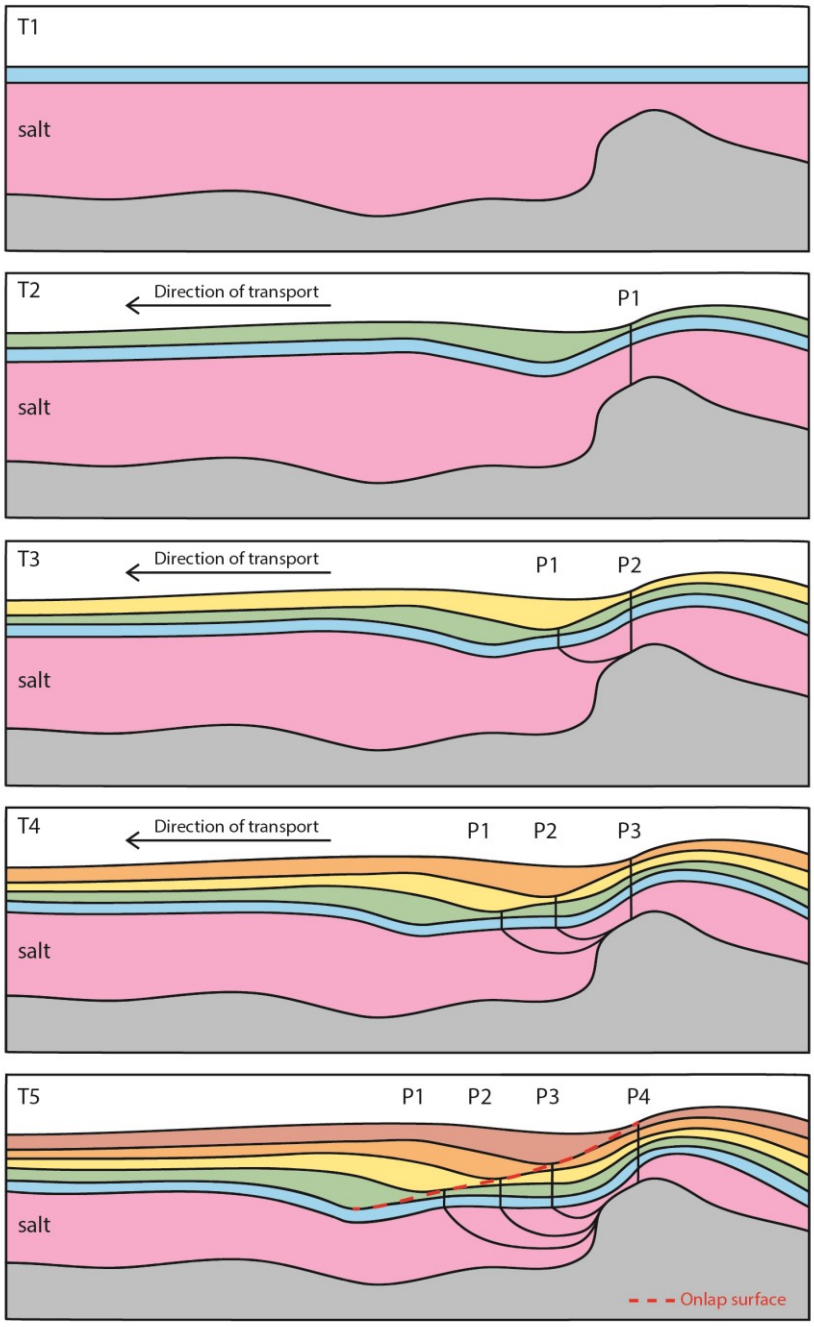

Figure 4.10 Co-development of ramp syncline basins and fluid escape pipes. Successive RSB depocentres and pipes are progressively translated away from the base-salt high. Pipe age may therefore be constrained by the age of the onlap that the terminus connects to at the base of the RSB.

Given that each onlap originally formed at the RSB hinge before being buried and translated basinward, the total translation is given by the horizontal distance from the first onlap to the present RSB hinge (Fig. 4.2). We round distance measurements to the nearest 100 m to allow for the uncertainty related to seismic resolution, and incorporate a possible error up to 100 m in picking the precise position of the onlap. This method assumes that the position of the RSB hinge has been stable through time, which we believe to be a valid assumption based on the results of numerical analogue models (Pichel et al. 2018).

The total amount of translation for each RSB varies between 5.0 and 7.0 km (±100 m) (Onlap 10 in Fig. 4.11a). This represents a scatter of up to 17% about the mean of 6.0 km (±100 m), with an average absolute deviation of 0.6 km. There does not appear to be a systematic spatial trend from north to south along the margin (i.e. increasing or decreasing magnitudes of translation from north to south), but there is evidently some lateral variability in the average rate of overburden translation; from c. 2.8 mm/yr up to 3.9 mm/yr (±1 mm/yr), assuming that the 1.8 Ma horizon represents the onset of gravity gliding. RSB 6 has the largest magnitude of translation (7.0 km) and is located 60 km from RSB 2, which has the smallest magnitude of translation (5.0 km). We do not identify any discrete strike-slip faults accommodating these differential rates within the overburden. This means that the rigid overburden has accommodated a very modest shear strain of c. 0.03 (2 km/60 km), with an angular shear of 2°.

The basinward translation of RSBs is accommodated updip by a network of salt-detached normal faults (Fig. 4.4b and Fig. 4.5). Summing the horizontal components of slip (i.e. heave) of faults in the extensional domain gives a horizontal translation estimate that we can compare to the RSB-derived estimates of total translation (Fig. 4.12). This method yields extension values of 4.7-7.0 km, which are largely consistent with translation estimates from the RSBs (Fig. 4.12). Profile 1 sums to 7.0 km of horizontal displacement, which is consistent with the 7.0 km of translation recorded by RSB 6 downdip. Profiles 3, 4 and 5 give 6.1-6.6 km of horizontal displacement, which is consistent with the 6.7 and 6.3 km of translation recorded by RSB 4 and RSB 5, respectively. Conversely, the horizontal displacement estimate derived from Profile 2 (5.5 km) is significantly less than that recorded by RSB 6 downdip (7.0 km), likely due to missing strain accommodated by sub-seismic scale faults. Overall, translation estimates from fault heaves support the apparent lateral variability in translation rates along the margin derived from the RSBs (Fig. 4.12). Note that we cannot measure fault heaves updip of RSBs 1, 2 or 3 due to the domain of diapiric growth, or for RSBs 7 and 8 due to the southern limit of the dataset (Fig. 4.12).

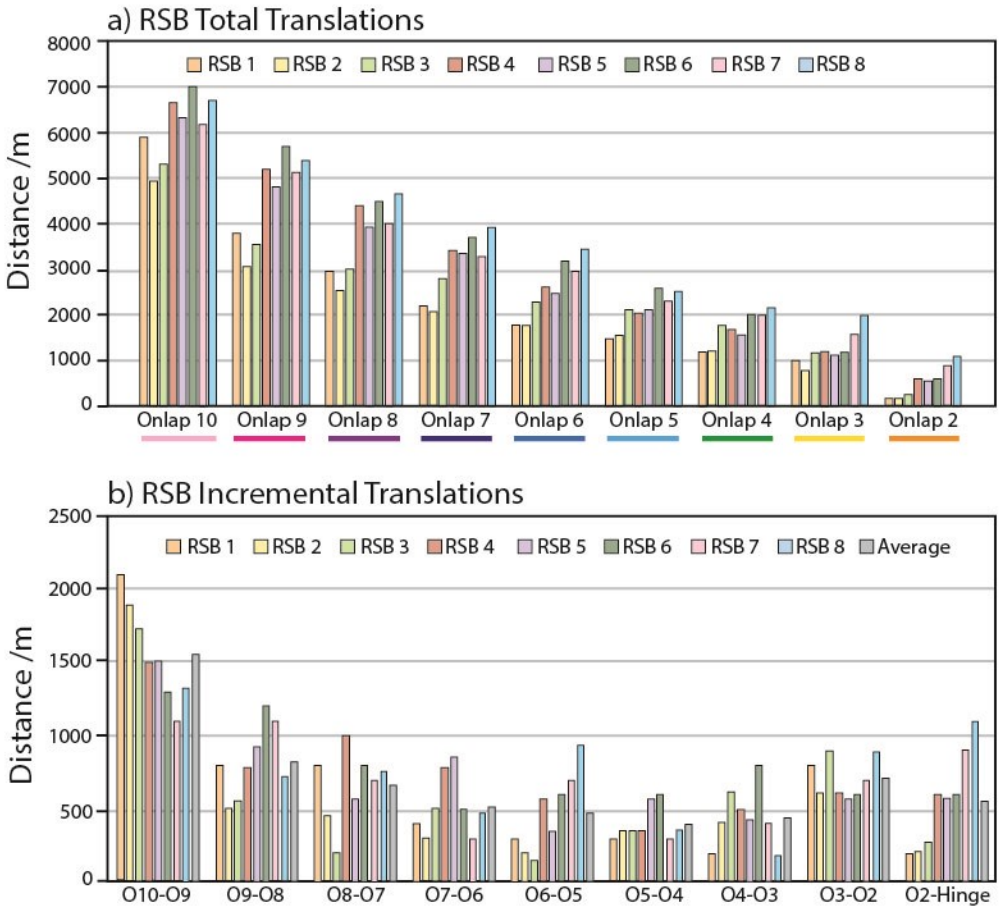

Figure 4.11 (a) Magnitudes of translation measured for intra-RSB onlaps of equivalent ages in each RSB. The magnitude of translation given by the oldest onlap (Onlap 10) represents the total translation experienced by each RSB. (b) Magnitudes of translation during different time periods, given by the difference between total onlap translations. O10-O9 represents the oldest increment of time, with O2-Hinge representing the most recent increment of time.

As well as total translation estimates, we can compare the translation magnitudes for other intra-RSB horizons of equivalent ages (Fig. 4.11a), and use these to calculate the incremental translation during different time intervals (Fig. 4.11b). For example, the distance between Onlap 10 and Onlap 9 gives the distance that each RSB moved during that interval of time (Fig. 4.11b). We can therefore use this to compare the relative translation rates of the RSBs through time. This approach assumes that the correlated intra-RSB horizons represent temporally equivalent surfaces across the margin, which we believe to be valid based on the lack of seismic-scale unconformities in the overburden and apparently continuous sediment aggradation since the Messinian (e.g. Fig. 4.5). These incremental translations show significantly more variability between different RSBs than the total translations, with some time intervals showing a scatter of up to 80% about their average (e.g. O6-O5 gives values

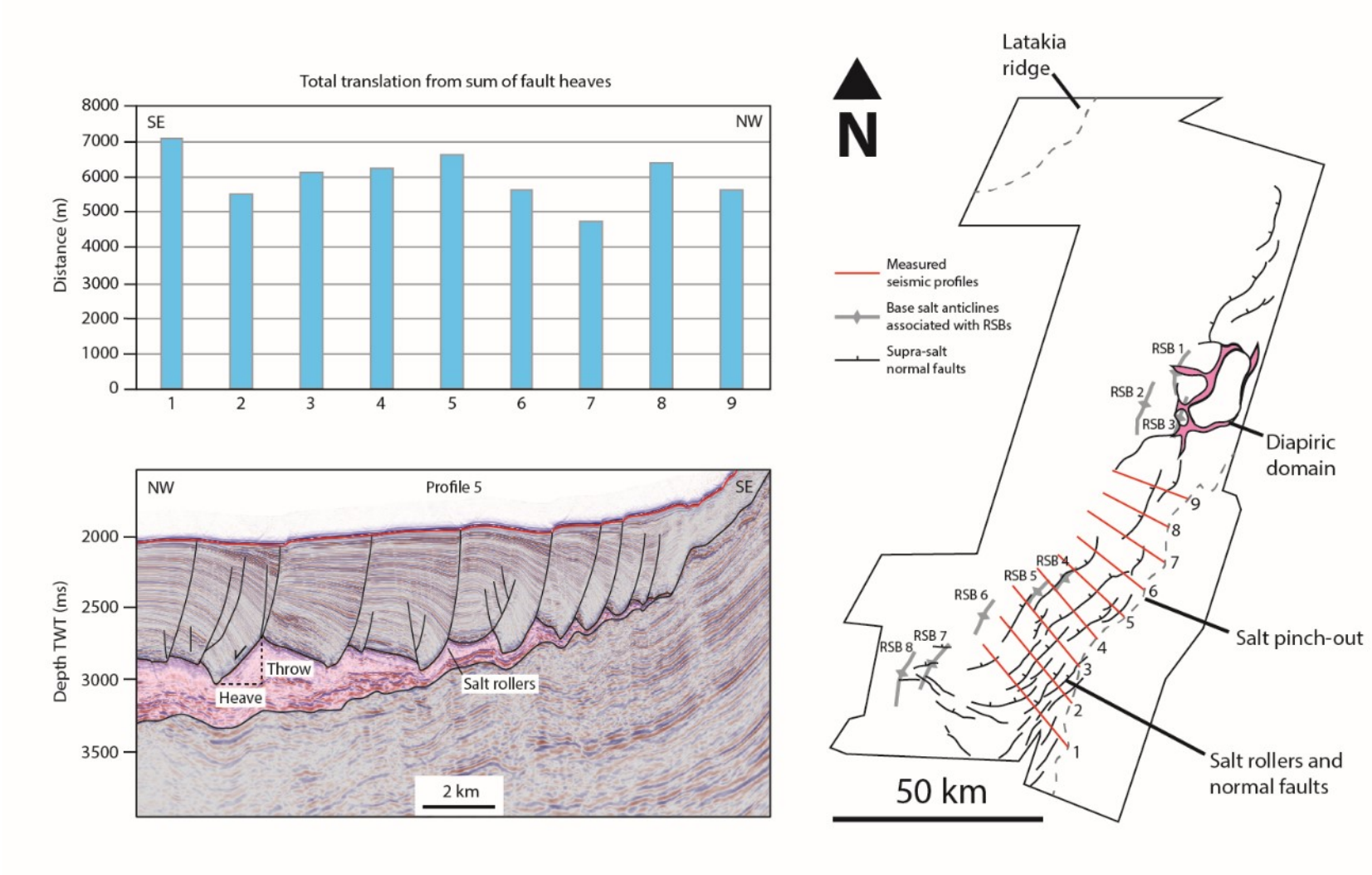

Figure 4.12 Total translation magnitudes calculated from summing the heaves (horizontal components of fault slip) of normal faults in the updip extensional domain. Red lines show locations of measured seismic profiles.

within a the range 100-900 m with an average of 500 m) (Fig. 4.11b). Furthermore, we see that the relative velocity of each RSB varies through time (i.e. the fastest and slowest RSBs on average, RSB 6 and RSB 2 respectively, have not been consistently fastest or slowest through time) (Fig. 4.11b). For example, the incremental translations show that the relatively large magnitude of translation recorded by RSB 8 is primarily due to a very recent episode of increased velocity that was not experienced by the other RSBs. In fact, all RSBs appear to experience 'pulses' of faster translation rates punctuated by periods of slower translation rates, such that the seemingly random variability observed on short (c. 100-200 Kyr) timescales averages out over longer (c. 1-2 Myr) timescales. After one RSB experiences a faster 'pulse', it then slows relative to the others, such that all RSBs 'keep-up' with each other to a certain degree over long enough timescales. This means that the average translation rate would eventually converge to a common value for all RSBs along the margin given a long enough time period.

4.5 Discussion

The young and active RSBs offshore Lebanon provide an excellent stratigraphic record of the magnitude and timing of salt-detached gravity gliding. As the rigid overburden slides on the ductile salt layer, the RSB depocentres and onlapping strata are progressively transported downdip from the adjacent causal anticline, allowing us to quantify the incremental basinward translation through time. The direction of translation is constrained by tracing the RSB depocentres through time, or by using the orientation of fluid escape pipe trails, which track a single point through time and thus give a direct kinematic vector.

The temporal correlation of the oldest onlap surface between the RSBs suggests that they developed at approximately the same time, and therefore that the onset of gravity gliding was broadly synchronous across the entire margin (c. 1.8 Ma). This roughly coincides with the age of the oldest fluid escape pipes in the region, though not all pipe trails initiated at this time (see also Oppo et al., 2020). Therefore, the initiation of gravity gliding and fluid escape is broadly contemporaneous across the entire northern Levantine Basin, suggesting a single trigger for both events. The most recent phase of uplift of the Levantine margin was recorded by a change in drainage direction in northern Israel starting at c. 1.8 Ma (Matmon et al., 1999).

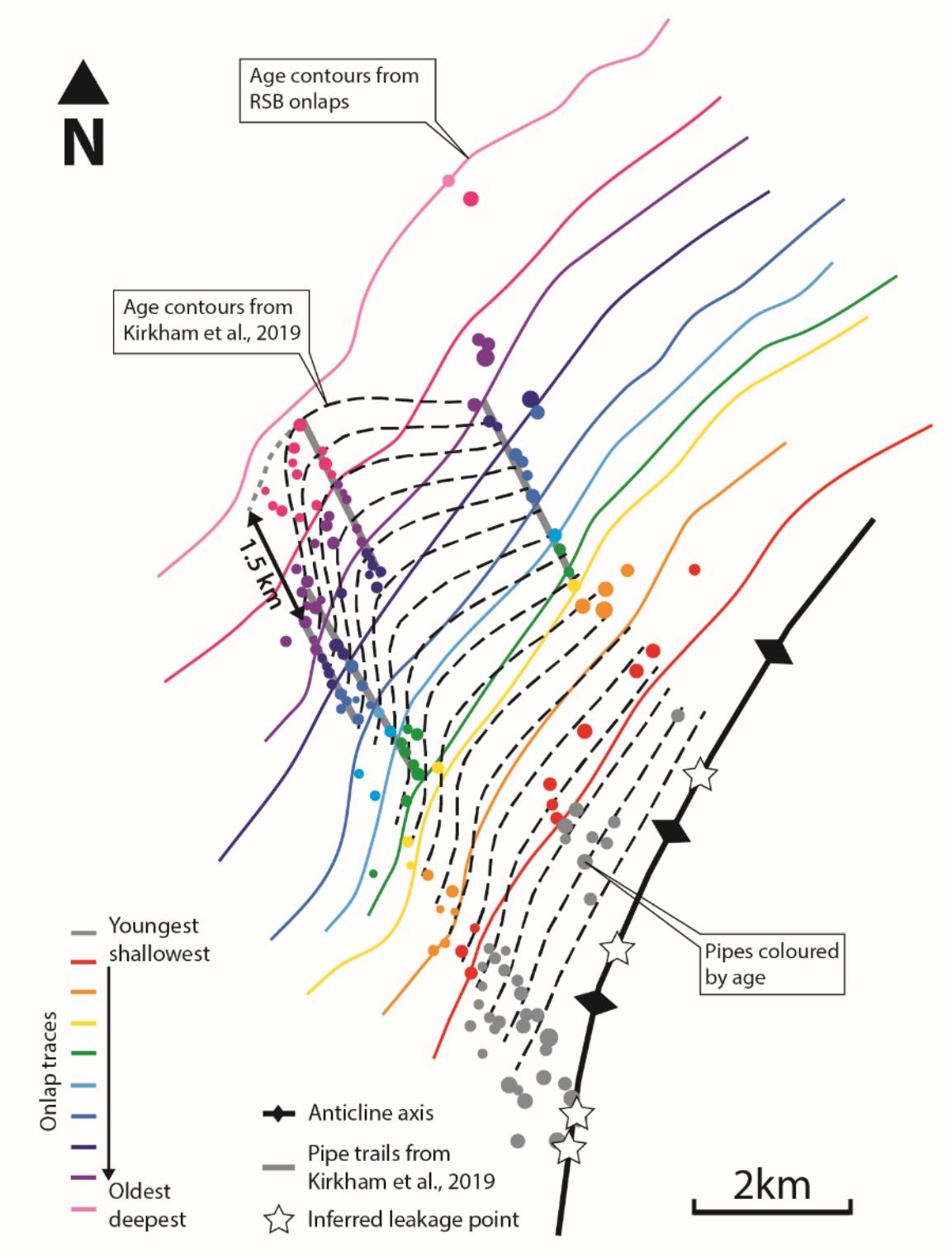

Figure 4.13 Coloured lines show age contours given by onlap traces for RSB 8. Pipes coloured by age of corresponding intra-RSB unit. Dashed lines show age contours inferred by Kirkham et al., (2019) assuming equivalent age of first pipe in each trail. Sub-parallel onlap traces show uniform translation away from the base-salt anticline.

This uplift could have increased the tilt of the base-salt enough to generate gravitational instability and initiate post-Messinian gravity gliding. At the same time, the basin tilt would have also favoured updip fluid (e.g. oil and gas) migration from the deep basin towards the anticlines along the basin margin (Oppo et al., 2020). The combination of updip fluid migration filling the sub-salt traps, and the exsolution of gas from oil due to a decrease in pressure (linked to erosion of the overburden), could together have led to supra-lithostatic overpressure within the anticlines, thus triggering cross-evaporite fluid escape (Oppo et al., 2020).

The original study to identify a pipe trail associated with an anticline in the deep Levantine Basin (termed the Oceanus structure) used the horizontal distance from the oldest pipe to the present emission point to estimate the magnitude of translation (3.4 km) (Cartwright et al., 2018). Assuming this to be the total translation since deposition of the 1.8 Ma marker horizon, the authors calculate an average translation rate of 2.0 mm/yr. However, the RSBs onlaps show that translation actually initiated prior to the emission of the first pipe, and that the distance from the first onlap onto the 1.8 Ma horizon to the present-day RSB hinge in fact suggests 4.6 km of translation in this time (see Fig. 4.2b in Cartwright et al., 2018). This yields a faster translation rate of 2.7 mm/yr (i.e. 35% higher than that estimated from the pipes alone). The RSB onlaps also show that the overburden has thickened through time, from a thin (c. 120 m) pre-kinematic layer at 1.8 Ma to the present-day thickness (c. 400 m). This means that the stress acting on the salt has increased through time and it is therefore more accurate to use a time-averaged overburden thickness than present-day overburden thickness when calculating viscosity (ratio of shear stress to shear strain rate; see supplementary info in Cartwright et al., 2018). However, the recalculated viscosity (1.1×10^{18} Pa s) using the newly constrained translation rate (2.7 mm/yr) and time-averaged overburden thickness (260 m assuming constant sedimentation rate) is of the same order of magnitude as that estimated by the previous study (2.3×10^{18} Pa s; Cartwright et al., 2018). Both values fall within the expected viscosity range derived from other natural examples and from laboratory experiments of rock salt rheology (Urai and Spiers, 2007; Urai et al., 2008; Mukherjee et al., 2010).

Another previous study investigated four closely spaced pipe trails within RSB 8, associated with the southernmost anticline in the present dataset (Saida-Tyr structure; Fig. 4.3) (Kirkham

et al., 2019). The authors postulate the presence of 'streams' of fast-flowing salt based on the assumption that the first pipe in each trail formed at the same time (Fig. 4.13). However, using the intra-RSB onlaps to constrain the relative ages of the first pipes, which are not in fact the same age, we show that c. 1.5 km of translation had actually occurred between the formation of the oldest pipe in trail STP 1 and the oldest pipein trail STP 3 (Fig. 4.13). This observation does not support large differences in salt flow velocity across a single RSB and questions the presence of fast-flowing salt streams. In fact, the sub-parallel intra-RSB onlaps mapped show that local rates of basinward translation are approximately uniform over individual km-scale anticlines (i.e. we do not see any major rotation or deformation of onlaps as they are translated away from the anticline; Fig. 4.13).

However, our correlation of horizons between different RSBs along the margin shows that both the direction and rate of translation *do* vary significantly through space and time over a larger spatial scale. This leads us to discuss two possible mechanisms that may be controlling this lateral variability in translation rate along the margin.

4.5.1 Salt Flux Imbalance and Cyclical 'Pulses' of Salt Flow

Thinning of the salt over the crests of the anticlines leads to an imbalance in salt flux. On the updip flank of the anticlines there is a large volume of salt forced to squeeze through a relatively small gap between the sub-salt anticline and relatively strong clastic overburden. Physical analogue models show that salt flux imbalances such as this can cause temporal variations in salt (and overburden) velocity (Dooley et al., 2017). A simple experiment modelling salt flow up onto a base-salt high shows that during the early stages of deformation, the salt slows down and inflates as flow lines converge (see Fig. 4.18 in Dooley et al., 2017). Subsequently, as the salt above the high thickens, the effects of basal drag are minimised and the salt accelerates. Some anticlines in the present study show evidence of inflation on the updip flank of subsalt anticlines (e.g. Fig. 4.2), and we therefore propose a similar mechanism may play a role in modulating local rates of salt and overburden translation here (Fig. 4.14).

In the first instance, pressure builds within the salt on the updip flank due to the volumetric mismatch (more salt input than output) (Fig. 4.14a). This may also be associated with inflation, though the confining pressure from the overburden weight resists this. On the downdip flank the flux imbalance causes the salt to thin and overburden to subside (more salt output than input),

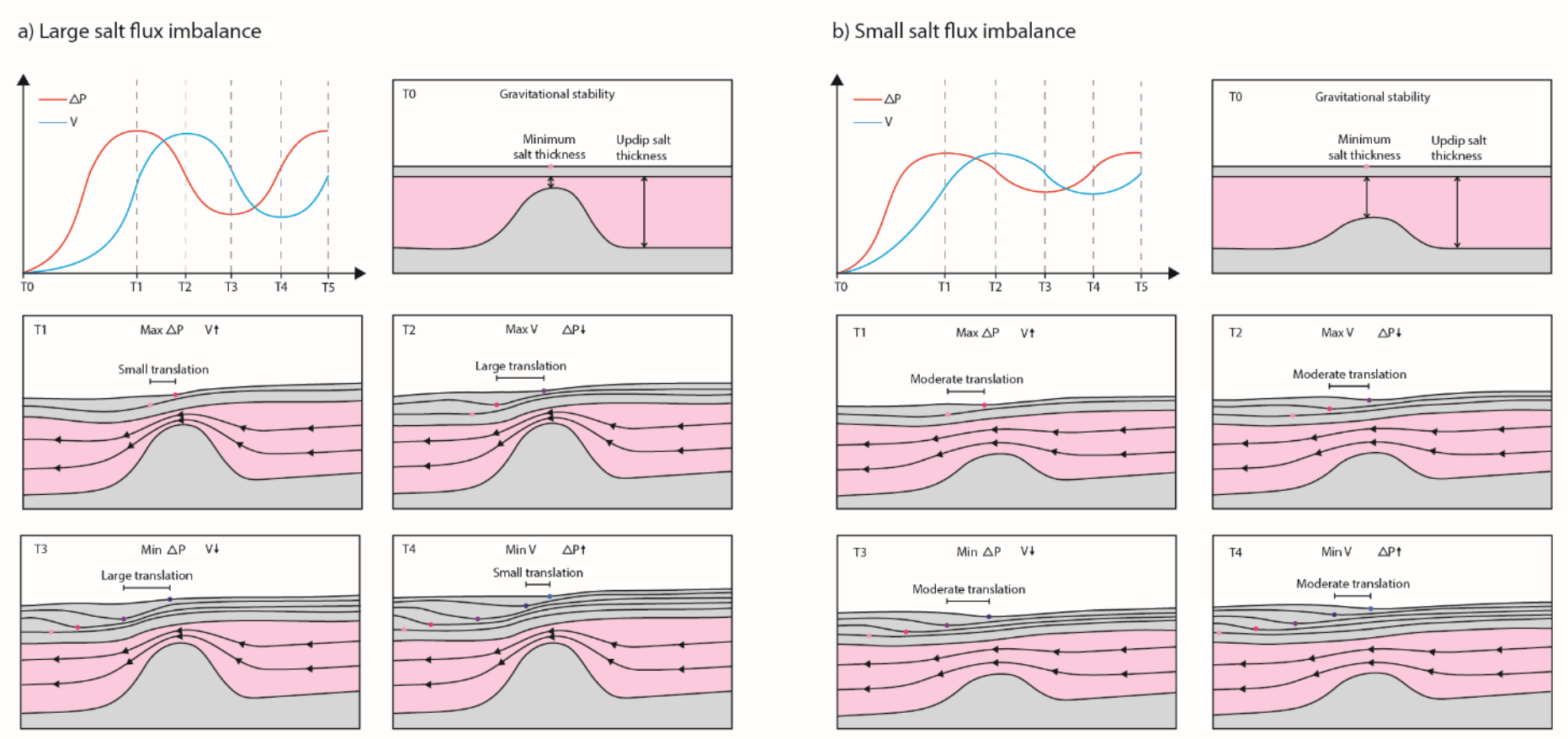

Figure 4.14 Schematic showing time-varying evolution of pressure and velocity during salt flow over a base-salt anticline. In the first instance, pressure builds within the salt on the updip flank due to the volumetric mismatch (more salt input than output). This process gradually increases the pressure difference (ΔP) across the anticline (T0-T1). In turn, this pressure difference increases the stress acting upon the salt, and since stress is proportional to strain rate, the velocity of salt flow across the anticline increases (T0-T1). The acceleration of the salt flow is proportional to the pressure difference across the anticline, such that maximum acceleration occurs when ΔP is at its peak (T1). This velocity increase reduces the volumetric imbalance across the anticline and allows the pressure difference to drop (T1-T2). As the system approaches equilibrium, the stress acting on the salt is reduced and it begins to decelerate (T2-T3). The pressure difference across the anticline then starts to build up again, and the process repeats (T3-T4). The feedback between pressure difference and velocity therefore causes them to vary in a cyclical nature. Pressure and velocity variations are more extreme for a large salt flux imbalance (a) than a small salt flux imbalance (b).

creating the RSB depocentre adjacent to the anticline. This process gradually increases the pressure difference (ΔP) across the anticline (Fig 14a T0-T1). In turn, this pressure difference increases the stress acting upon the salt, and since stress is proportional to strain rate, the velocity of salt flow across the anticline increases (Fig 14a, T0-T1). The premise that stress is proportional to strain rate applies to Newtonian fluids, which is a valid approximation in this case where the stress is relatively low and pressure solution is the dominant mechanism of salt flow (Spiers et al., 1990; Van Kekan et al., 1993; Urai et al., 2008). The acceleration of the salt flow is proportional to the pressure difference across the anticline, such that maximum acceleration occurs when ΔP is at its peak (Fig. 4.14a, T1). This velocity increase reduces the volumetric imbalance across the anticline and allows the pressure difference to drop (Fig. 4.14a, T1-T2). As the system approaches equilibrium, the stress acting on the salt is reduced and it begins to decelerate (Fig. 4.14a, T2-T3). The pressure difference across the anticline then starts to build up again, and the process repeats (Fig 14a, T3-T4). This mechanism would allow for cyclical 'pulses' of faster salt flow (and overburden translation) during certain time intervals. The timing of the salt 'pulses' would vary for different anticlines depending on the thickness of the salt over the anticline, the adjacent salt thickness updip, and the thickness of the overburden, amongst other variables.

The anticlines associated with the RSBs in this study have maximum heights between 220-820 ms (430 m up to 1.6 km). The thickness of salt over the anticlines tends to be inversely proportional to their height, with larger anticlines generally capped by thinner salt over their crests (Fig. 4.15a). The difference between the adjacent thickness of salt updip, and the thickness of salt over the crest, can be used as a proxy for salt flux imbalance (Fig. 4.15a). This means that we would expect anticlines with a large thickness of adjacent salt and very thin salt over their crest to have a large salt flux imbalance. Some anticlines are therefore associated with larger salt flux imbalances than others (Fig. 4.15a).

This observation and inference could explain why some RSBs demonstrate more extreme 'pulses' of salt flow than others (Fig. 4.11b). In order to evaluate this variability quantitatively, we calculate the average absolute deviation for each RSB, and find that this is proportional to the salt flux imbalance with an R^2 value of 0.9 (Fig. 4.15b). This means that RSBs with a greater salt flux imbalance deviate more from the average magnitude of translation at each time step (Fig. 4.15b). We suggest that this is because where the volumetric imbalance is relatively small

(i.e. salt thickness is more uniform across the anticline), pressure differences are released more easily (Fig. 4.14b). Consequently, the 'pulses' of faster and slower translation are less extreme, and translation rates are generally more consistent over time (Fig. 4.14b). This is the case for RSBs 4 and 5 (Fig. 4.15b). Conversely, the anticlines with the greatest flux imbalance show more extreme variability because they must build up a greater pressure difference in order to equilibrate over the anticline (Fig. 4.14a). This is the case for RSBs 2, 3 and 8 (Fig. 4.15b). We note that there may have been some post-Messinian amplification of these anticlines absorbed by salt thinning, which would further augment the salt flux imbalance over time, but the lack of stratigraphic evidence for overburden uplift suggests that this would have been relatively minor.

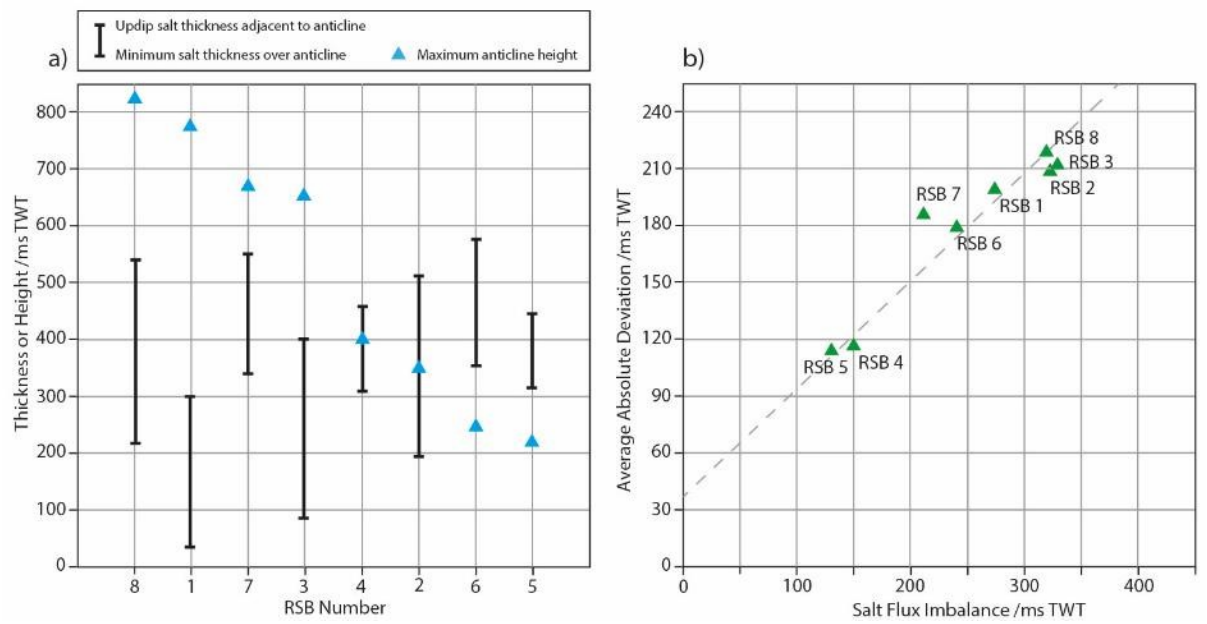

Figure 4.15 (a) Plot of anticline height, adjacent salt thickness and minimum salt thickness over the crest for each RSB, ordered from largest to smallest anticline height. The difference between adjacent updip salt thickness and minimum thickness over the crest is a proxy for the magnitude of salt flux imbalance. (b) The absolute average deviation of each RSB is proportional to its salt flux imbalance. This means that RSBs with a large salt flux imbalance show more extreme variability in relative translation rate with respect to the average at each time interval than those with a small salt flux imbalance. The R^2 value for this correlation is 0.9.

This mechanism could also explain why even the dual RSBs (2 and 3) show slightly different rates of translation (Fig. 4.11). The anticlines associated with RSB 2 and RSB 3 are 10 km apart and parallel to one another (Fig. 4.6 and Fig. 4.8e). They record translation on the same part of the margin, but show slightly different magnitudes of total translation. It appears that the landward RSB has translated further than the basinward RSB (5.3 km and 4.9 km respectively), as well as experiencing slightly different magnitudes of incremental translation through time

(Fig. 4.11b). The anticlinal geometry of the landward intra-RSB strata could suggest that the additional 400 m of translation may have been accommodated via large-scale folding, as well as possible cryptic lateral compaction (Fig. 4.6) (e.g. Butler and Paton, 2010).

While salt flux imbalances may play a key role in modulating local rates of translation over base-salt anticlines, there are other key controls that we also need to consider. The Couette flow profile inferred from the geometry of the deformed pipes indicates that drag on the top-salt surface is the dominant driver of salt deformation in this area (Cartwright et al., 2017; Kirkham et al., 2019). This means that it is the translation of the overburden that drives salt deformation, and not vice versa. We must therefore consider mechanisms that facilitate the basinward translation of the overburden, and their key controls, in order to fully understand the differential rates of overburden translation.

4.5.2 Overburden Mechanics and Elastic Strain

An alternative or additional mechanism that could be controlling translation rates of the salt and its overburden is the distribution of elastic stress and strain in the relatively rigid overburden. If we treat the overburden as a uniform sheet (Fig. 4.16a) and apply a tilt (Fig. 4.16b), the gravitational force acting on the tilted overburden, and therefore the tectonic stress, is approximately constant along the margin but increases updip (where the weight of the downdip sheet is greatest). This causes elastic strain to build up within the overburden, which is proportional to the applied stress and therefore also increases updip (Fig. 4.16b). When the stress exceeds the strength of the overburden, brittle failure occurs and faults develop (Fig. 4.16c-f). The development and growth of these faults thus facilitates the basinward translation of the overburden (Fig. 4.5).

However, the extent to which these faults control the rate of translation in the translational domain downdip is unclear, and depends largely on whether the mechanical behaviour of the overburden is dominantly plastic or dominantly elastic. In a dominantly plastic deformation model, where materials deform at constant stress, the translational domain is permitted to pull away at a uniform rate, with faults updip locally releasing the elastic strain when brittle failure occurs (Fig 16c-d). In a dominantly elastic deformation model, where strain is directly

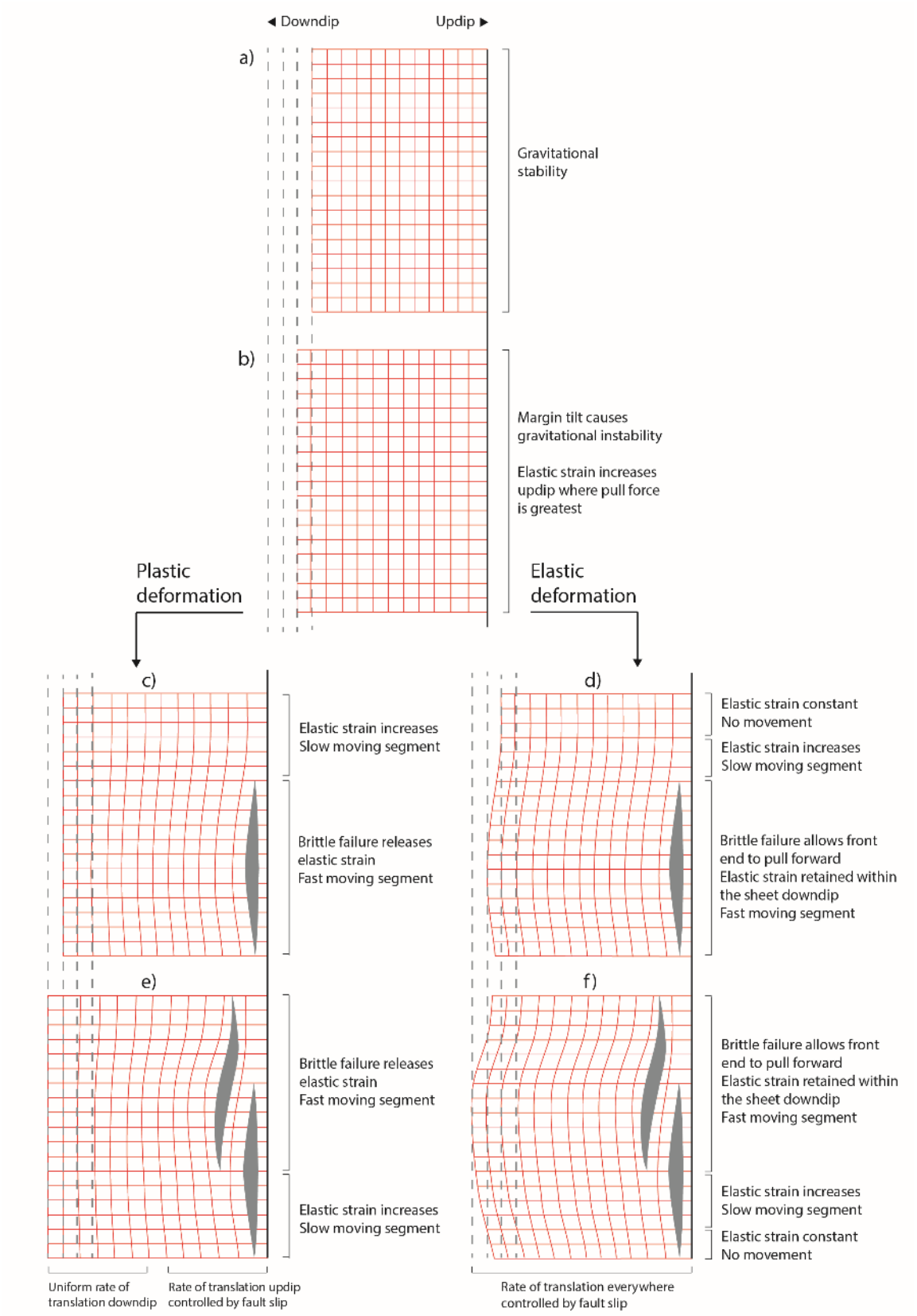

Figure 4.16 Schematic showing two models for elastic strain build-up and release within the overburden. A dominantly plastic overburden allows the translational domain to pull away at a uniform rate and the faults in the updip domain rupture as and when they reach a critical stress, locally releasing the elastic strain build-up. A dominantly elastic overburden remains under tension and the ruptures updip allow the sheet to pull forward by a magnitude dictated by the fault slip.

proportional to stress, the tension in the sheet is maintained and the faults updip allow the sheet downdip to pull forward by a magnitude dictated by the fault heave (Fig. 4.16e-f). In reality, the mechanical behaviour of the overburden at the margin scale is elasto-plastic (Weijermars et al., 1993) and therefore the actual overburden deformation is a hybrid of these two end-member models. In either case, this means that the rate of basinward translation in the extensional and upper translational domains, where the majority of RSBs are located, is intrinsically linked to the slip rate on the faults (Fig. 4.16). These faults move at different times, due to a number of independent variables in the system (rheological heterogeneity, geometry of the fault plane, fluid circulation, etc.) that make it very difficult to predict when or in which order the different fault segments will slip. This phenomenon is well-documented on fault networks in areas of active extension, with many studies showing that fault activity is inherently episodic and that slip rates vary through time and space (e.g. Mitchell et al. 2001; Benedetti et al. 2002; Friedrich et al. 2003; Bull et al. 2006; Nicol et al. 2006; McClymont et al. 2009; Schlagenhauf et al. 2010, 2011; Cowie et al., 2012). This may explain some of the seemingly random variability in rates of translation along the margin. Note that this simplified model considers only the mechanics of the updip extensional and translational domains, and further complexity may be introduced by incorporating stresses within the contractional domain downdip. Nevertheless, this gives valuable insights into some key controls in the updip region where the RSBs are situated.

Furthermore, these faults transfer elastic strain and stress between different segments of the overburden during each slip event (e.g. Cowie 1998; Robinson et al. 2009; Cowie et al., 2012). If one part of the relatively rigid overburden sheet is moving faster than the adjacent segment, as the RSBs have shown, this difference would have to be accommodated by a discrete NW-trending strike-slip fault, or distributed over a wider zone and stored as shear strain. Strike-slips faults are observed in the overburden offshore Israel where they offset subaqueous channels (Cartwright et al., 2012; Clark and Cartwright, 2009; Kartveit et al., 2018), and likely accommodate differential rates of salt-detached translation between different segments of the margin. However, we do not identify similar salt-detached strike-slip faults in the overburden offshore Lebanon, and therefore infer that the differential translation must be accommodated by distributed elastic shear strain. Since the overburden is a relatively rigid sheet, it can only accommodate a certain amount of elastic strain without brittle failure. This

means that when one fault ruptures and a segment moves locally, this increases the elastic strain in neighbouring segments, thus bringing them closer to failure (Fig. 4.16c-d). This strain is then released when the neighbouring segments slip and 'catch up' with the first segment (Fig. 4.16e-f). We therefore envisage that the distribution of stress and storage of elastic strain in the overburden could explain the fact that all segments appear to 'keep-up' with each other over long timescales.

Essentially, this demonstrates that over margin-scale lengths the overburden undergoes a process of tectonic 'stretching and squeezing' as it translates basinward, rather than uniformly translating as a perfectly rigid material. Since the overburden in the Levantine Basin is relatively young and shallowly buried, it may be able to accommodate more elastic strain than thicker, more compacted and consolidated clastic overburdens in other basins (Butler and Paton, 2010; Burberry, 2015). We conclude that the interplay between the cyclical 'pulsing' of salt flow over base-salt anticlines and the mechanical behaviour of the overburden control differential rates of basinward translation on the Levant Margin, and similar processes are expected to occur in other salt basins (e.g. Gulf of Mexico, North Sea, West African margin).

4.6 Conclusions

- The well-developed ramp syncline basins offshore Lebanon are excellent records of translation on a salt-influenced passive margin dominated by gravity-gliding
- Pipe trails provide direct vectors of transport direction, and the relative ages of the pipes can be determined by correlating intra-RSB horizons across the margin
- Rates of basinward translation are approximately uniform at the km-scale but show significant lateral variability at the margin-scale
- Differential translation rates may be a result of pulsed salt flow due to volumetric imbalance over the base-salt anticlines
- The overburden deforms as it translates, with the distribution of stress and elastic strain ensuring that translation rates average out over long timescales

References

Aal, A.A., El Barkooky, A., Gerrits, M., Meyer, H., Schwander, M. and Zaki, H., 2000. Tectonic evolution of the Eastern Mediterranean Basin and its significance for hydrocarbon prospectivity in the ultradeepwater of the Nile Delta. The Leading Edge, 19(10), pp.1086-1102.

Al-Balushi, A.N., Neumaier, M., Fraser, A.J. and Jackson, C.A., 2016. The impact of the Messinian salinity crisis on the petroleum system of the Eastern Mediterranean: a critical assessment using 2D petroleum system modelling. Petroleum Geoscience, 22(4), pp.357-379.

Albertz, M. and Ings, S.J., 2012. Some consequences of mechanical stratification in basin-scale numerical models of passive-margin salt tectonics. Geological Society, London, Special Publications, 363(1), pp.303-330.

Allen, H., C.A.-L. Jackson and A.J. Fraser, 2016, Gravity-driven deformation of a youthful saline giant: the interplay between gliding and spreading in the Messinian basins of the Eastern Mediterranean: Petroleum Geoscience, v. 22, p. 340-356.

Barnes, A., 2016. Handbook of Poststack Seismic Attributes. Society of Exploration Geophysicists.

Ben-Avraham, Z., 1978. The structure and tectonic setting of the Levant continental margin, eastern Mediterranean. Tectonophysics, 46(3-4), pp.313-331.

Benedetti, L., Finkel, R., Papanastassiou, D., King, G., Armijo, R., Ryerson, F., Farber, D. & Flerit, F., 2002. Post-glacial slip history of the Sparta fault (Greece) determined by 36Cl cosmogenic dating: evidence for non-periodic earthquakes, Geophys. Res. Lett., 29, 1246, doi:10.1029/2001GL014510.

Brown, A.R., 2011. Interpretation of three-dimensional seismic data. Society of Exploration Geophysicists and American Association of Petroleum Geologists.

Brun, J.P. and Fort, X., 2011. Salt tectonics at passive margins: Geology versus models. Marine and Petroleum Geology, 28(6), pp.1123-1145.

Bull, J.M., Barnes, P.M., Lamarche, G., Sanderson, D.J. Cowie, P.A., Taylor S.K. & Dix, J.K., 2006. High-resolution record of displacement accumulation on an active normal fault: implications for models of slip accumulation during repeated earthquakes, J. Struct. Geol., 28, 1146–1166.

Burberry, C.M., 2015. Spatial and temporal variation in penetrative strain during compression: Insights from analog models. Lithosphere, 7(6), pp.611-624.

Butler, R.W.H. and Paton, D.A., 2010. Evaluating lateral compaction in deepwater fold and thrust belts: How much are we missing from “nature’s sandbox”. GSA Today, 20(3), pp.4-10.

Cartwright, J., Kirkham, C., Bertoni, C., Hodgson, N. and Rodriguez, K., 2018. Direct calibration of salt sheet kinematics during gravity-driven deformation. Geology, 46(7), pp.623-626.

Cartwright, J. and Santamarina, C., 2015. Seismic characteristics of fluid escape pipes in sedimentary basins: implications for pipe genesis. Marine and Petroleum Geology, 65, pp.126-140.

Cartwright, J., Jackson, M., Dooley, T. and Higgins, S., 2012. Strain partitioning in gravity-driven shortening of a thick, multilayered evaporite sequence. Geological Society, London, Special Publications, 363(1), pp.449-470.

Cartwright, J.A. and Jackson, M.P.A., 2008. Initiation of gravitational collapse of an evaporite basin margin: The Messinian saline giant, Levant Basin, eastern Mediterranean. Geological Society of America Bulletin, 120(3-4), pp.399-413.

Clark, I.R. and Cartwright, J.A., 2009. Interactions between submarine channel systems and deformation in deepwater fold belts: Examples from the Levant Basin, Eastern Mediterranean sea. Marine and Petroleum Geology, 26(8), pp.1465-1482.

Coleman, A.J., Jackson, C.A.L. and Duffy, O.B., 2017. Balancing sub-and supra-salt strain in salt-influenced rifts: Implications for extension estimates. Journal of Structural Geology, 102, pp.208-225.

Cowie, P.A., 1998. A healing-reloading feedback control on the growth rate of seismogenic faults, J. Struct. Geol., 20, 1075–1087.

Cowie, P.A., Roberts, G.P., Bull, J.M. and Visini, F., 2012. Relationships between fault geometry, slip rate variability and earthquake recurrence in extensional settings. Geophysical Journal International, 189(1), pp.143-160.

Davison, I., Alsop, I. and Blundell, D., 1996. Salt tectonics: some aspects of deformation mechanics. Geological Society, London, Special Publications, 100(1), pp.1-10.

Dooley, T.P., Hudec, M.R., Carruthers, D., Jackson, M.P. and Luo, G., 2017. The effects of base-salt relief on salt flow and suprasalt deformation patterns—Part 1: Flow across simple steps in the base of salt. Interpretation, 5(1), pp.SD1-SD23.

Evans, S.L. and Jackson, C.A.L., 2019. Base-salt relief controls salt-related deformation in the Outer Kwanza Basin, offshore Angola. Basin Research. DOI: 10.1111/bre.12390.

Evans, S. L., and Jackson, C.A.L., 2020. Intrasalt Structure and Strain Partitioning in Layered Evaporites: Implications for Drilling Through Messinian Salt in the Eastern Mediterranean. EarthArXiv. DOI: 10.31223/osf.io/8pkbz.

Feng, Y.E., Yankelzon, A., Steinberg, J. and Reshef, M., 2016. Lithology and characteristics of the Messinian evaporite sequence of the deep Levant Basin, eastern Mediterranean. *Marine Geology*, *376*, pp.118-131.

Feng, Y.E. and Reshef, M., 2016. The Eastern Mediterranean Messinian salt-depth imaging and velocity analysis considerations. Petroleum Geoscience, 22(4), pp.333-339.

Feng, Y.E., Steinberg, J. and Reshef, M., 2017. Intra-salt deformation: Implications for the evolution of the Messinian evaporites in the Levant Basin, eastern Mediterranean. Marine and Petroleum Geology, 88, pp.251-267.

Friedrich, A.M., Wernicke, B.P., Niemi, N.A., Bennett, R.A. & Davis, J.L., 2003. Comparison of geodetic and geologic data from the Wasatch region, Utah, and implications for the spectral character of Earth deformation at periods of 10 to 10 million years, J. geophys. Res., 108, doi:10.1029/2001JB000682.

Gautier, F., G. Clauzon, J.P. Suc, J. Cravatte and D. Violanti, 1994, Age and duration of the Messinian salinity crisis: R. Acad. Sci., Paris (IIA) 318, p. 1103–1109.

Gardosh, M.A. and Druckman, Y., 2006. Seismic stratigraphy, structure and tectonic evolution of the Levantine Basin, offshore Israel. Geological Society, London, Special Publications, 260(1), pp.201-227.

Ghalayini, R., Daniel, J.M., Homberg, C., Nader, F.H. and Comstock, J.E., 2014. Impact of Cenozoic strike-slip tectonics on the evolution of the northern Levant Basin (offshore Lebanon). Tectonics, 33(11), pp.2121-2142.

Ghalayini, R., Homberg, C., Daniel, J.M. and Nader, F.H., 2017. Growth of layer-bound normal faults under a regional anisotropic stress field. Geological Society, London, Special Publications, 439(1), pp.57-78.

Ghalayini, R., Nader, F.H., Bou Daher, S., Hawie, N. and Chbat, W.E., 2018. Petroleum systems of Lebanon: an update and review. Journal of Petroleum Geology, 41(2), pp.189-214.

Gvirtzman, Z., M. Reshef, O. Buch-Leviatan and Z. Ben-Avraham, 2013, Intense salt deformation in the Levant Basin in the middle of the Messinian salinity crisis: Earth and Planetary Science Letters, 379, 108–119.

Gvirtzman, Z., Manzi, V., Calvo, R., Gavrieli, I., Gennari, R., Lugli, S., Reghizzi, M. and Roveri, M., 2017. Intra-Messinian truncation surface in the Levant Basin explained by subaqueous dissolution. Geology, 45(10), pp.915-918.

Hall, J., Calon, T.J., Aksu, A.E. and Meade, S.R., 2005. Structural evolution of the Latakia Ridge and Cyprus Basin at the front of the Cyprus Arc, eastern Mediterranean Sea. Marine Geology, 221(1-4), pp.261-297.

Hawie, N., Gorini, C., Deschamps, R., Nader, F.H., Montadert, L., Granjeon, D. and Baudin, F., 2013. Tectono-stratigraphic evolution of the northern Levant Basin (offshore Lebanon). Marine and petroleum geology, 48, pp.392-410.

Hudec, M.R. and Jackson, M.P., 2007. Terra infirma: Understanding salt tectonics. Earth-Science Reviews, 82(1-2), pp.1-28.

Inati, L., Zeyen, H., Nader, F.H., Adelinet, M., Sursock, A., Rahhal, M.E. and Roure, F., 2016. Lithospheric architecture of the Levant Basin (Eastern Mediterranean region): A 2D modeling approach. Tectonophysics, 693, pp.143-156.

Jackson, M.P.A., B.C. Vendeville and D.D. Schultz-Ela, 1994, Structural dynamics of salt systems: Annual Review of Earth and Planetary Sciences, 22(1), pp.93-117.

Jackson, M.P. and Hudec, M.R., 2005. Stratigraphic record of translation down ramps in a passive-margin salt detachment. Journal of Structural Geology, 27(5), pp.889-911.

Jackson, M.P., Hudec, M.R., 2017. Salt Tectonics: Principles and Practice. Cambridge University Press.

Jones, I.F. and Davison, I., 2014. Seismic imaging in and around salt bodies. Interpretation, 2(4), pp.SL1-SL20.

Kartveit, K.H., Omosanya, K.O., Johansen, S.E., Eruteya, O.E., Reshef, M. and Waldmann, N.D., 2018. Multiphase structural evolution and geodynamic implications of Messinian salt-related structures, levant basin, offshore Israel. Tectonics, 37(5), pp.1210-1230.

Kirkham, C., Cartwright, J., Bertoni, C., Rodriguez, K. and Hodgson, N., 2019. 3D kinematics of a thick salt layer during gravity-driven deformation. Marine and Petroleum Geology, 110, pp.434-449.

Kirkham, C., Bertoni, C., Cartwright, J., Lensky, N.G., Sirota, I., Rodriguez, K. and Hodgson, N., 2020. The demise of a 'salt giant'driven by uplift and thermal dissolution. Earth and Planetary Science Letters, 531, p.115933.

Marton, L.G., Tari, G.C. and Lehmann, C.T., 2000. Evolution of the Angolan passive margin, West Africa, with emphasis on post-salt structural styles. Geophysical Monograph-American Geophysical Union, 115, pp.129-150.

Matmon, A., Enzel, Y., Zilberman, E. and Heimann, A., 1999. Late Pliocene and Pleistocene reversal of drainage systems in northern Israel: tectonic implications. Geomorphology, 28(1-2), pp.43-59.

McClymont, A.F., Villamor, P. & Green, A.G., 2009. Fault displacement accumulation and slip rate variability within the Taupo Rift (New Zealand) based on trench and 3-D ground-penetrating radar data, Tectonics, 28, TC4005, doi:10.1029/2008TC002334.

Meilijson, A., Hilgen, F., Sepúlveda, J., Steinberg, J., Fairbank, V., Flecker, R., Waldmann, N.D., Spaulding, S.A., Bialik, O.M., Boudinot, F.G. and Illner, P., 2019. Chronology with a pinch of salt: Integrated stratigraphy of Messinian evaporites in the deep Eastern Mediterranean reveals long-lasting halite deposition during Atlantic connectivity. Earth-Science Reviews.

Mitchell, S.G., Matmon, A., Bierman, P.R., Enzel, Y., Caffee, M. & Rizzo, D., 2001. Displacement history of a limestone normal fault scarp, northern Israel, from cosmogenic 36Cl, J. geophys. Res., 106, 4247–4264.

Mukherjee, S., Talbot, C.J. and Koyi, H.A., 2010. Viscosity estimates of salt in the Hormuz and Namakdan salt diapirs, Persian Gulf. Geological Magazine, 147(4), pp.497-507.

Nader, F.H., Inati, L., Ghalayini, R., Hawie, N. and Daher, S.B., 2018. Key geological characteristics of the Saida-Tyr Platform along the eastern margin of the Levant Basin, offshore Lebanon: implications for hydrocarbon exploration. Oil & Gas Science and Technology–Revue d'IFP Energies nouvelles, 73, p.50.

Nicol, A.,Walsh, J., Berryman, K. & Villamor, P., 2006. Interdependence of fault displacement rates and paleoearthquakes in an active rift, Geology, 34, 865–868.

Oppo, D., Evans, S., Iacopini, D., Kabir, M., Maselli, V., Jackson C. A-L., 2020. Leaky salt: pipe trails record the history of cross-evaporite fluid escape in the northern Levant Basin, Eastern Mediterranean, EarthArXiv.

Peel, F.J., 2014. The engines of gravity-driven movement on passive margins: Quantifying the relative contribution of spreading vs. gravity sliding mechanisms. Tectonophysics, 633, pp.126-142.

Pichel, L.M., Peel, F., Jackson, C.A. and Huuse, M., 2018. Geometry and kinematics of salt-detached ramp syncline basins. Journal of Structural Geology, 115, pp.208-230.

Pichel, L.M., Jackson, C.A.L., Peel, F. and Dooley, T.P., 2019. Base-salt relief controls salt-tectonic structural style, São Paulo Plateau, Santos Basin, Brazil. Basin Research, 32(3), pp.453-484.

Quirk, D.G., Schødt, N., Lassen, B., Ings, S.J., Hsu, D., Hirsch, K.K. and Von Nicolai, C., 2012. Salt tectonics on passive margins: examples from Santos, Campos and Kwanza basins. Geological Society, London, Special Publications, 363(1), pp.207-244.

Raith, A.F., Strozyk, F., Visser, J. and Urai, J.L., 2016. Evolution of rheologically heterogeneous salt structures: a case study from the NE Netherlands. Solid Earth, 7(1), p.67.

Reiche, S., Hübscher, C. and Beitz, M., 2014. Fault-controlled evaporite deformation in the Levant Basin, Eastern Mediterranean. Marine Geology, 354, pp.53-68.

Robinson, R., Nicol, A., Walsh, J.J. & Villamor, P., 2009. Features of earthquake recurrence in a complex normal fault network: results from a synthetic seismicity model of the Taupo Rift, New Zealand, J. geophys. Res., 114, B12306, doi:10.1029/2008JB006231.

Roveri, M., R. Flecker, W. Krijgsman, J. Lofi, S. Lugli, V. Manzi, F.J. Sierro, A. Bertini, A. Camerlenghi, G. De Lange, R. Govers, F.J. Hilgen, C. Hübscher, P.T. Meijer, & M. Stoica, 2014, The Messinian salinity crisis: Past and future of a great challenge for marine sciences: Marine Geology, 352, 25–58.

Rowan, M.G., Urai, J.L., Fiduk, J.C. and Kukla, P.A., 2019. Deformation of intrasalt competent layers in different modes of salt tectonics. Solid Earth, 10(3), pp.987-1013.

Ryan, W.B.F., 2009, Decoding the Mediterranean salinity crisis: Sedimentology 56, 95–136.

Schlagenhauf, A., Gaudemer, Y., Benedetti, L., Manighetti, I., Palumbo, L., Schimmelpfennig, I., Finkel, R. & Pou, K., 2010. Using in situ Chlorine-36 cosmonuclide to recover past earthquake histories on limestone normal fault scarps: a reappraisal of methodology and interpretations, Geophys. J. Int., 182, 36–72, doi:10.1111/j.1365-246X.2010.04622.x.

Schlagenhauf, A., Manighetti, I., Benedetti, L., Gaudemer, Y., Finkel, R., Malavieille, J.&Pou, K., 2011. Earthquake supercycles in central Italy inferred from 36Cl exposure dating, Earth planet. Sci. Letts., 307, 487–500, doi:10.1016/j.epsl.2011.05.022.

Schultz-Ela, D.D., 2001. Excursus on gravity gliding and gravity spreading. Journal of structural geology, 23(5), pp.725-731.

Spiers, C.J., Schutjens, P.M.T.M., Brzesowsky, R.H., Peach, C.J., Liezenberg, J.L. and Zwart, H.J., 1990. Experimental determination of constitutive parameters governing creep of rocksalt by pressure solution. Geological Society, London, Special Publications, 54(1), pp.215-227.

Steinberg, J., Gvirtzman, Z., Folkman, Y. and Garfunkel, Z., 2011. Origin and nature of the rapid late Tertiary filling of the Levant Basin. Geology, 39(4), pp.355-358.

Urai, J.L., and Spiers, C.J., 2007. The effect of grain boundary water on deformation mechanisms and rheology of rocksalt during long-term deformation, in Wallner, M., et al., eds., Proceedings of the 6th Conference on the Mechanical Behaviour of Salt: Understanding of THMC Processes in Salt Rocks: London, Taylor and Francis, p. 149–158.

Urai, J.L., Schléder, Z., Spiers, C.J., and Kukla, P.A., 2008, Flow and transport properties of salt rocks, in Littke, R.,et al., eds., Dynamics of Complex Intracontinental Basins: The Central European Basin System: Berlin, Heidelberg, Springer-Verlag, p. 277–290.

Van Keken, P.E., Spiers, C.J., Van den Berg, A.P. and Muyzert, E.J., 1993. The effective viscosity of rocksalt: implementation of steady-state creep laws in numerical models of salt diapirism. Tectonophysics, 225(4), pp.457-476.

Weijermars, R., Jackson, M.T. and Vendeville, B., 1993. Rheological and tectonic modeling of salt provinces. Tectonophysics, 217(1-2), pp.143-174.

5 Analogue Modelling

This chapter presents my initial findings of analogue modelling work that took place over 3 weeks at IFP Energies Nouvelles in February 2019. I will be consolidating these results and preparing the manuscript after PhD submission.

Acknowledgements

Sylive Schueller, Jean-Marie Mengus and Juliette Hello were instrumental in facilitating the modelling work at IFP Energies Nouvelles. AAPG and the Geological Society of London awarded grants to fund this work. I would also like to thank my supervisor, Chris Jackson, for valuable discussions that guided my interpretation of the data, and help with editing the chapter.

Abstract

I ran a series of physical analogue models in order to test how variations in salt thickness and salt heterogeneity affect the coupling between sub- and supra-salt structures during gravity-driven translation. I designed a simple base-salt geometry and ran experiments with different thicknesses and compositions of the ductile salt analogue. Models were run within a CT scanner to image internal structure during model evolution. Results show that thicker and more homogeneous salt units experience more vertical movement (i.e. minibasin subsidence and diapiric rise) and exhibit less coupling to the base-salt relief. Conversely, thinner and more heterogeneous salt units are dominated by lateral movement, and the resulting distribution of depocentres and supra-salt structures is more closely coupled to the geometry of the base-salt surface. These results highlight the role of base-salt relief in the subsequent structural evolution of salt basins.

5.1 Introduction

In the previous chapters I used 3D seismic reflection datasets from the Kwanza Basin, offshore Angola and the Levantine Basin, offshore Lebanon to investigate how the structural development of salt basins may be influenced by: (i) relief on the base-salt surface, and (ii) the lithological heterogeneity of the evaporite sequence, both of which may locally affect salt flow and supra-salt structure. Our analysis suggests that in the translational domain offshore Angola, local stress fields associated with the base-salt steps have had a greater influence on the local development of salt structures than the regional tectonic regime. Offshore Lebanon, lithological heterogeneity controls the way in which strain is accommodated within the deforming evaporite sequence, while volumetric imbalances over base-salt anticlines modulate local rates of salt flow and overburden translation.

However, seismic reflection data reveal only finite structural style, whereas models (physical or numerical) can help us to better understand how, when and where supra-salt structures evolve. Physical analogue models test these concepts by creating a 3D scaled-down replica of the system, colloquially referred to as a 'sandbox' model. They allow us to observe the development of salt structures over human timescales (i.e. minutes to weeks, rather than millions of years), and have played a vital role in achieving our present understanding of salt tectonic systems (e.g. Vendeville and Cobbold, 1988; Vendeville, 1988, 1989; Cobbold et al., 1989; Richard, 1991; Vendeville and Jackson 1992a,b). They also allow us to investigate the influence of specific variables (e.g. salt viscosity, strain rate, overburden thickness) under precisely controlled boundary conditions. This method therefore gives us an opportunity to test and further develop the interpretations made in previous chapters.

5.1.1 Salt Rheology

In order to be able to create scaled physical models of natural systems, we must first have good constraints on the rheology of the natural rock types (i.e. clastic sediments and salt). The termed 'ductile' is used when the dominant mode of deformation is plastic creep, whereas 'brittle' refers to dominant deformation by frictional slip.

Salt has an elastic yield strength on short timescales and under high differential stresses, such as those involved in drilling and mining operations, and as such may behave in a brittle

manner under these conditions. Over geological timescales, however, it behaves as a viscoplastic material and will flow in response to small applied stresses (Weijermars et al., 1993).

The way that salt responds to applied stresses varies under different conditions (temperature, pressure, fluid presence, etc.), depending on the dominant mechanism of flow. Dislocation creep dominates at high temperatures, relatively high strain rates (>10^{-14}/s), and for coarse grain sizes (c. 30 mm), whereas solution-precipitation creep dominates at moderate temperatures, relatively low strain rates (<10^{-12}/s), and for relatively fine grain sizes (c. 5 mm) (Fig. 5.1; Jackson and Hudec, 2017). The rheology of salt therefore obeys a combined flow law for these two processes, and the dominant mechanism of deformation may vary through time and space.

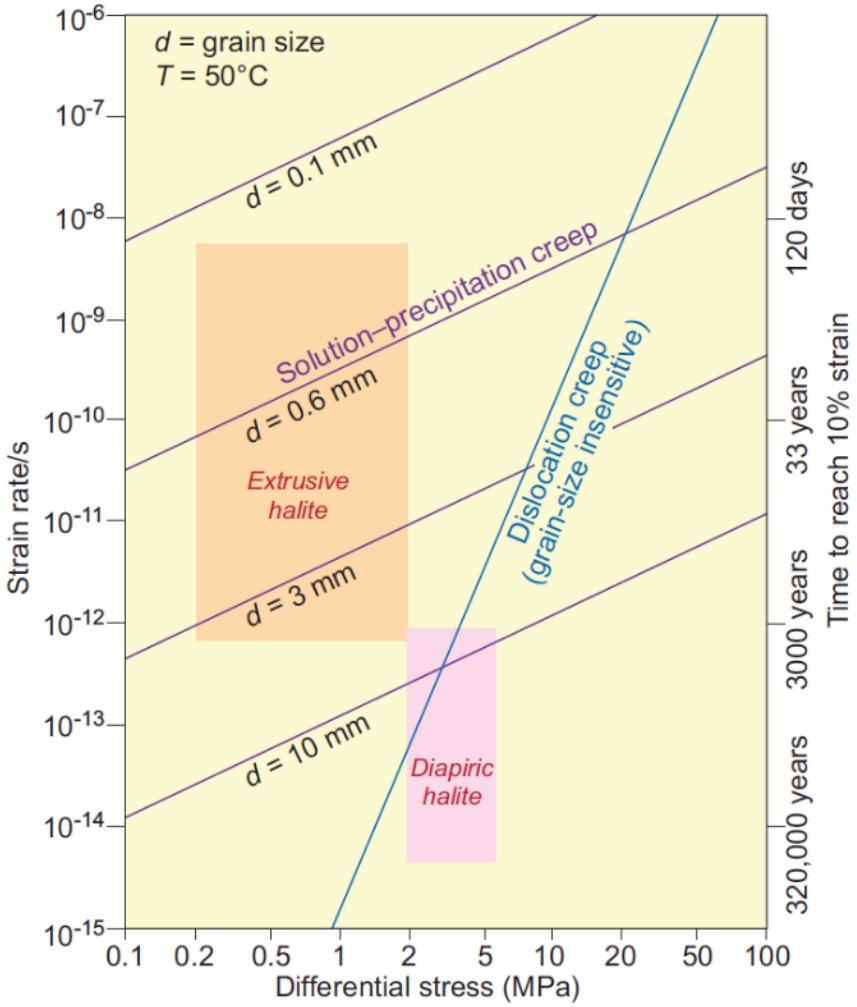

Figure 5.1 Experimentally-derived flow laws for damp, pure halite. The strain rate of solution–precipitation creep depends on grain size, whereas the rate of dislocation creep is grain-size insensitive. Where the line for dislocation creep crosses the lines for solution–precipitation creep, the two types of creep are equally effective. The most significant crossing point is in the field for diapirism (pink), where stress is about 3 MPa, strain rate is about 10–13/s, and grain size is 10 mm. Solution-precipitation creep dominates in extrusive salt glaciers. From Jackson and Hudec (2016) (after Urai et al., 2008).

Where dislocation creep dominates, the viscosity of the salt depends on strain rate (power-law viscous). This means that the salt deforms plastically at constant stress (known as the 'yield stress'). Where solution–precipitation creep dominates the viscosity is constant (Newtonian viscous). This means that stress and strain rate are directly proportional, and the ratio between them gives the viscosity of the fluid. Once the salt reaches steady-state creep, it yields a single value for viscosity, which is useful for comparisons and also for scaling physical models of salt tectonics.

Increasing the grain size from 5 to 30 mm increases the viscosity of halite by two orders of magnitude (Jackson and Hudec, 2017). For a grain size of 10 mm, which is typical for diapiric salt, a viscosity of 10^{19} Pa s is representative of salt at the surface, and 10^{18} Pa s for salt at depth. However, these diapiric values of viscosity (10^{18} to 10^{19} Pa s) are much higher than in extremely fine-grained, mylonitized salt in the distal reaches of salt glaciers (Talbot 1998; Schléder and Urai 2007), where viscosity is locally as low as 10^{15} Pa s. The viscosity of salt is also very sensitive to temperature and water content, with an increase in either lowering the viscosity. Natural salt viscosities are therefore variable, but generally fall within the range 10^{19} – 10^{15} Pa s.

5.1.2 Dynamic Scaling

In order to replicate geological processes on human timescales and length scales, we must scale down the physical properties of the natural systems. The rheological behaviour of the analogue materials must replicate processes that naturally occur over millions of years and over tens of kilometres. A key part of this is the scaling relationships between the different parameters. For example, scaling the length down from 50 km to 50 cm gives a scaling factor of 100,000 (50,000/0.5) and all other lengths (thicknesses, depths etc.) should be scaled by the same factor. Similarly, physical parameters must be scaled proportionally (e.g. viscosity of the salt, cohesive strength of the overburden) as well as time-dependent variables (e.g. translation rates, sedimentation rates). Historically, even unscaled models have helped us to better understand some qualitative concepts in salt tectonics (e.g Nettleton, 1934), but an accurate analogue model, from which quantitative data can be extrapolated to nature, requires the consideration of dynamic scaling relationships. Even then the extrapolation of laboratory data to natural systems must be done with care because they are measured at

strain rates at least six orders of magnitude faster than in nature (Carter and Tsenn, 1987; Paterson, 1987). Experiments must therefore be carefully designed such that the scaling results in analogue materials behaving in broadly the same manner as their natural equivalents.

Early models of salt tectonics treated the overburden as a fluid, with viscous salt rising buoyantly into a higher density fluid (e.g. Nettleton, 1934). However, we now know that this theory of Rayleigh-Taylor instability due to density contrasts does not represent the physical reality of salt systems. Observations and experimental rock mechanics have shown that natural clastic overburdens deform dominantly by brittle failure, and the analogue materials used in physical models must therefore replicate this behaviour. Some early physical models used wet clay or concrete to simulate brittle failure, but the cohesive strength of these materials was too great, resulting in the formation of tension rather than shear fractures (i.e. faults) (e.g. Ramberg, 1981). Nettleton and Elkins (1947) were the first to use a granular overburden with proper consideration of scaling parameters of shear strength, friction coefficient, cohesion and density. They were also the first to model a complete gravity gliding system by tilting the substrate to generate updip extension and downdip contraction, a structural style common on many salt-influenced passive margins (Jackson et al., 1994).

Using sand to model brittle overburdens fracturing above a ductile substratum has four advantages: finite shear strength, brittle mode of deformation, low cohesion, and the ability to simulate syn-kinematic sedimentation (Weijermars et al., 1993; Koyi, 1997). Granular materials such as sand may be regarded as a continuous medium (prior to fault propagation) if the mechanics is studied at a scale much larger than that of the characteristic grain size. A common criticism of sandbox experiments is that, if scaled back to natural dimensions, the size of the grains would be unrealistically large. However, sand is chosen as a model material because it successfully imitates the *bulk* mechanical properties of the natural overburden. At the basin-scale, the overburden acts as an elasto-plastic sheet; sand deforms elastically at the grain contacts, but if stressed beyond the elastic limit, plastic deformation initiates (Weijermars et al., 1993). The range of estimated cohesion values for loose sand at normal gravity meets the scaling criterion that the cohesion in sandbox models should be 300 Pa or less (Weijermars et al., 1993). As long as the other parameters of the model are proportionally

scaled and boundary conditions remain similar, model and nature should remain dynamically similar even after faulting has occurred.

Silicone polymers are commonly used as analogues for salt due to their viscous behaviour. Silicone behaves as a Newtonian fluid, which may accurately replicate salt tectonic systems dominated by solution-precipitation creep, but may differ in some respects from salt tectonic systems dominated by non-Newtonian, power-law dislocation creep (see Section 1.1.2). However, silicone is thought to be an appropriate analogue material in many cases since solution-precipitation creep generally dominates over dislocation creep at the low strain rates characterising many subsurface salt basins (Fig. 5.1) (Weijermars, 1993; Jackson et al., 1994; Koyi, 1997).

Silicone polymers lack a yield strength, such that they spread under their own weight to a thin sheet confined only by surface tension. In order to replicate dynamic similarity with natural systems, the ratio of densities between the model overburden and silicone should be the same as the ratio between natural salt and its overburden (Koyi, 1997). Geometric and rheological scaling of model and nature will then be sufficient to ensure that the stress field in the model corresponds to that of the natural system (Weijermars et al., 1993; Koyi, 1997). Due to the temperature control, viscosity may vary with depth in natural salt basins, but in models it is practical and convenient to assume a depth-averaged viscosity. The strain rate of the model scales with viscosity, density and thickness. The strength of the salt analogue is typically of the order of 1 Pa, with viscosity of the order of 10^4 Pa s and typical model strain rates of 10^{-4} s^{-1} (Weijermars et al., 1993).

Model design requires not only scaling of rheologies (Weijermars and Schmeling, 1986) but also careful consideration of the initial geometry and boundary conditions in both nature and experiments (Hubbert, 1937; Ramberg, 1981). This includes basal slope and mechanical properties of layer boundaries, as well as the initial thickness of the salt and its overburden. If syn-kinematic sedimentation is included, the thickness of these layers, as well as rates of erosion and sedimentation, must be also scaled proportionally.

Models with silicone polymer substrata and sand overburdens therefore provide reliable, rheologically-scaled analogues of salt overlain by clastic overburdens (Weijermars, 1993; Jackson et al., 1994; Koyi, 1997). This means that the structural evolution of salt tectonic systems can be simulated in scale models using a ductile substratum overlain by an elasto-

plastic overburden, i.e. silicone polymer for the salt and fine-grained sand for the clastic overburden. For gravity gliding-dominated systems, scaling of the geometries, rheologies and densities is adequate for achieving dynamic similarity between models and nature. Such experiments have produced fault patterns and structures that are remarkably similar to those in depth-converted seismic sections of salt-detached sedimentary sequences (e.g. Nettleton and Elkins, 1947; Vendeville and Cobbold, 1988; Vendeville et al., 1987; Vendeville, 1988; Cobbold et al., 1989; Dooley and Hudec, 2017; Ferrer et al., 2017). The dynamic scaling parameters used in this study are listed in Table 5.1.

Quantity	Model	Nature	Ratio
Overburden density ($kg \cdot m^{-3}$)	1500 - 1700	2300	0.65 - 0.74
Overburden coefficient of friction	0.7	0.8	0.88
Salt density ($kg \cdot m^{-3}$)	987	2200	0.45
Salt viscosity (Pa·s)	$5 \cdot 10^{4}$	$5 \cdot 10^{18}$	10^{-14}
Gravity ($m \cdot s^{-2}$)	9.81	9.81	1

Table 5.1 Dynamic scaling parameters used in physical analogue models in this study.

5.2 Experiment Design

We ran a series of physical analogue models designed to investigate the relationship between overburden deformation and base-salt relief for different thicknesses and rheological properties of the salt. In Chapter 2 we proposed that supra-salt structures in the transitional domain offshore Angola have been influenced by salt flow over fault scarps on the base-salt surface. We proposed that the strong coupling between the sub- and supra-salt structures was due to the large magnitude of relief relative to the thickness of the salt sheet itself. We therefore designed a model to test how the depositional salt thickness affects the coupling of supra-salt structures to features on the base-salt. Furthermore, in Chapter 3 we suggested that the thickness and lithology of the intrasalt units may control the way in which strain is partitioned within the evaporite sequence. If the intrasalt heterogeneity controls the distribution of strain within the salt, it follows that this will also affect the distribution of strain

within the overburden. We therefore ran the models for heterogeneous salt analogues as well as varying the salt thickness to investigate how intrasalt heterogeneity can also affect the interaction between base-salt relief and supra-salt structure.

The model consists of three basin-facing steps on the base-salt surface at different orientations (Fig. 5.2), and we varied the thickness and heterogeneity of the salt analogue in controlled experiments to isolate the effects of these variables (Fig. 5.3; Table 2). The base-salt steps were designed to reflect base-salt geometries observed in our seismic reflection dataset from the Kwanza Basin, offshore Angola, but in a simplified form that explicitly shows the influence of the base-salt steps on salt and supra-salt structure (Fig. 5.4). The steps are reminiscent of the large, basin-dipping syn-rift faults that typically accommodate thick-skinned extension during rifting. Since the salt is often deposited shortly after rifting, overlying these remnant fault scarps, basin-dipping steps are common structural features of base-salt surfaces.

The experiments were run within a CT scanner, which images the internal structure of the models during deformation. This approach allows us to monitor the internal structural development of the model as it evolves (c.f. Colletta et al., 1991; Adam et al., 2013; Zwaan and Schreurs, 2017), in contrast to traditional approaches which permit only a 2D analysis of the model top or base during its evolution. Such models must be sliced open after they have run to completion to reveal their internal structure (e.g. Dooley et al., 2017), whereas the CT scanning approach is non-destructive. The resulting evolution of the analogue models is then used to constrain the tectono-stratigraphic interpretations of natural salt structures identified in seismic reflection data. This gives unprecedented insight into how the structures evolve in 4D, exploring the extent to which base-salt relief and intrasalt heterogeneity control the

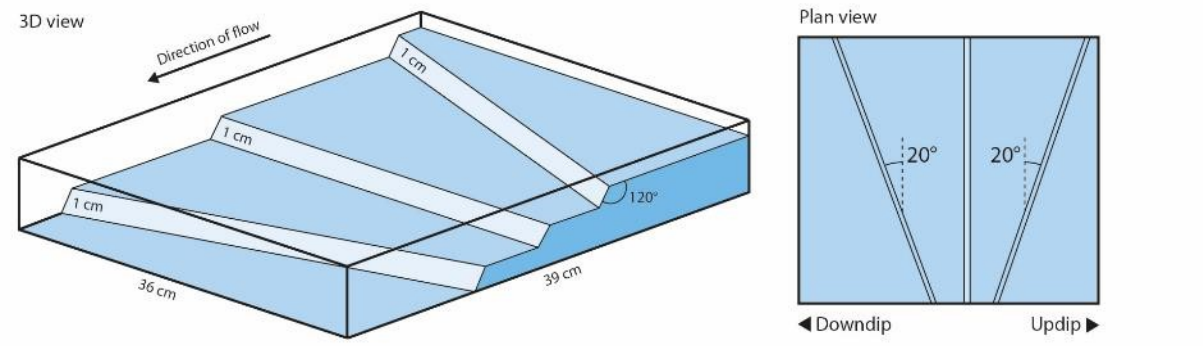

Figure 5.2 Base-salt geometry of physical analogue models designed to investigate the development of supra-salt structures during gravity-translation. The model consists of three basin-facing steps oriented at different angles. Steps represent inherited topography of syn-rift fault scarps on passive margins.

distribution and style of intra- and supra-salt structure. This allows us to compare with the predictions of classic models of gravity gliding and spreading on salt-detached slopes.

Dynamic scaling relationships were calculated based on real-world natural examples (Table 1). These models do not aim to replicate the entire kinematically-linked gravitational system from updip extension to downdip contraction, but rather focus on modelling salt flow over base-salt steps at a relatively narrow portion of the margin, comparable to the scale considered in our seismic reflection-based study of salt structures in the Kwanza Basin, offshore Angola. We therefore use a scaling factor of 1 cm: 1 km. The width of the model (along-strike) was 36 cm (c. 36 km) and the length (across-strike) 39 cm (c. 36 km) (Fig. 5.2). The edges of the model were excluded from the final analysis to remove the effects of boundary drag. Base-salt steps were 1 cm high (c. 1 km; equivalent to the height of base-salt steps offshore Angola) (Fig. 5.2). The corner of each step was slightly rounded, with the basin-facing plane dipping at an angle comparable to typical rift-related normal faults (60^{o}). A silicone polymer (polydimethylsiloxane SGM-36) was used to represent the ductile salt layer (dynamic scaling parameters given in Table 1) and left to settle for a minimum of 24 hours after application to ensure cohesion. The silicone was applied with the model back-tilted to resemble the initial post-rift basin geometry, such that the salt thickens uniformly over each step into the centre of the basin (Fig. 5.3).

Model	Salt thickness (updip - downdip)	Intrasalt layers (4 mm)
Thin salt	6 - 13	0
Intermediate salt	9 - 21	0
Intermediate salt	16 - 21	1
Thick salt	24 - 33	0
Thick salt	29 - 34	1
Thick salt	25 - 31	2

Table 5.2 Variable parameters for each model run: thickness of the viscous salt analogue and number of brittle intrasalt layers. All other parameters and boundary conditions were kept constant.

A pre-kinematic overburden (4 mm; c. 400 m) was added prior to model initiation, equivalent to the minimum thickness of the pre-kinematic Albian interval identified offshore Angola (Evans and Jackson, 2020). Deformation was induced by tilting the model basinward to initiate gravitational instability, given that the ramp syncline basins record >20km of downdip translation and indicate that gravity-gliding was the dominant driver of salt tectonics (Hudec and Jackson, 2004; Evans and Jackson, 2020). Models were tilted by 1° in the initial stages and increased to 3° at approximately halfway through the model duration, reflecting the natural tilting of the margin caused by post-rift subsidence in the deep basin. Syn-kinematic sedimentary layers were added as the model developed, infilling basin topography to create

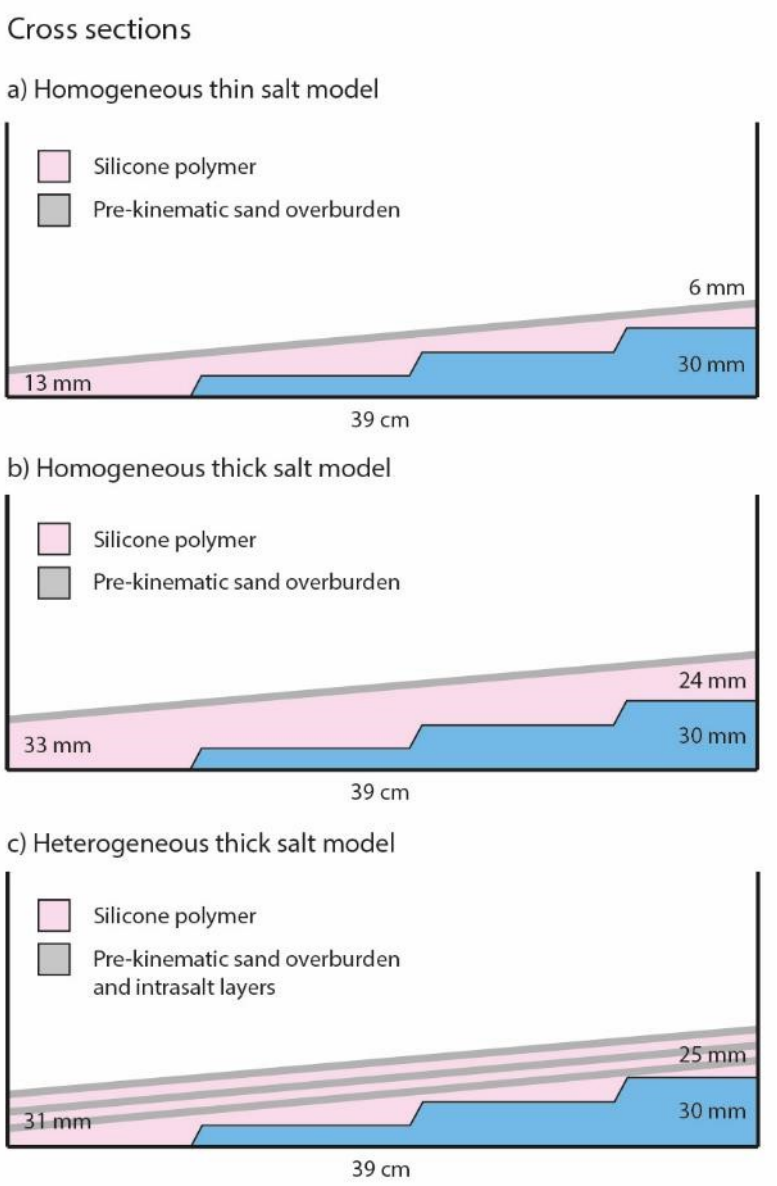

Figure 5.3 Initial set-up of three physical analogue models with variable thicknesses and compositions: a) homogeneous thin salt, b) homogeneous thick salt, and c) heterogeneous thick salt. All models thicken downdip and start with a thin pre-kinematic overburden.

growth strata in the overburden. Alternating layers of fine sand and pyrex with a grain size of 100 µm were used to represent clastic sedimentary layers (as their density contrast is sufficient for them to be imaged by the CT scanner). Sedimentary layers were applied with minor basinward thinning, but lateral uniform distribution, to reflect realistic thickness changes across the designated length-scale. Since we are modelling a relatively narrow portion of a much wider margin we cut the model at the downdip end at regular time intervals to allow continued translation over the steps, therefore simulating an 'open-toe' salt tectonic system (cf. Gaullier et al., 1993; Dooley et al., 2017).

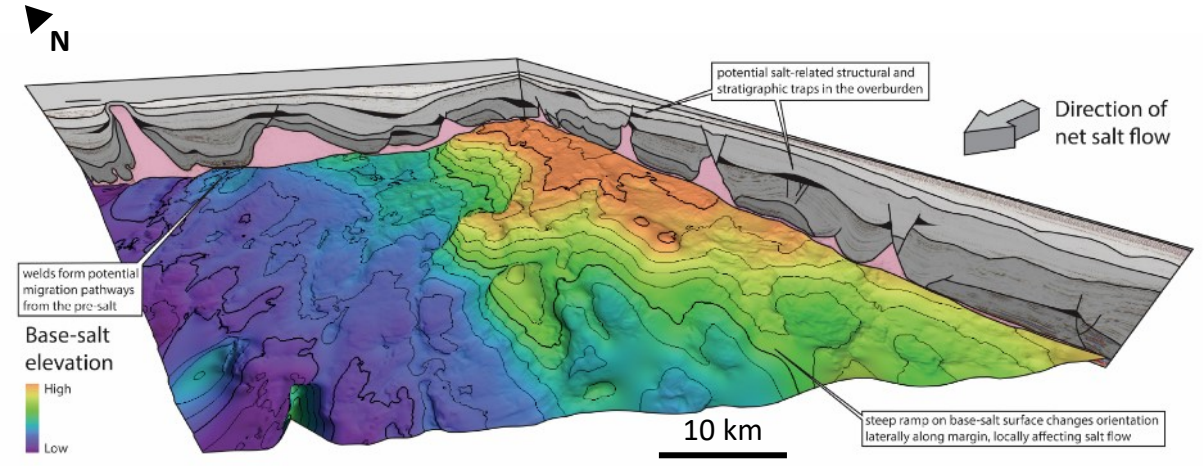

Figure 5.4 Complex base-salt geometry and associated supra-salt structures in the Outer Kwanza Basin, offshore Angola.

In total we ran six experiments with base-salt steps (Table 2). We varied the initial thickness and heterogeneity of the salt layer for each experiment, and kept all other parameters constant between runs in order to isolate the effects of the chosen variables on basin evolution. The minimum updip salt thickness and maximum downdip salt thickness for each experiment are reported in Table 2, along with the number of intrasalt layers. Here we present results of three selected models: thin homogeneous salt, thick homogeneous salt, and thick heterogeneous salt. Interpretation of the remaining models is ongoing and will form the basis of future work for publication.

5.3 Results

5.3.1 Homogeneous Thin Salt

Immediately after translation begins, the model with a thin initial salt layer develops three linear depocentres downdip of each base-salt step (Figs. 5.5a-i, 5.6a-i and 5.7a-i). The syn-kinematic sediments thicken into the depocentres and onlap the pre-kinematic layer, thus developing three ramp syncline basins (RSBs) adjacent and parallel to each of the base-salt steps (Fig. 5.5a-ii). As described in detail in previous chapters, RSBs form when salt translates over relief on the base-salt surface, creating local accommodation and landward-dipping growth strata (Hudec and Jackson, 2004; Pichel et al., 2018; Evans and Jackson, 2019).

As the RSB depocentres subside, the underlying salt thins, which increases the basal friction (Figs. 5.5a-iii and 5.8a). The thicker salt downdip of the depocentre pulls away more easily, stretching the overburden and forming graben structures at the downdip edge of each depocentre (Figs. 5.5a-iii, 5.7a-i and 5.8a). The grabens initiate at the southern end where the steps are closest together and rapidly propagate across the model (Fig. 5.7a-ii). The stretched and thinned overburden creates space into which the salt can flow, thus forming three linear reactive diapirs parallel to each base-salt step (Figs. 5.5a-iv and 5.6a-ii). Asymmetric subsidence causes the overburden to form monoclines over each step (Figs. 5.5a-v and 5.7a-ii).

The RSBs become progressively deeper and wider, and the salt walls continue to accommodate extensional strain (by widening) as they translate downdip (Figs. 5.5a-v, 5.6a-iii and 5.7a-iii). When the reactive salt walls reach the downdip base-salt step, their basinward flanks subside rapidly over the step and generate a pronounced asymmetry (Fig. 5.9). This transforms the symmetrical grabens into basinward-dipping normal faults directly above the base-salt step (Fig. 5.9). The linear salt walls therefore become distorted in plan view as they reach the steps first at the southern end of the model but continue to translate at the northern end of the model where the steps are more widely spaced (Figs. 5.6a-iii and 5.7a-iii). The diapirs then collapse completely as they translate over the step and into the RSB depocentre, where they become buried (Fig. 5.9), leaving no expression of the structure at the seabed (Fig. 5.7a-iii). The RSBs subside to the point that they effectively weld against the

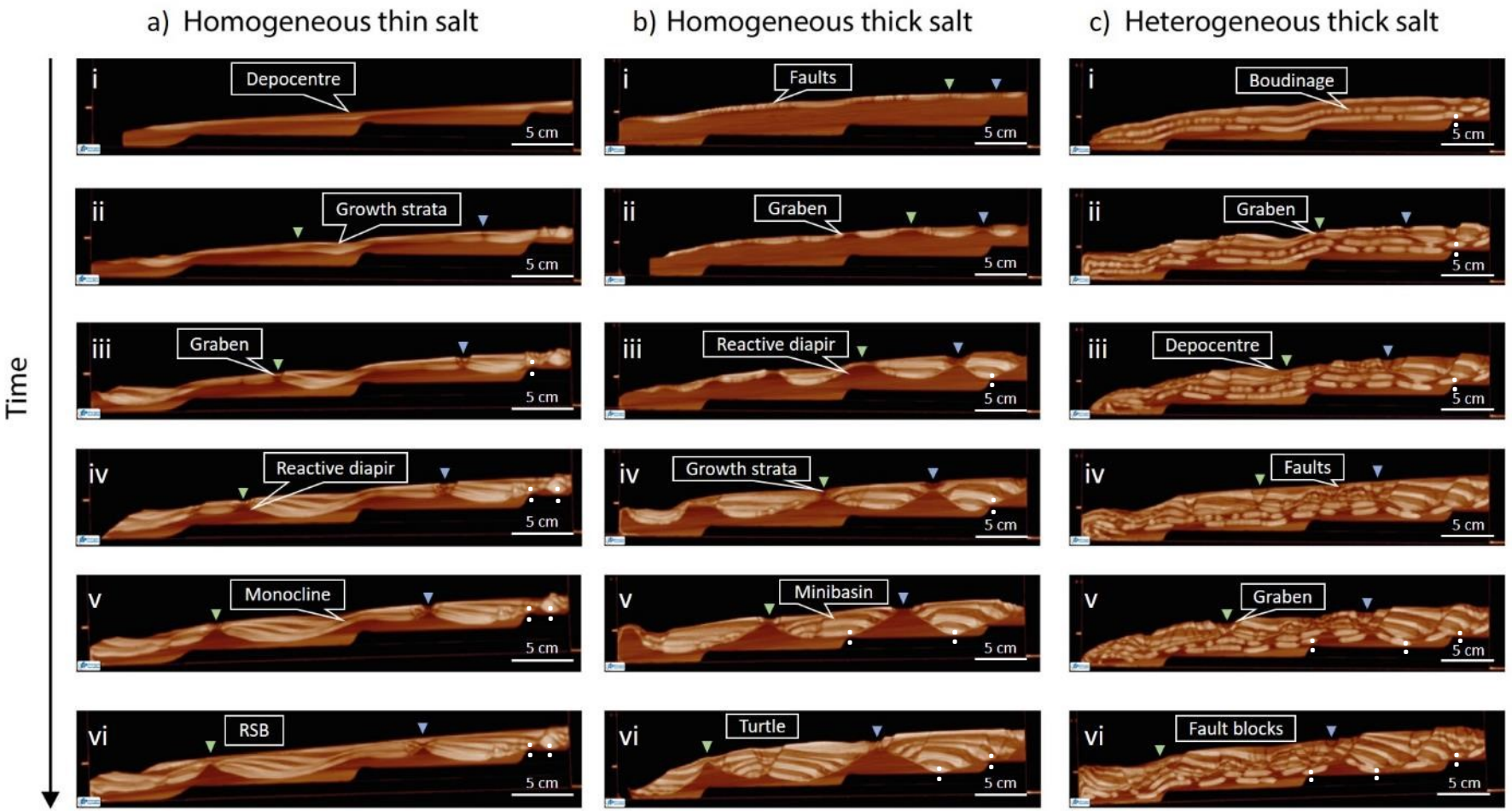

Figure 5.5 CT-scan cross sections through physical analogue models showing the structural evolution of a) thin, b) thick and c) heterogeneous models. Key features of interest are annotated. The homogeneous thin salt model develops reactive diapirs and ramp syncline basins. The homogeneous thick salt model develops reactive diapirs and turtle minibasins. The heterogeneous thick salt model develops boundinaged intrasalt layers and supra-salt fault blocks. The blue and green triangular markers track the position of selected structures in order to measure translation and extension across the model. White dots show weld locations. See Appendix A for enlarged CT scan sections.

base-salt, but still continue to translate at a reduced rate (Fig. 5.5a-vi). The updip RSB is the first to weld as this is where the salt layer was initially (i.e. depositionally) thinnest, followed by the downdip RSBs.

There is a clear relationship between the underlying steps and the distribution and orientation of the overburden structure. Even in the late stages of the model the expression of the steps is clearly shown by the top-salt surface, with all of the dominant structures (i.e. faults, reactive diapirs, and ramp-syncline and graben-like depocentres) trending parallel to the adjacent updip base-salt step (Figs. 5.6a-iii and 5.7a-iii). The base-salt relief therefore has a clear influence on the structural development of the model.

We can measure the total translation by tracking the position of the two major salt walls as the model evolves (Fig. 5.5a-vi). The distance from the original position of the updip diapir to its final position reveals c. 5 cm (5 km) of downdip translation, while the downdip diapir reveals c. 6 cm (6 km) of translation (indicating 1 cm of cumulative syn-kinematic extension between the diapirs).

5.3.2 Homogeneous Thick Salt

In contrast to the thin salt model where extension is localised within grabens early on, leaving the rest of the overburden relatively undeformed, the early stages of the thick salt model show much more distributed overburden extension. This means that the extension is accommodated by a series of normal faults with very small throws across a wide surface area (Figs. 5.5b-i, 5.7b-i and 5.8b). The faults forming over the downdip and middle steps are aligned with the orientations of the underlying base-salt step (Fig. 5.7b-i). The faults at the updip end of the model are, however, oblique to the underlying base-salt step and perpendicular to the translation direction (Fig. 5.7b-i). They do, however, terminate laterally where they meet the edge of the step, such that the expression of the underlying step can still be seen at the seabed (Fig. 5.7b-i).

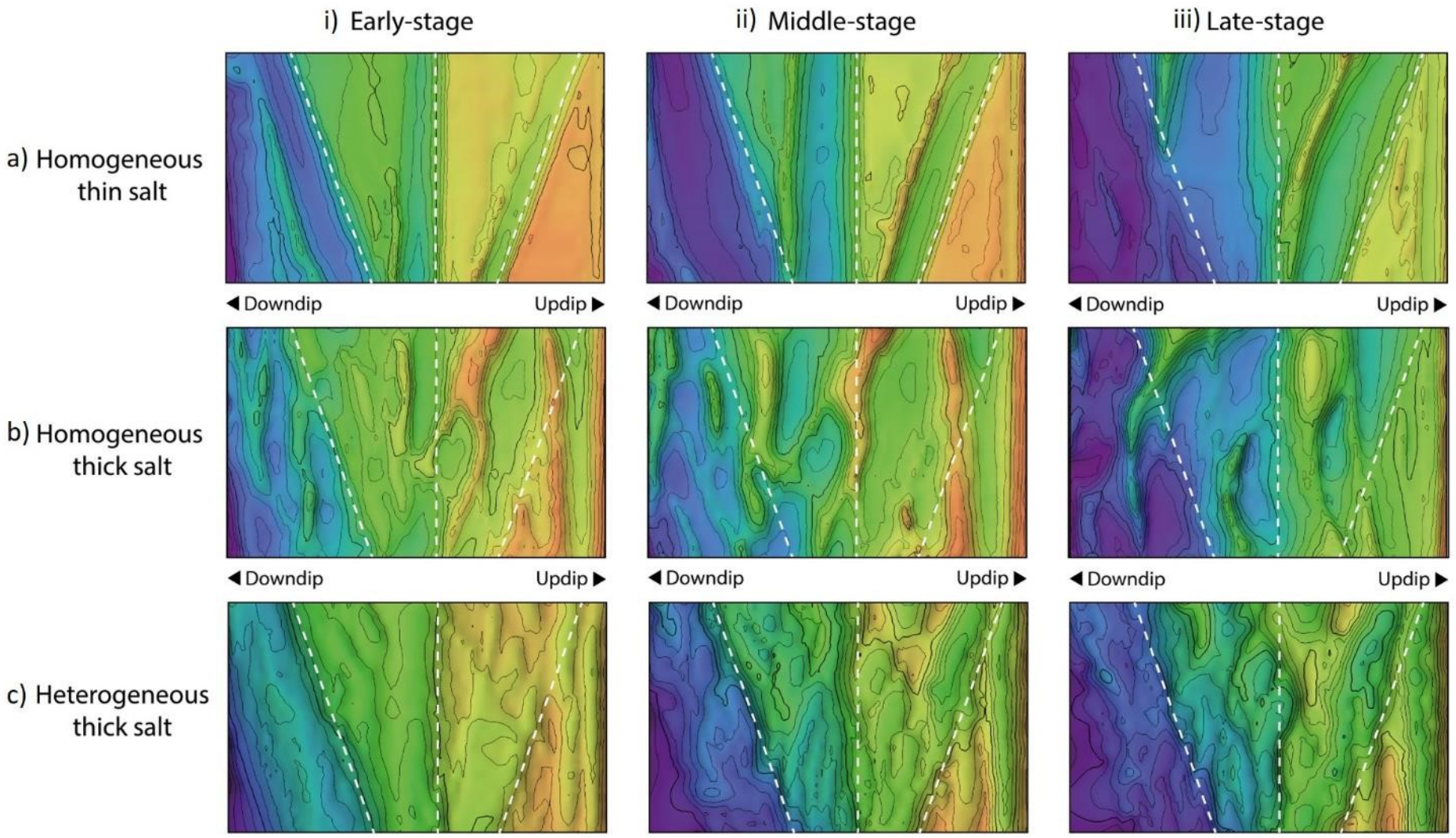

Figure 5.6 Plan-view evolution of the top-salt surface for a) thin, b) thick and c) heterogeneous models. Note that in all images the edges of the model have been cut off to eliminate the effects of boundary drag.

As the model evolves and the overburden thickens, the strain localises into discrete grabens and most of the smaller faults die out (Figs. 5.5b-ii and 5.7b-ii). As in the thin salt model, the localised extension leads to the development of reactive diapirs (Figs. 5.5b-iii and 5.6b-i). Sediments thicken across the crests of the diapirs, whose flanks subside as extension continues (Fig. 5.5b-iv). This creates minibasins with antiformal internal growth strata, known as turtle structures, separated by broad, triangular salt walls (Fig. 5.5b-v). The salt walls are oriented sub-perpendicular to the translation direction and have a curvilinear geometry in plan view (Fig. 5.6b-ii).

As the salt walls move over the downdip base-salt steps, they subside asymmetrically as observed in the thin salt model (Fig. 5.5b-vi). However in this case they do not collapse completely, but instead continue to widen when they reach the flat of the next step. By the late stages of the model there is no clear spatial relationship between the distribution and trend of structures in the overburden and the base-salt steps (Fig. 5.6b-iii), and no development of ramp syncline basins (Fig. 5.5b-vi). Instead, structures form sub-perpendicular to the translation direction (Figs. 5.6b-iii and 5.7b-iii). The final structure of the model does not bear a spatial resemblance to the geometry of the base-salt surface, indicating a weak influence of the steps on the overburden structure (Figs. 5.6b-iii and 5.7b-iii).

As with the thin salt case, we can track the position of the two broad reactive diapirs during model evolution to reveal the magnitude of horizontal translation (Fig. 5.5b-vi). The distance from the original position of the updip diapir to its final position reveals c. 12 cm (12 km) of downdip translation, whereas the downdip diapir reveals a significantly larger magnitude c. 23 cm (23 km) of translation (indicating 11 cm of cumulative syn-kinematic extension between the diapirs). Both the total magnitude of translation and the magnitude of extension are therefore larger than that observed in the thin salt model.

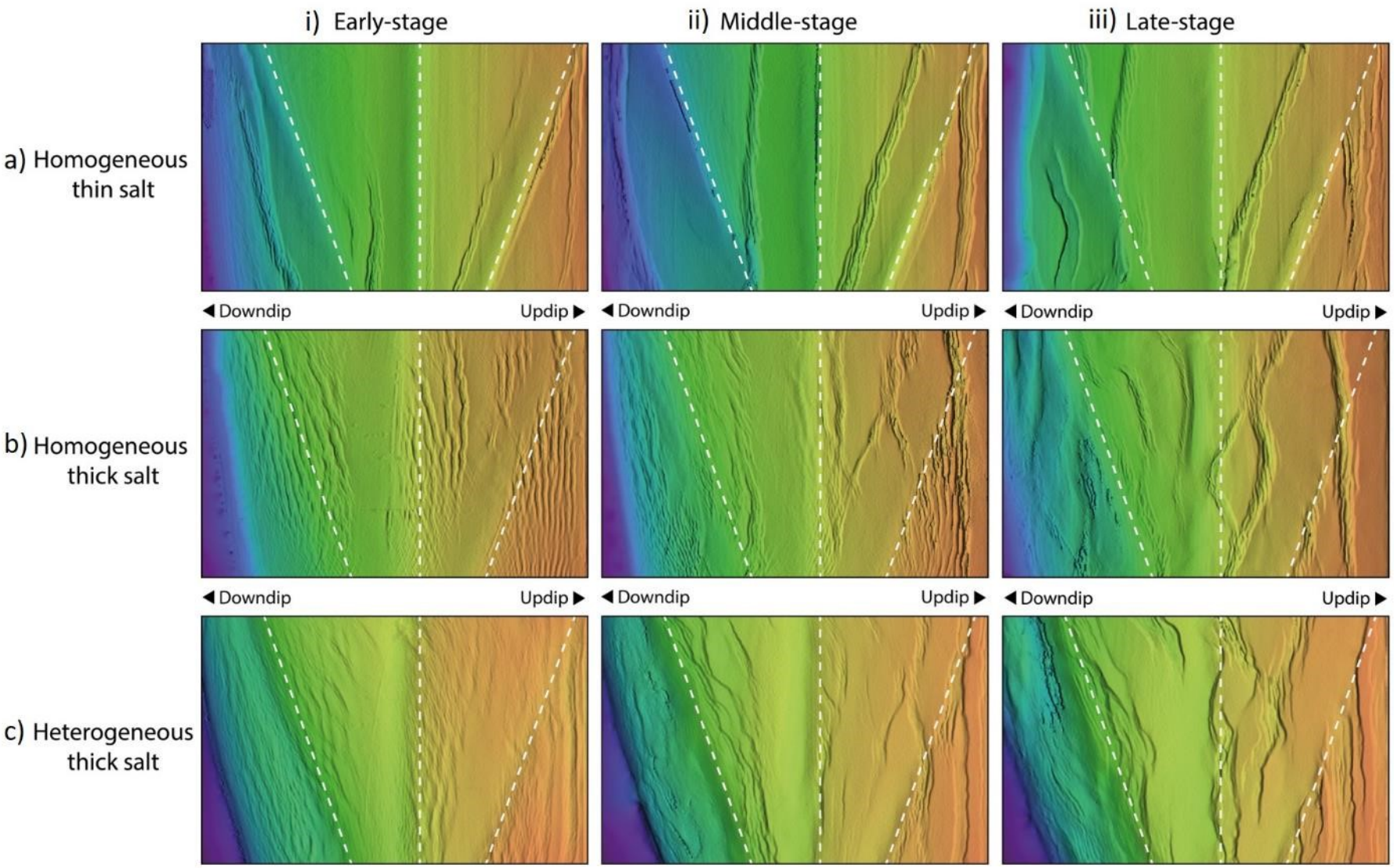

Figure 5.7 Plan-view evolution of the seabed surface for a) thin, b) thick and c) heterogeneous models. Note that in all images the edges of the model have been cut off to eliminate the effects of boundary drag.

5.3.3 Heterogeneous Thick Salt

The thick salt model was run with two sand layers encased within the silicone to investigate the impact of intrasalt heterogeneity (Fig. 5.3c). We use a sand composition for the layers, analogous to the clastic interbeds identified in the Levantine Basin, but may be representative of any dominantly brittle interbeds. The total thickness of the salt layer was the same as the homogeneous thick salt model (Table 2), and all other physical parameters and boundary conditions were kept constant.

The early stages of the model show distributed strain in the overburden, similar to that observed in the early stages of the homogeneous thick salt model (Figs. 5.5c-i and 5.7c-i). Forced folds form above the steps and the intrasalt layers boudinage as they stretch (Fig. 5.5c-i).

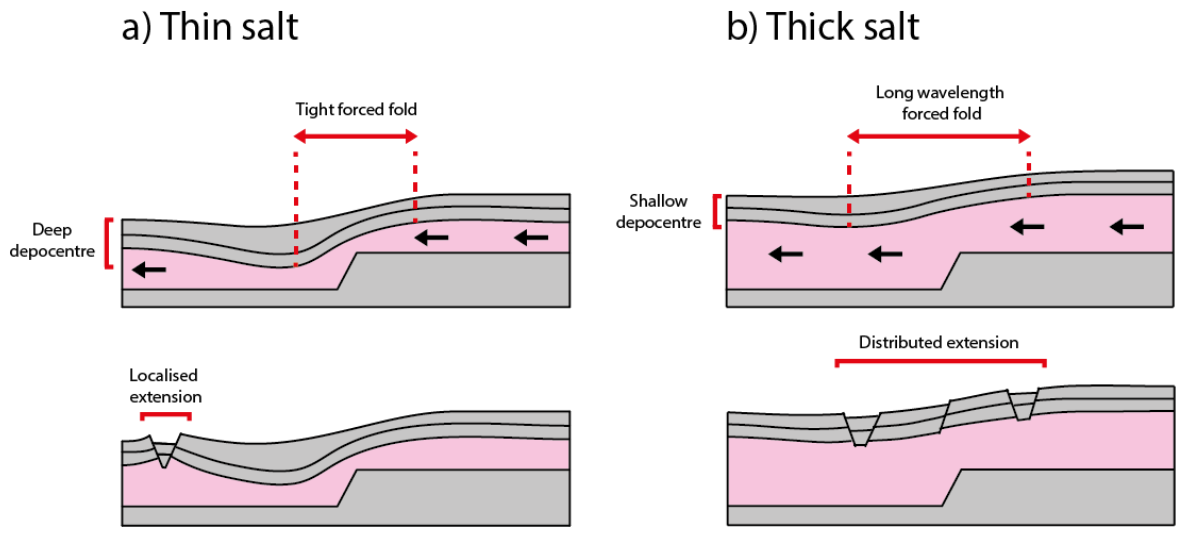

Figure 5.8 Schematic diagram highlighting key differences between the early-stage development of the a) homogeneous thin salt, and b) homogeneous thick salt models. In the thin salt model, the salt flux imbalance across the step creates a deep RSB depocentre, increasing basal friction adjacent to the step and localising the extensional strain. In contrast, there is little salt flux imbalance across the step in the thick salt model, and consequently the RSB depocentre is shallow and the strain distributed.

Grabens develop in the overburden, but the intrasalt layers prevent salt from being drawn into reactive diapirs and inhibit vertical subsidence (Figs. 5.5c-ii, 5.7c-ii and 5.10). This means that strain does not localise within salt walls and therefore cannot develop the turtle minibasins that formed in the homogeneous thick salt model (Figs. 5.6c-i and 5.10). Instead, the inhibited vertical movements mean that lateral motion dominates, which creates depocentres adjacent to the base-salt steps and this promotes RSB development (Figs 5.5c-iii

and Fig. 5.7c-ii). However, the lack of strain localisation means that RSB development is frequently disrupted by normal fault development (Fig. 5.5c-iv). Basinward-dipping normal faults form above the base-salt steps, thus disrupting the continuous translation required to form RSBs and instead resulting in landward-dipping growth strata in the hangingwall (Fig. 5.5c-v). Faults also form within the basins themselves, creating complex patterns of growth strata that overprint the landward-thickening trend typically characterising RSBs (Fig. 5.5c-v).

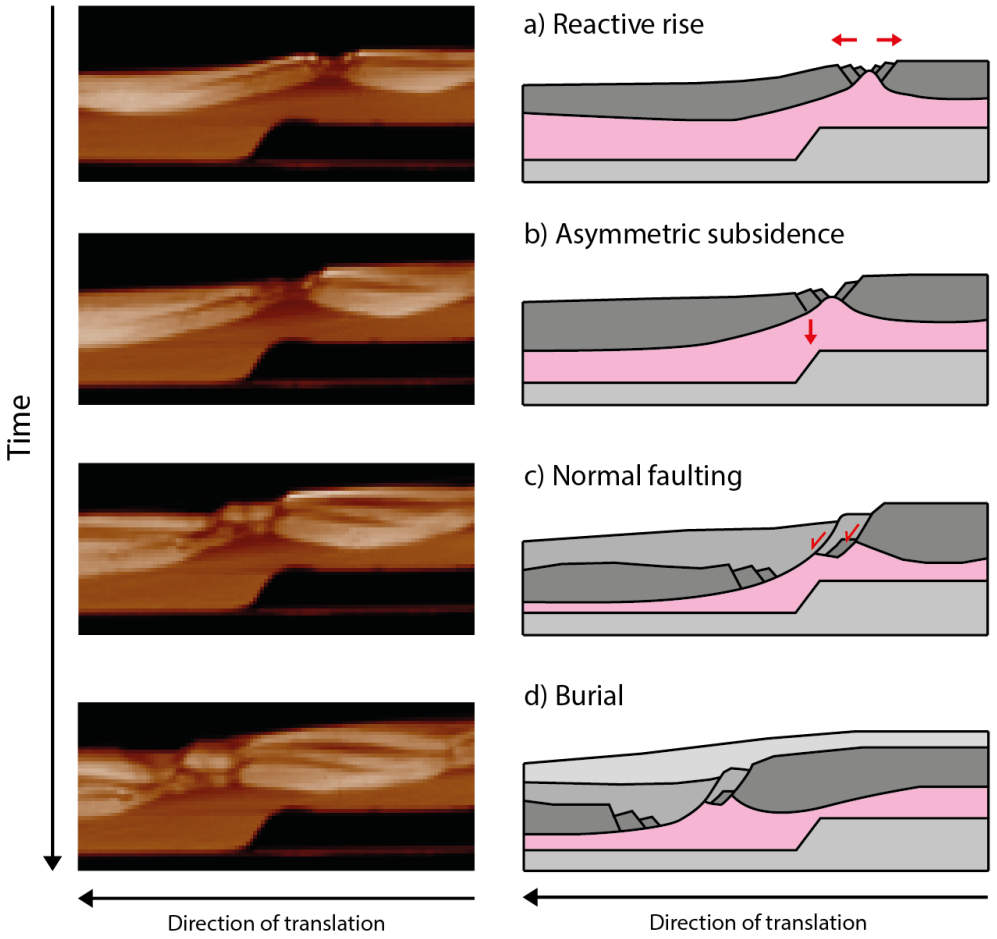

Figure 5.9 Zoom-in CT-scan cross sections and schematic illustrations showing diapir collapse as it translates over the base-salt step (homogeneous thin salt model).

The final structure of the model is therefore dominated by basinward-dipping and associated antithetic normal faults that give rise to a series of displaced blocks above the boudinaged intrasalt layers (Fig. 5.5c-vi). The orientation and distribution of structures shows some relationship with the base-salt steps, although most are oriented sub-perpendicular to the translation direction (Figs. 5.6c-iii and 5.7c-iii). The overall structural development of the heterogeneous thick salt model shares some characteristics with both the homogeneous thick salt model and the thin salt model, but differs in several key ways from both. First, neither

extensional turtle structures nor ramp syncline basins develop; instead, overburden structure is characterised by the formation of fault blocks.

Tracking the position of a couple of the major structures as the model evolves shows c. 7 cm (7 km) of horizontal translation in the updip domain and c. 15 cm (15 km) of translation in the downdip domain (indicating 8 cm of cumulative syn-kinematic extension across the model). These the magnitudes of translation and extension are intermediate values between the thin salt model and homogeneous thick salt model.

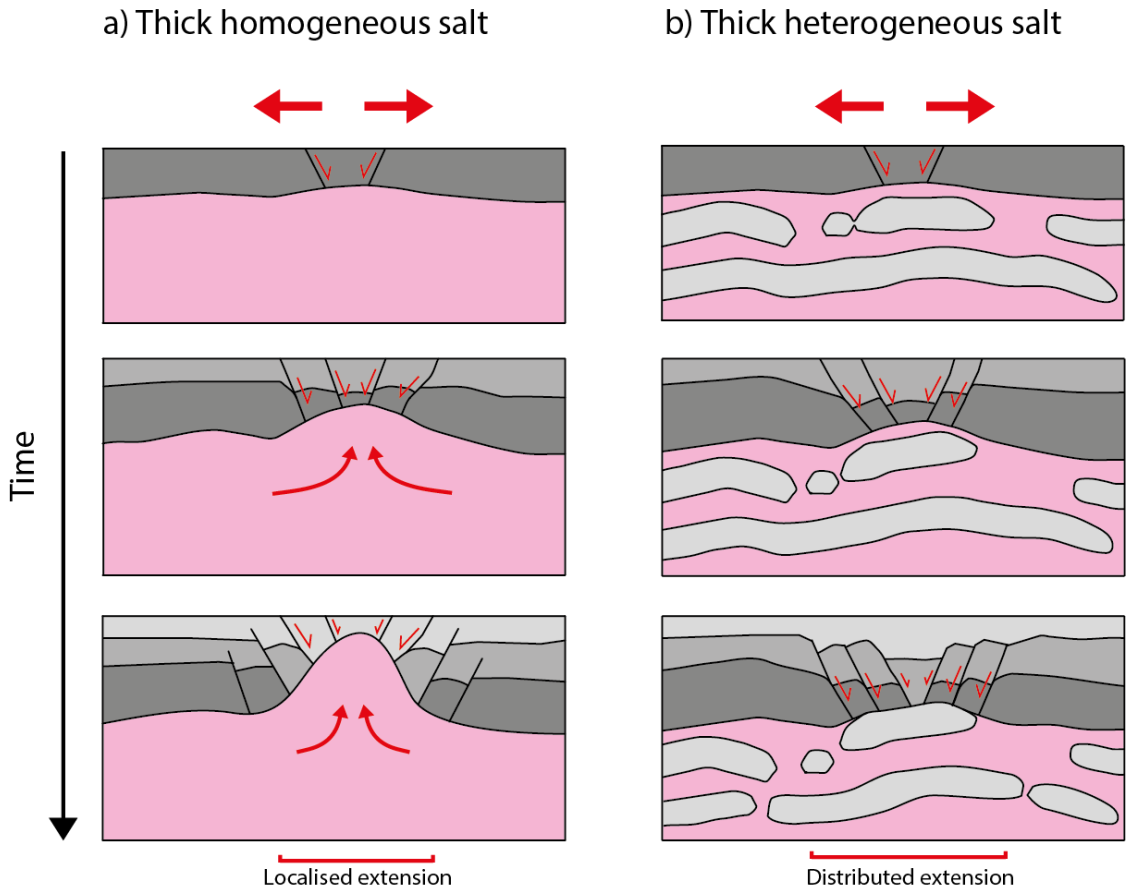

Figure 5.10 Schematic illustration comparing extensional strain development in a) thick homogeneous salt, and b) thick heterogeneous salt models. The thick homogeneous salt model promotes diapiric rise and localises strain within reactive diapirs, whereas the heterogeneous salt model prevents diapiric rise and therefore strain remains distributed.

5.4 Discussion

As discussed in previous chapters, the traditional end-member models of salt tectonics in common usage (i.e. gravity gliding and spreading of homogeneous salt on a smooth base-salt surface) are insufficient to explain the complexity and diversity of structural styles documented in different salt basins around the world. The physical models presented here highlight the structural complexity introduced by the interplay between base-salt relief, salt thickness and intrasalt lithological heterogeneity during thin-skinned, gravity-driven salt tectonics.

5.4.1 Salt Thickness

The structural evolution of the thin salt model was significantly different from the thick salt model, despite the experimental setup and all other physical parameters being kept constant (Fig. 5.5). The thin salt model developed mature RSBs, whereas the thick salt model preferentially formed extensional turtle structures (Fig. 5.5). Overall, the thin salt model shows a much greater degree of coupling between the sub- and supra-salt structures, indicating strong control of the base-salt geometry on the deformation of the salt and overburden (Figs. 5.6 and 5.7). By contrast, the thick salt model is dominated by structures sub-perpendicular to the direction of gliding and lacks coherence with the sub-salt structure, indicating a weaker influence of the base-salt steps (Figs. 5.6 and 5.7).

Note that these differences do not relate directly to the absolute salt thickness, but rather the ratio of salt thickness to the height of the base-salt relief. This means that even basins with very thick salt deposits may be influenced by base-salt relief if the magnitude of the relief is also very large (e.g. Santos Basin offshore Brazil; Pichel et al., 2018). The model results presented here clearly demonstrate that this ratio is a first-order control on the structural and stratigraphic development of the overburden. Where the ratio is low (i.e. salt is thin relative to the height of relief), the geometry of the base-salt has a profound impact on the subsequent structural evolution of the salt and overburden. The salt flow over the base-salt steps acts to control the distribution and orientation of supra-salt depocentres and structures. This is largely done through spatial variations in volumetric flux and flow velocity. Similar mechanisms were proposed for the Kwanza Basin in Chapter 2 and the Levantine Basin

in Chapter 4. In the homogeneous thick salt model, these variations are less pronounced and therefore the resulting deformation is only weakly coupled to the base-salt relief. Thicker salt also promotes more vertical motion whereas thin salt models are dominated by lateral motion. Furthermore, thick salt margins are characterised by faster translation rates and larger magnitudes of translation (as they do not weld as quickly).

The extensional turtle structures that developed in the homogeneous thick salt model closely resemble seismically-imaged structures found offshore Gabon and Angola, in the Campos Basin offshore Brazil, and in the Gulf of Mexico (Fig. 5.11) (Mauduit et al., 1997; Demercian et al., 1993; Jackson and Hudec, 2016). As noted above, this observation alone does not necessarily mean that these areas had a thick initial salt layer, but that they had a high ratio of salt thickness to base-salt relief ratio, and thus little influence from the base-salt geometry during their structural development.

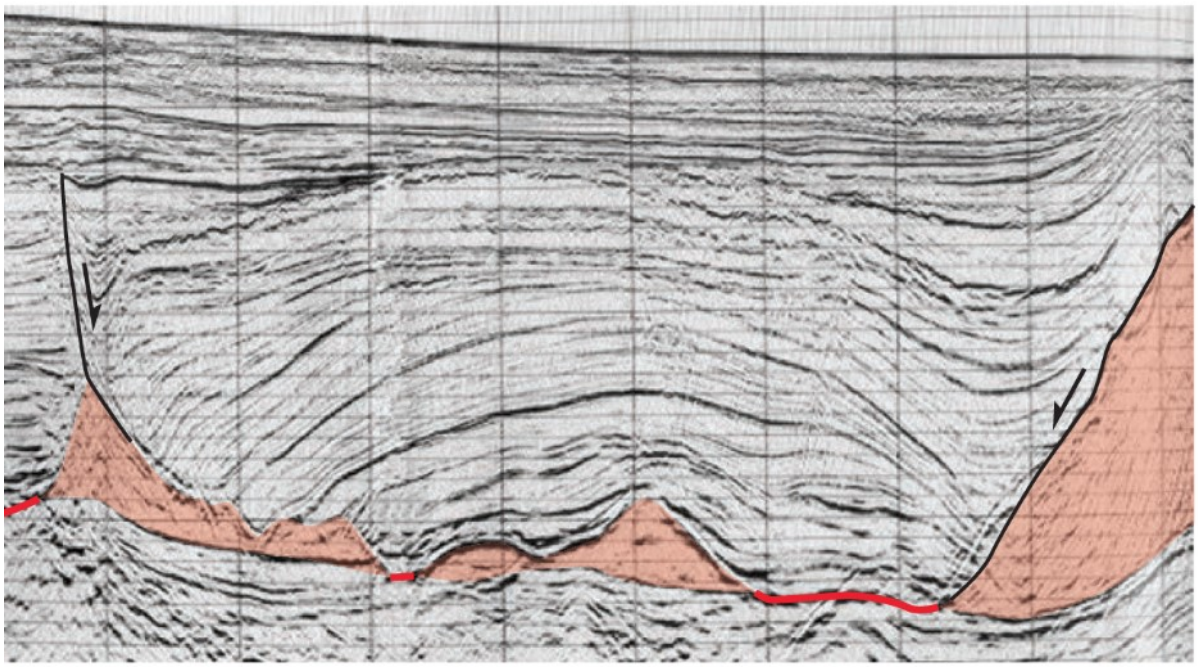

Figure 5.11 Seismically-imaged example of an extensional turtle anticline bounded by diapirs from offshore Brazil. Structure closely resembles those formed in the homogeneous thick salt model. From Jackson and Hudec, 2017.

The RSBs that developed in the thin salt model are similar to those identified in the Kwanza Basin offshore Angola, the Santos Basin offshore Brazil, and on the Levant margin offshore Lebanon (Fig. 2.6) (Pichel et al., 2018; Evans and Jackson, 2019; Evans et al., 2020). RSB development demonstrates strong coupling between the base-salt geometry and supra-salt development, and therefore a relatively low ratio of salt thickness to base-relief. Strong

coupling, and RSB development, can occur even in basins with very thick salt if the magnitude of relief on the base-salt surface is large enough.

Because both the salt thickness and the magnitude of relief vary spatially across individual basins, it is possible to have strongly coupled structures developing contemporaneously with weakly coupled structures in the same basin. Some parts of the basin may be characterised by a low ratio (i.e. the base-salt is highly rugose or the salt is thin, and therefore coupling is strong) whereas other parts may have a high ratio (i.e. the base-salt is very flat or the salt is thick, and therefore coupling is weak). For example, both turtle back anticlines and RSBs are found in the extensional and translational domains of the Kwanza Basin, offshore Angola.

Structures may also be translated through areas of both high ratio and low ratio during their development. Structures developed updip with no influence from the base-salt relief may be subsequently translated into an area strongly coupled to the base-salt relief as the overburden translates basinward. We may therefore expect to see structural overprinting during different phases of translation as the system evolves, adding further complexity to the system.

5.4.2 Salt Heterogeneity

The addition of intrasalt layers to the thick salt model increases the degree of coupling between the overburden structure and base-salt relief. By inhibiting vertical motion, the dominance of lateral translation promotes the distribution of depocentres adjacent to the base-salt steps, as observed in the thin salt model (Fig. 5.5). However, the inhibited vertical motion and intrasalt stringers also prevent strain localisation and salt wall development, which results in distributed normal faulting throughout model evolution (Fig. 5.10). Despite the lack of strain localisation, the orientation of the structures align more closely with the base-salt steps than those formed in the homogeneous thick salt model (Figs. 5.6 and 5.7). The final structure of the model is therefore unique but shares some attributes with both the thin salt model and homogeneous thick salt model.

Intrasalt heterogeneity results from spatial and temporal changes in the depositional environment. The lithological composition of evaporite sequences can therefore vary drastically between different basins depending on the oceanographic conditions, basin

physiography, and nature of clastic input, but can also vary across individual basins on relatively short length scales. This could explain some of the observed spatial variability in structural styles on salt-influenced passive margins. For example, in Chapter 3 we showed that salt walls develop locally at one part of the Levant margin but are absent elsewhere, despite the wide extensional domain (Figure 3.7). Perhaps the clastic interbeds are inhibiting diapiric development along most of the margin, but a local increase in the ductile-to-brittle ratio of the salt sheet has allowed local reactive rise and salt wall development.

It is difficult to assess the impact of intrasalt heterogeneity in more mature basins due to limitations in seismic imaging which gives poor constraints on the composition of the salt sheet. However, rare reflectivity is observed within the Aptian salt in the Santos Basin, offshore Brazil, and spatial variations in the both the intrasalt composition and the structural style have been mapped (Rodriguez et al., 2018). There appears to be a connection between the increasing proportion of halite in the deep basin and increased prevalence of diapiric structures, in contrast to the inboard portion of the margin where intrasalt reflectors appear to have prevented vertical subsidence and diapiric rise (Figure 5.12). This also implies that structures in the inboard portion of the margin should exhibit greater coupling with the base-salt relief, but further work is needed to investigate this.

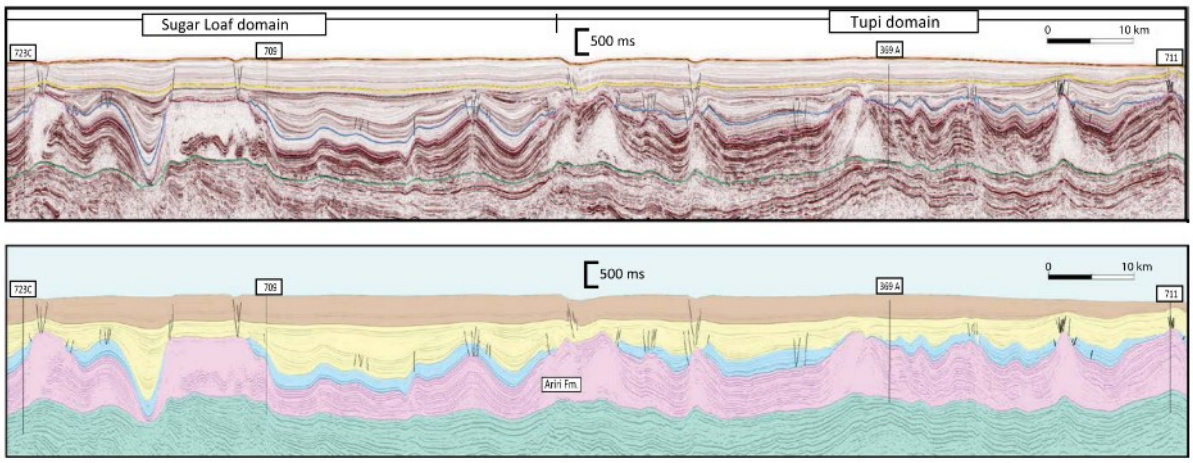

Figure 5.12 Seismic cross section through heterogeneous layered evaporites in the Santos Basin, offshore Brazil. Some diapiric structures have locally pierced the overburden, but the overall thickness of the salt sheet remains much more continuous than the Kwanza Basin (situated on the conjugate margin), likely indicating vertical motion is inhibited as observed in the heterogeneous physical model. From Rodriguez et al., 2018.

5.4.3 Wider Implications

Although conceptually based on our observations of base-salt relief and supra-salt structure in the Kwanza Basin, offshore Angola, the implications of these physical models reach much further, given that many other salt basins, such as the Gulf of Mexico and offshore Brazil, are also characterized by heterogeneous salt and/or base-salt relief. These variables could partially explain why we observe such contrasting styles of deformation in different salt basins around the world, and especially on salt-influenced passive margins. Many of the structures developed in the models closely resemble natural examples imaged in seismic data, providing valuable insights into controls on their kinematic development. In petroleum exploration, this will enable better assessment of the geometries and distribution of salt-related traps on hydrocarbon-bearing margins, as well as constraining the timing of trap generation (so that the timing can be assessed relative to phases of hydrocarbon expulsion and migration through the basin and thus reduce the charge risk).

A low ratio of salt thickness to base-salt relief and/or a high brittle-ductile ratio within the evaporite sequence increases the coupling between supra-salt and sub-salt structures, and thus promotes RSB development. As demonstrated in Chapters 2 and 4, a key benefit of RSB development is that they record, and therefore allow us to measure, the magnitude of salt-detached translation. This allows us to reconstruct the original position of translated salt structures on the margin, and in doing so unravel some of the structural complexity in the context of salt flow interaction with base-salt relief.

The well-defined RSBs developed in the thin salt model mean that we can easily measure the amount of translation over each base-salt step from just its final structure, using the distance from the first intra-RSB onlap to the RSB hinge (Fig. 5.5). In the homogeneous thick salt model, however, it would be very difficult to constrain the magnitude of translation just from its final structure (Fig. 5.5). Only by tracking the position of the diapirs through time during the model evolution can we show that a significant amount of downdip translation has actually occurred (Fig. 5.5). This means that even in salt tectonic systems where no RSBs or other indicators of lateral translation have been identified, the supra-salt structures may still have been translated a significant distance downdip. This information is pertinent to petroleum systems analysis because it may affect the charge of supra-salt trap structures if we assume vertical

migration of fluids from the sub-salt. This means that a structure which is today located directly above an area with mature, quality source rock may have been located much further updip and out of range at the time of fluid expulsion. Equally, a structure which is today located in area with poor quality or immature source rock may have been charged when it was located further updip and subsequently translated here. Using these models we can constrain where and how welds develop, and therefore map the possible fluid migration pathways at different time intervals, showing how they evolve as the structure of the basin develops. This gives a much more accurate picture of fluid distribution in the supra-salt overburden. The models can also be used to aid in the prediction of reservoir quality distribution, as sand-rich units proximal to the margin may have been translated a significant distance downdip, thus opening up new plays in the deep basin.

Of course, physical modelling has its limitations. Any scientist worth their salt (pun intended) must think long and hard about the reliability of their experiments, what they show - and perhaps most importantly - what they do not show. As the famous quote goes, 'All models are wrong, but some are useful'. The models presented here are inherently oversimplifications of natural systems, where base-salt geometries may be infinitely more complex and have many other variables at play, but by reducing the complexity of the system in this way we have succeeded in isolating the influence of certain parameters to further our understanding of specific geological processes. The models clearly show that the magnitude of base-salt relief relative to salt thickness is an important first-order control on the structural evolution of the basin, and that intrasalt heterogeneity affects the extent to which supra-salt structures are coupled to the base-salt relief.

5.5 Conclusions

- The magnitude of salt thickness to base-salt relief is an important first-order control on the supra-salt structural evolution of a basin
- Low ratios result in strong coupling between the base-salt relief and supra-salt structure, characterised by RSB development and salt walls/depocentres aligned with orientation of base-salt relief
- High ratios result in weak coupling between the base-salt relief and supra-salt structure, characterised by turtle back anticlines and salt walls/depocentres oriented sub-perpendicular to the dominant translation direction
- Intrasalt heterogeneity inhibits vertical movement and strain localisation, and promotes greater coupling with the base-salt relief

References

Adam, J., Klinkmüller, M., Schreurs, G. and Wieneke, B., 2013. Quantitative 3D strain analysis in analogue experiments simulating tectonic deformation: Integration of X-ray computed tomography and digital volume correlation techniques. Journal of Structural Geology, 55, pp.127-149.

Brace, W.F. and Kohlstedt, D.L., 1980. Limits on lithospheric stress imposed by laboratory experiments. Journal of Geophysical Research: Solid Earth, 85(B11), pp.6248-6252.

Byerlee, J.D., 1968. Brittle-ductile transition in rocks. Journal of Geophysical Research, 73(14), pp.4741-4750.

Byerlee, J.D., 1975, January. The fracture strength and frictional strength of Weber sandstone. In International Journal of Rock Mechanics and Mining Sciences & Geomechanics Abstracts (Vol. 12, No. 1, pp. 1-4). Pergamon.

Byerlee, J., 1978. Friction of rocks. In Rock friction and earthquake prediction (pp. 615-626). Birkhäuser, Basel.

Carter, N.L. and Tsenn, M.C., 1987. Flow properties of continental lithosphere. Tectonophysics, 136(1-2), pp.27-63.

Cobbold, P., Rossello, E. and Vendeville, B., 1989. Some experiments on interacting sedimentation and deformation above salt horizons. Bulletin de la Société Géologique de France, (3), pp.453-460.

Colletta, B., Letouzey, J., Pinedo, R., Ballard, J.F. and Balé, P., 1991. Computerized X-ray tomography analysis of sandbox models: Examples of thin-skinned thrust systems. Geology, 19(11), pp.1063-1067.

Demercian, S., Szatmari, P. and Cobbold, P.R., 1993. Style and pattern of salt diapirs due to thin-skinned gravitational gliding, Campos and Santos basins, offshore Brazil. Tectonophysics, 228(3-4), pp.393-433.

Dooley, T.P., Hudec, M.R., Carruthers, D., Jackson, M.P. and Luo, G., 2017. The effects of base-salt relief on salt flow and suprasalt deformation patterns—Part 1: Flow across simple steps in the base of salt. Interpretation, 5(1), pp.SD1-SD23.

Dooley, T.P. and Hudec, M.R., 2017. The effects of base-salt relief on salt flow and suprasalt deformation patterns—Part 2: Application to the eastern Gulf of Mexico. Interpretation, 5(1), pp.SD25-SD38.

Evans, S.L. and Jackson, C.A.L., 2020. Base-salt relief controls salt-related deformation in the Outer Kwanza Basin, offshore Angola. Basin Research, 32(4), pp.668-687.

Ferrer, O., Gratacós, O., Roca, E. and Muñoz, J.A., 2017. Modeling the interaction between presalt seamounts and gravitational failure in salt-bearing passive margins: The Messinian case in the northwestern Mediterranean Basin. Interpretation, 5(1), pp.SD99-SD117.

Fossum, A. F., and J. T. Fredrich, 2002, Salt mechanics primer for near-salt and sub-salt deepwater Gulf of Mexico field developments: Albuquerque, NM, Sandia National Laboratories, report SAND2002-2063.

Gaullier, V., Brun, J.P., Gue, G. and Lecanu, H., 1993. Raft tectonics: the effects of residual topography below a salt de´ collement. Tectonophysics, 228(3-4), pp.363-381.

Goetze, C. and Evans, B., 1979. Stress and temperature in the bending lithosphere as constrained by experimental rock mechanics. Geophysical Journal International, 59(3), pp.463-478.

Hubbert, M.K., 1937. Theory of scale models as applied to the study of geologic structures. Bulletin of the Geological Society of America, 48(10), pp.1459-1520.

Hudec, M.R. and Jackson, M.P., 2004. Regional restoration across the Kwanza Basin, Angola: Salt tectonics triggered by repeated uplift of a metastable passive margin. AAPG bulletin, 88(7), pp.971-990.

Jackson, M.P.A. and Hudec, M.R., 2016. Principles and practice of salt tectonics. Cambridge University Press.

Jackson, M.P., Vendeville, B.C. and Schultz-Ela, D.D., 1994. Structural dynamics of salt systems. Annual Review of Earth and Planetary Sciences, 22(1), pp.93-117.

Koyi, H., 1997. Analogue modelling: from a qualitative to a quantitative technique—a historical outline. Journal of Petroleum Geology, 20(2), pp.223-238.

Kusznir, N.J. and Park, R.G., 1986. Continental lithosphere strength: the critical role of lower crustal deformation. Geological Society, London, Special Publications, 24(1), pp.79-93.

Mauduit, T., Gaullier, V., Brun, J.P. and Guerin, G., 1997. On the asymmetry of turtle-back growth anticlines. Marine and Petroleum Geology, 14(7-8), pp.763-771.

Nettleton, L.L., 1934. Fluid mechanics of salt domes. AAPG Bulletin, 18(9), pp.1175-1204.

Nettleton, L.L. and Elkins, T.A., 1947. Geologic models made from granular materials. Eos, Transactions American Geophysical Union, 28(3), pp.451-466.

Paterson, M.S., 1987. Problems in the extrapolation of laboratory rheological data. Tectonophysics, 133(1-2), pp.33-43.

Pichel, L.M., Peel, F., Jackson, C.A. and Huuse, M., 2018. Geometry and kinematics of salt-detached ramp syncline basins. Journal of Structural Geology, 115, pp.208-230.

Ramberg, H., 1981. Gravity, deformation and the earth's crust: in theory, experiments and geological application. Academic press, London, 452 pp.

Ranalli, G. and Murphy, D.C., 1987. Rheological stratification of the lithosphere. Tectonophysics, 132(4), pp.281-295.

Richard, P., 1991. Experiments on faulting in a two-layer cover sequence overlying a reactivated basement fault with oblique-slip. Journal of Structural Geology, 13(4), pp.459-469.

Rodriguez, C.R., Jackson, C.A.L., Rotevatn, A., Bell, R.E. and Francis, M., 2018. Dual tectonic-climatic controls on salt giant deposition in the Santos Basin, offshore Brazil. Geosphere, 14(1), pp.215-242.

Schléder, Z. and Urai, J.L., 2005. Microstructural evolution of deformation-modified primary halite from the Middle Triassic Röt Formation at Hengelo, The Netherlands. International Journal of Earth Sciences, 94(5-6), pp.941-955.

Schléder, Z. and Urai, J.L., 2007. Deformation and recrystallization mechanisms in mylonitic shear zones in naturally deformed extrusive Eocene–Oligocene rocksalt from Eyvanekey plateau and Garmsar hills (central Iran). Journal of Structural Geology, 29(2), pp.241-255.

Schléder, Z., Burliga, S. and Urai, J.L., 2007. Dynamic and static recrystallization-related microstructures in halite samples from the Kłodawa salt wall (central Poland) as revealed by gamma-irradiation. Neues Jahrbuch für Mineralogie-Abhandlungen: Journal of Mineralogy and Geochemistry, 184(1), pp.17-28.

Schoenherr, J., Reuning, L., Kukla, P.A., Littke, R., Urai, J.L., Siemann, M. and Rawahi, Z., 2009. Halite cementation and carbonate diagenesis of intra-salt reservoirs from the Late Neoproterozoic to Early Cambrian Ara Group (South Oman Salt Basin). Sedimentology, 56(2), pp.567-589.

Sibson, R.H., 1974. Frictional constraints on thrust, wrench and normal faults. Nature, 249(5457), pp.542-544.

Spiers, C.J., Urai, J.L. and Lister, G.S., 1988. The effect of brine (inherent or added) on rheology and deformation mechanisms in salt rock. Second Conference on the Mechanical Behaviour of Salt, Hanover,FRG, September 24-28, 1984, Transtech Publ., Clausthal-Zellerfeld, pp. 89-102.

Spiers, C.J. and Carter, N.L., 1998. Microphysics of rocksalt flow in nature. Series on rock and soil mechanics, pp.115-128.

Talbot, C. J., 1998, Extrusions of Hormuz salt in Iran, in D. J. Blundell, and A. C. Scott, eds., Lyell: The past is the key to the present: London, Geological Society, Special Publication 143, pp.315–334.

Urai, J.L., Spiers, C.J., Zwart, H.J. and Lister, G.S., 1986. Weakening of rock salt by water during long-term creep. Nature, 324: 554-557.

Urai, J. L., Z. Schléder, C. J. Spiers, and P. A. Kukla, 2008, Flow and transport properties of salt rocks, in R. Littke, U. Bayer, D. Gajwski, and S. Nelskamp, eds., Dynamics of complex intracontinental basins: The central European basin system: Berlin, Springer, 277–290.

Vendeville, B., 1988. Modèles expérimentaux de fracturation de la couverture contrôlée par des failles normales dans le socle. Comptes rendus de l'Académie des sciences. Série 2, Mécanique, Physique, Chimie, Sciences de l'univers, Sciences de la Terre, 307(8), pp.1013-1018.

Vendeville, B.C., 1989. Scaled experiments on the interaction between salt flow and overburden faulting during syndepositional extension. In SEPM Gulf Coast Section, 10th Annual Research Conference, Houston, Program and Extended Abstracts, pp. 131-136.

Vendeville, B. and Cobbold, P.R., 1988. How normal faulting and sedimentation interact to produce listric fault profiles and stratigraphic wedges. Journal of structural Geology, 10(7), pp.649-659.

Vendeville, B. and Cobbold, P.R., 1987. Glissements gravitaires synsédimentaires et failles normales listriques: modèles expérimentaux. Comptes rendus de l'Académie des sciences. Série 2, Mécanique, Physique, Chimie, Sciences de l'univers, Sciences de la Terre, 305(16), pp.1313-1318.

Vendeville, B., Cobbold, P.R., Davy, P., Brun, J.P. and Choukroune, P., 2002. Physical models of extensional tectonics at various scales. In: Extensional tectonics: faulting and related processes, 2, pp.171-183.

Vendeville, B.C. and Jackson, M.P., 1992a. The rise of diapirs during thin-skinned extension. Marine and Petroleum Geology, 9(4), pp.331-354.

Vendeville, B.C. and Jackson, M.P.A., 1992b. The fall of diapirs during thin-skinned extension. Marine and Petroleum Geology, 9(4), pp.354-371.

Weijermars, R., Jackson, M.T. and Vendeville, B., 1993. Rheological and tectonic modeling of salt provinces. Tectonophysics, 217(1-2), pp.143-174.

Weijermars, R. and Schmeling, H., 1986. Scaling of Newtonian and non-Newtonian fluid dynamics without inertia for quantitative modelling of rock flow due to gravity (including the concept of rheological similarity). Physics of the Earth and Planetary Interiors, 43(4), pp.316-330.

Zwaan, F. and Schreurs, G., 2017. How oblique extension and structural inheritance influence rift segment interaction: Insights from 4D analog models. Interpretation, 5(1), pp.SD119-SD138.

6 Discussion

The research presented in this thesis offers new insights into the ways in which base-salt relief and intra-salt heterogeneity can affect the tectono-stratigraphic development of gravity-driven salt basins using two case studies: the Levantine Basin, offshore Lebanon; and the Kwanza Basin, offshore Angola. I have used a multifaceted approach, integrating different seismic interpretation-based methods and physical analogue models, to explore key controls on the distribution of intra- and supra-salt strain on passive margins.

The weakly deformed supra-salt structure of the Levantine Basin differs in many respects from the complex salt structures characterising the Kwanza Basin. The most obvious differences are due to the fact that the Messinian salt in the Mediterranean is much younger than the Aptian salt on the Atlantic Margin, and consequently deformation in the Kwanza Basin is much more mature than in the Levantine Basin. We could therefore suggest that the Levant Margin provides an analogue for early-stage, gravity-driven deformation on the Angolan Margin. To what extent would this analogy be valid? This final chapter will summarise the main findings of this body of work in the context of cross-cutting themes that compare and contrast the two study areas to further our understanding of salt tectonic systems.

6.1 Tectonic Setting

In terms of their tectonic settings, both the Levantine and Kwanza datasets are situated on passive margins. Despite this, the Kwanza Basin has evolved under a very different tectonic regime to that of the present Levant. As discussed previously, the Aptian salt was deposited during the early opening stages of the South Atlantic Ocean, which developed into an oceanic spreading system as the African and South American plates pulled apart (Fig. 1.15; Bryant et al., 2012). The Aptian salt deposits were consequently divided, with the opposing basins forming the Santos and Campos Basins on the conjugate margin, offshore Brazil (Fig. 1.15; Bryant et al., 2012). The Messinian salt sheet, on the other hand, was deposited in (and is still in) a region of tectonic compression due to the convergence of the northward-migrating African plate and the stable Eurasian plate (Fig. 1.16; Roveri et al., 2014). This section will address the influence of these different tectonic regimes on the post-salt structural evolution of both basins.

Ductile salt units act as detachment layers which allow decoupling of sub-and supra-salt structures. However, this detachment does not mean that the thin- and thick-skinned systems act completely independently. For example, the regional tectonic regime controls both the tilting and the loading of the margin, thus inducing the gravitational instability that triggers and drives salt deformation. Specifically, the tilt is controlled by margin uplift and basin subsidence, while the loading is controlled by the uplift of the hinterland and associated erosion rates and drainage systems that supply clastic material to the basin. We can therefore say that to some extent the thick-skinned tectonic setting determines the relative contributions of gliding and spreading, which affects the supra-salt structural development.

In the Outer Kwanza Basin, c. 25 km of basinward translation has been driven by a combination of tilting due to thermal subsidence or margin uplift, and spreading due to sediment loading on the continental shelf (see Chapter 2). The three main phases of salt tectonic deformation are thought to be linked to thick-skinned tectonic events that altered the basin configuration (and therefore the influence of gliding and spreading) (Hudec and Jackson, 2004). For example, in Chapter 2 I showed that an increase in the tilt of the basin (due to mantle plume-related Miocene uplift of the West African margin; Walford and White, 2005) rejuvenated gravity gliding and caused an abrupt increase in the rate of basinward translation (as well as increased sediment supply; Bond, 1978).

In the Levantine Basin, we observe both spatial and temporal variations in the contributions of gliding and spreading, resulting in different structural styles across the basin. Gravity spreading dominates the salt tectonic regime in the southern Levantine Basin due to the northward progradation of the Nile Delta (creating the circum-Nile deformation belt; Zucker et al., 2020), whereas deformation on the Levant Margin, where our dataset is situated, is predominantly driven by gravity gliding (Cartwright et al., 2018). However, deformation on the margin may not always have been dominated by gravity gliding. The distribution and orientation of structures offshore Lebanon support two main phases of gravity-driven salt movement; an early syn-depositional phase followed by a later post-depositional phase (Netzeband et al., 2006; Gvirtzman et al., 2013; Feng et al., 2017; Kartveit et al. 2018; see Chapter 3). In Chapter 3, based on the intra-salt strain distribution, I proposed that the early phase could have been driven by gravity spreading (generating a Poiseuille flow), followed by an increase in tilt on the margin (attributed to the ongoing continental collision

between the African, Arabian and Eurasian plates) causing a transition to a gliding-dominated system (and associated Couette flow). Contemporaneous activity on the transpressional Dead Sea fault network onshore Lebanon, adjacent to the margin, may have affected the basin indirectly by modulating the rate of sediment supply, and thus the contribution from gravity spreading.

As well as controlling the driving mechanisms, the tectonic setting also determines the local boundary conditions for salt flow. The opening of the South Atlantic and the slow rate of deep-water sedimentation allowed the advance of the Angolan Salt Nappe from the Late Cretaceous to the Miocene (Hudec and Jackson, 2004). This 'open-toe' tectonic setting allowed extreme extension to take place in the updip domain, creating raft blocks and turtle structures, which was relatively unbalanced by contractional structures downdip (Jackson and Hudec, 2009; see Chapter 2). The eventual blockage of this advance due to burial of the nappe toe in the Plio-Pleistocene forced contractional squeezing of diapirs in the downdip domain (Jackson and Hudec, 2009).

In the northern Levant, the influence of the thick-skinned boundary conditions can be seen around the Latakia Ridge, a compressional structure accommodating the N-S direction of plate convergence. In Chapter 3, I observed that this restricts salt flow in the northern basin, generating a supra-salt fold belt that runs proximal and parallel to the ridge. This compressional zone reaches up to c. 35 km from the ridge itself (Fig. 3.7). The same can be said for the Eratosthenes Seamount to the west, which is associated with local contraction and backflow of the salt within c. 40 km (Allen et al., 2016). This confined system contrasts with the open-toed system that allowed sustained basinward salt flow in the Kwanza Basin.

Despite these differences, the regional-scale supra-salt structure of both margins is broadly similar. The confinement of the salt in the Levantine Basin did not prevent the development of kinematically linked zones of updip extension and downdip contraction associated with gravity gliding, also observed in the Kwanza Basin. This means that while the thick-skinned, basement-involved tectonic regime has played an important role in the post-salt evolution of both basins by controlling the local gravitational drivers (i.e. gliding and spreading), and the boundary conditions that either restrict or promote salt flow, the geometries and distribution of the developing structures may still be broadly analogous.

However, this isn't the full story. As discussed in Chapter 2, the orientation and distribution of supra-salt structures in the translational domain of the Outer Kwanza Basin cannot be explained in terms of simple gliding and spreading models, or in terms of thick-skinned tectonic events. My tectono-stratigraphic analysis of salt structure evolution showed that contractional structures developed shortly after salt deposition, and local contraction occurred throughout the basin evolution, despite evolving in a dominantly extensional, 'open-toe' tectonic setting (see Chapter 2). Furthermore, synchronous extension and contraction took place in adjacent salt structures, and the wide range of orientations does not reflect the dominantly ENE-WSW direction of extension (see Chapter 2).

Similarly, the differential rates of translation recorded along the Levant margin cannot be explained in terms of the interplay between gliding and spreading or varying boundary conditions in a thick-skinned tectonic regime. To explain these nuanced observations we must appeal to another important way that the thick-skinned tectonic regime affects the thin-skinned salt tectonic system: through the development and preservation of base-salt relief.

6.2 Base-Salt Relief

The different pre-salt tectonic histories of the Kwanza and Levantine Basins have resulted in significantly different base-salt surface geometries. The base-salt on the Angolan Margin is characterised by a relatively flat updip domain, a highly rugose central domain (Atlantic Hinge Zone), and a smoothly dipping downdip domain (Angolan Salt Nappe) (Hudec and Jackson, 2004; Fig. 2.3). The rugose central domain comprises several large, basin-dipping steps on the base-salt surface, thought to be relict fault scarps inherited from the syn-rift phase (Marton et al., 2000). In contrast, the base-salt surface on the Levant Margin is characterised by a series of large anticlines in the updip domain, becoming smoother and flatter into the deep basin (Fig. 3.6). These anticlines are thought to be fault-propagation folds related to structurally deeper thrust faults, generated during a regional plate reorganisation in the late Miocene (Ghalayini et al., 2014).

In both study areas, the salt flux imbalance generated by flow over the positive relief (i.e. steps or anticlines) has led to the development of ramp syncline basins (RSBs) (Pichel et al., 2018; see Chapters 2 and 4). RSB development is thought to be characteristic of strong coupling between the sub- and supra-salt structures (see Chapter 5). The RSBs therefore

provide a key commonality between the two margins and, as demonstrated in Chapters 2 and 4, allow us to analyse their respective histories of salt-detached translation.

Despite the development of RSBs on both margins, in detail the different base-salt geometries produce different patterns of salt flow, thus resulting in different strain distributions. The base-salt ramp offshore Angola produces a large salt flux imbalance, which generates a significant stress field during salt flow. Because it has a complex geometry that changes orientation along strike (Fig. 2.5), the stress field is equally complex. This results in a complex distribution of extensional and contractional supra-salt structures that also vary in orientation, as described in Chapter 2. The base-salt anticlines offshore Lebanon also generate a salt flux imbalance. However, they compensate the salt flux deficit by intermittently increasing the local rate of salt flow (creating cyclical 'pulses' of salt flow as proposed in Chapter 4). This limits the magnitude of stresses in the overburden, and the anticlines are therefore not associated with significant supra-salt strain (see Chapter 4).

These different base-salt geometries could partially explain why supra-salt structures formed very early in the Albian when the overburden was very thin, whereas the Messinian has accumulated a large overburden thickness with relatively little deformation (see Chapters 2, 3 and 4). These differences could have set the two margins on a very different path early on, since it is easier to reactivate existing structures (either extensionally or contractionally) than it is to form completely new structures, especially as the overburden strengthens as it thickens through time. This means that the distribution and orientation of structures developed during the early stages of basin evolution play a key role in its subsequent structural development. Essentially, if two basins develop differently in their early stages, those differences will likely persist, and even be exaggerated, as the basins evolve.

Physical analogue modelling results support my interpretations in the Kwanza and Levantine Basins, showing how spatial variations in velocity and volumetric flux, related to base-salt relief, can determine the structural style of the salt and overburden (see Chapter 5). In this way, the pre-salt tectonic history of a basin may be very important in controlling the structural evolution of a basin. Since the Kwanza and Levantine Basins have different base-salt geometries, they are likely to develop different structural styles. This indicates that the structural evolution of the Levant Margin may differ in some important ways from the early-stage salt tectonics of the Angolan margin. These differences introduced by base-salt relief

may be further compounded by differences in the thickness and lithological heterogeneity of the evaporite sequence itself.

6.3 Salt Thickness and Composition

Evidence suggests that the lithological composition of the evaporite sequence varies widely between different basins and even spatially within individual basins (Rowan et al., 2019), but the effects of salt thickness and intra-salt heterogeneity on structural development are even more nuanced and difficult to ascertain than those of base-salt relief. Firstly, in mature basins it is difficult to reconstruct the original, depositional thickness of the salt sheet from just the final basin structure. Secondly, it is difficult to precisely constrain the lithological composition of subsurface salt bodies because the heterogeneous intra-salt layers are difficult to image in seismic reflection data (Jones and Davison, 2014), and even where drilled the lateral continuity of the layers remains unknown (Fig. 1.13).

In Chapter 3 I showed that because it is shallow and weakly deformed, the Messinian is one of few subsurface salt giants where intra-salt reflectivity allows internal strain to be mapped across the basin. However, I also debated that seismically-derived strain measurements may not represent the true distribution of intra-salt strain because the rheology of the intra-salt units affects the way in which strain is accommodated within the deforming evaporite sequence, and seismic data resolves only the strain accommodated by macro-scale structures (see Chapter 3).

Due to the limitations associated with seismic-based methods and poor lithological constraints, in Chapter 5 I tested the influence of salt thickness and intra-salt heterogeneity using physical analogue models. These models revealed the significant impact that the thickness and rheological properties of the salt could have on the structural evolution of a basin. The ratio of salt thickness to base-salt relief controls the degree of coupling between sub- and supra-salt structures (see Chapter 5). For basins, or local areas of basins, with a low ratio, the base-salt geometry constitutes a first-order control on the supra-salt structural development, whereas those with a high ratio may be largely decoupled (see Chapter 5). Increasing the proportion of competent, brittle layers within the sequence inhibits vertical motion (i.e. subsidence and diapiric rise), prevents strain localisation and promotes increased coupling to the base-salt geometry (see Chapter 5).

In addition to differences caused by base-salt geometry, this may also account for some of the observed variability in structural style across different salt basins. For example, intra-salt reflectivity is present in both the western and eastern Mediterranean basins, but the seismic stratigraphy is different. The western Mediterranean has the classic 'trilogy' of units (UU, MU, and LU), each with distinct seismic facies, whereas the eastern Mediterranean has three discrete packages of brittle intra-salt reflectors embedded within a halite-rich background (Camerlenghi et al., 2020). These different stratigraphies will therefore respond to stress differently, and develop different patterns of intra- and supra-salt strain. This could contribute to the observed prevalence of diapiric structures in the western Mediterranean, compared to the Levant Margin that is dominated by immature salt structures such as rollers.

Similarly, differences in salt composition, as well as thickness, may partially explain the different structural styles of the Kwanza Basin versus the Santos and Campos Basins on the conjugate margin. We have few constraints on the internal composition of the Aptian salt but its transparent and chaotic seismic facies offshore Angola contrasts markedly with the high-amplitude reflectivity characterising the Aptian in the Santos Basin, offshore Brazil. The salt in the Kwanza could therefore be interpreted as more halite-rich and therefore more viscous and able to form large diapiric structure and welded minibasins, whereas the layered evaporites in the Santos Basin maintain a more consistent thickness (see Chapter 5). Of course the different geological settings of the two basins will also contribute to their different structural styles, but since the overall tectonic histories of the two basins are similar we can speculate that the role played by different salt compositions and rheologies is perhaps greater than previously thought.

Ultimately, this relates back to the palaeogeographic and oceanographic conditions under which the salt is deposited. Proximity to sources of freshwater or clastic input to the basin, as well as the connectivity and geometry of the different sub-basins, give rise to salt bodies with very different compositions even within the same basin. There is evidence that the connection between the western and eastern Mediterranean was largely cut off during the Messinian by the intervening Sicily Ridge (Camerlenghi et al., 2020), and similarly restricted connectivity for the West African and Brazilian sub-basins during early Atlantic rifting (Lentini et al., 2010; Rodriguez et al., 2018).

This means that care must be taken when comparing the deformation of the heterogeneous Messinian salt on the Levant Margin with the halite-rich Aptian salt on the Angolan Margin, given that thickness compositional differences in layered salt bodies can have important implications for structural evolution.

6.4 Summary

Scientists are said to be divided into 'lumpers' and 'splitters' (a quote that originated in a letter from Charles Darwin in 1857, but has been widely used since). Given a set of samples to analyse, lumpers will focus on the shared characteristics that unite them, while splitters will focus on the differences that set them apart. While the term was first applied in the context of species classification, the same approach can be taken with sedimentary basins. When comparing salt basins, we can either focus on what is similar about them, or what is different about them.

From a lumper's point of view, both the Angolan and Levant Margins are gravity-driven salt tectonic systems situated on passive margins. They both have kinematically-linked domains of updip extension and downdip contraction. In this sense at least, they both fit the predictions of classic gravity gliding and spreading models, as do almost all documented examples of passive margin salt tectonics. There are also commonalities in the types of structures developed, such as ramp syncline basins, which allow us to draw similarities between different basins. And so in that respect, salt-influenced basins and margins are remarkably similar on a regional scale.

Splitters, however, would observe the great variability in the distribution and orientation of structures on a local scale. This variability represents the fingerprints of base-salt relief and intra-salt heterogeneity, as well as other variables related to the tectonic setting. In this sense, the structural development of every salt basin is unique. Ideally we would look at salt basins of different ages and use them to form a complete temporal evolution of the natural system, but, as I have shown in the work compiled in this thesis, there are many local variables at play which overprint the broad-scale similarities. The geometry of the base-salt surface, and the thickness and composition of the salt sheet, appear to be equally (if not more) important in controlling the intra- and supra-salt strain as the regional, thick-skinned tectonic setting. This

results in structural overprinting, where the thick-skinned stresses drive large-scale basinward translation and local factors control how the thin-skinned deformation manifests.

When asking broad questions such ‘How do supra-salt faults link and grow in the extensional domain?’, the Levant Margin can provide some valuable insights into early-stage gravity gliding that can be applied to more evolved margins such as Angola. But while analogous at a regional scale, the structural evolution of the Levant Margin may differ in some important ways from the early-stage salt tectonics of the Angolan Margin. When asking more specific questions about the relative timing of events or the distribution of structures such as ‘At what stage do welds develop?’ or ‘How are reactive diapirs distributed across the margin?’, answers from the Levant are unlikely to be transferrable to the Kwanza. The base-salt steps which cause such structural complexity in the translational domain of the Kwanza are absent in the Levant. The intra-salt layers which inhibit vertical subsidence and diapiric rise in the Levant are absent in the Kwanza.

I would advocate that the early-stage, gravity-driven structural development of the Levant Margin be used with care as an early-stage analogue for gravity-driven deformation of the Angolan Margin. The key is to know when to lump and when to split. Salt basins contain some of the most complex structures in the world, and if we are to fully understand the evolution of these complex systems, we must recognise the key differences that set them apart.

6.5 Wider Applications

Salt tectonics has long been a focus of the petroleum industry, and the themes discussed here have clear implications for hydrocarbon exploration; trap development, drilling, velocity modelling and fluid migration all benefit from a better understanding of the salt kinematics. But now, as society embraces the energy transition and we enter a new phase of energy production with renewable and sustainable resources at the forefront, what might become of the field of salt tectonics? Is there anything that salt tectonics can contribute to the challenges of the future?

Firstly, for all the same reasons we care about salt in the context of hydrocarbon exploration and production, we must care about salt for carbon capture and storage. Salt may provide an excellent seal for long-term subsurface fluid storage thanks to its impermeable nature, but injecting fluids into structurally complex regions requires a deep understanding of the local

and basin-scale kinematics (Underhill et al., 2009; Li et al., 2006; Roberts et al., 2017). This will help de-risk prospective CCS targets in terms of subsurface stress fields and possible fluid migration pathways.

Another low-carbon resource that may help us to bridge the energy transition is nuclear power. This means long-term storage solutions for highly radioactive waste materials, and shallow salt bodies are one of the most viable options due its excellent sealing properties (Pollok et al., 2018). In a similar vein, large-scale, long-term, shallow subsurface storage solutions will be required if hydrogen or compressed air are to become widely used energy storage systems, providing a buffer between supply and demand as more intermittent renewable energy sources are connected to the grid (Ozarslan, 2012; Michalski et al., 2017; Dooner and Wang, 2019; Caglayan et al., 2020). The safe and effective storage of these materials requires an understanding of the long-term stability of complex deformed and layered salt bodies. This includes the development of detailed geometric models of suitable salt structures and their in situ- and palaeo-stress distributions, to test their stability and sensitivity to stress changes.

Finally, salt giants may also have a role to play in geothermal resource development. Salt perturbs patterns of subsurface heat flow distribution due to its high thermal conductivity, which may provide a new geothermal exploration target for higher energy recovery at shallower depths (Daniilidis and Herber, 2017). This would require a good understanding of the salt structure geometries, their mechanical properties, and the associated distribution of stress in and around the salt bodies to safely and effectively drill and inject fluids into the subsurface in salt-influenced regions.

For any of these solutions to be successfully implemented, we must understand the complex distribution of intra- and supra-salt strain. The body of work presented here has elucidated some of the key controls in these complex systems, and is therefore highly relevant to the petroleum industry and beyond.

6.6 Future Work

This thesis has focussed primarily on two case studies (the Levantine and Kwanza Basins) to highlight the role of base-salt relief and intra-salt heterogeneity in salt tectonic systems, and how they add complexity to the classic models of gravity-driven intra- and supra-salt strain distribution on passive margins. The results presented here may be directly applied to other gravity-driven, salt-influenced margins (e.g. Gulf of Mexico). The generalised learnings (importance of salt rheology, base-salt geometry and local boundary conditions) are transferrable to different types of salt basins such as multi-phase rifts (e.g. North Sea) or foreland basins (e.g. Paradox Basin), but further work is required to investigate the role that these parameters play in such cases, and to develop these concepts for different base-salt geometries and more complex salt rheologies.

Future work on the influence of intra-salt heterogeneity should focus on integrating available well/outcrop data, and constructing depositional models to better constrain the stratigraphy of the evaporite sequence and its lateral variability, as well as its rheological behaviour. The number of possible stratigraphic combinations comprising different viscosities, bed thicknesses and strengths of brittle layers is very large. Numerical modelling offers a practical solution to efficiently testing a large number of different scenarios, and this method has become increasingly widespread in the geosciences thanks to technological advances. The increasing computational capacity allows for increasing model sizes and better resolutions to solve complex problems. Numerical models allow full control of parameters, material laws and boundary conditions, but this blessing can also be a curse. Models underpinned by the wrong underlying physics will produce incorrect results, and numerical errors can be easily overlooked. Empirical flow laws derived from lab experiments and assigned to numerical models do not fully capture the spectrum of deformation processes that occur in nature. This means that the rheological behaviour of the numerical models may not be representative of their natural equivalent. We should therefore be cautious about relying on these results too heavily.

In order to increase confidence in the results, physical analogue models (such as those described in Chapter 5) can be used to ground-truth numerical modelling results. Although potentially more expensive and time-consuming than numerical models, the advantage of

physical models is that they happen naturally, so that if the scaling is accurate they should have the same underlying physics as the naturally occurring processes. It is also relatively easy to change and test different base-salt geometries, and they could help to find scaling laws for processes where the underlying physics is not yet completely understood (which is needed to model them numerically). I would therefore advocate for an integrated approach to further explore the roles of base-salt relief and intra-salt heterogeneity using data from natural salt basins and experimenting with different variables using numerical and physical models.

Salt tectonics has a pertinent role to play in the changing face of geoscience, and we should apply our existing knowledge in these emerging sectors as we continue to build our understanding of these complex processes.

Fin.

References

Allen, H., Jackson, C.A.L. and Fraser, A.J., 2016. Gravity-driven deformation of a youthful saline giant: the interplay between gliding and spreading in the Messinian basins of the Eastern Mediterranean. Petroleum Geoscience, 22(4), pp.340-356.

Bond, G., 1978. Evidence for late Tertiary uplift of Africa relative to North America, South America, Australia and Europe. The Journal of Geology, 86(1), pp.47-65.

Bryant, I., Herbst, N., Dailly, P., Dribus, J.R., Fainstein, R., Harvey, N., McCoss, A., Montaron, B., Quirk, D. and Tapponnier, P., 2012. Basin to basin: Plate tectonics in exploration. Oilfield Review, 24(3), pp.38-57.

Caglayan, D.G., Weber, N., Heinrichs, H.U., Linßen, J., Robinius, M., Kukla, P.A. and Stolten, D., 2020. Technical potential of salt caverns for hydrogen storage in Europe. International Journal of Hydrogen Energy, 45(11), pp.6793-6805.

Camerlenghi, A., Del Ben, A., Hübscher, C., Forlin, E., Geletti, R., Brancatelli, G., Micallef, A., Saule, M. and Facchin, L., 2020. Seismic markers of the Messinian salinity crisis in the deep Ionian Basin. Basin Research, 32(4), pp.716-738.

Cartwright, J., Kirkham, C., Bertoni, C., Hodgson, N. and Rodriguez, K., 2018. Direct calibration of salt sheet kinematics during gravity-driven deformation. Geology, 46(7), pp.623-626.

Daniilidis, A. and Herber, R., 2017. Salt intrusions providing a new geothermal exploration target for higher energy recovery at shallower depths. Energy, 118, pp.658-670.

Dooley, T.P., Hudec, M.R., Carruthers, D., Jackson, M.P. and Luo, G., 2017. The effects of base-salt relief on salt flow and suprasalt deformation patterns—Part 1: Flow across simple steps in the base of salt. Interpretation, 5(1), pp.SD1-SD23.

Dooner, M. and Wang, J., 2019. Potential exergy storage capacity of salt caverns in the cheshire basin using adiabatic compressed air energy storage. Entropy, 21(11), p.1065.

Feng, Y.E., Steinberg, J. and Reshef, M., 2017. Intra-salt deformation: Implications for the evolution of the Messinian evaporites in the Levant Basin, eastern Mediterranean. Marine and Petroleum Geology, 88, pp.251-267.

Ghalayini, R., Daniel, J.M., Homberg, C., Nader, F.H. and Comstock, J.E., 2014. Impact of Cenozoic strike-slip tectonics on the evolution of the northern Levant Basin (offshore Lebanon). Tectonics, 33(11), pp.2121-2142.

Gvirtzman, Z., M. Reshef, O. Buch-Leviatan and Z. Ben-Avraham, 2013, Intense salt deformation in the Levant Basin in the middle of the Messinian salinity crisis: Earth and Planetary Science Letters, 379, 108–119.

Hudec, M.R. and Jackson, M.P., 2004. Regional restoration across the Kwanza Basin, Angola: Salt tectonics triggered by repeated uplift of a metastable passive margin. AAPG bulletin, 88(7), pp.971-990.

Jackson, M. and Hudec, M., 2009, October. Interplay of basement tectonics, salt tectonics, and sedimentation in the Kwanza Basin, Angola. In AAPG Search and Discovery Article 30091, presented at the AAPG International Conference and Exhibition, Cape Town, South Africa (Vol. 26, p. 29).

Jones, I.F. and Davison, I., 2014. Seismic imaging in and around salt bodies. Interpretation, 2(4), pp.SL1-SL20.

Kartveit, K.H., Omosanya, K.O., Johansen, S.E., Eruteya, O.E., Reshef,M. and Waldmann, N.D., 2018. Multiphase structural evolution and geodynamic implications of Messinian salt-related structures, levant basin, offshore Israel. Tectonics, 37(5), pp.1210-1230.

Lentini, M.R., Fraser, S.I., Sumner, H.S. and Davies, R.J., 2010. Geodynamics of the central South Atlantic conjugate margins: implications for hydrocarbon potential. Petroleum Geoscience, 16(3), pp.217-229.

Li, Z., Dong, M., Li, S. and Huang, S., 2006. CO2 sequestration in depleted oil and gas reservoirs—caprock characterization and storage capacity. Energy Conversion and Management, 47(11-12), pp.1372-1382.

Marton, L.G., Tari, G.C. and Lehmann, C.T., 2000. Evolution of the Angolan passive margin, West Africa, with emphasis on post-salt structural styles. Geophysical Monograph-American Geophysical Union, 115, pp.129-150.

Michalski, J., Bünger, U., Crotogino, F., Donadei, S., Schneider, G.S., Pregger, T., Cao, K.K. and Heide, D., 2017. Hydrogen generation by electrolysis and storage in salt caverns: Potentials, economics and systems aspects with regard to the German energy transition. International Journal of Hydrogen Energy, 42(19), pp.13427-13443.

Netzeband, G. L., C. P. Hübscher, & D. Gajewski, 2006, The Structural Evolution of the Messinian Evaporites in the Levantine Basin: Marine Geology, 230(3–4), 249–73.

Ozarslan, A., 2012. Large-scale hydrogen energy storage in salt caverns. International journal of hydrogen energy, 37(19), pp.14265-14277.

Pichel, L.M., Peel, F., Jackson, C.A. and Huuse, M., 2018. Geometry and kinematics of salt-detached ramp syncline basins. Journal of Structural Geology, 115, pp.208-230.

Pollok, L., Saßnowski, M., Kühnlenz, T., Gundelach, V., Hammer, J. and Pritzkow, C., 2018, September. Geological exploration and 3D model of the Asse salt structure for SE expansion of the Asse II mine. In Proc. 9th Int. Conf. on the Mechanical Behavior of Salt (SaltMechIX).

Roberts, J.J., Wilkinson, M., Naylor, M., Shipton, Z.K., Wood, R.A. and Haszeldine, R.S., 2017. Natural CO2 sites in Italy show the importance of overburden geopressure, fractures and faults for CO2 storage performance and risk management. Geological Society, London, Special Publications, 458(1), pp.181-211.

Rodriguez, C.R., Jackson, C.L., Rotevatn, A., Bell, R.E. and Francis, M., 2018. Dual tectonic-climatic controls on salt giant deposition in the Santos Basin, offshore Brazil. Geosphere, 14(1), pp.215-242.

Roveri, M., Flecker, R., Krijgsman, W., Lofi, J., Lugli, S., Manzi, V., Sierro, F.J., Bertini, A., Camerlenghi, A., De Lange, G. and Govers, R., 2014. The Messinian Salinity Crisis: past and future of a great challenge for marine sciences. Marine Geology, 352, pp.25-58.

Rowan, M.G., Urai, J.L., Fiduk, J.C. and Kukla, P.A., 2019. Deformation of intrasalt competent layers in different modes of salt tectonics. Solid Earth, 10(3), pp.987-1013.

Underhill, J.R., Lykakis, N. and Shafique, S., 2009. Turning exploration risk into a carbon storage opportunity in the UK Southern North Sea. Petroleum Geoscience, 15(4), pp.291-304.

Walford, H.L. and White, N.J., 2005. Constraining uplift and denudation of west African continental margin by inversion of stacking velocity data. Journal of Geophysical Research: Solid Earth, 110(B4).

Zucker, E., Gvirtzman, Z., Steinberg, J. and Enzel, Y., 2020. Salt tectonics in the Eastern Mediterranean Sea: Where a giant delta meets a salt giant. Geology, 48(2), pp.134-138.

7 Appendix A: Enlarged CT Scans

7.1 Homogeneous Thin Salt Model

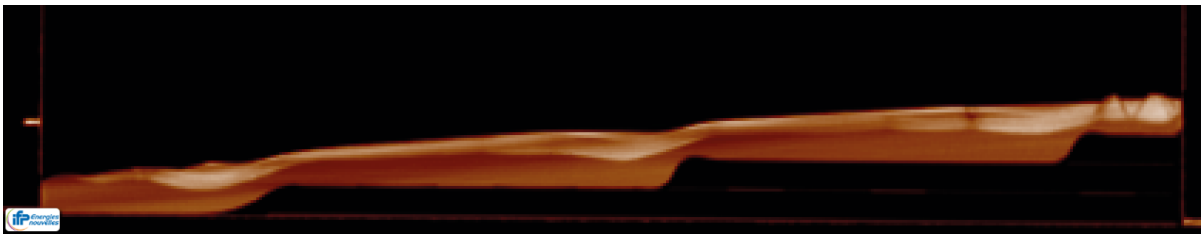

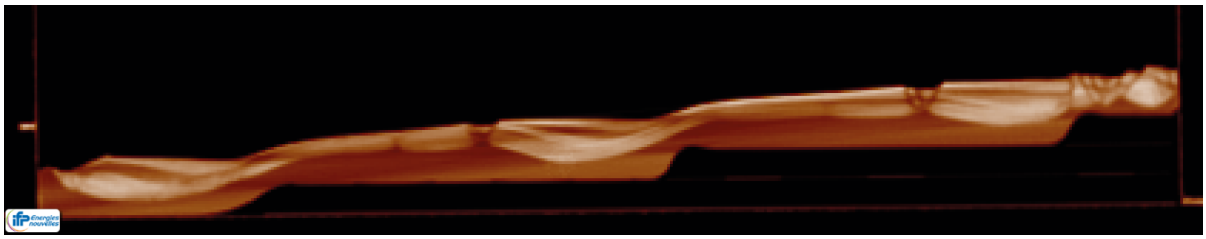

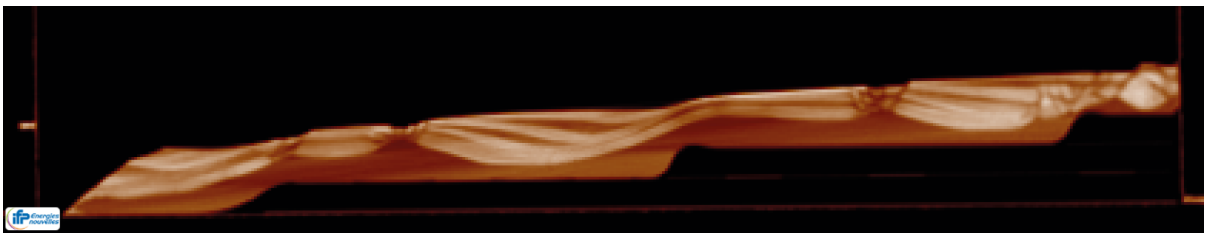

7.2 Homogeneous Thick Salt Model

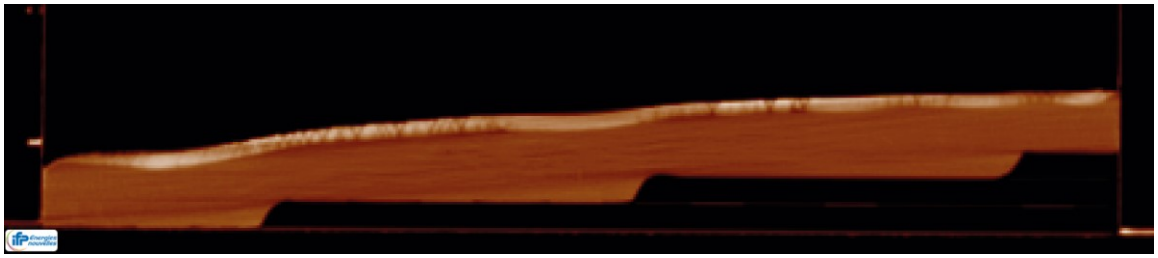

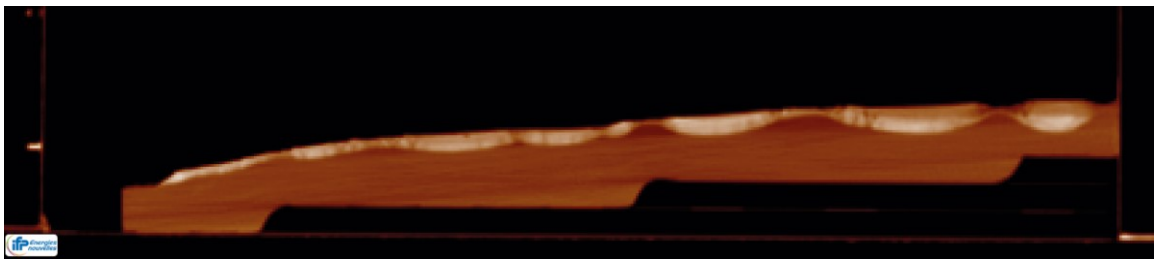

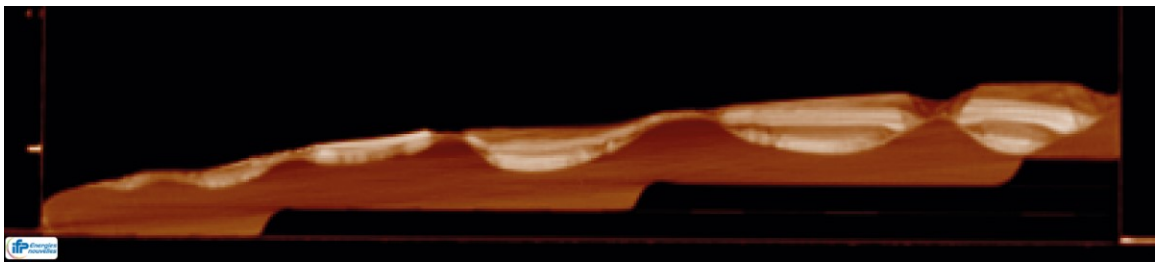

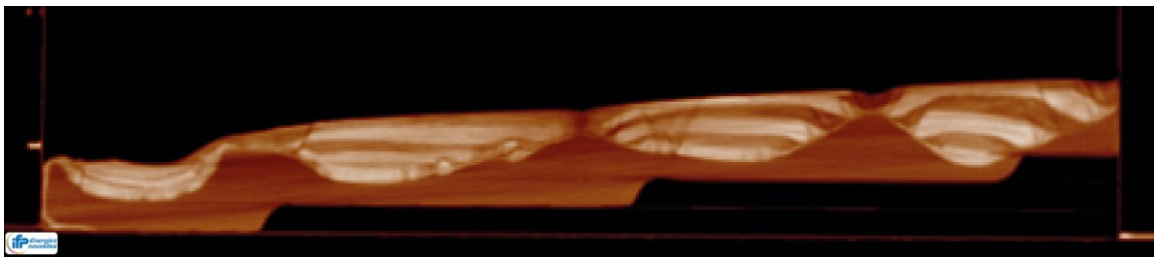

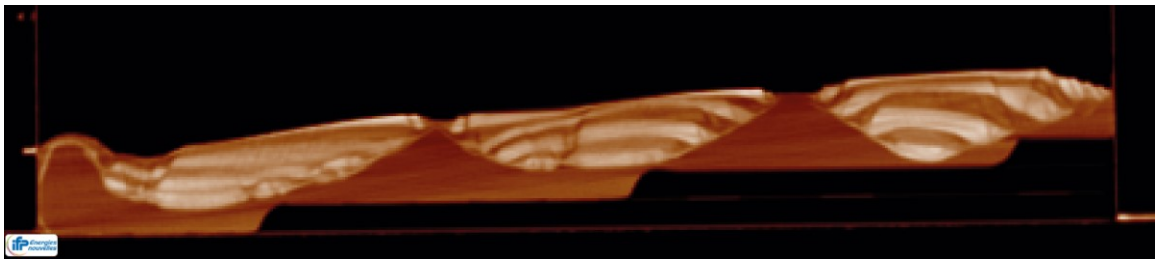

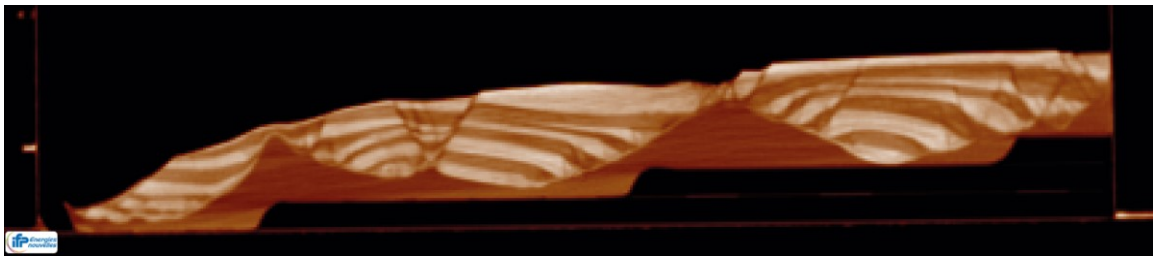

7.3 Heterogeneous Thick Salt Model